Topics in Current Chemistry 351

Barbara Kirchner *Editor*

Electronic Effects in Organic Chemistry

Springer

351
Topics in Current Chemistry

Aims and Scope

The series Topics in Current Chemistry presents critical reviews of the present and future trends in modern chemical research. The scope of coverage includes all areas of chemical science including the interfaces with related disciplines such as biology, medicine and materials science.

The goal of each thematic volume is to give the non-specialist reader, whether at the university or in industry, a comprehensive overview of an area where new insights are emerging that are of interest to larger scientific audience.

Thus each review within the volume critically surveys one aspect of that topic and places it within the context of the volume as a whole. The most significant developments of the last 5 to 10 years should be presented. A description of the laboratory procedures involved is often useful to the reader. The coverage should not be exhaustive in data, but should rather be conceptual, concentrating on the methodological thinking that will allow the non-specialist reader to understand the information presented.

Discussion of possible future research directions in the area is welcome.

Review articles for the individual volumes are invited by the volume editors.

Readership: research chemists at universities or in industry, graduate students.

More information about this series at
http://www.springer.com/series/128

Barbara Kirchner
Editor

Electronic Effects in Organic Chemistry

With contributions by

C.B. Aakeröy · K. Ansorg · P.W. Ayers · J. Becker · M. Brehm · M. Brüssel · E. Echegaray · B. Engels · K. Epa · C. Grebner · A. Guevara-García · O. Hollóczki · S. Jenkins · B. Kirchner · S.R. Kirk · W. Lee · S.B.C. Lehmann · L. Nyulászi · A. Paasche · A.S. Pensado · M. Schöppke · T.C. Schmidt · A. Stark · A. Toro-Labbe

Springer

Editor
Barbara Kirchner
Mulliken Center for Theoretical Chemistry
Institut für Physikalische und Theoretische Chemie
Universität Bonn
Bonn
Germany

ISSN 0340-1022 ISSN 1436-5049 (electronic)
ISBN 978-3-662-43581-6 ISBN 978-3-662-43582-3 (eBook)
DOI 10.1007/978-3-662-43582-3
Springer Heidelberg New York Dordrecht London

Library of Congress Control Number: 2014952317

Printed on acid-free paper

Springer is part of Springer Science+Business Media (www.springer.com)

Preface

A wide range of keywords can be drawn from the topic "electronic effects in organic chemistry" since a lot of topics are connected with this area. While it is simple to define organic chemistry – see any textbooks on general chemistry – it is much more difficult to define electronic effects, especially if we want to avoid simply repeating the terms "effects which are governed by electrons". What can be considered as such electronic effects? All consequences concerning changes caused by the (valence) electrons of organic molecules?

This volume deals with the concepts of electronic structure and associated methods in the context of organic chemistry and provides some answers to the questions above. As all authors are considering some kind of electronic effects, the main emphasis of the book lies in theoretical contributions, because one of the most important sections in theoretical chemistry is electronic structure theory. Nevertheless, important experimental work is highlighted or reviewed at the appropriate position. Hydrogen bonding always plays an important role when it comes to electronic effects, and throughout the book hydrogen bonding always emerges on the surface or plays an indirect role.

The volume begins with a contribution by Oldamur Hollóczki and László Nyulászi on the hot topic of carbenes from ionic liquids, which is also the title of their chapter. It deals with the fact that within ionic liquids–although their direct detection has been impossible so far–carbenes can be accessed by deprotonation of the cation at the appropriate position. This opens the possibility to use ionic liquids as, e.g. organocatalysts, which makes their investigation even more exciting. In the next chapter, Guevara-García et al. elaborate on conceptual density functional theory, which is a very exciting development, in order to describe organic reactivity, and which is thus at the heart of the topic of this book. Instead of considering electron-following, the electron-preceding picture (described by the stress tensor) identifies favourable changes in the electronic structure. Bernd Engels and co-workers review the application of a multi-scale method, namely QM/MM (quantum mechanics/molecular modelling), – which has been mainly applied to biochemical problems – to organic chemistry questions. With regard to organic

reactions, it is important to stress that most of these reactions are carried out in a condensed phase environment, or via complex interactions between the substrate and, for example, a catalyst, which renders the use of such methods – describing the electronic structure at least partly – indispensable. Hydrogen bonding in supramolecular assemblies is one the main origins of the control mechanisms as discussed by Aakeröy and Epa. The authors conclude that p*K*a values are less practical for retaining information whenever different functional groups are involved. They suggest the employment of molecular electrostatic potential surfaces for guiding the synthesis of binary and ternary co-crystals. The same difficulty in the context of ionic liquids and their mixtures, namely the reasonable description of hydrogen bonding, is highlighted in the final chapter by Stark and co-workers.

As editor of the volume, I hope this collection of fine chapters reflects the importance of theoretical methods and conceptual work in this interesting field of "electronic effects in organic chemistry" in a broad review style, while at the same time highlighting possible future directions. I would like to thank Prof. em. Dr. Dr. h.c. Sigrid Doris Peyerimhoff, Prof. Dr. Stefan Grimme and also my group members for fruitful discussions. To all the contributing authors I am indebted for providing this volume with such excellent and thorough chapters, and, finally, I would also like to thank the contributing authors for their patience.

Bonn, Germany
August 2013

Barbara Kirchner

Contents

Top Curr Chem (2014) 351: 1–24
DOI: 10.1007/128_2012_416

Published online: 29 March 2013

Carbenes from Ionic Liquids

Oldamur Hollóczki and László Nyulászi

Abstract In the last decade an explosive development has been observed in the fields of both ionic liquids (ILs) as potential chemically inert solvents with many possible technical applications, and N-heterocyclic carbenes (NHCs) as catalysts with superb performance. Since the cations of many ILs can be deprotonated by strong bases yielding NHCs, this two fields are inherently connected. It has only recently been recognized that some of the commonly used basic anions of the ILs (such as acetate) are able to deprotonate azolium cations. While the resulting NHC could clearly be observed in the vapor phase, in the liquid – where the mutual electrostatic interactions within the ion network stabilize the ion pairs – the neutral NHC cannot be detected by commonly used analytical techniques; however, from these ionic liquids NHCs can be trapped, e.g., by complex formation, or more importantly these ILs can be directly used as catalysts, since the NHC content is sufficiently large for these applications. Apart from imidazole-2-ylidenes, the formation of other highly reactive neutral species ("abnormal carbenes," 2-alkylideneimidazoles, pyridine-ylidenes or pyridinium-ylides) is feasible in highly basic ionic liquids. The cross-fertilizing overlap between the two fields may provide access to a great advance in both areas, and we give an overview here on the results published so far, and also on the remaining possibilities and challenges in the concept of "carbenes from ionic liquids."

O. Hollóczki
Wilhelm-Ostwald Institute of Physical and Theoretical Chemistry, University of Leipzig, Linnéstr. 2, 04103 Leipzig, Germany
e-mail: holloczki@gmail.com

L. Nyulászi (✉)
Department of Inorganic and Analytical Chemistry, Budapest University of Technology and Economics, Szent Gellért tér 4, 1111 Budapest, Hungary
e-mail: nyulaszi@mail.bme.hu

Keywords 1-Ethyl-3-methylimidazolium acetate · Acid–base equilibria · Basic ionic liquids · Carbene · Catalysis · CO_2 capture · DFT calculations · Hydrogen bonding · Ionic liquids · Mass spectroscopy · N-Heterocyclic carbenes · Organocatalysis · Photoelectron spectroscopy · Proton transfer · Synthesis · Vaporization mechanism

Contents

List of Abbreviations and Symbols

$[C_2C_1Im][CH_3SO_3]$	1-Ethyl-3-methylimidazolium methanesulfonate
$[C_2C_1Im][OAc]$	1-Ethyl-3-methylimidazolium acetate
$[C_2C_2Im][OAc]$	1,3-Diethylimidazolium acetate
$[C_nC_1Im][OAc]$	1-Alkyl-3-methylimidazolium acetate
$[C_nC_1Im][OH]$	1-Alkyl-3-methylimidazolium hydroxide
$[C_nC_mIm][HCO_3]$	1,3-Dialkylimidazolium hydrogen carbonate
DFT	Density functional theory
DIPP	2,6-Diisopropylphenyl group
IL	Ionic liquid
Im-IL	Imidazolium-based ionic liquid
NHC	N-Heterocyclic carbene
Tf_2N^-	Bis(trifluoromethanesulfonyl)imide
TfO^-	Triflate

1 Introduction

Among ionic liquids [1–3] (ILs), 1,3-dialkylimidazolium salts (Im-ILs) are undoubtedly one of the most popular and most investigated classes. They are widely used in a great variety of applications, such as solvents for many synthetic chemical processes [1–3]. One of the reasons for their success as solvents involves the fact that these compounds are often considered inert, since their electrochemical window is wide, and they neither possess easily dissociating protons nor energetically easily available lone pairs.

However, it is also well known that from 1,3-dialkylimidazolium salts imidazole-2-ylidenes, the most important class of N-heterocyclic carbenes (NHCs) [4–10] can be derived by a single deprotonation (Fig. 1), albeit under strongly basic conditions (alcoholate, alkali-hydrides, etc.), connecting inherently the chemistry

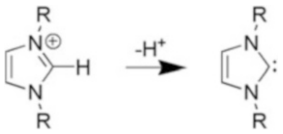

Fig. 1 Deprotonation of the imidazolium cation – connection between ILs and NHCs

of these two families of compounds. Proton/deuteron exchange at position 2 of 1,3-dimethylbenzimidazolium iodide had already been observed by Breslow in 1958 [11], suggesting the intermediacy of the corresponding carbene (often called "zwitterion" or "betaine" in the early literature). Accordingly, in highly basic media the non-inert nature of Im-ILs has been indicated [12–17], as carbene-derived decomposition products could be observed. Also, the synthesis of imidazol-2-ylidenes from imidazolium salts by alcoholates (e.g., by *t*BuOK) has been patented [18]. However, given that NHCs can also be used in a great variety of highly important applications, e.g., as organocatalysts [19–22] or ligands in organometallic catalysts [4, 23–29], this possibility is not merely a possible decomposition mechanism for Im-ILs but also an opportunity to unite the advantageous properties of these two groups of compounds into a novel and powerful chemistry. In the last few years there has been a significant advance in the overlap of these fields, showing that, in the presence of appropriate external bases or, as was shown very recently [30], even in the case of sufficiently basic anions, carbenes may form in ILs. Here we summarize this knowledge, by presenting the recent results and the still open challenges in this topic.

2 Chemistry and Applications of NHCs

Although there are many recent reviews – including a thematic issue of Chemical Reviews – on carbenes [4–10, 31], and in particular on NHCs, which discuss their structure, stability, and applications, we think it is important for the non-specialized reader to give a short overview here. NHCs are divalent carbon derivatives incorporated into a nitrogen-containing heterocycles. Unlike the parent carbene CH_2 [5, 32], NHCs possess a singlet electronic ground state (Fig. 2) [4, 5]. In these structures the carbene empty orbital interacts with the nitrogen lone pair(s) (note that one of the substituents at the divalent carbon might also be another kind of atom), providing significant stabilization [4, 5], often with some further contribution from aromaticity (see below). Due to all these interactions with the vacant orbital, the electrophilicity of NHCs is reduced, while the carbon-based lone pair (Fig. 2) makes NHCs a strong nucleophile [4, 5]. The competing triplet state can be considered a highly unstable biradical (Fig. 2), being able to dimerize with the formation of a double bond; thus, the stability of carbenes can generally be correlated to the singlet/triplet gap [5, 33, 34], and therefore to the extent of the stabilizing interaction between the heteroatoms and the carbene center. The energy of the isodesmic reaction ($\Delta E_{\text{carbene}}$) in Fig. 3 provides an easily computable and

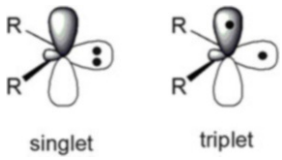

Fig. 2 Singlet and triplet electronic ground state of carbenes

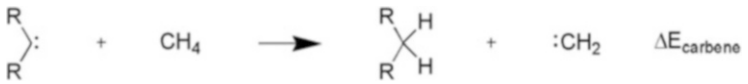

Fig. 3 Isodesmic reaction, used as a measure of carbene stability

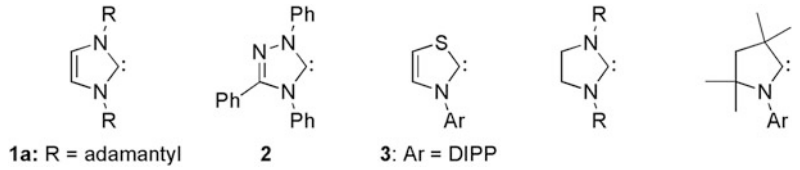

Fig. 4 Some already synthesized NHCs

good approximation for the stability of the carbenes, also being in good correlation with the dimerization energies [35]. The stabilization of the carbene is not only interesting from the apparent point of view of the synthesizability, but it also has an important effect on the reactivity, including the catalytic activity [36].

According to these stabilization principles, many stable NHCs (and also other carbenes) have been synthesized [5, 6]. The first free NHC, 1,3-diadamantylimidazole-2-ylidene [37] **1a** (Fig. 4), synthesized by Arduengo and co-workers in the early 1990s, has a melting point at 240°C without any sign of decomposition [37], and can be stored under an inert atmosphere for a prolonged period; while the $\Delta E_{\text{carbene}}$ is the largest (ca. 110 kcal/mol) for this carbene among all hitherto investigated structures [35, 36]. This stability is induced not only by the interaction of the carbene center with the heteroatoms but also by a significant aromatic character [38, 39], which has been evaluated (Fig. 5) using the elegant concept of isomerization stabilization energy (ISE, [40]) to be ca. 14 kcal/mol [41, 42]. It is worth mentioning that the synthesis of this NHC has been followed by a series of analogous carbenes, including other imidazole-2-ylidene derivatives, triazole-5-ylidene **2** [43], and thiazole-2-ylidene[1] **3** [44].

The presence of the lone pair and the low-lying empty orbital provides NHCs with a unique structure, making them analogous to transition metals [45]. Indeed, NHCs (particularly derivatives of **1, 2**, and **3**) are very effective and versatile

[1] It should be noted that while the first thiazole-2-ylidene derivative was isolated in 1997 – see [44] – its catalytic activity was shown by Breslow as early as 1958 – see [11].

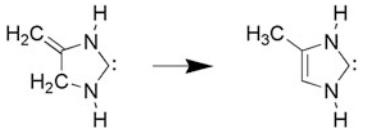

Fig. 5 Isomerization stabilization energy, an isodesmic reaction applied to evaluate the aromaticity of imidazole-ylidenes

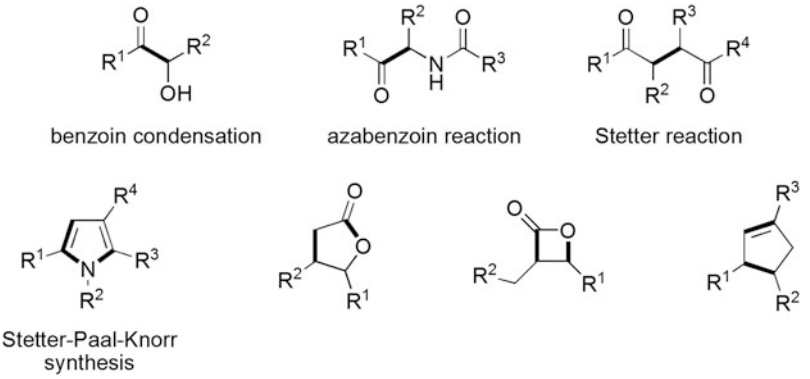

Fig. 6 Some examples for structures that can be built by NHC catalysis [19–22]. The bonds that are formed by the corresponding synthetic approach are highlighted as *thick lines*

organocatalysts [19–22, 46], providing simple routes via "umpolung" toward, for example, C–C couplings that are important for synthetic strategies, such as – among others – the benzoin condensation and the Stetter (or Stetter–Michael) reaction (Fig. 6). Making them even more valuable, most of these reactions can also be performed stereoselectively if chiral substituents are attached to the carbene ring [19–22]. The efficiency and generality of the catalytic activity of NHCs in C–C couplings is also indicated by the fact that biological systems also apply NHC catalysis by thiamine for analogous transformations, e.g., in the carbohydrate metabolism [11, 47, 48]. Beside these transformations, the activation of many small molecules, such as P_4 [49, 50], H_2 [51, 52], N_2 [53], NH_3 [51], CO_2 [54–56], and CS_2 [55], and also the stabilization of main group element allotropes [57, 58] including, e.g., Si_2 or C_1 [59] by NHCs are also important to note, offering interesting solutions for chemistry in terms of alternative building blocks.

In many cases of organocatalytic reactions an azolium (e.g., imidazolium) salt is used as pre-catalyst, which is in situ deprotonated by the added external base to release the NHC catalyst itself [19–22]. In some work these salts have also been used as an IL solvent for the reaction, defining therefore a "pre-catalytic solvent" [13, 16, 60–63]. It is also worth mentioning that not only can additional bases be used to prepare the NHC catalyst from the IL solution, but also the electrochemical reduction of the imidazolium cation to the corresponding NHC is a viable possibility [12, 17, 64–66]. It is worth noting that, apart from the apparent carbene precursor

azolium cations, the CO_2 [67–70], borane [71], and silane complexes [72–75], and, as has been shown very recently, carbeniophosphanes [76] can also be used as carbene sources.

As the presence of the carbon-based lone pair already suggests, these compounds possess strong Lewis-base properties, making them excellent proton acceptors and also very good ligands for transition metal [4, 23–29] and even main group element complexes [73, 74, 76, 77]. Their complexing ability is clearly presented by the significantly higher stabilities of carbene-derived penta- and hexacoordinate silicon derivatives, compared to those of the known amine and phosphine analogues [73]. In good accordance, the NHC complexes of transition metals often exhibit higher stability and better catalytic properties compared to the corresponding – and also very popular – phosphine derivatives [4, 27]. Accordingly, these structures have a high impact on modern synthetic chemistry. Since such complexation may also occur at transition metal (e.g., gold) surfaces [78], this field may also hold some future applications in material sciences and nanotechnology.

Given that this strong basicity facilitates proton abstraction even from weak acids, and that it is directly relevant in the aforementioned organocatalytic applications, there are measured [79] and several computational data [80–82] in the gas phase, and spectroscopic measurements [83–86] in the liquid phase, to determine the basicity of these compounds. For imidazole-2-ylidene gas phase protonation energies about 260 kcal/mol have been obtained depending on the level of theory applied [80–82], in reasonable agreement with the collision-induced dissociation measurements (251.3 $\pm$ 4 kcal/mol) [79]. According to the high proton affinities these compounds can be termed as superbases. The pK_a data were usually measured by the rate of H/D exchange of the corresponding protonated species, or by partial deprotonation by using similarly strong bases. It should be noted that, while the pK_a value of imidazol-2-ylidenes varies between 21 and 24 depending on the solvent (including water) and the substituents on the nitrogen atoms [81, 83–86], the pK_a of water shows a much larger dependence on the solvent between 15.6 (water) and 32 (DMSO) [87]. Interestingly, although the position 2 of the imidazolium ring possesses the most acidic hydrogen [88, 89], the position 4 (and 5) of the ring is not entirely innocent, and "abnormal carbenes" [29] are accessible by deprotonation at the rear of the ring, as shown by H/D exchange studies [90, 91] and also by complexation reactions [24, 29, 171, 172]. An imidazol-2-ylidene at position 4 could also be lithiated, resulting in an anionic dicarbene [92]. Recently, even a free "abnormal carbene" could be synthesized with a substituent at position 2 of the imidazolium ring [93].

The lone pair of the NHCs allows them not only to act as proton acceptors but also to form strong hydrogen bonds. This increased hydrogen bonding ability of carbenes results in the possible formation of even C- - -H–C type bonds, as shown between imidazole-2-ylidene and imidazolium cation via the position 2 hydrogen atom [94], and even between two imidazole-2-ylidenes via the position 4 hydrogen atom [95] – note the involvement of the "abnormal carbene" [29] structure. The strength of the hydrogen bond between a water molecule and 1,3-dimethylimidazole-2-ylidene is about 10 kcal/mol according to theoretical

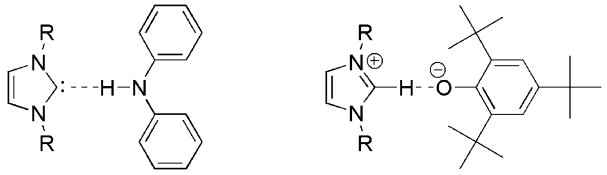

Fig. 7 Two "acid"-NHC systems investigated by Clyburne and co-workers [99]

calculations (at various levels of theory) [96], which is ca. 50% stronger than that between two water molecules [96] at the same level of theory! In this respect it is worth mentioning that, although carbenes are considered to be very sensitive to water, with traces of moisture (up to a few equivalents of water) the reaction of imidazole-2-ylidenes has been shown to be very slow (the full conversion may take several months), resulting in ring opened products [72, 96, 97]. Moreover, calculations also showed that proton transfer from the water to the carbene – yielding imidazolium-hydroxides – is only viable with bigger water clusters [96], where the acidity of the water cluster is high enough to protonate the carbene, in agreement with some early findings [88] that indicate the lack of imidazolium-hydroxide-like structure when a single water molecule is present. According to these theoretical observations [88, 96], the corresponding NHC-water H-bonded structures could be detected by IR and NMR spectroscopies [96]. It is notable that, while the synthesis and catalytic activity of an imidazolium hydroxide has been claimed [98, 173], no detailed structural characterization of the obtained substance has been reported.

A further important observation of NHC-hydrogen bonded structures was reported by Clyburne and co-workers [99]. They showed that while with diphenylamine the carbene simply forms a hydrogen bond, with 2,4,6-tri(tert-butyl)phenol proton transfer occurs, and an ion pair-like structure was obtained [99]. Both structures could be confirmed by X-ray crystallography, and the difference in their bonding is in good accordance with the acidity difference between these two H-boding partners [12] (Fig. 7). Later it was shown that the non-ionic carbene-phenol structure would be more stable in the gas phase, but steric effects of the bulky *t*Bu groups together with the mutual interaction between the particles stabilize the ionic isomer [30]. Interestingly, these two structures exhibit similar C–N and C–O distances, indicating that the interaction in the overall assembly itself is only slightly affected by the position and bonding mode of the hydrogen atom [99].

These results suggest that by altering the acidity of the hydrogen bonding partner of the carbene, or by altering the basicity of the anion in imidazolium salts (like Im-ILs), the system can be switched between the two alternative structures in Fig. 8, and carbene precursor ionic liquids can be designed.

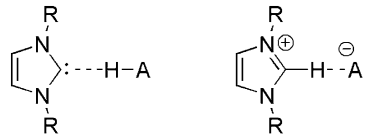

Fig. 8 Two possible isomers of carbene–acid or imidazolium salt ion pair systems [30]

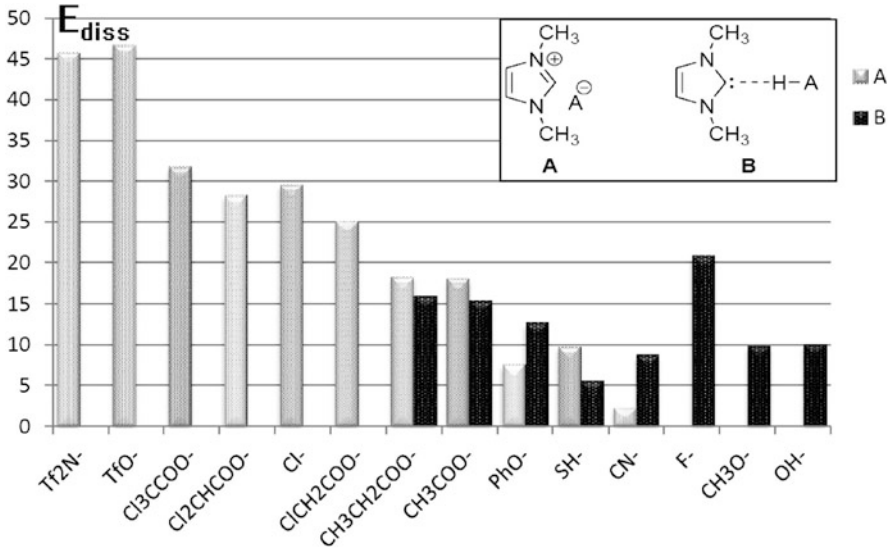

Fig. 9 Structure and dissociation energy (E_{diss} to the carbene and the corresponding acid) of possible isomers of imidazolium salts with anions having different basicities (increasing from *left* to *right*)

3 Carbenes from Ionic Liquids

The first systematic investigation on the effect on the anion's basicity on the protonation/deprotonation equilibrium in Im-IL ion pairs, and their dissociation to a carbene and the conjugate acid of the anion, has been carried out by theoretical methods on the model series of dimethylimidazolium salts [30]. The two isomeric structures are shown in Fig. 9. In the case of the least basic anions – which are in fact the most widely used in ILs – only the expected ionic isomer **A** could be optimized, and the corresponding dissociation to the carbene has been found to be highly endothermic [100]. By increasing the basicity of the anion (thus resulting in a basic IL [101]) to that of the carboxylates, however, other structures appear on the potential energy surface. The most interesting from the point of view of the carbene formation is isomer **B**, which is composed of a carbene attached by an H-bond to the conjugate acid of the anion.

The dissociation energies (to the carbene and the corresponding acid) of isomer **A** type structures show a gradual decrease by the increasing proton affinity of the anion, from the ca. 45–47 kcal/mol value for Tf_2N^- and TfO^- to the 2.3 kcal/mol of the cyanide. For the three most basic investigated anions (F^-, MeO^-, OH^-) this isomer could not even be optimized. On the other hand, dissociation energies of isomer **B** structures show no direct dependency on the basicity of the anion; it is rather connected to the well-known H-bonding ability of the corresponding conjugate acids: those possessing an O–H bond form strong (10–15 kcal/mol) H-bonds, HF bonds somewhat stronger, while HCN and H_2S exhibit weaker bonding to the carbene. Since the dissociation energies are calculated with respect to the same reference structures (viz. the free carbene and acid) in the case of both isomers, the difference in these values can be rationalized as relative energies between the two isomeric structures. Thus, the isomer having higher dissociation energy is the more stable. Accordingly, considering the aforementioned differences in stabilities by the increasing basicity of the Im-IL anion, it can be expected that the relative stability of the carbene-containing isomer **B** will increase. From the investigated basic[2] anions, clearly the acetate is the most interesting, since $[C_2C_1Im][OAc]$ is commercially available and generally applied in synthetic and technical chemistry, e.g., in cellulose processing [103]. For this IL the energies of isomers **A** and **B** are close. While for the energy of the carbene complex a somewhat higher value has been reported than that of the ion pair in the gas phase [104], using larger basis sets this energy difference decreases, and at some levels **B** turned out to be even the most stable structure [30]. The dissociation energy of $[C_2C_1Im][OAc]$ ion pairs to the corresponding carbene and acetic acid has been found to be ca. 15–18 kcal/mol, depending on the level of theory. This value indicates a strongly bound system (cf. with the stability of the water dimer, as discussed above), in which the stronger H-bond with the acetic acid is completed by another (albeit much weaker) interaction between the methyl group and the carbonyl oxygen atom of the acid. Nevertheless, these dissociation energies might be low enough for the dissociation to occur at elevated temperatures and under lower pressures in the gas phase.

Considering the observations that vaporized ILs [105] consist of single ion pairs [106–108], these aforementioned gas phase calculations on these structures directly represent the vapor of ILs. Thus, photoelectron and mass spectroscopies could be applied to confirm directly the results of the theoretical calculations [30]. Interestingly, under the conditions of photoelectron spectroscopy (ca. 10^{-2} mbar, 420 K), the first reported isomer **B** carbene-acetic acid **H**-bonded system – and not the ion pair A – has been observed [30], in contrast to previous findings for ILs, containing less basic anions [105–108]. This result indicates that the stability of isomer **A** is slightly overestimated by some of the theoretical methods applied. A further important observation for the vapor phase structure comes from the MS spectrum, which clearly shows all the characteristic peaks of acetic acid (base peak at

[2] Related to the basicity it should be noted that the nucleophilicity of the acetate anion in $[C_2C_1Im][OAc]$ is sufficiently large to esterify alkyl halides directly [102].

60 amu), and one distinct peak at m/z = 110 amu that corresponds to 1-ethyl-3-methylimidazol-2-ylidene, together with other peaks characteristic for the carbene fragmentation [30]. These findings could only be rationalized by considering the formation of the *isolated carbene* and *acetic acid* prior to ionization, showing that dissociation occurs under the higher vacuum of the MS measurements (10^{-6} mbar) [30]. The analogous $[C_2C_1Im][CH_3SO_3]$, possessing a less basic anion, showed no peaks of the imidazol-based carbene, rather that of the imidazolium cation at m/z = 111 a.u. [30]. These results suggested for the first time that – in spite of the generally accepted term "non-protic IL" – for 1,3-dialkylimidazolium ionic liquids possessing sufficiently basic anions a similar vaporization mechanism may hold to that of the so-called protic ILs (viz. generally protonated amines [109], which release protons easier than CH acids), involving neutral species formed by a proton transfer from the cation to the anion.

While the presence of acetic acid and the free carbene (at high temperature and low pressure) in the vapor phase has clearly been demonstrated, the concentration of the free carbene in the ionic liquid can still be small, since the ion network of the condensed phase is shown to stabilize ionic structures [110, 111]. Thus, the question arises whether this carbene content is observable at all in the liquid phase. Indeed, the carbene could not be detected by any direct spectroscopic methods in $[C_2C_1Im][OAc]$, nor in a recently published X-ray structure on the analogous $[C_2C_2Im][OAc]$ [112]. Nevertheless, its presence could be surmised according to ab initio molecular dynamics simulations [113], where significantly increased C–H and decreased O–H bond lengths have been observed also in the bulk, alleviating the above discussed H/D exchange. In agreement, the NHC had been trapped as Pd^{2+} complex when $Pd(OAc)_2$ had been dissolved in Im-ILs even with less basic anions [114, 115]. In the light of the above discussed role of the acetate ion in the carbene formation it became apparent that the strong basicity of the acetate counterion of Pd^{2+} had played a crucial role in the formation of the carbene (in its complex).

Rogers and co-workers used a series of trapping experiments to provide further indirect evidence for the presence of carbenes in this apparently very complex IL system. Apart from the formation of the Pd^{2+} complex with $Pd(OAc)_2$ (which had been noted before in other Im-ILs [114, 115] – see discussion above), imidazole-2-thiones could be isolated in the reaction mixture of equimolar amount of S_8 in $[C_2C_1Im][OAc]$ (24 h at 25°C, Fig. 10), with a yield of nearly 50% [116]. Similarly, typical carbene-like reactivity resulting in adduct formation with elemental Se, and benzaldehyde could also be observed (Fig. 10) [116]. Since no reaction with the sulfur occurred if the acetate was changed to Cl^-, HSO_4^-, SCN^-, $CH_3SO_3^-$, tosylate, TfO^-, or CF_3COO^-, the effect of the anion's basicity is clearly shown.

Rogers and co-workers also speculated about the need for the H-bond between the acetate ion and the acetic acid released during the carbene formation [116], which had previously been observed in acetate-acetic acid systems within ILs (see Fig. 10) [117, 118]. In apparent agreement, the presence of extra hydrogen bond donor molecules, such as acetic acid and water, suppressed the thione formation.

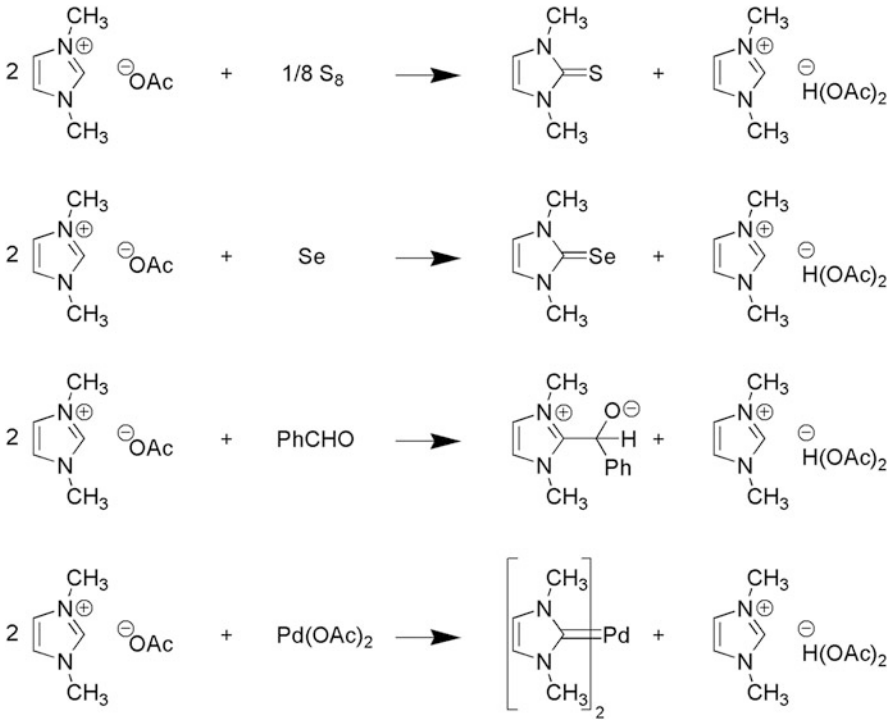

Fig. 10 Trapping reactions of carbenes in $[C_2C_1Im][OAc]$ [116]

The occurrence of the $H(OAc)_2^-$ complex anions also provides an explanation for the observed 50% upper limit of yields in the trapping reactions, given that after 50% conversion there are no free acetates to accommodate the acetic acid [116]. The formation of the acetic acid–acetate complex has been clearly demonstrated in the X-ray structure obtained from the product of the subsequent carbene trapping experiment with CO_2 [112] (see below for details). Undoubtedly, this H-bond stabilizes the acetic acid, shifting the equilibrium of the proton transfer between the cation and the anion towards the carbene formation; however, we believe that these observations still do not necessitate the direct involvement of these complex anions in the carbene formation. In this context it is worth mentioning that no such structure had been documented in the case of the previous carbene trapping reactions of Im-ILs with $Pd(OAc)_2$ [114, 115]. Apparently, in the case of a sufficiently stable reaction product the additional effect of the acetic acid removal is not needed. Besides, if the accessibility of these structures were the condition of the carbene formation, no isomer **B** structures would have been observed previously in the vapor phase, where the carbene–acetic acid complex was shown to evaporate [30]. Moreover, the lack of trapping reactions in the presence of acetic acid (!) or water [116] (cf. basicities of water [87] and imidazole-2-ylidenes [81, 83–86], see above) can be rationalized by the decrease in basicity due to the presence of the

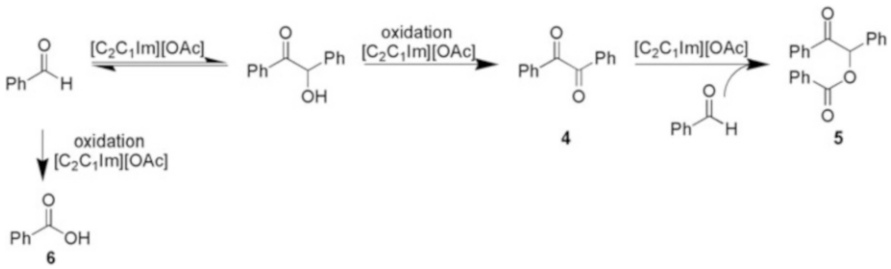

Fig. 11 Proposed catalytic network of the $[C_2C_1Im][OAc]$–benzaldehyde system [119]

additional protons. Recent ab initio molecular dynamics data support this idea [113], showing that by the addition of water to $[C_2C_1Im][OAc]$, it competes with the ions for the interactions sites; thus, the anion–cation assembly is disrupted, which results in the shortening of the C2–H2 bonds (viz. suppression of carbene formation) compared to the "dry" system.

We aimed to show the presence of carbenes by a different approach, via investigating the organocatalytic activity of $[C_2C_1Im][OAc]$ in the benzoin condensation [119], which is a classical example of an NHC organocatalyzed reaction. Thus, benzaldehyde was added to a sample of this IL in excess, and was stirred at 60°C under argon for 6 h. Indeed, the product benzoin was isolated in reasonable yields (67%, which could be further increased to 76% by the careful purification of benzaldehyde from benzoic acid), showing indirectly that carbenes are indeed present in the liquid to an extent that provides observable catalytic activity for this reaction.

Interestingly, by performing the reaction under air, the products of the catalytic process altered; benzyl **4**, 2-oxo-1,2-diphenylethyl benzoate **5**, and benzoic acid **6** have been isolated from the reaction mixture (Fig. 11) [119]. Considering the differences between the two reactions and the fact that all products are oxidized and no reduced species have been obtained, it is reasonable to assume that (one component of) air has served as oxidizing agent. Recently, CO_2 has been proposed to oxidize aldehydes in NHC catalysis [120, 121], although its role as an oxidizing agent has been questioned [122–124], and it has been considered that in these reactions traces of oxygen oxidized the substrates. Nevertheless, we obtained the same products under CO_2 atmosphere, while we clearly observed the formation of CO by IR spectroscopy (Kelemen Z, Pasinszki T, Hollóczki O, Nyulászi L, unpublished), which has been surmised as a possible product of the CO_2's reduction in the analogous NHC catalyzed reactions [120, 121]. These results suggest that CO_2 may indeed have a role in this oxidation process [119], although the reproducibility of this reaction has turned out to be poor.

The formation of **5**, however, cannot be concluded by a single oxidation step, and therefore the benzaldehyde/$[C_2C_1Im][OAc]$/air system should exhibit a rather complex multistep reaction mechanism. NHCs are also known to catalyze the so-called hydroacylation reactions, in which the addition of aldehydes to ketones occurs, and esters are formed [125]. Accordingly, we proposed a mechanism

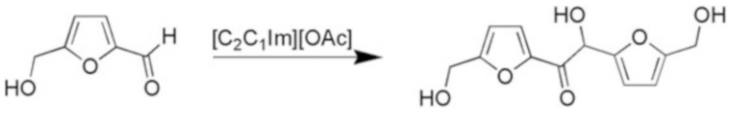

Fig. 12 Catalytic reaction of $[C_2C_1Im][OAc]$, applied in biomass processing [126]

involving the initial formation of **4** by the oxidation of benzoin, followed by a hydroacylation coupling step between **4** and the substrate benzaldehyde [119]. To check the feasibility of this assumption, first we mixed **4** and benzaldehyde in $[C_2C_1Im][OAc]$ at room temperature. Indeed a fast and highly exothermic reaction occurred, with good yields (87%). In a different experiment we checked the viability of the benzoin → **4** oxidation step by dissolving benzoin in the IL under air. Interestingly, not only has the oxidation to **4** been observed, but also the formation of **5** and **6**. These surprising results necessitate not only the oxidation but also the presence of non-reacted benzaldehyde in the system, clearly showing the reversibility [36] of the benzoin condensation between two benzaldehyde molecules. Thus, according to these experimental results, the NHC catalytic activity of $[C_2C_1Im][OAc]$ in the presence of air can be concluded to be as depicted in Fig. 11 [119].

Very recently [126] the above described catalytic activity of $[C_2C_1Im][OAc]$ in the benzoin condensation has been reported to provide a novel route for biomass processing. 5-Hydroxymethylfurfural – that can be produced effectively from plant biomass resources such as glucose or cellulose [127] – can undergo a facile benzoin condensation (see Fig. 12) in $[C_2C_1Im][OAc]$, catalyzed by the solvent itself under very mild conditions (60–80°C) with excellent yields (up to 98% within 1 h). The product of the reaction, 5,5′-di(hydroxymethyl)furoin has been suggested for use as a possible C_{12} kerosene/jet fuel [126]. Later, also a redox esterification reaction has been reported in this ionic liquid [174].

In light of the above results a particularly intriguing problem is the CO_2 trapping in the form of a carbene complex in $[C_2C_1Im][OAc]$. Im-ILs generally absorb CO_2 so efficiently [128–131] that they have been suggested as absorbents for the neutralization of industrial waste gases. This behavior can be related to the recently recognized specific weak interactions between CO_2 and imidazolium cations [132]. Interestingly, $[C_nC_1Im][OAc]$ ILs possess even significantly higher CO_2 solubility, which has been tentatively rationalized by chemical absorption according to the phase diagrams [133]. The fact that CO_2 could be electrochemically reduced in $[C_2C_1Im][OAc]$ [134] opens up further possibilities for the utilization of the captured CO_2. Carbenes have also been known since the late 1990s to form adducts with CO_2 (Fig. 13) [54, 55, 135, 136] when generated by external bases from ILs [137], and therefore the presence of carbenes in these ILs provides an apparent explanation for this interesting behavior of acetate-based Im-ILs. Rogers and co-workers could isolate the forming species [112] which was indeed in accordance with the expected products according to the NMR spectra and the X-ray crystallography. The reaction is indicated to be rather slow under atmospheric pressure (36 h),

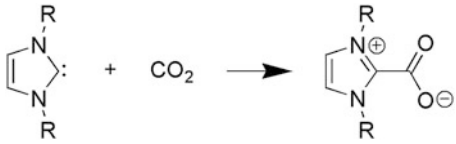

Fig. 13 Reaction of carbenes with CO_2, reported by Kuhn in the 1990s [54]

but at 20 bar it is facilitated and the precipitation of the crystalline product has been observed even after 2 h. Similarly to the aforementioned carbene trapping experiments [116], a maximum yield of 50% has also been observed in this case, due to the gradual increase in acidity by the formation of acetic acid, and also partly due to the complex anion formation [116]. The $[C_2C_1Im][OAc]$–CO_2 system has recently been intensely studied, and the formation of the adduct has also been evidenced by NMR spectroscopy and microcalorimetric measurements [138]. Investigation of the related $[C_4C_1Im][OAc]$–CO_2 system by NMR and Raman spectroscopies [139–141] also revealed the presence of the NHC–CO_2 complex. The assignment of the measured spectral features has been supported by DFT calculations on IL clusters to rationalize the spectra [140], involving the detailed analysis of the additional physical absorption of CO_2 in the IL, occurring after the chemical absorption by the reaction with the carbene is completed [140].

The presence of the $H(OAc)_2^-$ anions has been observed directly in the X-ray measurements [112]. In the presence of water, however, this adduct has not been formed, and imidazolium hydrogen carbonates have been obtained [112]. Considering the aforementioned suppression of carbene formation by the addition of H-bonding substances to the IL, this product has presumably been formed by a direct reaction with the water in the basic medium provided by the acetate anions. In a moist solution, however, the already formed adduct can also be hydrolyzed, as shown by the Rogers group [112] and previously also by Kuhn in the 1990s [54]. Later it has been proven by NMR spectroscopy and supported by DFT calculations that in solution these hydrogen carbonates are in equilibrium with the NHC–CO_2 adduct, and the equilibrium is shifted toward the hydrogen carbonate in protic solvents, or by adding a few drops of water [142].

Since the hydrogen carbonate anion is also a strong base, similar to the acetate, it is not surprising that very recently $[C_nC_nIm][HCO_3]$ derivatives have been reported [70, 142] to exhibit carbene-like reactivity, similar to $[C_2C_1Im][OAc]$. Trapping of the carbene from this IL has been performed by CS_2, $[Pd(allyl)Cl]_2$, and $Au(SMe)_2Cl$, yielding the corresponding adducts (Fig. 14). Apart from the trapping reactions, the organocatalytic carbene activity has been shown in benzoin condensation and also in a ring opening polymerization reaction using imidazolium hydrogen carbonate itself (Fig. 15). The similarities between the acetate and hydrogen carbonates show the robustness of NHC-forming ILs, allowing many different anions to obtain NHC chemistry with ILs.

It might be of further interest that by the use of different anions (with different basicity) the carbene concentration (and the catalytic activity) can be influenced in the ILs. In this respect imidazolium-hydroxide (with an apparently highly basic anion) should be mentioned. The synthesis of $[C_4C_1Im][OH]$ has been reported

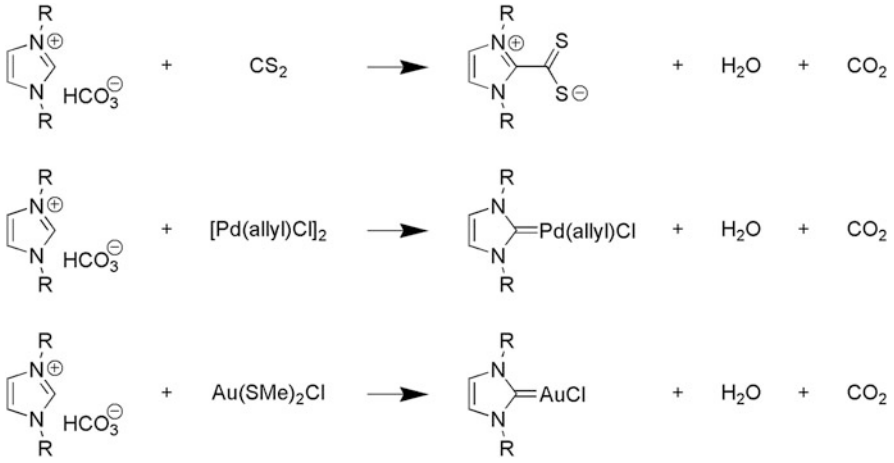

Fig. 14 Trapping reactions performed by 1,3-dialkylimidazolium hydrogen carbonates [142]

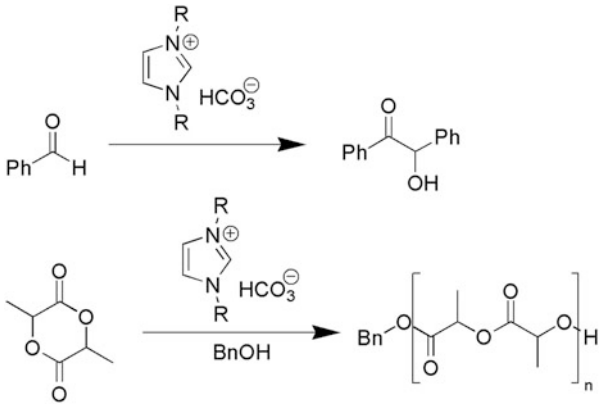

Fig. 15 Reactions catalyzed by 1,3-dialkylimidazolium hydrogen carbonates [70, 142]

together with the corresponding IR and ^{1}H and ^{13}C NMR spectra [98]; however, the viscous oil could not be structurally characterized.[3] It has been reported as an active catalyst in Michael addition [98], aza-Michael addition [144], and Knoevenagel condensation [145] without observation of carbene catalyzed products. The fact that no such product has been obtained could be explained by the fast reaction between aldehydes and active methylene compounds. In contrast to the above results, a successful dechlorination of PVC by $[C_4C_1Im][OH]$ has been reported [146], and the high efficiency of the process has been attributed to the carbene

[3] It should be noted that a 5 % aqueous solution of $[C_4C_1Im][OH]$ has been produced [143], and has been used for the combinatorial synthesis of other ILs.

content of the imidazolium salt, which should apparently be rather high in the presence of the basic hydroxide counteranion [30, 96]. It is worth noting that the substitution of the halogens in CH_2Cl_2 (by $[OAc]^-$) has also been reported in $[C_2C_1Im][OAc]$ [102] in a process, where the involvement of the carbene has not been necessitated, as it has been discussed above. Regarding the reactivity of $[C_4C_1Im][OH]$ it should also be mentioned that, due to the nucleophilic attack of the hydroxide anion at the C2 carbon atom of the imidazolium cation, these compounds are known to be unstable at high hydroxide concentrations [147], while in 0.1 M concentration no decomposition has been observed in the case of 1,3-bis(2,6-diisopropylphenyl)imidazolium hydroxide [96]. Very recently [148] a polymeric benzimidazole-hydroxide has been reported, in which the position 2 of the ring has been shielded by a bulky group. This polymer turned out to be stable and exhibited hydroxide conducting properties. Considering the above discussed differences in reactivity and in light of the possible ring opening decomposition of the imidazolium ring in extremely strong media [147], it seems to be desirable to characterize those ILs, which are reported as imidazolium-hydroxides in more detail.

4 Formation of Other Kinds of Neutral Species from ILs

Although the main aim of the present review is to investigate the possibility of carbene formation in ionic liquids, it is important to note that the formation of other neutral species is also possible from Im-ILs. The first indications came from H/D exchange reactions. As we have already mentioned above, apart from the H/D exchange at position 2 of the imidazolium ring [11], subsequent studies showed the exchange at positions 4 and 5 of the same ring as well [90, 91], and even the proton of the 2-methyl substituent in 1,2,3-trialkylimidazolium salts turned out to be exchangeable in deuterated solvents [149]. The high temperature deprotonation of 1,2,3-trialkylimidazolium salts at montmorillonite surfaces [150], or their irreversible reaction with strong bases like NaH [151], yields alkylidene-imidazoles. This class of compounds (also named recently as "deoxy Breslow intermediate" [152, 153]) exhibit an unusual, polarized electron distribution, resulting in "umpolung," which generally allows unusual chemical reactivity, making this concept highly important in organic chemistry.

We have investigated [42] the possibility of proton transfer in 1,2,3-trialkylimidazolium salts, modeled by 1,2,3-trimethylimidazolium derivatives. The B3LYP/6-31 + G^* deprotonation energies at the position 2 methyl group are only slightly higher than the energy demand for the removal of the position 2 proton in the 1,3-dimethylimidazolium cation at the same level. It is worth noting that the deprotonation energy at the position 4 of the ring (yielding the "abnormal" 1,3-dimethylimidazol-4-ylidene) is 18.1 kcal/mol higher at the same level, although it should be mentioned that in our calculations the isolated gas phase cation has been considered, and thus the relative stabilities of these isomeric structures may be

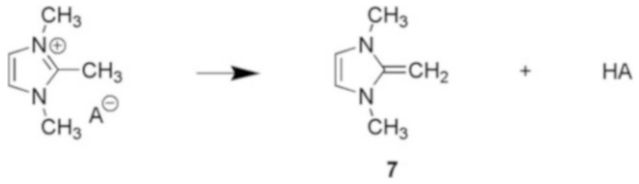

Fig. 16 Proposed proton transfer in 1,2,3-trialkylimidazolium ILs [42]

influenced by the interactions with the IL. It is also important to note that hydrogen bonds have been detected between basic anions (such as acetate) and the methyl hydrogen atoms for the first time, being similar in strength to those in the 1,3-dialkyl species [42].[4] Also, dissociation energies of 1,2,3-trimethylimidazolium ion pairs to 2-alkylideneimidazole 7 (Fig. 16) and the corresponding acid were similar to those for the analogous 1,3-dimethylimidazolium ion pairs [30], suggesting that in the case of basic anions dissociation may occur under high vacuum and low pressures [42], similarly to the above discussed experiments for $[C_2C_1Im][OAc]$ [30]. All this behavior is in accordance with the zwitterionic structure of 2-alkylidene-imidazoles, which has also been shown before [42, 157, 158], and one might surmise that the aromaticity of these two five-membered rings (**1** and **7**) is similar [42]. However, it has been shown that the aromaticity measures of **7** are significantly reduced with respect to **1** [42]; furthermore, the NICS(1) values are close to those of the apparently non-aromatic saturated analogue [159]. In any case, **7** turned out to be a stable complexing agent to form complexes with $SnH_2W(CO)_5$ [160], and with $Au(PPh_3)$ [151]. Likewise, the phosphorus analogue of **7** (note the diagonal relationship between phosphorus and carbon "phosphorus the carbon copy" [161, 162]), was complexed by two BH_3 ligands [163].

For the also N-heterocyclic 1-alkylpyridinium ion pairs the formation of pyridine-2-ylidenes **8**, pyridinium-ylide **9**, and 1,2- or 1,4-dihydropyridine derivatives **10** and **11** has also been investigated (Fig. 17) [42]. The feasibility of the proton transfer is supported by the occurrence of position 2H/D exchange in basic solutions [164], and also by the isolation of **8**′s complexes in the presence of (amine or acetate) bases and transition metals [165–168, 175–178]. NHC **8** – with proper substituents – has also been surmised by theoretical calculations to be stabilizable, and synthesizable [41]. However, the energy demand to deprotonate this cation is significantly larger than for imidazolium salts, and hence generating of pyridine-2-ylidene derivatives is rather difficult [42]. Deprotonation at the N-alkyl group yielding the pyridinium-ylide **9** has been indicated to be more facile [41, 42], and deprotonation energies have been calculated similar to those for imidazolium salts [30, 42], due to the significant conjugative interaction between the forming $-CH_2^-$ moiety and the cationic ring in the zwitterionic product [42]. However,

[4] Interestingly, in previous literature data for the significantly less basic $[Tf_2N]^-$ anion considerable reduction in hydrogen bonding has been observed upon methylation at the position 2 of 1,3-dialkylimidazolium derivatives [154–156].

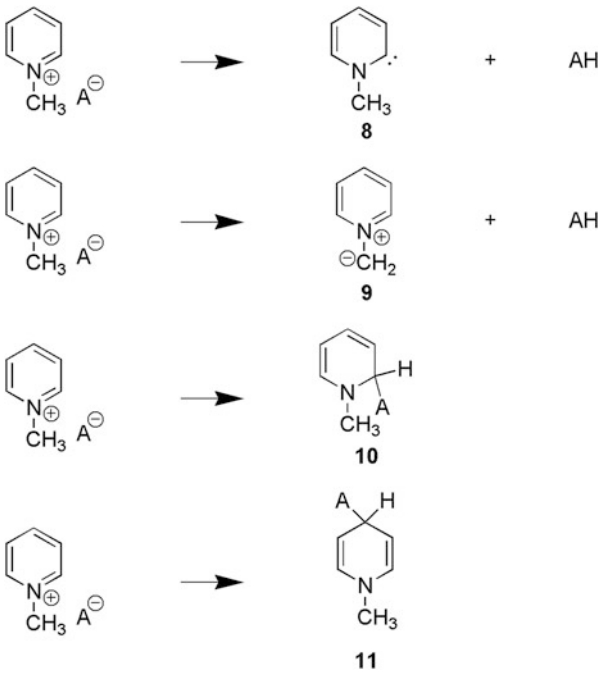

Fig. 17 Possible formation of neutral species from pyridinium-based ILs [42]

dissociation energies of the ion pairs to **9** and the corresponding acid have been found several kcal/mol higher compared to those for the analogous Im-ILs, presumably due to the stronger anion–cation interactions [42]. On the other hand, the higher electrophilicity of the pyridinium ring [169] – which can also be exploited in a number of synthetic approaches (see, e.g., the Chichibabin reaction) and is also of high biochemical importance in metabolic redox systems of the NAD^+ coenzyme [48] – results in very easy access to dihydropyridine derivatives **10** and **11**. Thus, unlike for Im-ILs [41, 42], for pyridinium based ILs possessing basic (and nucleophilic) anions the formation of these neutral species is expected [42].

Although the reactivity of fulvene **7**, ylide **9**, and the dihydropyridine derivatives **10** and **11** is much less explored than that of NHCs, these compounds exhibit unusual electronic distribution, rendering them highly basic and/or redox active. Thus, even if their concentration is small in basic ILs, they might significantly influence the chemical – including physicochemical – behavior of the IL, and therefore their accessibility must be considered in such IL systems. Accordingly, a detailed exploration of their formation and behavior in the IL media has an apparent impact on IL science. Moreover, the comparably high vapor pressure of protic ILs [109], and hence their good distillability, is directly attributed to their access to neutral species, which may also result in interesting applications for the present systems as well, e.g., in separation techniques.

5 Summary

The conclusion of the above described results in literature is that carbenes (and other neutral species) may form in Im-ILs, and therefore these two great fields of chemistry can be directly linked by IL NHC precursors, uniting the advantageous physical properties of ILs, and the chemical versatility of NHCs. Beyond the direct contribution to the advance of basic chemical concepts such as acid–base reactions, we believe that the already published trapping and catalytic reactions will be of direct applications, and may also serve as templates for novel chemistries. Clearly there are some obvious directions in which this field should and will advance. One of the most obvious extensions of $[C_2C_1Im][OAc]$'s applications is to use this IL for other kind of catalyses. According to the versatile chemistry of NHCs, and also the advantageous properties of this IL, this is indeed a promising topic for synthetic approaches. Furthermore, it has to be noted that the basicity of the acetate ions itself can provide considerable chemical activity, such as in the aldol dimerization or in the Claisen condensation, or the very facile halogen substitution reactions. The very recent results in the chemistry of tetraazafulvenes show that these highly redox active compounds can also be formed in the reaction of imidazolium salts with NHCs [170], which are inherently present in basic Im-ILs. A more detailed exploration of this aspect will undoubtedly open new chemistries.

Although only a few Im-ILs are known with basic anions (e.g., $[OAc]^-$, $[HCO_3]^-$, and tartarate [ref]) [179], it can be expected that in the future other anions will also be considered, allowing one to tune the concentration and thus the shifting of selectivities in the many possible reactions. Although – as noted in the introduction of this chapter – Im-ILs are very popular with respect to carbene formation and this type of catalytic activity, changing the cation to thiazolium [62] and triazolium salts – not necessarily as pure ILs, but as additives in Im-ILs – may also have significant potential. Apparently these azolium salts have been shown to have different catalytic properties, allowing one to fine tune chemical reactivities. As has also been mentioned, the position 4 (and 5) hydrogen atoms, and the methyl hydrogens at position 2 of the imidazolium ring, are also non-innocent; therefore they can also be removed by basic anions. Accordingly, the substituents on the ring of the anion may be tuned in order to show some alternative trapping reactions, or even alternative catalytic activity of the resulting "abnormal carbenes" and "deoxy Breslow intermediates." Our groups are continuously working on these topics, and the results are expected to be published throughout the following years.

Acknowledgment Funding from the New Széchenyi Plan TÁMOP-422B10-1-2010-0009 and OTKA K 105417, and financial support for Oldamur Hollóczki by the Alexander von Humboldt-Stiftung is gratefully acknowledged.

References

1. Hallett JP, Welton T (2011) Chem Rev 111:3508–3576
2. Rogers RD, Seddon KR, Volkov S (2002) Green industrial applications of ionic liquids. Kluwer Academic, Dordrecht
3. Wasserscheid P, Welton T (2007) Ionic liquids in synthesis, 2nd edn. Wiley-VCH, Weinheim
4. Díez-González S (2011) N-Heterocyclic carbenes: from laboratory curiosities to efficient synthetic tools. Royal Society of Chemistry, Cambridge
5. Bourissou D, Guerret O, Gabbaï FP, Bertrand G (2000) Chem Rev 100:39–92
6. Arduengo AJ, Bertrand G (2009) Chem Rev 109:3209–3210
7. Hahn FE, Jahnke MC (2008) Angew Chem Int Ed 47:3122–3172
8. Melaimi M, Soleilhavoup M, Bertrand G (2010) Angew Chem Int Ed 49:8810–8849
9. Droge T, Glorius F (2010) Angew Chem Int Ed 49:6940–6952
10. Martin D, Melaimi M, Soleilhavoup M, Bertrand G (2011) Organometallics 30:5304–5313
11. Breslow R (1958) J Am Chem Soc 80:3719–3726
12. Canal JP, Ramnial T, Dickie DA, Clyburne JAC (2006) Chem Commun 42:1809–1818
13. Dupont J, Spencer J (2004) Angew Chem Int Ed 43:5296–5297
14. Chowdhury S, Mohan RS, Scott JL (2007) Tetrahedron 63:2363–2389
15. Aggarwal VK, Emme I, Mereu A (2002) Chem Commun 1612–1613
16. Sowmiah S, Srinivasadesikan V, Tseng M-C, Chu Y-H (2009) Molecules 14:3780–3813
17. Gorodetsky B, Ramnial T, Branda NR, Clyburne JAC (2004) Chem Commun 40:1972–1973
18. Maase H, Massonne K (2005) WO 2,005,019,183
19. Marion N, Díez-González S, Nolan SP (2007) Angew Chem Int Ed 46:2988–3000
20. Enders D, Balensiefer T (2004) Acc Chem Res 37:534–541
21. Enders D, Niemeier O, Henseler A (2007) Chem Rev 107:5606–5655
22. Moore J, Rovis T (2009) Top Curr Chem 291:118–144
23. Cavallo L, Correa A, Costabile C, Jacobsen H (2005) J Organomet Chem 690:5407–5413
24. Arnold PL, Pearson S (2007) Coord Chem Rev 251:596–609
25. Frenking G, Sol M, Vyboishchikov SF (2005) J Organomet Chem 690:6178–6204
26. Diaz-Requejo MM, Perez PJ (2005) J Organomet Chem 690:5441–5450
27. Crabtree RH (2005) J Organomet Chem 690:5451–5457
28. Díez-González S, Marion N, Nolan SP (2009) Chem Rev 109:3612–3676
29. Schuster O, Yang L, Raubenheimer HG, Albrecht M (2009) Chem Rev 109:3445–3478
30. Hollóczki O, Gerhard D, Massone K, Szarvas L, Németh B, Veszprémi T, Nyulászi L (2010) New J Chem 34:3004–3009
31. Vignolle J, Cattoen X, Bourissou D (2009) Chem Rev 109:3333–3384
32. Yamaguchi Y, Sherrill CD, Schaefer HF (1996) J Phys Chem 100:7911–7918
33. Gronert S, Keeffe JR, O'Ferrall RAM (2011) J Am Chem Soc 133:3381–3389
34. Gronert S, Keeffe JR, O'Ferrall RAM (2011) J Am Chem Soc 133:11817–11818
35. Forró A, Veszprémi T, Nyulászi L (2000) Phys Chem Chem Phys 2:3127–3129
36. Hollóczki O, Kelemen Z, Nyulászi L (2012) J Org Chem 77:6014–6022
37. Arduengo AJ, Harlow RL, Kline M (1991) J Am Chem Soc 113:361–363
38. Boehme C, Frenking G (1996) J Am Chem Soc 118:2039–2046
39. Heinemann C, Muller T, Apeloig Y, Schwartz H (1996) J Am Chem Soc 118:2023–2038
40. Schleyer PvR, Pühlhofer F (2002) Org Lett 4:2873–2876
41. Hollóczki O, Nyulászi L (2008) J Org Chem 73:4794–4799
42. Hollóczki O, Nyulászi L (2011) Org Biomol Chem 9:2634–2640
43. Enders D, Breuer K, Raabe G, Runsink J, Teles H, Melder J-P, Ebel K, Brode S (1995) Angew Chem Int Ed 34:1021–1023
44. Arduengo AJI, Goerlich JR, Marshall WJ (1997) Liebigs Annalen 1997:365–374
45. Martin D, Soleilhavoup M, Bertrand G (2011) Chem Sci 2:389–399
46. Chiang P-C, Bode JW (2012) Science of synthesis: asymmetric organocatalysis, vol 1. Georg Thieme, Stuttgart

47. Kluger R, Tittmann K (2008) Chem Rev 108:1799–1833
48. Berg JM, Tymoczko J, Stryer L (2012) Biochemistry, 7th edn. Freedman, New York
49. Scheer M, Balázs G, Seitz A (2010) Chem Rev 110:4236–4256
50. Masuda JD, Schoeller WW, Donnadieu B, Bertrand G (2007) Angew Chem Int Ed 46:7052–7055
51. Frey GD, Lavallo V, Donnadieu B, Schoeller WW, Bertrand G (2007) Science 316:439–441
52. Runyon JW, Steinhof O, Rasika Dias HV, Calabrese JC, Marshall WJ, Arduengo AJI (2011) Aust J Chem 64:1165–1172
53. Park S-W, Chun Y, Cho SJ, Lee S, Kim KS (2012) J Chem Theory Comput 8:1983–1988
54. Kuhn N, Steinmann M, Weyers G, Henkel GZ (1999) Naturforsch 54B:427–433
55. Delaude L (2009) Eur J Inorg Chem 1681–1699
56. Tommasi I, Sorrentino F (2006) Tetrahedron Lett 47:6453–6456
57. Wang Y, Robinson GH (2012) Dalton Trans 41:337–345
58. Wang Y, Robinson GH (2011) Inorg Chem 50:12326–12337
59. Dyker CA, Bertrand G (2008) Science 321:1050–1051
60. Xu L-W, Gao Y, Yin J-J, Li L, Xia C-G (2005) Tetrahedron Lett 46:5317–5320
61. Estanger J, Leveque J-M, Turgis R, Draye M (2007) Tetrahedron Lett 48:755–759
62. Davis JHJ, Forrester KJ (1999) Tetrahedron Lett 40:1621–1622
63. Nyce GW, Glauser T, Connor EF, Möck A, Waymouth RM, Hedrick JL (2003) J Am Chem Soc 125:3046–3056
64. Feroci M, Chiarotto I, Orsini M, Inesi A (2010) Chem Commun 46:4121
65. Orsini M, Chiarotto I, Elinson MN, Sotgiu G, Inesi A (2009) Electrochem Commun 11:1013
66. Feroci M, Chiarotto I, Orsini M, Sotgiu G, Inesi A (2008) Adv Synth Catal 350:1355
67. Holbrey JD, Reichert WM, Tkatchenko I, Bouajila E, Walter O, Tommasi I, Rogers RD (2003) Chem Commun 28–29
68. Voutchkova AM, Feliz M, Clot E, Eisenstein O, Crabtree RH (2007) J Am Chem Soc 129:12834–12846
69. Voutchkova AM, Appelhans LN, Chianese AR, Crabtree RH (2005) J Am Chem Soc 127:17624–17625
70. Fevre M, Coupillaud P, Miqueu K, Sotiropoulos J-M, Vignolle J, Taton D (2012) J Org Chem 77:10135–10144
71. Ogata K, Yamaguchi Y, Kashiwabara T, Ito T (2005) J Organomet Chem 690:5701–5709
72. Bonette F, Kato T, Destarac M, Mignani G, Cossío FP, Baceiredo A (2007) Angew Chem Int Ed 46:8632–8635
73. Hollóczki O, Nyulászi L (2009) Organometallics 28:4159–4164
74. Ghadwal RS, Sen SS, Roesky HW, Tavcar G, Merkel S, Stalke D (2009) Organometallics 28:6374–6377
75. Böttcher T, Bassil BS, Zhechkov L, Heine T, Röschenthaler G-V (2013) Chem Sci 4:77–83
76. Canac Y, Maaliki C, Abdellahab I, Chauvin R (2012) New J Chem 36:17–27
77. Kuhn N, Kratz T, Blaser D, Boese R (1995) Chem Ber 128:245–250
78. Weidner T, Baio JE, Mundstock A, Große C, Karthäuser S, Bruhn U, Siemeling C (2011) Aust J Chem 64:1177–1179
79. Chen H, Justes DR, Cooks RG (2005) Org Lett 7:3949–3952
80. Graham DC, Cavell KJ, Yates BF (2005) J Phys Org Chem 18:298–309
81. Magill A, Cavell KJ, Yates BF (2004) J Am Chem Soc 126:8717–8724
82. Sauers RR (1996) Tetrahedron Lett 37:149–152
83. Kim Y-J, Streitweiser A (2002) J Am Chem Soc 124:5757–5761
84. Amyes TL, Diver ST, Richard JP, Rivas FM, Tóth K (2004) J Am Chem Soc 126:4366–4374
85. Chu Y, Deng H, Cheng J-P (2007) J Org Chem 72:7790–7793
86. Alder RW, Allen PR, Williams SJ (1995) J Chem Soc Chem Commun 1267–1268
87. Bordwell FG (1988) Acc Chem Res 21:456–463
88. Song Z, Wang H, Xing L (2009) J Solut Chem 38:1139–1154
89. Turner EA, Pye CC, Singer RD (2003) J Phys Chem A 107:2277–2288

90. Haake P, Bausher LP, McNeal JP (1971) J Am Chem Soc 93:7045–7049
91. Giernoth R, Bankmann D (2006) Tetrahedron Lett 47:4293–4296
92. Wang Y, Xie Y, Abraham MY, Wei P, Schaefer HF III, Schleyer PvR, Robinson GH (2010) J Am Chem Soc 132:14370–14372
93. Aldeco-Perez E, Rosenthal AJ, Donnadieu B, Parameswaran P, Frenking G, Bertrand G (2009) Science 326:556–559
94. Arduengo AJI, Gamper SF, Tamm M, Calabrese JC, Davidson F, Craig HA (1995) J Am Chem Soc 117:572–573
95. Leites LA, Magdanurov GI, Bukalov SS, West R (2008) Mendeleev Commun 18:14–15
96. Hollóczki O, Terleczky P, Szieberth D, Mourgas G, Gudat D, Nyulászi L (2011) J Am Chem Soc 133:780–789
97. Denk KD, Rodezno JM, Gupta S, Lough A (2001) J Organomet Chem 617–618:242–253
98. Ranu BC, Banerjee S (2005) Org Lett 7:3049–3052
99. Cowan J, Clyburne JAC, Davidson MG, Harris RLW, Howard JAK, Küpper P, Leech MA, Richards SP (2002) Angew Chem Int Ed 41:1432–1434
100. Diedenhofen M, Klamt A, Marsh K, Schäfer A (2007) Phys Chem Chem Phys 9:4653–4656
101. MacFarlane DR, Pringle JM, Johansson KM, Forsyth SA, Forsyth M (2006) Chem Commun 42:1905–1917
102. Zhao B, Greiner L, Leitnerac W (2011) Chem Commun 47:2973–2975
103. Sun N, Maxim ML, Metlen A, Rogers RD (2011) ChemSusChem 4:65–73
104. Dhumal NR, Kim HJ, Kiefer J (2009) J Phys Chem A 113:10397–10404
105. Earle MJ, Esperanca JMSS, Gilea MA, Lopes JNC, Rebelo LPN, Magee JW, Seddon KR (2006) Nature 439:831–834
106. Strasser D, Goulay F, Kelkar MS, Maginn EJ, Leone SR (2007) J Phys Chem A 111:3191–3195
107. Leal JP, Esperanca JMSS, Minas da Piedade ME, Lopes JNC, Rebelo LPN, Seddon KR (2007) J Phys Chem A 111:6176–6182
108. Armstrong JP, Hurst C, Jones RG, Licence P, Lovelock KRJ, Satterly CJ, Villar-Garcia IJ (2007) Phys Chem Chem Phys 9:982–990
109. Greaves TL, Drummond CJ (2008) Chem Rev 108:206–237
110. Lui MY, Crowhurst L, Hallett JP, Hunt PA, Niedermeyer H, Welton T (2011) Chem Sci 2:1491–1496
111. Hallett JP, Liotta CL, Ranieri G, Welton T (2009) J Org Chem 74:1864–1868
112. Gurau G, Rodrguez H, Kelley SP, Janiczek P, Kalb RS, Rogers RD (2011) Angew Chem Int Ed 50:12024–12026
113. Brehm M, Weber H, Pensado AS, Stark A, Kirchner B (2012) Phys Chem Chem Phys 14:5030–5044
114. Yoshizawa-Fujita M, Johansson K, Newmann P, MacFarlane DR, Forsyth M (2006) Tetrahedron Lett 47:2755–2758
115. Jin C-M, Twamley B, Shreeve JM (2005) Organometallics 24:3020–3024
116. Rodriguez H, Gurau G, Holbrey JD, Rogers RD (2011) Chem Commun 47:3222–3224
117. Treble RG, Johnson KE, Tosh E (2006) Can J Chem 84:915–924
118. Jonansson KM, Izgorodina EI, MacFarlane DR, Seddon KR (2008) Phys Chem Chem Phys 10:2972–2978
119. Kelemen Z, Hollóczki O, Nagy J, Nyulászi L (2011) Org Biomol Chem 9:5362–5364
120. Gu L, Zhang Y (2010) J Am Chem Soc 132:914–915
121. Nair V, Varghese V, Paul RR, Jose A, Sinu CR, Menon RS (2010) Org Lett 12:2653–2655
122. Chiang P-C, Bode JW (2011) Org Lett 13:2422–2425
123. Park JH, Bhilare SV, Youn SW (2011) Org Lett 13:2228–2231
124. Maji B, Vedachalan S, Ge X, Cai S, Liu X-W (2011) J Org Chem 76:3016–3023
125. Chan A, Scheidt KA (2006) J Am Chem Soc 128:4558–4559
126. Liu D, Zhang Y, Chen EY-X (2012) Green Chem 14:2738–2746
127. Zhao H, Holladay JE, Brown H, Zhang ZC (2007) Science 316:1597–1600

128. Anderson JL, Dixon JK, Brennecke JF (2007) Acc Chem Res 40:1208–1216
129. Cadena C, Anthony JL, Shah JK, Morrow TI, Brennecke JF, Maginn EJ (2004) J Am Chem Soc 126:5300–5308
130. Jutz F, Anderson J-M, Baiker A (2011) Chem Rev 111:322–353
131. Brennecke JF, Gurkan BE (2010) J Phys Chem Lett 1:3459–3464
132. Hollóczki O, Kelemen Z, Könczöl L, Szieberth D, Nyulászi L, Stark A, Kirchner B (2012) ChemPhysChem. doi:10.1002/cphc.201200970
133. Shiflett MB, Yokozeki A (2009) J Chem Eng Data 54:108–114
134. Barrosse-Antle LE, Compton RG (2009) Chem Commun 3744–3746
135. Duong HA, Tekavec TN, Aarif AM, Louie J (2004) Chem Commun 40:112–113
136. Van Ausdall BR, Glass JL, Wiggins KM, Aarif AM, Louie J (2009) J Org Chem 74:7935–7942
137. Wang C, Luo H, Luo X, Li H, Dai S (2010) Green Chem 12:2019–2023
138. Shiflett MB, Elliott BA, Lustig SR, Sabesan S, Kelkar MS, Yokozeki A (2012) Chemphyschem 13:1806–1817
139. Besnard M, Cabaco MI, Chávez FV, Pinaud N, Sebastiao PJ, Coutinho JAP, Mascetti J, Danten Y (2012) J Phys Chem A 116:4890–4901
140. Cabaco MI, Besnard M, Danten Y, Coutinho JAP (2012) J Phys Chem A 116:1605–1620
141. Besnard M, Cabaco MI, Chávez FV, Pinaud N, Sebastiao PJ, Coutinho JAP, Danten Y (2012) Chem Commun 48:1245–1247
142. Fevre M, Pinaud J, Leteneur A, Gnanou Y, Vignolle J, Taton D (2012) J Am Chem Soc 134:6776–6784
143. Himmler S, König A, Wasserscheid P (2007) Green Chem 9:935–942
144. Xu J-M, Wu Q, Zhang Q-Y, Zhang F (2007) Eur J Org Chem 1798–1802
145. Ranu BC, Jana R (2006) Eur J Org Chem 3767–3770
146. He X-L, Zhou Q, Li X-Y, van Kasteren JMN, Wang Y-Z (2012) Polym Degr Stab 97:145–148
147. Duclos JM, Haake P (1974) Biochemistry 13:5358–5362
148. Thomas OD, Soo KJWY, Peckham TJ, Kulkarni MP, Holdcroft S (2012) J Am Chem Soc 134:10753–10756
149. Handy ST, Okello M (2005) J Org Chem 70:1915–1918
150. Awad WH, Gilman JW, Nyden M Jr, Harris RH, Sutto TE, Callahan J, Trulove PC, DeLong HC, Fox DM (2004) Thermochim Acta 409:3–11
151. Fürstner A, Alcarazo M, Goddard R, Lehmann CW (2008) Angew Chem Int Ed 47:3210–3214
152. Biju AT, Padmanaban M, Wurz NE, Glorius F (2011) Angew Chem Int Ed 50:8412–8415
153. Knappke CEI, Arduengo AJ III, Jiao H, Neudcrfl J-M, von Wangelin AJ (2011) Synthesis 3784–3795
154. Peppel T, Roth C, Fumino K, Paschek D, Köckerling M, Ludwig R (2011) Angew Chem Int Ed 50:6661–6665
155. Wulf A, Fumino K, Ludwig R (2010) Angew Chem Int Ed 49:449–453
156. Fumino K, Peppel T, Geppert-Rybczyńska M, Zaitsau DH, Lehmann JK, Verevkin SP, Köckerling M, Ludwig R (2011) Phys Chem Chem Phys 13:14064–14075
157. Frison G, Sevin A (2002) J Chem Soc Perkin Trans 2:1692
158. Benassi R, Bertrarini C, Kleinpeter E, Taddei F (2000) J Mol Struct Theochem 498:217
159. Maji B, Horn M, Mayr H (2012) Angew Chem Int Ed 51:6231–6235
160. Al-Rafia MI, Malcolm AC, Liew SK, Ferguson MJ, McDonald R, Rivard E (2011) Chem Commun 47:6987–6989
161. Nyulászi L, Veszprémi T, Réffy JJ (1993) J Phys Chem 97:4011–4015
162. Mathey F, Nixon JF, Dillon K (1998) Phosphorus: the carbon copy. Wiley, New York
163. Arduengo AJ III, Carmalt CJ, Clyburne JAC, Cowley AH, Pyati R (1997) Chem Commun 981–982

164. Zoltewich JA, Helmick LS (1970) J Am Chem Soc 92:7547–7552
165. Owen JS, Labinger JA, Bercaw JE (2004) J Am Chem Soc 126:8247–8255
166. Piro NA, Owen JS, Bercaw JE (2004) Polyhedron 23:2797–2804
167. Alvarez E, Conejero S, Paneque M, Petronilho A, Poveda ML, Serrano O, Carmona E (2006) J Am Chem Soc 128:13060–13061
168. Kunz D (2007) Angew Chem Int Ed 46:3405–3408
169. Katritzky A (1997) Comprehensive heterocyclic chemistry 2, vol 5. Elsevier, Oxford
170. Jolly PI, Zhou S, Thomson DW, Garnier J, Parkinson JA, Tuttle T, Murphy JA (2012) Chem Sci 3:1675–1679
171. Grundemann S, Kovacevic A, Albrecht M, Faller JW, Crabtree RH (2001) Chem Commun 2274
172. Grundmann S, Kovacevic A, Albrecht M, Faller JW, Crabtree RH (2002) J Am Chem Soc 124:10473
173. Yuen AKL, Masters AF, Maschmeyer T (2013) Catal Today 200:9–16
174. Yu Y, Hua L, Zhu W, Shi Y, Cao T, Qiao Y, Hou Z (2013) Synth Commun 43:1287–1298
175. Quast H, Frankenfeld E (1965) Angew Chem Int Ed 4:691
176. Quast H, Schmitt E (1970) Liebigs Ann Chem 732:43–63
177. Quast E, Gelléri A (1975) Liebigs Ann Chem: 929–938
178. Quast E, Gelléri A (1975) Liebigs Ann Chem: 939–945
179. Rouch A, Castellan T, Fabing I, Saffon N, Rodrigez J, Constantieux T, Plaquevent JC, Génisson Y (2013) RSC Advances 3:413

Top Curr Chem (2014) 351: 25–102
DOI: 10.1007/128_2011_309

Published online: 6 March 2013

QM/MM Investigations Of Organic Chemistry Oriented Questions

Thomas C. Schmidt, Alexander Paasche, Christoph Grebner, Kay Ansorg, Johannes Becker, Wook Lee, and Bernd Engels

Abstract About 35 years after its first suggestion, QM/MM became the standard theoretical approach to investigate enzymatic structures and processes. The success is due to the ability of QM/MM to provide an accurate atomistic picture of enzymes and related processes. This picture can even be turned into a movie if nuclei-dynamics is taken into account to describe enzymatic processes. In the field of organic chemistry, QM/MM methods are used to a much lesser extent although almost all relevant processes happen in condensed matter or are influenced by complicated interactions between substrate and catalyst. There is less importance for theoretical organic chemistry since the influence of nonpolar solvents is rather weak and the effect of polar solvents can often be accurately described by continuum approaches. Catalytic processes (homogeneous and heterogeneous) can often be reduced to truncated model systems, which are so small that pure quantum-mechanical approaches can be employed. However, since QM/MM becomes more and more efficient due to the success in software and hardware developments, it is more and more used in theoretical organic chemistry to study effects which result from the molecular nature of the environment. It is shown by many examples discussed in this review that the influence can be tremendous, even for nonpolar reactions. The importance of environmental effects in theoretical spectroscopy was already known. Due to its benefits, QM/MM can be expected to experience ongoing growth for the next decade.

In the present chapter we give an overview of QM/MM developments and their importance in theoretical organic chemistry, and review applications which give impressions of the possibilities and the importance of the relevant effects. Since there is already a bunch of excellent reviews dealing with QM/MM, we will discuss

T.C. Schmidt, A. Paasche, C. Grebner, K. Ansorg, J. Becker, W. Lee, and B. Engels (✉)
Institut für Phys. und Theor. Chemie, Emil-Fischer-Strasse 42, Campus Hubland Nord, 97074 Würzburg, Germany
e-mail: bernd.engels@mail.uni-wuerzburg.de

fundamental ingredients and developments of QM/MM very briefly with a focus on very recent progress. For the applications we follow a similar strategy.

Keywords Application · Conformational search · Developments · EPR · Force fields · Hybrid approaches · NMR · Organic semiconductors · QM/MM · Reaction mechanism · Reaction pathways · Review · Solvent effects · Solvent shells · Spectroscopy · Theoretical organic chemistry · UV/Vis · VUV

Contents

1 Introduction

The QM/MM ansatz uses quantum chemical (QM) approaches for the description of the important part of a system while less expensive molecular mechanic (MM) methods are employed to account for the environmental influence of the rest of the system. For an enzymatic reaction, for example, a QM approach is used to describe a chemical reaction taking place in the active site while the impact of the enzyme environment on this reaction is taken into account by an appropriate force field. This division makes it possible to describe the process under investigation with very expensive but at the same time very accurate QM approaches without neglecting the influence of the rest of the system. Furthermore, QM/MM accounts for the molecular nature of the environment, hence it is more reliable than pure QM approaches which ignore the influence of the surroundings completely or mimic them by continuum approaches [1–3]. A recent comparison between both approaches was provided by Ryde and coworkers [4]. For proton-transfer reactions they showed that relative energies can still vary considerably for quite large QM systems. An important precondition for QM/MM approaches is of course that all parts are carefully chosen and the corresponding interfaces do not introduce artificial errors.

Due to its advantages, QM/MM is widely used to study biological and biochemical questions at an atomistic resolution. The first QM/MM approach was suggested

by Warshel and Levitt back in 1976 [5]. Their suggestion already contained many features of the present approaches. It was a visionary ansatz, but the time was not yet ripe. The formulation of Field, Bash and Karplus [6], who combined semi-empirical QM methods with the CHARMM force field [7], led to the first breakthrough of this method. Since then the relevance of QM/MM approaches has steadily increased. For 2000 the key word "QM/MM" gives 82 hits in the ISI web of knowledge [8]. For 2010, 310 hits are already found.

QM/MM has been established as the method of choice for biochemical investigations with atomistic resolution and it is also used in many other areas, e.g. solid state physics, hetero- and homogeneous catalysis, the description of reactions in solvents or medicinal chemistry. The development of QM/MM approaches together with applications from various fields, e.g. biochemical [9–36], solid state and material systems [37–45], chemical reactions in condensed phase [10, 34, 46–49] or photochemistry [50–53] with explicit solvent, homogeneous catalysis and asymmetric synthesis [37, 54–56], as well as medicinal chemistry [57] are well documented. So the question arises – why do we present just another review? The answer is twofold. Firstly, despite all the success the method is still rapidly developing and improving [33, 34, 36, 44, 46, 47, 50, 58–60]. Secondly, while many reviews focus on applications in biological or biochemical areas only a few concentrate on applications in organic chemistry which is the focus of the present review. The review is organized as follows. In Sect. 2 we describe methodological features of the QM/MM approach. However, since so many excellent reviews already discuss the various aspects [34, 49, 59, 61, 62] we will only briefly summarize the main aspects and concentrate on some recent developments. In the subsequent sections we will highlight some recent examples in which questions related to organic chemistry are investigated with QM/MM approaches.

2 Fundamentals of the QM/MM Approach

In QM/MM the whole system is divided into a smaller QM and a larger MM part. The QM part comprises the most important part of the system while the MM part includes the rest of the system. The accuracy of a given QM/MM computation depends on the accuracy of the employed QM and molecular mechanical methods, the interface between both and the covering of the phase space. Additionally, although quite large systems can be handled with QM/MM, an underlying realistic model is still essential. This includes reliable information about the geometrical structure of the system. To describe biological systems, for example, reliable structural data about the involved enzyme are necessary [5, 6, 34, 60]. They are usually taken from X-ray data which in most cases do not provide information about the position of hydrogen atoms. Hence, the protonation state of amino acids has to be carefully defined. In some cases NMR-data is used to build up the initial guess [32, 63], but its resolution is often even lower.

The way of dividing the complete system into QM and MM parts is important for the accuracy of the computations. For enzymatic reactions the parts of the active site directly involved in the reaction have to be known in advance, and even the possible participation of solvent molecules has to be considered [9, 11–32, 34, 60–62]. Similar considerations are also important for organic reactions in solution [9, 10, 46–49] or investigations about catalytic processes [37, 39, 54–56]. To describe an organic reaction which takes place in solution the QM part would in general consist of the reacting molecules while the influence of solvent molecules is taken into account by MM approaches. But if solvent molecules take part in the reaction actively, they have to be included in the QM part. One would assume that the accuracy of the QM/MM computation increases if the QM part is enlarged. However, this is not always the case, since some interactions are better described by force field approaches than by a given QM approach [4, 60, 61, 64]. One example is dispersion interactions, which are not accounted for by conventional DFT-functionals like B3LYP whereas they are implicitly included in the parameter set of common force field approaches.

2.1 QM Approaches Used in QM/MM Applications

For the selection of the QM method within QM/MM one can use the same criteria as for pure QM calculations. Nevertheless, one should take into account that QM/MM computations for large systems possess considerably more error sources than pure QM computations for small molecules. So, the accuracy of a high-end QM approach may be spoiled by less accurate force fields or problems in the preparation of the system or even other problems. For the electrostatic embedding scheme (see below) it is additionally necessary that the chosen QM method can treat the influence of an external point-charge field in an efficient way. Many investigations are performed with density-functional theory (DFT) [65–68] approaches since they possess a very favourable cost-benefit ratio. More accurate descriptions of ground state properties are obtained with wave-function based electron-correlation methods such as Møller–Plesset perturbation theory (e.g. up to second order [MP2]) or coupled-cluster (CC) theory with increasing accuracy [CCSD, CCSD (T)] [65, 66, 69, 70]. Linear scaling local correlation methods also allow the use of such methods for QM/MM investigations since they are able to treat QM parts containing several tens of atoms [71–74]. Such methods were used by Thiel, Werner, Mulholland and coworkers to benchmark the accuracy of the QM/MM description of enzymatic reactions [75–77]. They used the LCCSD(T0) method in combination with augmented triple-zeta basis sets to predict the reaction barriers of the hydroxylation reaction catalyzed by para-hydroxybenzoate hydroxylase (PHBH) and the Claisen rearrangement in the chorismate mutase (CM). The computed activation enthalpies deviate only about 1 kcal/mol from their experimental counterpart. Using low-level QM/MM approaches to estimate activation free energies by umbrella sampling [78, 79] for CM [80] or thermodynamic integration for PHBH

[81], similar deviations were found. It should be noted that in these cases the barrier height did not depend on the size of the QM region [75]. But it was necessary to take several reaction pathways into account. The geometries along these pathways were determined by B3LYP/aug-cc-pVTZ level of theory. LCCSD(T0) computations are still quite expensive. Using the considerably cheaper B3LYP/aug-cc-pVTZ level of theory the predicted activation enthalpies deviated about 2–4 kcal/mol from their experimental counterparts. The LMP2 method performed slightly better (2–3 kcal/mol).

Coupled cluster approaches are a good choice for closed shell systems possessing a large HOMO–LUMO gap [65, 66, 70]. However, they are less suited for open shell systems or molecules with a small energy difference between HOMO and LUMO. In such systems multi-reference (MR) approaches are often mandatory [69, 70]. Examples are radicals [66, 70, 82–85], biradicals [86–93] or transition metal complexes [60, 67, 94]. In the latter, an accurate description of the spin-state energetics is rather difficult. A review about recent multi-reference based investigations of heme-related systems was presented by Shaik, Thiel and coworker [35, 94]. Such systems were also investigated by Scherlis et al. [95, 96]. They used GGA (generalized-gradient approximation) functionals in combination with a self-consistent [97, 98] Hubbard-U-corrected electron–electron interaction term. As also shown in other applications, this correction considerably improves the description of the spin-state energetics of transition metal compounds [35, 94, 99]. This approach was also used in combination with Car–Parinello dynamics [100].

Multi-reference effects are also important to describe excited state processes [50, 51, 53, 101–103]. To describe, for example, photochemical processes, Robb and coworkers use CASSCF or related MR-approaches for the reliable descriptions of conical intersections [50]. But in most investigations less elaborate methods are used. For computations of spectral data, for example, TD-DFT [67, 104] is often chosen due to its high cost-benefit ratio although such approaches cannot yet describe excited state potential energy surfaces (PESs) in general [105]. Investigations of the accuracy of TD-DFT within QM/MM approaches have been carried out by some groups [106–109]. For zinc porphyrin in aqueous solution Govind et al. investigated the accuracy of long range-corrected functionals in comparison to high-level CC methods. For CAM-B3LYP [110, 111] and CAM-PBE0 [112] the results are in excellent agreement with the CR-EOM CCSD(T) results [113] if the asymptotic falloff is 1/r, and for approximations with an asymptotic falloff of 0.65/r only reasonable agreement is obtained. The uncorrected basis functionals B3LYP and PBE0 fail to describe the correct spectrum due to the well-known shortcomings of such functionals within the description of CT states [105, 114, 115]. Applications of Car–Parrinello simulations for excited states performed with the combination of QM/MM and TD-DFT are reviewed by Moret et al. [116]. The restricted open-shell Kohn–Sham (ROKS) represents another approach which is often used to describe excited-state dynamics [117–119]. This approach was also used in combination with Car–Parinello dynamics [100, 119–121].

The *ab initio* multiple spawning (AIMS) method is a time-dependent formulation of quantum chemistry which has been developed to carry out first principles

simulations of chemical reaction dynamics [103, 122, 123]. This approach includes quantum mechanical effects in nuclear dynamics, especially nonadiabatic effects which are crucial in modeling dynamics on coupled electronic PESs. This allows one to describe population transfers between two electronic states through conical intersections [124, 125] which are known to play a major role in nonradiative decay from excited electronic states [126–129]. It develops the nuclear wave function in a semilocal basis set of complex frozen Gaussians [130] to circumvent the problem that the solution of the nuclear Schrödinger equation needs information from the entire potential energy surface (PES). The basis functions have a position–momentum uncertainty as required by Heisenberg's uncertainty principle. The time-evolution of the wave packets is described by time-dependent complex coefficients of the basis functions. The centres of the basis functions move along classical trajectories. Quantum effects such as tunneling and electronic curve crossing are enabled through the use of an adaptive basis set expansion technique ("spawning"). An overview of the method used in combination with QM/MM PESs was presented by Virshup et al. [131]. More details about the method can be taken from the literature [101, 103, 122, 123, 132, 133]. Another approach for the description of conical intersections was provided by Robb and coworker [134, 135]. They also compared RASSCF, TD-DFT and MMVB results for the photophysics of the perylene radical cation [136].

The accuracies of QM/MM investigations depend on so many different ingredients that less accurate QM methods do not necessarily lower the overall reliability. Traditionally semi-empirical QM methods like MNDO [137, 138], AM1 [139], PM3 [140–142], to name but a few, have been most popular and they are still used very often especially for QM/MM molecular dynamics. Examples of new semi-empirical approaches are the DFT-inspired SCC-DFTB [143, 144] (self-consistent-charge density-functional tight-binding), the new pairwise distance directed Gaussian function (PDDG) ansatz developed by Jorgenson and coworker [46, 145] and the new OM-x approaches offered by Thiel and coworker [146–148]. Jorgenson and coworker also developed a new method which reintroduces the overlap matrix into MNDO [149]. The RM1 model is generally a copy of AM1's treatments in formulas, but chooses larger training sets and re-parametrizes more carefully [150]. The $RM1_{BH}$ modification which uses more Gaussian functions to improve the core repulsion function was developed for hydrogen-bonded systems [151]. The PM6 approach which stands in the continuity of PM3 [140–142] was proposed recently [152, 153].

A validation of the SCC-DFTB for reaction energies, vibrational frequencies and geometry parameter shows a mean absolute deviation vs. the G2 reference of 4.3 kcal/mol [154]. The corresponding value for the vibrational frequencies amounts to 75 cm^{-1} in comparison to BLYP/cc-pVTZ [154]. One critical problem of the SCC-DFTB method is its significant inaccuracy in describing proton affinity, especially in the case when highly charged anionic species are involved. For instance, the deprotonation energy of an isolated water molecule calculated by the SCC-DFTB method gives an error of around 40 kcal/mol compared to higher level of theory [143]. This is due to its dependency on the chemical hardness

(Hubbard parameter) evaluated for neutral atoms. However, this can be remedied by third order correction [155], which is simply the addition of one extra parameter per element. With this correction, the error mentioned above can be reduced to a few kcal/mol. Some recent developments in SCC-DFTB based QM/MM approaches were presented by Cui and coworker [156–158]. A comparison of SCC-DFTB and some NDDO-based semiempirical MO-approaches was performed by Jorgensen and coworker [159]. For enthalpy changes of 34 isomerizations of neutral molecules the computed mean absolute errors (MAEs) were 2.7, 3.2, 5.0, 5.1 and 7.2 kcal/mol from PDDG/PM3, B3LYP/6-31(d), PM3, SCC-DFTB and AM1, respectively. The computed heats of formation for 622 neutral, closed-shell molecules containing H, C, N and O atoms gave MAEs of 3.2, 4.4, 5.8 and 6.8 kcal/mol for PDDG/PM3, PM3, SCC-DFTB and AM1, respectively. A similar study (SCC-DFTB, MNDO, AM1 and OM2) was provided by Otte et al. who came to similar conclusions [160]. More details about the accuracy of the PDDG approaches can be taken from a review provided by Acevedo and Jorgensen [46]. Silva-Junior and Thiel [148] showed that OM-x approaches are also well suited for the description of electronically excited states. For 104 molecules the MAEs for vertical excitation energies were 1.35, 1.19, 1.41, 0.51, 0.51, 0.45, 0.50 and 0.45 for MNDO, AM1, PM3, OM1, OM2, OM3, INDO/S and INDO/S2, respectively. The accuracy of new semi-empirical approaches for hydrogen bonding was also investigated [151, 161].

Standard semi-empirical molecular orbital (MO) methods have significant shortcomings for carbohydrates, but reparametrized variants have been developed, which give better descriptions of their conformations. One example is the PM3CARB-1 approach which was developed by McNamara et al. [162]. A comparison to PM3CARB-1 and SCC-DFTB-D is given by Satelle and Almond [163]. Due to their advantageous cost-benefit ratio all of these methods are increasingly applied in QM/MM studies of ground and electronically excited states.

Most descriptions of the QM part rely on MO theories. Valence Bond (VB) approaches remain an important conceptual tool for chemists since the VB structures resemble the Lewis structures usually used by chemists [164–168]. For QM/MM applications this advantage was exploited by Warshel and coworkers [169, 170]. They developed the empirical valence-bond (EVB) method which is often used in QM/MM investigations involving biochemical [171–173] and catalytic topics [37, 39]. This method describes the reactive part of the system by interacting diabatic (resonance) states. The states are represented by simple empirical potential terms which incorporate the interaction of the charges with the environment. After a calibration with the help of experimental or ab initio data these curves are used to evaluate the free energy profile of the EVB surface by free energy perturbation (FEP) calculations [78, 174]. Then the free energy is calculated by moving back from the EVB to the *ab initio* surface. More information about the various approaches in VB can be taken from the literature [164, 175].

Valence-bond ideas are also employed within the molecular mechanics valence bond (MMVB) approach [50, 51, 53, 134, 135, 176–180]. It was originally developed to mimic CASSCF calculations for ground and excited states of conjugated

hydrocarbons. The MMVB approach is based on the idea that any CASSCF wave function can be transformed into a VB wave function via construction of an effective Heisenberg Hamiltonian [179, 181–184]. However, since geometries and calculated relative energies are surprisingly good [176] the method is now used with great success to describe photoinduced processes in large molecules. To describe the σ-bonded molecular framework MMVB currently uses the MM2 potential [185, 186]. MMVB works well for covalently excited states but delivers a poor description of zwitterionic states since a subset of electronic configurations with singly occupied localized orbitals is used.

The VB methods mentioned so far depend on various parametrization schemes [170, 187–195]. Shurki and coworker proposed a methodology that couples *ab initio* VB with MM using the concepts taken from the EVB method [172, 175, 196]. It has the capabilities of the EVB approach but the accuracy of the QM part does not rely on empirical parametrization. In their approach they only used a mechanical coupling scheme between QM and MM. They argue that this approach is sufficient since the electronic structures of the involved diabatic states do not change strongly along a coordinate [175, 196]. Application to an S_N2 reaction showed nice agreement with other studies and experimental results.

2.2 Force-Fields Used in QM/MM Applications

The most widely used force fields in biological chemistry are AMBER [197–200] which is especially for nucleic acids and CHARMM [201–205] which is parametrized for proteins and enzymes. There are also numerous other force fields like Gromos [206–208] and OPLS-AA [209–211] which, due to their parametrization, offer a more universal application. Organic molecules have a larger chemical diversity than biomolecules. Since force fields have to be adapted to the properties of the molecule under consideration, many force fields were developed for investigations in the field of organic chemistry. The MM2 force field [185, 186, 212] was primarily developed for conformational analysis of hydrocarbons and other small organic molecules. It was continuously refined and updated for many different classes of organic compounds leading to the MM3 [213–215] and MM4 [216–219] versions. Even older is the CFF which was developed by Warshel and Lifson [220–222]. According to its developers, the CFF95 represents a logical extension of the CFF [223, 224]. The Merck molecular force field (MMFF94) was developed at Merck for a broad range of molecules [225–231]. Other often used force fields are UFF [232, 233], Dreiding [234], Gromacs [235, 236], or the Tripos force field of the Sybyl molecular modeling package [237], to mention just a few. All of them have their strengths and weaknesses so that comparisons between the various possibilities are very important [229, 233, 238–245]. A nice compendium about all kinds of force fields is given in Wikipedia [246].

Developing MM parameters for (poly)saccharides is notoriously difficult [247]. With GLYCAM06 [36, 248] Woods and coworker presented a new consistent and

transferable parameter set for modeling carbohydrates and glycoconjugates which was also extended to enable the description of lipids, lipid bilayers, and glycolipids [249]. We have already mentioned the comparison between PM3CARB-1 and SCC-DFTB-D which was carried out by Satelle and Almond [163]. Hemmingsen et al. have tested the performance of various different carbohydrate force fields by a comparison to gas phase *ab initio* data [250].

Force fields are like complex machineries in which the gearwheels intertwine. Due to this sensitive balance, the mixing of different force fields is problematic. In medicinal chemistry sometimes problems arise since the enzyme is nicely described by a given force field but the parameters for a given ligand are missing. This problem was tackled by Vanommelslaeghe et al. They developed the CHARMM General Force Field (CGenFF) which extends the CHARMM force field to drug-like molecules [251–253].

While older force fields were calibrated with respect to experimental results the newer ones are more and more fitted with respect to computed *ab initio* data. As a consequence, total energies computed by force fields and more reliable QM approaches agree quite nicely. Nevertheless, deviations are found if the single contributions to the total interactions are compared [254]. Such comparisons are enabled through the Symmetry Adapted Perturbation Theory (SAPT) [255–261] which provides information about the individual terms. Attempts to parametrize intermolecular force fields based on SAPT can be taken from the literature [262–269]. Most obvious deviations exist between electrostatic and van der Waals terms [270–277]. The benzene dimer in the sandwich and the T-shape configuration is a good example [278]. The investigation includes the standard force fields OPLS-AA [209–211], MM3 [213–215], and AMOEBA [279] as implemented in the TINKER program package [280]. Van der Waals interactions are represented in these force fields with three different functional forms such as Lennard-Jones (OPLS-AA), modified Buckingham (MM3) and Buffered-14-7 (AMOEBA). We note that, in contrast to OPLS-AA and MM3, the AMOEBA force field is a polarizable one capable of including non-pairwise-additive many body effects in the force field via induced dipoles. The SAPT reference data were taken from van der Avoird et al. [281]. The comparison between the various contributions to the total binding energy shows that the force fields used underestimate the binding interactions resulting from electrostatics. However, this error is compensated since repulsion arising from van der Waals terms is also underestimated. So the total binding energies agree quite nicely for distances larger than 5 Å. However, at smaller distances for the sandwich and T-shape configurations of the benzene dimer, different effects are found to be dominant. Hence, OPLS-AA which is best suited for the sandwich configuration possesses larger errors for the T-shape configuration. For this configuration MM3 performs best.

Recently, Spackman [282] suggested that underestimations of the electrostatic binding effects result because charge penetration effects are not correctly taken into account. Such penetration effects arise if two atoms are so close that their charge densities can overlap and the shielding of the nuclear charge of each atom by its

own electron density decreases. They cannot be accounted for by the classical multipolar expansion. Spackman also showed that it is possible to estimate this contribution by a sum of classical coulomb interactions between spherical atomic charge densities. This expression can easily be incorporated into a force field since it can be reduced to a one-dimensional integration in reciprocal space [283]. Including this expression leads to excellent agreement between the force field and SAPT results for the electrostatic interaction. After reparametrizing the van der Waals term, we obtained an improved force field for polycyclic aromatic hydrocarbons with physically grounded electrostatics [278]. It differs from other approaches such as damping the long-range (multipolar) part of the electrostatic energy [284, 285]. It mimics to some extent a more computationally expensive representation of electrostatic interactions with the Gaussian Multipole Model [286] and is similar in spirit to recent work of Wang and Truhlar [287].

The very first QM/MM approaches [5, 288] and other early semi-empirical QM/MM implementations [58, 289–293] used polarizable force fields for the embedding scheme. However, since then biomolecular force fields normally treat non-bonded interactions as pairwise additive, where many-body contributions are included in an average manner [201, 209, 294–296]. This approach usually works well for homogeneous systems (pure liquids, mixtures of compounds of similar polarity). It may break down for more complicated systems with inhomogeneous electronic structures. For this kind of systems, the introduction of polarizability should and does lead to an improved description of the interactions [297–305]. The development of polarizable force fields, however, represents a problem since quantum effects are important. Polarizability can be included using different approaches [306, 307] such as the point polarizable dipole model (PPD) [5, 308, 309], the charge-on-spring (COS) model [310], also called the Drude oscillator [311] and the fluctuating charge (FQ) model [312]. The large number of new approaches for polarizable force fields shows the importance of this field [199, 211, 313–328]. The GROMOS polarizable force fields and software make use of the COS [329] model to integrate polarizability as it leads to simple formulas and is computationally efficient and compatible with the non-polarizable (GROMOS) force fields. For this model some recent developments and applications of the van Gunsteren group can be taken from the literature [295–297, 329–331]. Other approaches were provided by Swope et al. [332], Biswas and Gogonea [333], or Pliego [334]. The performance of scalable MD simulations with polarizable force fields based on classical Drude oscillators was shown by Jiang et al. [335]. The CHARMM polarizable force field is based on the same approach [336]. The code is implemented in the NAMD program package [337].

For embedding schemes, Zhang et al. proposed an efficient approach in which only the MM atoms at the boundary are polarized [338, 339]. In investigations about heterogeneous catalysis such polarizable force fields are successfully used to describe the interaction between inorganic surfaces and molecules [340–343]. This method is also applied to describe the chemistry taking place in the interstellar medium [344–347]. Polarizable force fields for the computation of excited states were also provided by Olsen et al. [348] and Slipchenko [349]. Decomposition of

fragment approaches were developed and applied by Mata and Cabral [350], Yoo et al. [351] and Fujimoto and Yang [352]. These approaches are related to frozen density approximations developed by Neugebauer and co-worker [353–357].

2.3 Handling of the QM/MM Partitioning and Coupling

The overall accuracy of QM/MM computations strongly depends on the coupling between the QM and the MM part. Traditionally, one differentiates between subtractive and additive coupling schemes. In the meantime, both are well developed so that the differences in accuracy become small [33]. Since many reviews contain excellent discussions on this topic [34, 36, 59–62, 358] we will only briefly differentiate between the main approaches.

For subtractive schemes, a MM calculation of the entire system and QM and MM calculations for the QM part are needed. The QM/MM energy of the whole system is given by the sum of the QM calculation of the QM part and the MM calculation of the entire system:

$$E_{\mathrm{QM/MM}} = E_{\mathrm{MM}}(\mathrm{all}) + E_{\mathrm{QM}}(\mathrm{QM}) - E_{\mathrm{MM}}(\mathrm{QM}).$$

The result of the MM calculation for the QM part is subtracted to avoid double counting. In this straightforward realization [359, 360], the subtractive scheme is very simple to implement; however, the coupling between the subsystems is handled entirely at the MM level, i.e. a polarization of the QM part by the MM part is not taken into account. Due to the simplicity of the approach, extensions to the combination of two QM approaches [361–363] or to the treatment of various layers are also possible. The latter approaches are known under the name ONIOM (our n-layered integrated MO and MM) [364–367]. Ryde and coworker also developed a subtractive scheme [32, 368, 369]. It is also used in Qpot developed by Sierka and Sauer [37, 39].

In the additive scheme, the MM computation is only performed for the MM part. The coupling between both parts is described by an additional term which has to include bonded, van der Waals and electrostatic interactions between the QM and MM atoms. The total QM/MM energy is obtained by the sum of the QM energy of the QM part, the MM energy of the rest of the system, and the coupling term between the two subsystems:

$$E_{\mathrm{QM/MM}} = E_{\mathrm{QM}}(\mathrm{QM}) + E_{\mathrm{MM}}(\mathrm{MM}) + E_{\mathrm{interact}}(\mathrm{QM} + \mathrm{MM}).$$

The additive scheme has the advantage that the coupling can be described in different ways. In the mechanical embedding scheme [34, 36, 59–62, 358], the QM MM electrostatic interaction is treated on the same footing as the MM MM electrostatics. The disadvantages of the mechanical embedding scheme are largely

eliminated by an electrostatic embedding scheme. Here, the QM calculation is performed in the presence of the MM charges, e.g. by incorporating them into the one-electron integrals of the QM calculation. In this respect the electrostatic embedding scheme resembles continuum approaches but one has to take into account that the molecular nature of the surrounding is more accurately mimicked. For drawbacks of the electrostatic approach we again refer to recent reviews [34, 60, 62, 358].

If QM and MM regions interact only through non-bonded terms (electrostatic and van der Waals), the implementation is straightforward. Cases in which the QM MM border cuts covalent bonds are more problematic. One important approach to handle this issue is the so-called link atom scheme in which the dangling bond is saturated by a capping atom. In most cases either hydrogen [288, 370] or fluorine atoms are used. Previous studies have shown that the choice of link atom scheme is generally as good as other schemes [64, 371–373]. Furthermore, it was shown that different variations of the link atom scheme result in comparable relative energies [371–376]. More accurate but more complicated to implement are methods which use precomputed frozen localized orbitals (FLO) that are placed instead of the ruptured bond [377]. Actually, this method dates back to the first suggestion of QM/MM by Warshel and Levitt [5]. Truhlar and coworker developed a related approach based on auxiliary hybrid orbitals [378, 379]. The usage of effective fragment or group potentials is in the same spirit [380–386]. All important physical interactions between the two fragments are considered explicitly via a set of one-electron potentials. This method is very accurate but the transferability between different types of fragments is problematic. In the related field-adapted adjustable density matrix assembler (FAADMA) the system is divided into fragments [387–389], all of which are computed by conventional QM considering its local environment. The more distant parts of the system are incorporated via point charges. In quantum capping potentials approaches the dangling bond is saturated with effective potentials [390–393].

For a detailed discussion of the various effects and approaches, we refer to a review of Senn and Thiel [60] which also contains newer approaches up to 2009. The recent review given by Salahub and coworker [34] also contains a comprehensive discussion of effects. A nice summary is also given by Komin and Sebastiani [394]. So we refrain from further discussion of these works but will only point to some recent developments. Truhlar and coworker developed the balanced redistributed charge (BRC) scheme which represents an improvement for H and F link atoms [375, 395]. Using this approach the mean unsigned error for average proton affinity decreases from 15–21 kcal/mol (unbalanced H link atom) and 16–24 kcal/mol (unbalanced F link atom) to 5–7 kcal/mol and 4–6 kcal/mol for balanced H and F link approaches. If the F link atom is additionally tuned by a pseudopotential to reproduce the partial charges the value drops to 1.3–4 kcal/mol.

First attempts to saturate dangling bonds by effective potentials (quantum capping potentials) were performed by DiLabio et al. [390, 391, 396] based on analytical effective core potentials of the Goedecker type [397, 398]. In line with

previous QM/MM studies, Sebastiani and coworker [394, 399] fitted the pseudo potential parameters under the constraint that the change in the quantum part of the QM/MM calculation is minimal with respect to the full-QM computations. The perturbative effects of the capping potentials were tested by means of geometrical parameters, proton affinities, and NMR chemical shifts, which are known to be sufficiently sensitive [400–402]. First optimizations were performed with an iterative Nelder–Mead downhill simplex minimization [403], and later a variation of the artificial bee colony algorithm [404–406] was employed [399]. The results look quite promising especially for the NMR parameters of the centers directly located at the QM/MM boundary. Capping approaches were also tested using the example of EPR parameter predicition by Salahub and coworker [407].

So far, we have reviewed approaches in which the QM/MM border is defined at the start and remain unchanged during the calculation. In adaptive schemes, the size of the QM subsystem can adjust during the calculation so that atoms or charges can move between QM and MM subsystems. First approaches were presented by Rode and co-workers (hot spot method) [408–411]. Other methods were proposed by Kerdcharoen and Morokuma (ONIOM-XS) [412–414] and by Zhang et al. (adaptive partitioning method) [338, 339, 415, 416]. A comparison of the various approaches was also provided by Zhang et al. [339]. For recent reviews about adaptive multiscale simulations we refer to the literature [417, 418].

Even QM/MM does not allow the treatment of an arbitrary number of atoms so that boundary effects result. For classical force fields periodic boundary conditions in combination with Ewald summations are realistic solutions [419–421]. Adaptations for QM/MM approaches using semiempirics [422, 423] and density functional theory (DFT) [424, 425] for the QM part were recently introduced. If periodic boundary conditions are not possible, boundary potentials are an attractive alternative to handling long-range electrostatic interactions [426–431]. In the boundary potential ansatz, the full system is subdivided into an inner and an outer part. The inner part comprises the active site, its neighboring residues and important solvent molecules. It is described atomistically, e.g. by the QM/MM approach. The outer part contains the rest of the enzyme and less important solvent molecules. Their influence on the inner region is mimicked by the boundary potential, e.g. a polarizable dielectric continuum (PDC). Benighaus and Thiel [432] implemented and compared a generalized solvent boundary potential (GSBP) [433] with the solvated macromolecule boundary potential (SMBP) [434, 435]. In the former, the solvent molecules are described by a PDC while for the outer macromolecule region fixed point charges are used. The SMBP is similar to the GSBP but are expected to be very efficient in geometry optimization. Additionally, it allows distinguishing between the influence of the outer macromolecule region and that of the bulk solvent. The investigation underlines the accuracy of the SMBP approach. It also shows an influence of the outer macromolecule region on the reaction energetic if strong charge transfers are associated with the reaction. If in such cases the outer macromolecule region is completely neglected, errors of

several kcal/mol have to be expected. In less polar reactions the influence is smaller than 2 kcal/mol. The bulk solvent is less important for polar reactions and negligible for apolar ones [432].

2.4 Sampling Techniques for Determining Structures and Reaction Paths

Reliable descriptions of molecules need accurate information about their geometrical arrangement at experimental temperatures. For small molecules, this geometrical arrangement corresponds to the global minimum of the PES. For very small rigid molecules this global minimum is easily accessible with simple minimization approaches, e.g. algorithms like Newton, quasi-Newton (e.g. L-BFGS) or Conjugate Gradients [174, 436].

Since characteristic QM/MM models for enzymes posses several thousand degrees of freedom a simple minimization leads to a local but not to the global minimum. Hence, global optimization routines are necessary, but nowadays even the most sophisticated algorithms for finding the global minimum are unable to describe, for example, the folding of a big protein from scratch (see the Critical Assessment of methods of protein Structure Prediction 2008, CASP8) [437]. Therefore, QM/MM investigations normally start from a Protein Data Base (PDB) structure obtained by X-ray or NMR. But this gives rise to the problem that neither information about the protons nor information about the orientation of the solvent molecules is included. Furthermore, the resolution of these structures is often limited. Hence, a careful preparation of the system is essential. This preparation includes the determination of the protonation state and the optimal orientation of the solvent molecules. This is obtained by long MD-runs which involve periods of heating and cooling. The MD is used since it covers the phase space reasonably well [33]. While the properties of small molecules are mainly determined by one single structure, the properties of macromolecules are determined, due to their flexibility, by an ensemble of geometric arrangements which are accessible at a given temperature. This does not only apply to stable structures but also to complete reaction paths connecting the reactants and products of a chemical reaction. Also, in this respect, sampling is absolutely necessary. Without this sampling, major errors are bound to happen [438], especially when evaluating, for example, the activation barrier for an enzymatic reaction. If the PES of the enzyme ligand complex is very rugged with many local minima, simple QM/MM minimization approaches may not be sufficient. Even larger problems arise when calculating, for example, the binding free energy. In this case, calculation of the ground state free energy is very problematic since one expects different results for different local minima. The only way to obtain reasonable results is again sampling. For these reasons, a wide variety of efficient approaches for sampling were developed and many reviews of this topic can be

found [33, 60, 174, 436–441]. To avoid duplication we only list the most important methods and concentrate on new developments in this field of research from the year 2009 to now.

2.5 *Conformational Search and Determination of Stationary Points*

To compute the property of a small rigid molecule the knowledge of the global minimum is sufficient. To determine the properties of large flexible molecules it is necessary to take an average over the ensemble of structures accessible at the given temperature. To generate such ensembles and to determine the global minimum structure (which is the most stable structure on the PES) conformational search algorithms are necessary [174, 436, 442–444]. The easiest part of the conformational search represents the minimization to the next local minimum on a given PES. Widely used algorithms for pure QM or MM computations are Newton, quasi-Newton (e.g. L-BFGS) or Conjugate Gradient methods [174, 436]. The most efficient coordinates for optimization are internal coordinates or hybrid delocalized coordinates (HDLC) which supplement the delocalized internal coordinates with Cartesian information [60].

The determination of the next local minimum in large molecular systems with QM/MM approaches is more difficult. Here, the concept of microiterations is used to speed up the convergence of the optimization. In principle there are two possibilities. On the one hand, the optimization of the QM and MM parts is done alternately, i.e. during optimization of the QM part the MM part is kept fixed and vice versa. These iterations are repeated until convergence is reached [33, 60]. On the other hand, after each optimization step within the QM part the MM part is completely relaxed. It is also known as adiabatic scheme. The calculation of the MM part requires less computational time than the QM part and by applying the adiabatic approach the number of energy and gradient calculations required until convergence can be reduced [33]. Besides minimization to the next minimum, conformational search algorithms must also contain parts which are able to leave this minimum to find the next possibly deeper one.

Conformational search algorithms can be divided into deterministic [445–448] and stochastic [449–452] procedures. Since the deterministic algorithms can only be used for small systems due to combinatorial explosion [174], a huge variety of specialized methods was developed over the past few years [452–456]. These methods include, for example, classical molecular dynamics (MD) [450, 457], mutually orthogonal Latin squares (MOLS) conformational search techniques [458], smoothing/deformation search techniques [459], Monte Carlo (MC) [460], simulated annealing (SA) [461, 462], potential flooding [463], energy leveling [464], metadynamics [465], and genetic algorithms [466].

A comparison of different algorithms usable for protein structure predictions is given by Scheraga et al. [467]. They compared the new Replica-Exchange Monte Carlo-with-Minimization (REMCM) with Monte Carlo-with-Minimization (MCM), Conformational Space Annealing (CSA) and Conformational Family Monte Carlo (CFMC). The REMCM approach often locates the global minimum faster and more consistently than the other methods. Furthermore, it shows a significant improvement to the traditional Replica Exchange method [467].

Some recent developments and improvements to conformational search algorithms are given by a new variant of a Tabu-Search method in combination with basin hopping (BH) ideas [468], a knowledge-based approach based on evolutionary algorithms [469], the PSAMD/GAc (Parallel Simulated Annealing Molecular Dynamics using Genetic Crossover with knot theory) method [470], the ConfGen approach for generating bioactive conformers [471], an approach for Systematic Screening of Conformers (SSC) [472], a new hybrid algorithm consisting of diffusion equation method (DEM), a SA algorithm and evolutionary programming (EP) elements [473]. For more details about the above-mentioned methods we refer to the references.

The publication about a new Tabu-Search based algorithm [468] includes a comparison of various conformational search algorithms (MD, SA, BH [474] or Monte Carlo minimization (MCM) [452], and Tabu-Search) with respect to their ability of finding the global minimum as well as their overall performance. The study also revealed the advantage of reasonable starting structures. Five-, six- and seven-membered intra-molecular ring structures closed by hydrogen bonds between hydrogen bond donors and acceptors seem to represent good starting structures. Their usage indeed speeds up the convergences of global optimization methods as well as increases the ability to locate the global minimum.

For the pentapeptide Glu–Lys–Ser–Cys–Pro, the MD and SA methods perform rather poorly in locating the global minimum (17.8 kcal/mol for MD and 6.2 kcal/mol for SA above the lowest lying minimum found in the whole study which we expect represents the global minimum). If the above-mentioned ring structures are used as starting points much better minima resulted (4.7 kcal/mol and 5.8 kcal/mol above the global minimum for MD and SA, respectively). The BH approach converges with and without usage of the above-mentioned starting structures to a minimum lying 0.7 kcal/mol above the global minimum, hence it is not able to locate the global minimum during the performed runs. The Tabu-Search finds the global minimum only when the better starting structures are used. A combined Tabu-Search/BH algorithm always finds the global minimum. If the above-mentioned starting structures are used the global minimum is found in 68% of all runs; if no starting structures are used the efficiency decreases to 37% [468].

We already mentioned that QM/MM investigations of solvated macromolecules deserve careful preparation of the system. It should lead to the optimal orientation of the macromolecule and of the surrounding solvent molecules. In this respect, the buildup of the solvent layers is an especially crucial point since X-ray structures only contain information about the conserved water molecules. By default this preparation is obtained by long MD runs involving heating and cooling periods. Several structures along the MD trajectory are manually selected and the

corresponding geometries are optimized. The resulting minima are then subjected to the QM/MM treatment. The accuracy of the obtained structures is disputable due to several reasons. As shown above, such MD simulations converge quite slowly. So the obtained minima can be expected to be considerably higher in energy and structurally far from the global minimum. Furthermore, the snapshots used for the subsequent minimization are selected on the basis of a visual inspection. This needs experience and might further bias the outcome [475].

To obtain improved structures Grebner et al. [475] developed a novel approach which uses the above-mentioned combined Tabu-Search/BH [452, 468, 474] approach for diversification of the search space and a dimer-method based strategy to escape from a local minimum [476–478]. In the Tabu-Search-based procedure the water shell can be built up by a step-wise procedure in which the complete solvation is obtained by a few microsolvation steps. After each step the water sphere is globally optimized. It is also possible to build up the water shell in one step. As a first test example, the new method was applied to obtain a solvated structure of the Chignolin protein (PDB-ID: 1UAO) [479]. The computations started from the NMR-structure provided by Honda et al. [479]. Previous computations were performed by Satoh et al. [480] and Suenaga et al. [481]. To get an insight into the suitability of the new approach the results of the Tabu-Search/BH were compared with those obtained from the standard approach (MD run with subsequent local optimization of all selected snapshots). The computational times required by both approaches are very similar. However, the Tabu-Search method locates a global minimum which lies approximately 100 kcal/mol below the best structures found by the standard approaches.

The investigation revealed another advantage of the new Tabu-Search-based approach. Depending on the procedure it can provide structures being as close as possible to the experimental information or to those geometries representing the global minimum within the used theoretical method. We will explain this difference for the given example. For the Chignolin peptide, the NMR structure shows a T-stacked orientation between the Trp9 and Tyr2 residues. This orientation is also predicted by DFT computations for a model system using continuum approaches to account for solvent effects. For the same model system the OPLS-AA force field employed for the simulation, however, predicts a distorted π-stacked orientation since the interactions which stabilized the T-stacked orientation are strongly underestimated. Due to this error in the force field the lowest lying structures found by the Tabu-Search- and MD-based preparations predict the wrong orientation.

However, using the step-wise buildup of the solvent shell the Tabu-Search-based approach conserves the right orientation if the peptide is kept fixed during the build-up of the first three solvation shells. This structure, which closely resembles the NMR structure, is still 40 kcal/mol lower in energy than the energetically lowest structure predicted by the MD which possesses the wrong orientation. Another big advantage of Tabu-Search-based approaches is the fact that the optimal structure can easily be taken from the optimization. A manual selection as needed within the MD-based procedure is rendered obsolete by the readily available internal ranking by the absolute energies of each individual minimum.

2.6 Determination of Reaction Pathways

The determination of local minima is well understood but finding the optimal transition state (TS) and the corresponding reaction pathway is still a problem [174, 436]. When the TS is found, the minimum energy pathway (MEP) can be found by following the gradients downhill, both forward and backward [482]. In principle, the TS can be found using information about the curvature of the PES given by the eigenvalues of the Hessian matrix and using a Newton algorithm to maximize the energy function. In practice, this approach cannot be used for large systems since the Hessian matrix is too expensive to be calculated.

Therefore, different approaches were developed which can be divided into surface walking algorithms (single-ended) and chain-of-states methods (double-ended) connecting different points on the surface [436, 477]. Surface walking algorithms follow the lowest curvature of the PES to reach the nearest TS and only need an initial guess for the calculation. These include, for example, the partitioned rational-function optimizer (P-RFO) [483–486] or the Dimer method [476–478]. In contrast, chain-of-states methods build up a sequence of different molecular geometries starting from product and reactant structures. Then the constructed points are relaxed to the MEP. The nudged-elastic-band (NEB) [487–489] and the growing string [478, 490] are chain-of-states methods. Furthermore, a reaction coordinate-driven approach was implemented which can also be seen as a chain-of-states or chain-of-replica method [34, 491]. An improvement to the NEB was given by the Climbing-Image-NEB (CI-NEB) [492]. Further improvements to TS search algorithms include modifications of the growing-string method [493–495] and a Dimer method combined with constrained Broyden minimization [496].

An investigation of reaction pathways in enzymes and sampling of possible transitions to give insights into temporal and dynamic information for barrier crossing was given by Schwartz et al. [497]. They showed that the standard view of a strongly bound TS in the thermodynamic equilibrium between the Michaelis complex and the product is not always correct. Furthermore, large time scale movements of the peptide backbone are crucial for an effective catalysis and have to be considered for artificial drug design.

Finally, sampling is needed to determine the free energy. The free energy is widely used for QM/MM studies containing explicit solvent molecules since it is the fundamental driving force of chemical reactions. An extensive overview about historically important work is given in the review of Senn and Thiel [60], whereas Zhang et al. [34] provide a comprehensive introduction into the theoretical background of QM/MM related free energy methods.

One major problem of free energy methods is the need for extensive sampling of the phase space, which can lead to a prohibitively large computational effort for the QM part. The unavailability of complete sampling also limits the estimation of entropy differences, whereas free energy differences can be determined routinely today since extensive sampling of only the relevant part where the two states differ

from one another is sufficient in these cases [498]. Therefore, various methods have been developed trying to circumvent these problems while retaining sufficient accuracy. A recommendable summary on the various free energy methods like free energy perturbation (FE or FEP) [499], thermodynamic integration (TI), umbrella sampling (US) [78, 500], metadynamics [501] and FEP methods employing reaction path optimization on the potential of mean force surface (MFEP) [502] can be found in reviews of Hu and Yang [47]. An overview of recent advances and applications for QM/MM simulations of organic reactions is provided by Acevedo and Jorgensen [46].

The FEP scheme is widely used and exists in more or less general formulations [499, 503–505], based on the Zwanzig equation [506]. The basic concept is to calculate the molecular ensemble of a given state while employing potential energy parameters of another state along a reaction coordinate. The two states should only differ by an incrementally small perturbation to ensure a large overlap of the two phase spaces and good error cancelation due to comparably incomplete sampling. Therefore, the calculation of free energy differences between two states is accessible from a sum of intermediate steps. QM/MM FEP method is usually the method of choice to study organic reactions in solvent environment when it is combined with MC method due to the advantage of MC method for sampling solvent molecules. In the most recent application this approach was used to study Diels–Alder reactions and Cope eliminations in aqueous solution [507]. In practice, FEP calculations are often conducted with fixed QM parts for every incremental step, represented by charges derived from the electrostatic potential (ESP), whereas only the MM part is sampled at every point along the predefined reaction pathway. This approach seems to work well for enzymatic reactions [508], but this does not necessarily hold for all reactions. Furthermore, the need for more than one single starting structure has been emphasized by recent studies about finite temperature effects if one aims to get accuracy of energy differences below 3 kcal/mol [509]. An interesting new approach uses a dipole-field/QM combination (DF/QM) to perform alchemical FEP calculations, from which dissociation free energies, entropies and absolute pK_a values can be obtained [510]. Another recent development does not rely on a single potential of mean force (PMF) but uses multi-dimensional PMFs, which are very useful for QM/MM studies of organic reactions [46, 511].

In contrast to the FEP methods, thermodynamic integration (TI) needs a continuous path connecting the two states. It was originally formulated by Kirkwood [512]. Here the free energy difference is obtained by integration of the thermodynamic path connecting the two states of interest, for which the energy gradient with respect to the path variable is needed. This is also a major drawback of the method compared to FEP approaches, since the calculation of gradients might be difficult in some applications [47]. Nevertheless, a recent QM/MM study shows that in practical use configuration sampling employing TI delivers similar results to umbrella sampling, deviating less than 1 kcal/mol. FEP results were found to deviate by 1–2 kcal/mol [509].

Umbrella sampling (US) is one of the most frequently used sampling methods to calculate the PMF. The original idea was first suggested by Torrie et al. [78, 500]

In this technique the difficulty in sampling the configurational space in high energy, which occurs with low probability is tackled by adopting biasing harmonic potential. Therefore, this method is suitable for computing the free energy profiles of processes with activation barriers. The combination of US methods with QM/MM scheme extends the scope of the problems it can deal with. Recent applications of this method to investigate intramolecular deprotonation mechanisms [513], reaction mechanisms of monoethanolamine with carbon dioxide [514] and *cis–trans* isomerization mechanisms [515, 516] can be found in the literature.

Metadynamics is another sampling method which was invented rather recently by Laio et al. [501]. In common with US methods it uses biasing potentials. However, metadynamics has its strength in employing history-dependent biasing potential. This potential is used to fill up the minima of the free energy surface (FES) that have already been visited. This encourages the system to explore the other minima, and to determine the FES accurately as a function of collective variables. So far, the metadynamics approach in the context of QM/MM scheme has been mostly applied to the research concerning chemical reactions in enzyme active sites [517–519].

More recently, another free energy calculation method in the context of QM/MM framework was developed by the Yang group [502]. The QM/MM FEP method is still not completely free from initial conformation dependency due to the fixation of the QM part during the sampling of the MM part. To lift such biases, a method, called QM/MM minimum free energy path (QM/MM MFEP) method, was invented as a need for solving this problem. The key idea of this method is based on the fact that the gradient of PMF for a certain reaction of interest, which can be obtained from QM/MM FEP calculation, is actually equivalent to an ensemble average of the gradient of QM atoms. Therefore, using this information in combination with an optimization method such as the nudged elastic band (NEB) method [487, 489] or Ayala–Schlegel method [520], the whole minimum free energy path for all conformations along the reaction path can be obtained. This method has been applied to organic problems such as computing redox free energy [521] and solvent contribution [522] as well as enzymatic reactions [4, 523]. One good example of applications of this method in enzymatic reactions is the study of the decarboxylation reaction in orotidine 5′-monophosphate decarboxylase. In this study, QM/MM MFEP calculations predicted an activation barrier of 16.5 kcal/mol, which is in good agreement with the experimental value of 15.2 kcal/mol [523].

3 Applications

Most QM/MM applications are devoted to biological questions. In this field QM/MM approaches are mandatory since the molecular nature of the enzymatic environment determines geometrical arrangements and the energetics of enzymatic processes. The use of continuum polarizable models is problematic since the dielectric constant, for example, is not well defined. For regions in the outer spheres

of the enzyme it is close to the value of water but decreases considerably for non-polar regions within the enzyme [524–526]. For questions within the field of organic chemistry the influence of the environment is substantially smaller. This is shown by many successful applications which completely neglect the environment and replace large alkyl side chains by methyl groups [527–531]. In other cases it is sufficient to approximate the solvent by polarizable continuum models [65, 66, 532–540]. Their success results from a careful adjustment to experimental data. Only in cases in which the molecular nature is important do QM/MM approaches also become essential for investigations within the field of organic chemistry. Important areas are investigations about solvent effects on chemical reactions in ground (thermochemistry) [46, 47, 49] and electronically excited states (photochemistry) [50, 51, 53, 541–544] and on spectroscopic data ranging from NMR and EPR through IR and Raman to UV-VIS (laut Langenscheidt) and X-ray absorptions.

Fields in which QM/MM approaches will become even more important are ionic liquids, organic semiconductors and medicinal chemistry. In all these fields, QM/MM is the method of choice since understanding and predicting desired properties is only possible if the influence of the surroundings is taken into account [545, 546]. An overview of different aspects of ionic liquids offers a recent themed issue in PCCP [547] and we will highlight some recent applications based on QM/MM. At the moment, most QM based investigations in medicinal chemistry characterize [548] ligand properties without considering the environment [549]. Reviews about pure QM investigations in this field are presented by Merz and co-worker [550, 551], LaPointe and Weaver [552] and Cavalli et al. [553]. In comparison, QM/MM applications which describe the reaction of the ligand in the enzyme are rare [527, 554–559] and a review containing further work was provided recently by Menikarachchi and Gascon [57]. To avoid duplications we will not discuss this topic in more detail.

Due to distinct properties, functional π-conjugated molecules with charge and energy transport properties possess a bright future [560–563]. For the understanding of the properties of these compounds, environmental effects have to be taken into account since the interesting effects only appear in bulk systems (crystals, thin films) [564–566] and optical as well as charge and energy transport properties of functional π-conjugated molecules strongly depend on intermolecular interactions and on the mutual orientation of the monomers [567–569]. Perylene bisimide (PBI) compounds are good examples. In diluted dissolution they all possess the same absorption spectra but the colors of PBI crystals range from red to black [570–572]. The electronic energy transfer (EET) properties of π-conjugated molecules was first explained by Förster [573–575] but a thorough explanation is also possible on the basis of the work of London and Eisenschlitz on van der Waals interactions [576]. Per definition at least the interaction between two neighbors has to be taken into account but it can be assumed that the environment will also influence this effect [577, 578]. At the moment the underlying interactions are taken into account using monomer computations together with empirical Hamilton operators which describe the Förster effect [579–586] or dimer computations

[580, 587–592]. The latter include higher order effects [593] but due to the size of the system and the complexity of the effects [594] they are limited to the isolated dimer only. Although they seem to be important even if the excitation is localized on a dimer, up to now only a few works exist which go beyond vacuum computations. Since QM/MM computations are still rare [354, 545, 546] in this field, a review should be postponed.

A strict separation between the field of organic chemistry and biological chemistry is impossible. Spectroscopic investigations about small peptides, for example, belong to both fields and many methodical improvements are tested at the hand of biological systems but offer important possibilities with the other field. The same holds for the field of transition metal chemistry and heterogeneous catalysis which can be related equally well to inorganic or organic chemistry. So our selection of applications is a matter of taste. Recent reviews represent further filters for our selection. To prevent a duplication of their contents we will mainly focus on applications published after 2008.

3.1 Structures in Solvents Due to Ions

Water as the most important chemical and almost solitary solvent in biological systems has been the subject of innumerable experimental and theoretical studies over the past years [48, 595–598]. Many of these investigations focus on the clarification of the "structure" of water, its influence on chemical reactions and its dependence on solvated molecules and ions. Although generally being accepted to be a "structured" liquid, up to now there has been no consensus on how to measure the degree of structure in aqueous solution. Early attempts by Bernal [599] divided the structure of a solvent into two descriptors, "coherence" and "fluidity". Later ones by Bennetto and Caldin [600–602] added a third, yielding "stiffness", "openness" and "order", derived from bulk properties of the solvent such as the work needed to create cavities, its free volume as well as the molar entropy. An explanation for the geometrical arrangement of solvent molecules around ions and reaction kinetics in condensed phase was first introduced by Frank and Wen [603] by an onion-like model, comprising an inner region of solvent molecules directly interacting with the central ion, a small intermediate region without specific interaction capabilities and thus low solvent densities as well as the bulk solvent regimen. Despite the simplicity, the quality of this model has proven astonishingly high as one can see from radial and angular distribution functions (RDF, ADF) available for a broad variety of ions [604–628]. Together with the mean residual time (MRT) of solvent molecules within a specific range around a centre, these values are quite easily accessible by experimental methods such as EXAFS [629–631], NMR [632, 633] and dielectric relaxation studies [634] as well as through theoretical MD investigations using MM with various parametrization schemes for water molecules [336, 635–640], pure QM [641–645] or combined QM/MM hybrid schemes [605, 615–619, 646].

Whereas the pure molecular mechanical methods are significantly less demanding than QM/MM or even pure QM, due to the pairwise additivity of interaction potentials they neglect important contributions and may deliver false geometries and energetics. Although these errors could be compensated by introducing suitable three- and many-body potentials, technical difficulties and the massive increase in computational power of present-day hardware make the hybrid QM/MM methods more favourable [604–606]. Consequently there have been numerous QM/MM studies within the last few years. While many investigations are focused on the quality and robustness of the employed theoretical methods [48, 604–606, 609, 614, 616–618, 621], lots of studies on the solvent shell structure around common ions [607–610, 612–617, 619, 624–628] or pure solvents [646] have also been published. Finding a compromise between the quality of the chosen QM method and the computational effort, most investigations are carried out on the HF or DFT level using medium size basis sets and effective core potentials (ECP) for transition metal ions within the QM subsystem combined with one of the many available force fields and an appropriate set of parameters for the solvent [336, 609, 635–640]. Both QM methods are known to have severe deficiencies, but the use of more sophisticated methods is, due to their enormous computational demands, limited to small reference systems and benchmark calculations. Whereas electron correlation effects, which might play an important role with respect to intermolecular interactions, are completely neglected within the HF approach, they are, to an uncontrollable extent, contained in the exchange correlation functional of DFT computations [611]. The latter ones are also known to overestimate the strength of hydrogen bonds and thus yield too rigid molecular arrangements and MRTs for solvent molecules around ions. Nevertheless, both methods are much better suited to describe experimental results than a description based on pure classical mechanics [608, 610, 613, 622, 628].

A principal step in finding an explanation for the interactions between solute and solvent and the resulting thermodynamics and kinetics is, of course, the understanding of the pure solvent. A recent study by Xenides [646] concentrates on the structural arrangement of the aqueous solvent around a single water molecule. Their results are in good agreement with data derived from X-ray and neutron diffraction experiments, but deliver additional insights into the individual H-bond patterns and the preferred coordination number. Similar investigations were put forward by Intharathep [613] on solvated hydronium ions with the focus on proton transfer properties. Their study is concentrated on clusters of the form $[H_{(2n+1)}O_n]^+$ and delivers an explanation for the decrease in the coordination number from about 4 in pure water to 3 for the hydronium ion by frequent conversions between the most stable, tetrahedral Eigen complexes $[H_9O_5]^+$ via transitional Zundel $[H_5O_2]^+$ structures. Another set of calculations of the same group [612] has been carried out for the ammonium ion. As expected from its structure, the ammonium ion is capable of forming one more H-bond to the solvent, making fourfold coordination possible. Nevertheless, with NH_4^+ being a much weaker hydrogen bond donor than H_3O^+, the solvation sphere is less rigidly bound, resulting in a higher rate of exchanging solvent molecules and making threefold coordination almost as probable as fourfold. Similar to the H_2O/H_3O^+ system, the NH_3/NH_4^+ possesses great

importance for many organic reactions and was studied by Tongraar [611]. The most interesting detail herein is probably the fact that the ammonium ion, due to its weak H-bond capabilities, acts as "structure breaker" in aqueous solution but changes to "structure making" effects in liquid ammonia.

Nearly as important as the detailed knowledge about the structure of the solvent itself is that of the influence of charged particles. Bucher [609] investigated the structural arrangement of the coordination sphere around sodium and potassium ions within the selectivity filter of the KcsA ion channel and compared them to the situation found in aqueous solution. They matched different force field methods together with a DFT based QM/MM scheme. Coordination numbers for both cations were estimated too large (up to 0.6 Å for K^+, 1.1 Å for Na^+) by all employed force fields whereas the QM/MM results have been within the experimental error range (5.9–6.4 Å for K^+, 4.4–5.4 Å for Na^+). The structures of solvated sodium and potassium ions were investigated in detail by Azam [608] and Tongraar [605], showing that the smaller Na^+ ion exhibits strong structure making effects, resulting in a very regularly shaped solvent shell of six water molecules. In contrast to that, the solvation shell of the larger K^+ ions is much more disordered and flexible with a higher frequency for exchanging solvent molecules. It was attributed to the weaker bond strength between the water molecules and the central cation. This behaviour is also reflected in the RDF and ADF values. The value for the first minimum in the RDF is almost zero for sodium, indicating a clear separation of the first two solvent shells, whereas that for potassium shows significant population or fluctuation between them. Similar differences can be found in the ADF plots, which show two distinct peaks and thus a very regular structure around Na^+, but broadly distributed values in the case of K^+, indicating a high degree of disorder and strong fluctuations. Fluctuations can also be seen from the MRTs within the first two hydration shells amounting to 7.4 and 3.4 ps in the case of sodium but only 3.2 and 2.2 ps for potassium. Care has to be taken going from the alkali to alkaline earth metals. Recent investigations by Tongraar [607] showed that the size of the QM region plays a significant role for the coordination number of Ca^{2+} ions, caused by effects ranging at least up to the second solvation shell but not being described by additive potential schemes.

Similar considerations hold for the case of transition metal ions as recently presented by Mohammed [615]. Although classical molecular mechanics (CMD) with added three-body corrections could quite well reproduce the experimentally determined coordination numbers, QM/MM methods are essential for describing the molecular motion. Sufficient flexibility of the water molecules can only be provided by including at least the first solvation shell into the QM part. Fatmi [618] even suggested a two-shell quantum mechanical treatment to improve the results, although the estimated increase of computational time amounts to a factor of about 80 compared to the single-shell approach. Nevertheless, this effort seems necessary to describe preferred solvation of transition metal ions such as Zn^{2+} by different ligands as recently done by Fatmi [619]. Zinc(II)-diamine complexes in aqueous solution were studied for thermodynamic as well as dynamic properties of the different geometries. Armunanto [647] investigated the coordination of silver

ions in a mixed solvent, comprising ammonia and water. In good agreement with simple chemistry experiments, they found Ag^+ to be preferably coordinated with ammonia rather than water molecules. Whereas the RDF for the NH_3 molecules exhibits a distinct peak, which is clearly separated from the bulk solvent, that of water is fairly broadened and population can be found between this peak and the bulk. From these results in connection with the geometries observed during the simulation, Armunanto concluded that the preferred coordination shell of Ag^+ ions consists of two tightly bound ammonia and about 2.8 frequently exchanging water molecules.

Investigations focusing on the halide anions F^-, Cl^- and I^- have been carried out by Tongraar [622, 627]. In the former of the two studies, they show that classical mechanics are unable to reproduce the finer differences in the solvation between F^- and Cl^-. Consequently, they used QM/MM methods to clarify the solvation of all three halide anions. All measures, such as RDF and ADF values, MRTs and the molecular motion of water molecules, indicate that the solvent shell, being highly ordered for fluoride, gets significantly disordered and weakened along the series. The effects are so strong that, although F^- and Cl^- tend to increase the rigidity of the solvent, I^- is considered to be structure breaking. The consequences of this series, the propensity of ions for the water/vapor interface or the bulk, respectively, have been part of a piece of work by Yagasaki [623]. They concluded that the propensity for the interface is caused by a subtle balance between the energetic destabilization and the counteracting entropic stabilization at the interface compared to the bulk solvent.

While the coordination of monoatomic anions is relatively simple with virtually only a single orientation between the ions and the solvent molecule, the situation gets significantly more complicated for complex oxygen rich anions such as NO_3^-, ClO_4^{2-}, SO_4^{2-}, PO_4^{2-} or CrO_4^{2-}. Whereas Tongraar [628] concentrated on reproducing structural and dynamical data by means of QM/MM, detailed investigations on the interactions between the central anion and individual water molecules are provided by Pribil [625, 626] and Hinteregger [624]. It has been shown that the preferred arrangement of water molecules is a threefold coordination of a single oxygen atom of the anion. Nevertheless, there are also notable amounts of structures with water molecules bridging two oxygen centres by donation of a single or both hydrogen atoms as well as structures with both water hydrogens bound to a single oxygen atom of the central ion. All of the investigated anions have structure making properties in the order $ClO_4^{2-} < SO_4^{2-} < CrO_4^{2-} < PO_4^{2-}$.

All the references mentioned so far are mostly considering the accuracy and the quality of QM/MM methods in reproducing experimental data on rather small model systems. With the established set of methods, further investigations on the interaction of ions with larger organic molecules as well as reactions involving the occurrence of charged species are now possible. Santosh [648] has investigated the interaction of transition metal ions and the glycylglycine dipeptide as model system for protein systems. They found smaller ions, such as Cu^{2+} or Zn^{2+}, to interact more strongly with the dipeptide than the larger ones, e.g. Fe^{2+}. Furthermore, the preferred interaction does not occur as naked cations, but as charged

complexes of the form $[M(H_2O)_6]^{2+}$. Real chemical reactions were in the focus of a study by Marchi investigating the solvation and ionization process of alkali metals in liquid ammonia [649]. Whereas sodium and caesium tend to dissociate into a cation and a solvated electron, lithium remains a contact-ion pair upon ionization.

3.2 QM/MM Applications of Solvent Effects for Organic Reactions

Chemical reactions and their mechanisms are central in chemical research. Especially for the clarification of reaction mechanisms, computations become more and more important. But, while nearly all chemical reactions are carried out in solvent, most calculations are still performed in the gas phase. Solvent effects are also often taken into account by continuum models but they incorporate mainly bulk effects [532, 535, 650–652]. QM/MM approaches allows a more exact description of the molecular nature of solvent and surrounding. Usually the subsystems directly involved in the reaction represent the QM part, while the solvent is taken into account within the MM part.

Jorgensen, Acevedo and coworkers carefully investigated the effects of solvation on the reactants, products and TS structures to compute the resulting influence on the rates of organic reactions [46, 653, 654]. In most investigations they used the PDDG/PM3 approach within the QM part. We have already mentioned that the accuracy of this semi-empirical approach is astonishing. This is also proven by the investigation about solvent effects, which are always in close agreement with experimental observations. It should be mentioned that in most cases only QM/MM approaches were able to reproduce the experimental trends accurately. This underlines the importance of effects connected with the molecular nature of the solvent.

To estimate the impact of these molecular solvent effects the division of solvents into protic (H-bond donor and acceptor) and aprotic (at most H-bond acceptor) ones is very helpful since the formation of specific hydrogen bonds often increases or decreases the reaction rate drastically. The rate for Kemp decarboxylations of benzisoxazole-3-carboxylic acid derivatives accelerate by a factor of about 10^8 when the solvent character changes from polar protic to polar aprotic. Hydrogen bonds between the reacting anion and the protic solvent were determined to be the most important factor for this acceleration [655, 656].

For the nucleophilic aromatic substitution reaction (S_NAr) it has been discussed whether the addition of the nucleophile, the elimination of the leaving group is the rate limiting step or if this depends on the solvent. Taking the S_NAr reaction between azide ion and 4-fluoronitrobenzene as an example, QM/MM calculations indicate that solvation effects cause the highest barrier for the elimination step. As a function of the solvent the experimental free energies of activation for these reactions are (values are given in kcal/mol): H_2O: 28.1/MeOH: 27.5/MeCN:

21.8/DMSO: 21.8. The computed counterparts with QM/MM employing the PDDG/PM3 approximation for the QM part are: H_2O: 35.3/MeOH: 27.5/MeCN: 21.1/DMSO: 19.9 [657]. In contrast B3LYP/6-311+G(2d,p) in combination with the continuum approach PCM fails to describe the strong influence of the solvent: H_2O: 27.6/MeOH: 27.9/MeCN: 27.1/DMSO: 27.9. This shows that the rate increases going from a protic (water) to dipolar aprotic (DMSO) solvent are only reproduced by the QM/MM methodology, i.e. if the molecular nature of the solvent is taken into account [657].

Acevedo and Jorgenson reviewed investigations about solvent effects on S_N2 reactions up to 2009 [46]. More recently Chen et al. studied the influence of solvation on the overall steric effects [658] and Geerke et al. characterized S_N2 reactions at nitrogen centres [659].

Ene reactions have also been investigated. The traditional ene reaction mechanism for the reaction between $_1O^2$ and tetramethylethylene contains a rate-limiting TS featuring a perepoxide, a diradical or a zwitterionic intermediate. DFT and CCSD(T) computations by Singleton, Houk, Foote et al. [660] proposed a "two-step no-intermediate" mechanism. In the QM/MM approach of Sheppard and Acevedo [511] the solute is treated by PDDG/PM3 while water as solvent is represented by the TIP4P model. The OPLS force field is used to describe a nonaqueous solvent (cyclohexane, DMSO, acetonitrile and methanol). For electrostatic contributions CM3 charges [661] were obtained for the solute-solvent energy with a scaling factor of 1.14. The study of the $_1O^2$ ene reaction shows a change in the reaction pathway from the gas-phase "two-step no-intermediate" mechanism to a stepwise reaction [511]. This happens since the charge separation present in the perepoxide intermediate is extremely sensitive to solvent polarity and hydrogen bonding ability. Hence, if the solvent polarity increases, the perepoxide becomes more stable (free energy changes, ΔG (kcal/mol) H2O: −4.3/DMSO: 1.8/cyclohexane: 5.0). This in turn increases the energy barrier for the product formation (free energy changes, ΔG (kcal/mol) H2O: −23.2/DMSO: −46.3/cyclohexane: −54.0).

A study of the reaction between 4-phenyl-1,2,4-triazoline-3,5-dione (PTAD) and tetramethylethylene also shows the solvent influence on ene reactions [662]. Initially believed to proceed via a concerted pericyclic mechanism, experiments have established that the reaction follows a stepwise route. The calculations are in good quantitative accord with experimentally measured free activation energies ($\Delta G^{\ddagger}$ (kcal/mol) MeCN exp.: 15.0 calc.: 14.9). A stepwise mechanism was confirmed and the addition of PTAD to the alkene was found to be the rate-determining step. The traditional supposed mechanism in which an aziridinium imide is formed following the rate determining TS structure could not be proven. Instead, the calculations predict that the reaction proceeds directly to an open intermediate.

QM/MM applications with Cope elimination reactions [663], numerous Diels–Alder cycloadditions and dimerizations, Claisen rearrangements and electrocyclic ring openings [664–668] indicate that effects connected with the molecular nature of the solvent influence their reaction rates as well. At first glance this is astonishing since these reactions are assumed to be rather nonpolar. Again, only the

QM/MM methodology reproduced the large rate increases in proceeding from aprotic solvents to water.

Due to its properties, water is one of the most interesting solvents. For reactions of physiological and biological relevance water is the most important solvent but also organic reactions often take place in aqueous solution. This is especially true in the area of green chemistry although nonaqueous media become more and more important. The effects of aqueous solvation on methyl-transfer reactions from dimethylammonium (A), tetramethylammonium (B) and trimethylsulfonium (C) to dimethylamine were computed with DFT, MP2, CBS-QB3 methods [669]. In the gas phase the free activation energies for reaction A are 17.9, 19.9 and 19.4 for B3LYP/6-31G(d,p), MP2/6-31+G(d,p) and CBS-QB3, respectively (all values in kcal/mol). An estimation of solvent effects by a single point B3LYP/6-31G(d) calculation in combination with the continuum approach CPCM predicts an increase of 16.9 kcal/mol. The resulting values of 34.8, 36.8 and 36.3 for B3LYP/6-31G(d,p), MP2/6-31+G(d,p) and CBS-QB3, respectively correspond nicely to the experimental value of 34.4 kcal/mol.

The PDDG/PM3 gas-phase activation enthalpies 31.3 kcal/mol differed notably from the CBS-QB3 gas phase value. QM/MM MC simulations utilizing free-energy perturbation and the PDDG/PM3 semiempirical Hamiltonian in combination with explicit TIP4P water molecules predict a solvent effect of 17.9 kcal/mol. This is comparable to the value estimated with the considerably cheaper continuum approach (16.9 kcal/mol) and shows that the molecular nature of the solvent is less important for reaction A.

For reaction B a slightly different picture emerges. Combining the CBS-QB3 gas phase result (24.8 kcal/mol) with the B3LYP/6-31 G(d)//CPCM value for solvent effects (8.2 kcal/mol) a free activation energy of 33.0 kcal/mol is obtained which is in perfect agreement with the experimental counterpart (33.5 kcal/mol). As for reaction A the PDDG/PM3 gas phase value for B (50.1 kcal/mol) deviates considerably from the CBS-QB3 counterpart. But in contrast to A the estimate of solvent effects using QM/MM MC (13.5 kcal/mol) differs from the continuum approach prediction. A combination of this value with the CBS-QB3 gas phase value leads to a worse agreement than obtained with the continuum approach. For C both estimates for the free activation barrier deviate (CBS-QB3//B3LYP/CPCM: 23.8 kcal/mol; CBS-QB3//QM/MM MC: 30.5 kcal/mol) from the experimental value (28.1 kcal/mol).

The reaction of peroxynitrite with carbon dioxide in aqueous solution shows a significant barrier in the free energy profile of the reaction in solution (exp.: ~12 kcal/mol; calc.: 12.4 kcal/mol). The barrier vanishes completely for the reaction in vacuum. This difference again results since the solvation pattern implicates the breaking and forming of several hydrogen bonds [670].

A work of Alexandrova et al. [671] addresses the decomposition of urea in neutral aqueous solution, which is most relevant as reference point for biological processes. Joint ab initio and QM/MM studies on alternative reaction pathways were carried out to identify preferred routes for the hydrolytic and ammonia-eliminative processes. The activation barrier for the direct ammonia elimination

from the QM/MM FEP calculations (36.6 kcal/mol) is somewhat higher than the reported experimental values of 28.4–32.4 kcal/mol. It is still lower than the barrier of the alternative addition–elimination mechanism (39.9 kcal/mol) [671]. This indicates that a direct elimination, which was proposed by Estiu and Merz [672], takes place.

While these reactions happen in a homogeneous solvent, reactions at interfaces are of special interest. Jung and Marcus computed the cycloaddition of quadricyclane with dimethyl azudicarboxylate [673, 674] to elucidate reasons for the remarkable catalysis taking place at the organic/water phase boundary [675]. Similar work on the aromatic Claisen rearrangement was performed by Zheng and Zhang [676] and Acevedo and Armacost [677]. The interplay between experiment, theory and computations for this interesting effect was highlighted in a recent review [678]. Radak et al. investigated the reactivity of gases with a liquid surface by simulating the scattering process of atomic fluorine with liquid squalane [679].

Ionic liquids are a unique class of solvents, generally defined as a material containing only ionic species with a melting point below 100 °C. These "designer" solvents are typically composed of organic cations and a weakly coordinating inorganic or organic anion with a diffuse negative charge [680]. Gao et al. had in the early 1990s already referred to the computation of the solvent-enhanced Menshutkin reaction, which is a good way to prepare phase transfer catalysts (PTC) and ionic liquids [681]. An interesting observation from this study is the strong change of the TS structure due to solvent effects. The MC simulation indicates that the TS of the Menshutkin reaction occurs much earlier in water than in the gas phase. Since solvent effects stabilize the products the result is in line with the Hammond postulate [9].

OPLS-AA force field parameters have been created and validated for use in the simulation of 68 unique combinations of room temperature ionic liquids. This was necessary to enable computationally accurate representation of the reaction medium for use in QM/MM calculations [680]. The newly developed force field parameters were tested for the Kemp elimination of benzisoxazole with piperidine in [BMIM][PF_6]. The calculated free energy of activation (25.2 kcal/mol) is in good agreement with the experimental value of 22.6 kcal/mol.

The solvation effect of an ionic liquid on nucleophilic substitution reactions of halides was investigated by Arantes et al. [682]. The simulations indicate that this substitution reaction is slower in the ionic liquid than in nonpolar molecular solvents. This is because the anionic reactants are more stabilized by the ionic liquid than the TS, which possesses a more delocalized electronic structure. The effect results from solute–solvent interactions in the first solvation shell which contains several hydrogen bonds. They are formed or broken in response to charge density variation along the reaction coordinate [682].

The impact of acidic and basic ionic liquid melts (1-ethyl-3-methylimidazolium chloride) on the rates of the Diels–Alder reaction between cyclopentadiene and methylacrylate has been investigated with the PDDG/PM3 method for the QM part and the OPLS force field for the solvent molecules. The ability of the ionic liquid to act as hydrogen bond donor (cation effect), moderated by its hydrogen bond

accepting ability (anion effect), has been proposed previously to explain observed *endo*/*exo* ratios [683]. Acevedo et al. investigated molecular effects which influence the TS using a QM/MM/MC approach and could relate the acceleration to specific hydrogen bonding effects [665].

Due to their importance for research but also for industrial chemistry, transition metal based catalysts are intensively investigated. Ananikov et al. [684] reviewed various applications of hybrid ONIOM methods within this field. This review involves reaction mechanisms and enantioselective reactions of transition metal complexes, e.g. Ti-catalyzed cyanation of benzaldehyde [685], Cu-catalyzed cyclopropanation [686], Mn-porphyrin catalyzed epoxidation of alkene [687], and Mo-catalyzed nitrogen activation [688]. These approaches involve QM/QM as well as QM/MM approaches.

A QM/MM study on the oxidation of a disulfide by a vanadium containing complex explains satisfactorily the remarkable dependence of the selectivity of the reaction on the nature of the ligand. The computations even quantitatively reproduce the experimental trends so that a rational design would be possible. Analysis of the computational results leads finally to the formulation of a simple model that can explain the large influence of ligands on the enantioselectivity [689].

The dihydroxylation of terminal aliphatic *n*-alkenes (propene, 1-butene, 1-pentene, 1-hexene, 1-heptene, 1-octene, 1-nonene and 1-decene) catalyzed by osmium tetroxide, a powerful method to enantioselectively introduce chiral centres into organic substrates, has been computationally studied by the hybrid QM/MM IMOMM-(B3LYP:MM3) method. The analysis of the results, in particular the partition of the total IMOMM energy into its components, allows the responsibility for the selectivity to be identified [690].

The rhodium-catalyzed asymmetric hydrogenation of prochiral enamides was investigated by Feldgus and Landis [691, 692]. They demonstrated that computational methods reproduce the α-substituent effect in enamide hydrogenation catalysis and probe how the interaction of the enamide C=C bond and the catalyst varies with the structure of the substrate. The picture that emerges emphasizes the complex interaction of both electronic (i.e. those effects that do not depend on the size of the model system) and steric effects in controlling the stereochemistry of enamide hydrogenation reactions [691, 692].

Chiral compounds have a broad range of applications as drugs, polymers, probes of biological function and new materials. Their synthesis represents an important branch of modern organic chemistry. Balcells and Maseras reviewed QM/MM studies about asymmetric catalysis. For such applications the molecular natures of solvent and catalyst have to be taken into account since *ee* rates strongly depend on the subtle interplay of the various effects. In these studies, the QM part typically includes the metal and these parts of the system which are directly involved in the reaction. Bulky chiral ligands are normally embedded within the MM part [55]. This review highlights pure QM investigations for the (1,2)-asymmetric induction in the nucleophilic addition to chiral carbonyl compounds and the proline-catalyzed asymmetric aldol reaction. They also review QM/MM studies about Diels–Alder

cycloadditions, asymmetric dihydroxylation and hydrogenation of olefins, and vanadium-catalyzed syntheses of chiral sulfoxides.

Heterogeneous catalysis is an important branch of chemistry which combines solid state physics (catalyst) with all parts of chemistry (substrate). A full description is out of range of the present review. We only want to point to some recent works on the activation of C–H bonds [42], methanol synthesis from syngas [41, 693], the partial epoxidation of alkenes [42] and the electron trapping at the oxygen terminated polar surfaces of ZnO and related surface F centres [43]. In the European project QUASI (Quantum Simulation in Industry, project EP25047) a flexible QM/MM scheme was developed [44]. It was employed to study a range of industrial problems like the catalytic decomposition of N_2O by Cu-containing zeolites, the modeling of enzyme structures and the methanol synthesis reaction catalyzed by Cu clusters deposited on ZnO surfaces. For the latter two Cu clusters and ZnO surfaces are involved in the catalytic cycle. We also want to mention some work which was performed by Sierka, Sauer and co-workers [37, 39, 694, 695].

Electron transfer (ET) reactions are important processes in chemistry and biology. Theoretical studies of processes are challenging because of the quantum nature of the processes and the complicated roles of the solvent. An ab initio QM/MM approach for electron transfer reactions based on DFT calculations with the fractional number of electrons approach (FNE) was reported by Zeng et al. [696]. With this method the oxidation free energies and the diabatic FES for the electron transfer process of Ru and Fe complexes in aqueous solution could be computed. The accurate oxidation free energies and the FES obtained from the calculation indicate that the FNE is an efficient order parameter that can be used to describe the redox reaction process and sample the solvent conformations along the reaction [696]. The method is related to the EVB method proposed by Warshel and Aqvist [169] or the ansatz of the Marcus theory.

3.3 QM/MM Based Computational Spectroscopy

Spectroscopy is the main tool to gain information about the structural properties, dynamic behaviour as well as the electronic character of molecules. Various spectroscopic techniques ranging from NMR to X-ray absorption spectroscopy exist to measure the experimental data but in most cases the interpretation of these data deserves reliable theoretical models. Theoretical chemistry approaches become more and more important in this field since they not only provide qualitative consideration as selection rules but also enable quantitative predictions. This started in the middle of the last century with computations regarding gas phase spectra of di- and triatomic molecules. The debate about the singlet-triplet gap of methylene represents a very famous example. It took about 20 years and more than 14 scientists from 7 labs from 4 countries to obtain the final answer and this final answer was only possible because theory and experiment interacted very closely [697–701]. In the 1980s and 1990s the methods for the computation

of all kinds of spectroscopy were considerably refined. Due to their increasing capabilities the computational approaches used today not only provide the spectroscopic parameters but also are able to simulate the complete spectra. In such cases deviations resulting from the extractions of parameters out of measured data are no longer present. This improves the comparison between theory and experiment since it takes place on the level of raw data so that deviations resulting from the extractions of parameters from measured data are no longer present. It also allows the clarification of the interplay between the various effects which determine the spectra.

QM/MM approaches offer the possibility to account for environmental effects and to extend the investigations to molecules or aggregates which are too large for pure QM approaches. The extension is possible since most spectroscopic processes are very local, so that a separation of the whole system into the QM and MM parts introduces negligible errors. For computations in solvents the division is quite simple and straightforward. For larger aggregates or macromolecules the borders may cut through covalent bonds. In such cases the same techniques as used for enzymes are employed.

The present review is devoted to applications in organic chemistry. For reviews of spectroscopic properties of biological systems we refer to some recent reviews [60, 62, 702–705]. Reviews of QM/MM applications in topics related to organic chemistry were, for example, provided by Barone and co-worker [541–543] in some cases together with a pedagogical introduction to the definition of various spectroscopic parameters [544] or the formulation of time-dependent and -independent approaches [541]. Bearpark et al. offered a tutorial overview of CASSCF/MM computations for larger molecules [50, 53] while, as already mentioned above, Virshup et al. provided a review of photodynamics in complex environments [131]. A review of electronic properties of disordered organic semiconductors was given by Difley et al. [546].

Before we address single applications in the field of theoretical spectroscopy we would like to discuss QM/MM approaches which are used to analyze and to interpret the experimental raw data. X-Ray data about biological systems are often refined by means of force field computations [706]. For NMR-based structure investigations of enzymes, similar concepts are used. The conclusions drawn from the underlying force field simulations are reliable as long as the force field is adapted to the bonding situation of the measured system. For unusual bonding situations problems may arise. As suggested by Ryde and coworker, such situations cannot occur if QM/MM approaches are used for the refinement, since the QM part will provide a reliable picture. It could be shown that this more flexible approach leads to considerably improved structural data [707–716]. Similar approaches were used for NMR [63, 717] and EXAFS [368, 718, 719] data. A related approach was also developed by Merz and co-workers [720].

A tool to determine the link between the shape of a Raman optical activity (ROA) spectrum and the structure of the system under investigation has been provided by Hudecova et al. [721]. They also provided the corresponding simulations for the VCD spectrum [722].

Nuclear Magnetic Resonance (NMR) represents the most important spectroscopic tool of organic chemistry to provide information about the composition and structure of a given molecule. Gas phase computations regarding the corresponding chemical shifts σ represent standard applications of theoretical chemistry [723–728]. The corresponding spin-coupling constants J are more difficult to compute but also here well developed methods are available [729–733]. NMR chemical shifts can be computed for quite large systems due to linear scaling approaches [734–736]. A discussion about the use of continuum solvent models in magnetic resonance parameter calculations were provided by Ciofini [737]. Calculations in solids and liquids using periodic boundary conditions were reviewed by Pickard and Mauri [738]. In principle also QM/MM can be used to account for environmental effects but for NMR parameters the size of the QM space strongly influences the results. This is shown by Johnson and Dilabio [739] who computed the chemical shifts for a glycine residue within a protein as a function of the size of the QM part. They found that all amino acids within a distance of 6 Å have to be included to reach convergence. In this case the slow convergence seems to result due to significant charge transfer effects which cannot be taken into account across QM/MM borders. As an indicator for convergence in such cases, they suggested the use of Mulliken atomic charges.

A similar convergency behaviour was described for ^{29}Si and ^{17}O chemical shifts of SiO_2 polymorphs [544, 740]. They showed that the ONIOM approach delivers similar values as cluster approaches when three complete atomic shells around the computed Si or O centre are included either in the cluster or in the QM part of the QM/MM approach. If only one surrounding shell is included in the QM part of the QM/MM approach, shifts computed with the ONIOM approach deviates 65 ppm from the converged value (490 ppm). The related cluster calculation which also includes only one additional shell only deviates by 15 ppm. This points to some error cancelation effects taking place in the cluster approach. This result also indicates that chemical shifts are quite local properties which do not strongly depend on long range electrostatic interactions. The authors also compared the accuracy of different DFT functionals for the ^{29}Si chemical shift tensor. The averaged errors of computed principal components were found to be 0.6, 1.9, 1.6, 1.0 and 1.7 ppm for HF, B3LYP, PBE0, M05-2X and CAM-B3LYP, respectively. This agreement is excellent but not found for all silicon-containing compounds. For substituted silanes, Heine et al. [741] found, for example, that the deviation between theory and experiment increases with an increasing number of hydrogen atoms bound to the silicon centre. For these compounds, B3LYP performs considerably better than HF. More information about the accuracy of theoretical methods for the computation of chemical shifts and spin–spin coupling constants can be taken from recent reviews provided by van Wüllen [742], Gauss and Stanton [743] and Helgaker and Pecul [744].

Tests regarding the ability of current computational approaches to reproduce ^{51}V NMR properties were provided by Bjornsson et al. [745, 746]. They predicted a small gas-to-liquid shift for the isotropic shielding constants. This again indicates that environmental effects on NMR shifts are well captured by cluster approaches. Gester et al. [747] investigated the gas-to-liquid shift for liquid ammonia.

Considering only one ammonia molecule in an electrostatic embedding predicts a wrong sign for the chemical shift. If solvent molecules are included in the QM part a correct sign is obtained and the computed vapor-to-liquid shift (−25.2 ppm) is in good agreement with experiment (−22.6 ppm). For the coupling parameter between N and H [J(N,H)] the vapor-to-liquid shift is negligible since geometrical relaxation and pure solvent effects cancel each other.

The interactions of the electron spin **S** with the spins of the nuclei $\mathbf{I_N}$ and an external magnetic field **B** lead to the EPR spectrum [748–750]. Due to the sensitivities of the connected parameters it presents an important tool to obtain information about the geometrical arrangements, the electronic structure (e.g. spin distribution) and tautomeric and isomeric forms of a radical under consideration. However, since the relations are not clear-cut, such information can only be gained from investigations in which theory and experiment closely interact. An overview of different aspects of modern EPR spectroscopy offers a recent themed issue in PCCP [751].

The electronic g-tensor describes the Zeeman effect (**S** with **B**) which leads to the splitting of the $(2S+1)M_S$ magnetic sublevels [748–750]. In the 1970s pioneering work on the general theory and computations about the g-tensor were presented by McWeeny and Harriman [748, 752]. Modern computations of the g-tensor were first presented by Grein and Lushington [753–755]. They used truncated sums over states approaches together with restricted open shell Hartree–Fock and multireference configuration-interaction wave functions to compute the g-tensor up to second order [753–755]. Since this approach is quite expensive, DFT approaches were used to compute larger systems [725, 756–758]. The various developments of wave function based approaches for the computation of the g-tensor underline the importance of this topic [759–767]. New coupled cluster based approaches recently presented by Gauss et al. [768] allow benchmark computations for the g tensor to elucidate the accuracy of less sophisticated approaches. In line with previous results they showed that HF approaches are not sufficiently accurate for qualitative predictions for small molecules containing light atoms. In the framework of DFT, the B3LYP functional seems to be best suited while BP86, for example, is considerably worse. Investigations of the suitability of DFT functionals were also performed by Abuznikov et al. [769–771].

The interaction between **S** and the spins of the nuclei $\mathbf{I_N}$ is described by the isotropic hyperfine coupling constant A_{iso} and the anisotropic hyperfine tensor A_{DIP} which are obtained for each nucleus **N** [748–750]. A_{iso} represents the spin-density at a given magnetic nuclei. It is difficult to compute for radicals with singly occupied π-orbitals and doubly occupied σ-type orbitals. In such cases A_{iso} solely results from correlation effects since the direct contributions from the singly occupied π-orbitals vanish due to their nodal plane at the nucleus [84, 772–775]. Furthermore, the contributions from the various closed shells are often similar in size but differ in sign [83, 776–779]. DFT approaches provide considerably better agreement with the experimental values [769–771, 780–784]. However, this success may arise from error cancelation since the agreement is not consistently found in all cases [785–788]. Molecules with singly occupied σ-type orbitals have

large positive contributions already from the singly occupied orbitals so that they are easier to compute. In many cases, vibrational effects cannot be neglected [789–794] especially if the movement of the nuclei leads to a coupling between two or more electronic states [777, 795, 796].

Reviews about their recent work in the field of theoretical EPR spectroscopy were provided by Barone and coworker [541, 542, 544]. The authors used the general liquid optimized boundary (GLOB) model [541, 797–801] to account for environmental effects and also took the influence of vibrational motions into account. In the GLOB model the complete system is divided into an explicit part which is embedded into a suitable cavity of a dielectric continuum. The explicit part consists of the solute along with a few solvent molecules. The interactions between this subsystem and the continuum account for long-range electrostatic and short-range dispersion-repulsion contributions. While the influence of the former on the explicitly treated part of the system is taken into account in line with the COSMO approach [532, 535, 802], the latter is presented as a classical mean force not perturbing the electronic density of the explicitly treated part. If the explicit part is treated with QM methods, the approach is very related to a usual continuum approach; however, additional short-range repulsion interactions are taken into account. If the inner part is described by QM/MM, the approach becomes related to the methods of Benighaus and Thiel [432] described above. They neglect short range effects but use considerably larger inner parts.

Barone and coworker employed their methods to determine the most stable tautomer of the uracil radical [803]. Pure energy computations employing B3LYP/6-31+G(2d,2p) in combination with the CPCM model [651, 804–806] predicted the wrong stability sequence but a comparison between experimental and theoretical EPR parameters [803, 807] definitely came to the right conclusion. This work shows the influence of solvent and dynamical effects but it also elucidates that they cancel each other quite often. In such cases simple gas-phase calculations are sufficiently accurate. This also seems to be true for uracil and aliphatic and aromatic nitroxides. For these investigations [544, 789, 793, 808–819] and recent biologically oriented works, we refer to the literature [60, 94, 820, 821]. The paper of Bernini et al. [822] is also biologically oriented but it allows an insight into the possibilities of DFT-based approaches to assign EPR experiments. They computed the EPR parameters of tryptophan and tyrosyl radical intermediates involved in the catalytic cycle of the *Pleurotus eryngii* peroxidase and its W164Y variant, respectively for calibration purposes of a B3LYP/CHARMM approach. The study indicates that a comparison of experimental EPR parameters with the related computed data obtained for different geometrical arrangements of a given hydrogen bonding network is able to elucidate the structure of the network if all values obtained for various centres are included in the analysis. Pure energy computations would be too uncertain because the corresponding differences are too small. In their approach, the deviations between the computed and the measured data are in the range of 0–20%. Approximations based on PCM or vacuum computations which include one water molecule to account for molecular solvent effects are not sufficiently accurate. The authors also compare different levels of theory within the QM part.

An insight into the slow convergence of a selected Multi-Reference Møller Plesset Perturbation (MRPT) based approach [823] as a function of the underlying CAS space is provided by Mattar and Durelle using the 4,5-dihydro-1,3,2-dithiazolyl radical as a typical example [824]. The MRPT based approaches converge slowly as a function of the CAS space. Therefore, the question arises as to whether the influence of the neglected configurations on the coefficients of the selected configuration might be important. A similar observation was made earlier for A_{iso} [84, 825]. The UB1LYP functional [826] provides values which deviate similarly to the MRPT data. However, while MRPT overestimates the g-values, UB1LYP underestimates them.

Vibrational spectroscopy is an important tool to obtain information about the secondary structure of proteins [827]. The ability to relate protein conformations to infrared vibrational bands was established very early in the pioneering work of Elliot and Ambrose before any detailed X-ray results were available [828]. Vibrational circular dichroism (VCD) provides sensitive data about the main chain conformation [829, 830]. The Raman optical activity (ROA) signal results from sampling of different modes but is especially sensitive to aromatic side chains [831, 832]. A theoretical prediction for the ROA phenomenon was developed by Barron and Buckingham [833, 834], and the first ROA spectra were measured by Barron, Bogaard and Buckingham [835, 836]. First ab initio predictions were provided by Polavarapu [837]. In 2003, Jalkanen et al. showed that DFT approaches in combination with explicit water molecules and a continuum model reproduce the experimental spectra much better [838]. DFT-based approaches to VCD spectra were, for example, pioneered by Stephens et al. [839]. To extract the local structural information provided by ROA, Hudecova et al. [721] developed multiscale QM/MM simulation techniques.

Kaminski et al. extended the SCC-DFTB method for the calculation of vibrational Raman spectra employing the Fourier Transform of Time-Correlation Function (FTTCF) formalism [327]. The molecular polarizability was accessed via second order numeric derivatives with respect to the components of an external electric field during MD simulations. The new approach is compared to the standard normal mode analysis at the same and at higher levels of theory (BLYP/aug-cc-pVTZ). For ten small organic compounds good agreement is found but for QM/MM test calculations of L-phenylalanine in aqueous solution larger deviations are observed.

A new approach to simulate multidimensional infrared spectroscopy was suggested by Jeon and Cho [840]. They compute the third-order vibrational response function in the classical limit using MD simulations in combination with QM/MM. In this investigation it could be shown that QM/MM approaches are needed for reliable predictions. Conventional classical force fields are too inaccurate since they cannot describe the intramolecular vibrational anharmonicities which are essential for the production of the nonlinear signal. QM/MM force fields are found to reproduce 2D spectra for *N*-methylacetamide and carbon monoxide, each solvated in water, in nice agreement with their experimental counterparts.

ONIOM based approaches employing QM/QM or QM/MM schemes were used to describe the vibrational spectra of some molecules of biological interest [841] and of boldine hydrochloride [842]. Further examples of the computation of vibrational spectra with QM/MM approaches are reviewed in recent overviews of Barone and co-worker [541, 544]. A description of state-of-the-art modeling of IR spectra to elucidate secondary-structure information of peptides and proteins is provided by Amadei et al. [843, 844].

UV-Vis and VUV spectroscopy offer important insights into the electronic structure of molecules. Absorption processes normally induce vertical excitations so that the spectra provide information about the nature of the electronically excited state and the shape of the corresponding PESs in the vicinity of the ground state equilibrium geometry. Since the shape of the PES of the ground state does not necessarily resemble the shape of the electronically excited states, such absorption induces nuclear motions leading to reorganization of the molecule. In most cases, this reorganization happens on the surface of the lowest lying electronically excited state since populations of higher lying states are very fast quenched to the lowest excited state [126, 129, 845]. The emission processes back to the ground state then take place from local minima on this surface. Hence, in contrast to the absorption spectra, emission spectra provide information about the PES of the electronically excited state in the vicinity of its local minima.

As a consequence, the description of absorption spectra is considerably easier than the simulation of emission spectra since the latter has to include the description of the photo-physical processes taking place after the excitation [126, 129, 845, 846]. A careful discussion of the various QM/MM applications to electronically excited states deserves at least its own review and would be out of the scope of the present one. Hence, we only list a few applications which might be of interest to provide a starting point for further reading. Again we will mainly focus on publications newer than 2008.

The already mentioned recent overviews of Barone and co-workers [541, 544] also contain information about recent computations of vibrationally resolved absorption spectra including environmental effects. Recent developments and applications of TD-DFT in combination with Car–Parrinello dynamics for the description of photochemical processes in complex systems were described by Moret et al. [116, 847] and Buda [848]. We have also already mentioned recent works of Bearpark, Robb et al. [50, 134–136] and Martinez and co-worker [103, 131, 133]. For recent applications concerning biologically oriented questions we again refer to the excellent review of Senn and Thiel [60] and some other works [702–704].

Many investigations are concerned with the description of the photophysics of biologically related molecules like amino acids or nucleic bases. Examples are investigations of uracil, cytosine, or guanine [108, 849–851], glycine [852] and poly-glutamic acid [853] to mention a few. The excitation energies were obtained from MR-CI approaches [849, 850, 852], TD-DFT using the CAM-B3LYP functional [851] or the conventional B3LYP functional [108]. The CC2 approach and the DFT/MRCI approach of Grimme and Waletzke [854] were also employed

[851]. Most investigations provide information about the size of the solvent effects and careful evaluations of the accuracy of the underlying QM approach.

Similar works were performed for the description of the photo-physics of formamide in an Ar matrix [855], the nonadiabatic deactivation of azomethane in gas phase, water and *n*-hexane [856], the *cis–trans* isomerization of *N*-methyl-acetamide in water [516] and the ultrafast nonadiabatic dynamics of NaI in a water cluster [857]. By comparing to an older work of Koch et al. [857] the latter study allows an insight into the importance of polarizable force fields for the description of charge-transfer (CT) states. Solvent effects on the vertical spectra of small carbonyl compounds were computed by Malaspina et al. [858], Nielsen et al. [859] and Lin and Gao [860]. Using CASSCF approaches in combination with the solvent model based on the polarizable NEMO force field [861], Hermida-Ramon et al. studied the influence of water as a solvent on the balance between zwitterionic and biradical valence structures of methylene peroxide [862].

3.4 Summary and Perspectives

The present review highlights recent progress in the QM/MM approach and summarizes newer applications in theoretical organic chemistry. Most of them underline that it is important to account for the molecular nature of the environment (solvent or catalyst) but some cases also show that conventional approaches employing pure QM with a continuum approach is at least sufficiently accurate. In some cases they are even more accurate than the considerably more expensive QM/MM approach. This indicates that, despite the rapid progress in QM/MM methodology, some improvements are still needed.

A strong progress will result from improvements in the QM and the MM methodology. Due to better hardware and software in future, considerably improved methods can be used for the QM and the MM part and it can be predicted that polarizable force fields will become standard. Another improvement will result from the number of layers. In most present QM/MM computations the whole world only consists of the QM and MM part. In future, this strict black and white world will be displaced by multi-layered simulations as is already possible in the ONIOM approach. They perhaps include different levels of quantum-chemical methods together with MM parts, possibly consisting of a polarizable force field around the outer QM level followed by a non-polarizable force field and completed by a continuum approach to describe also the long range electrostatic effects correctly. Some approaches are already known but they are not yet standard. Related with this we assume that methods like frozen-density embedding schemes will change from niche products to standard approaches in this field.

To describe structure and dynamics of complex biological systems like ion channels or membranes, combinations between the atomistic views of standard QM/MM approaches and coarse grained models are highly desirable. The future will show to what extent such approaches will also be helpful in theoretical organic

chemistry, e.g. to improve the description of the dynamics of macromolecules. For their treatments more efficient methods for sampling are also needed. They are even more important for macromolecules than for biologically oriented studies. The latter can start from X-ray structures which are mostly not available for macromolecules, thin films or amorphous material. The necessary determination of the global minimum and all thermally accessible structures is still a problem which is only partially solved despite the progress described in this work.

We have highlighted some recent developments for adaptive schemes in which the QM part is not fixed for the whole computation but can adapt to the problem. They are essential for CT processes but they would also lead to more reliable descriptions of the interactions between a metal surface and organic compounds. The higher reliability results since such adaptive schemes can better account for the effects of charge transfers. This is especially important for the description of heterogeneous catalysis. In this respect, also the improved description of metal surfaces is standing on the wish list.

As in all fields of theoretical chemistry, for QM/MM the calibration of theoretical approximation is also very important. However, the situation is not as simple as for gas phase computations of small molecules. The experimental determination of accurate relative energies and activation energies is difficult so that it is not easy to estimate the reliability of computed energy data. Comparisons of measured and computed geometrical parameters are also not clear cut, since X-ray data of large, very flexible molecules only give a picture for the crystal which does not necessarily equal the situation in the solvent in which the reaction takes place. Additionally it is even more problematic to compare geometrical data about the orientation of solvent molecules. In this respect, the simulation of spectroscopic data ranging from NMR to X-ray absorption spectra will become more and more important to validate the accuracy of a given theoretical approach.

Finally, we would like to point out that a great step towards more accurate calculations on more complex systems will result from electronic entertainment devices. The desperate wish for more and more detailed graphical representations enforces the development of more and more powerful graphic processing units (GPU). At the moment only a few programs can fully exploit the advantages resulting from their highly parallel architecture. The resulting advantages can be seen in the NAMD program package, which takes full advantage of this architecture. Using the new parallelized code on four GTX 480 GPU leads to an acceleration of 10 with respect to 8 Nehalem CPUs (2.9 GHz). This indicates another increase of computer power for the next few years. Bearing this advantage in mind it is easy to predict that the importance of theory will further increase in future. It can be foreseen that QM/MM will also become more standard in theoretical organic chemistry, although the necessary computations are more difficult than pure QM computations.

Acknowledgement Financial support by the DFG (Deutsche Forschungsgemeinschaft) in the framework of the SFB 630 and the GRK1221 and by the Volkswagen Stiftung is gratefully acknowledged.

References

1. Himo F (2006) Quantum chemical modeling of enzyme active sites and reaction mechanisms. Theor Chem Acc 116:232–240
2. Siegbahn PEM, Blomberg MRA (2000) Transition-metal systems in biochemistry studied by high-accuracy quantum chemical methods. Chem Rev 100:421–437
3. Siegbahn PEM, Borowski T (2006) Modeling enzymatic reactions involving transition metals. Acc Chem Res 39:729–738
4. Hu LH et al (2009) Do quantum mechanical energies calculated for small models of protein-active sites converge? J Phys Chem A 113:11793–11800
5. Warshel A, Levitt M (1976) Theoretical studies of enzymic reactions - dielectric, electrostatic and steric stabilization of carbonium-ion in reaction of lysozyme. J Mol Biol 103:227–249
6. Field MJ, Bash PA, Karplus M (1990) A combined quantum-mechanical and molecular mechanical potential for molecular-dynamics simulations. J Comput Chem 11:700–733
7. Brooks BR et al (2009) CHARMM – Chemistry at HARvard Macromolecular Mechanics (22 and higher) available at: http://www.charmm.org
8. ISI Web of Knowledge at http://www.isiknowledge.com. Accessed 2011
9. Gao J (1996) Hybrid quantum and molecular mechanical simulations: an alternative avenue to solvent effects in organic chemistry. Acc Chem Res 29:298–305
10. Gao J (2007) Methods and applications of combined quantum mechanical and molecular mechanical potentials. In: Lipkowitz KB, Boyd DB (eds) Reviews in computational chemistry. Wiley, New York
11. Cunningham MA, Bash PA (1997) Computational enzymology. Biochimie 79:687–689
12. Gao J (1998) Hybrid quantum mechanical/molecular mechanical (QM/MM) methods. In: Schleyer PV et al (eds) Encyclopedia of computational chemistry. Wiley, Chichester
13. Amara P, Field MJ (1998) Combined Q/M. In: Schleyer PV et al (eds) Encyclopedia of computational chemistry. Wiley, Chichester
14. Ruiz-López MF, Rivail J-L (1998) Combined quantum mechanics and molecular mechanics approaches to chemical and biochemical reactivity. In: Schleyer PV et al (eds) Encyclopedia of computational chemistry. Wiley, Chichester
15. Merz KMJ, Stanton RV (1998) Divide and conquer for semiempirical MO methods. In: Schleyer PV (ed) Encyclopedia of computational chemistry. Wiley, Chichester
16. Friesner RA, Beachy MD (1998) Quantum mechanical calculations on biological systems. Curr Opin Struct Biol 8:257–262
17. Beck B, Clark T (1998) Some biological applications of semiempirical MO theory. Perspect Drug Discov 9–11:131–159
18. Mordasini TZ, Thiel W (1998) Combined quantum mechanical and molecular mechanical approaches. Chimia 52:288–291
19. Monard G, Merz KM (1999) Combined quantum mechanical/molecular mechanical methodologies applied to biomolecular systems. Acc Chem Res 32:904–911
20. Hillier IH (1999) ChemInform abstract: chemical reactivity studied by hybrid QM/MM methods. ChemInform 30:45–52
21. Amara P, Field MJ (1999) Hybrid potentials for large molecular systems. In: Leszczynski J (ed) Computational molecular biology. Elsevier, Amsterdam
22. Bruice TC, Kahn K (2000) Computational enzymology. Curr Opin Chem Biol 4:540–544
23. Sherwood P (2000) Hybrid quantum mechanics/molecular mechanics approaches. In: Grotendorst J (ed) Modern methods and algorithms of quantum chemistry 2. John von Neumann Institute of Computing, Jülich
24. Lyne PD, Walsh OA (2001) Computer simulation of biochemical reactions with QM-MM methods. In: Becker OM et al (eds) Computational biochemistry and biophysics. Decker, New York

25. Mulholland AJ (2001) The QM/MM approach to enzymatic reactions. In: Eriksson LA (ed) Theoretical biochemistry: processes and properties of biological systems. Elsevier, Amsterdam
26. Field MJ (2002) Simulating enzyme reactions: challenges and perspectives. J Comput Chem 23:48–58
27. Gogonea V (2002) The QM/MM method. An overview. Internet Electron J Mol Des 1:173–184
28. Gao JL, Truhlar DG (2002) Quantum mechanical methods for enzyme kinetics. Annu Rev Phys Chem 53:467–505
29. Monard G et al (2003) Determination of enzymatic reaction pathways using QM/MM methods. Int J Quantum Chem 93:229–244
30. Ridder L, Mulholland AJ (2003) Modeling biotransformation reactions by combined quantum mechanical/molecular mechanical approaches: from structure to activity. Curr Top Med Chem 3:1241–1256
31. Náray-Szabó G, Berente I (2003) Computer modelling of enzyme reactions. J Mol Struct THEOCHEM 666–667:637–644
32. Ryde U (2003) Combined quantum and molecular mechanics calculations on metalloproteins. Curr Opin Chem Biol 7:136–142
33. Kästner J (2011) QM/MM: Quantenmechanik und empirische Kraftfelder. Nachr Chem 59:286–288
34. Zhang R et al (2010) A guide to QM/MM methodology and applications. In: Sabin JR, Brandas E (eds) Advances in quantum chemistry. Elsevier Academic, San Diego
35. Chen X et al (2011) Reaction pathway and free energy profile for butyrylcholinesterase-catalyzed hydrolysis of acetylcholine. J Phys Chem B 115:1315–1322
36. van der Kamp MW et al (2008) Biomolecular simulation and modelling: status, progress and prospects. J R Soc Interface 5:S173–S190
37. Sierka M, Sauer J (2005) Hybrid quantum mechanics/molecular mechanics methods and their application. In: Yip S (ed) Handbook of materials modeling. Springer, Dordrecht
38. Eichler U, Kolmel CM, Sauer J (1997) Combining ab initio techniques with analytical potential functions for structure predictions of large systems: method and application to crystalline silica polymorphs. J Comput Chem 18:463–477
39. Sauer J, Sierka M (2000) Combining quantum mechanics and interatomic potential functions in ab initio studies of extended systems. J Comput Chem 21:1470–1493
40. Sherwood P et al (1997) Computer simulation of zeolite structure and reactivity using embedded cluster methods. Faraday Discuss 106:79–92
41. French SA et al (2003) Identification and characterization of active sites and their catalytic processes - the Cu/ZnO methanol catalyst. Top Catal 24:161–172
42. Catlow CRA et al (2005) Computational approaches to the determination of active site structures and reaction mechanisms in heterogeneous catalysts. Philos T R Soc A 363:913–936
43. Sokol AA et al (2004) Hybrid QM/MM embedding approach for the treatment of localized surface states in ionic materials. Int J Quantum Chem 99:695–712
44. Sherwood P et al (2003) QUASI: a general purpose implementation of the QM/MM approach and its application to problems in catalysis. J Mol Struct-Theochem 632:1–28
45. Bernstein N, Kermode JR, Csanyi G (2009) Hybrid atomistic simulation methods for materials systems. Rep Prog Phys 72:1–25
46. Acevedo O, Jorgensen WL (2010) Advances in quantum and molecular mechanical (QM/MM) simulations for organic and enzymatic reactions. Acc Chem Res 43:142–151
47. Hu H, Yang WT (2009) Development and application of ab initio QM/MM methods for mechanistic simulation of reactions in solution and in enzymes. J Mol Struct-Theochem 898:17–30
48. Rode BM et al (2005) Coordination and ligand exchange dynamics of solvated metal ions. Coord Chem Rev 249:2993–3006

49. Hu H, Yang WT (2008) Free energies of chemical reactions in solution and in enzymes with ab initio quantum mechanics/molecular mechanics methods. Annu Rev Phys Chem 59:573–601
50. Bearpark MJ et al (2007) CASSCF calculations for photoinduced processes in large molecules: choosing when to use the RASSCF, ONIOM and MMVB approximations. J Photochem Photobiol A 190:207–227
51. Bearpark MJ et al (2006) Excited states of conjugated hydrocarbons using the molecular mechanics-valence bond (MMVB) method: Conical intersections and dynamics. Theor Chem Acc 116:670–682
52. Garavelli M (2006) Computational organic photochemistry: strategy, achievements and perspectives. Theor Chem Acc 116:87–105
53. Blancafort L et al (2005) Computational investigations of photochemical reaction mechanisms. In: Kutateladze AG (ed) Computational methods in photochemistry. Taylor & Francis, Boca Raton
54. Corbeil CR, Moitessier N (2010) Theory and application of medium to high throughput prediction method techniques for asymmetric catalyst design. J Mol Catal A-Chem 324:146–155
55. Balcells D, Maseras F (2007) Computational approaches to asymmetric synthesis. New J Chem 31:333–343
56. Maldonado AG, Rothenberg G (2010) Predictive modeling in homogeneous catalysis: a tutorial. Chem Soc Rev 39:1891–1902
57. Menikarachchi LC, Gascon JA (2010) QM/MM approaches in medicinal chemistry research. Curr Top Med Chem 10:46–54
58. Gao JL, Thompson MA (1998) Combined quantum mechanical and molecular mechanical methods. American Chemical Society, Washington
59. Senn HM, Thiel W (2007) QM/MM studies of enzymes. Curr Opin Chem Biol 11:182–187
60. Senn HM, Thiel W (2009) QM/MM methods for biomolecular systems. Angew Chem Int Ed 48:1198–1229
61. Lin H, Truhlar DG (2007) QM/MM: what have we learned, where are we, and where do we go from here? Theor Chem Acc 117:185–199
62. Senn HM, Thiel W (2007) QM/MM methods for biological systems. In: Reiher M (ed) Atomistic approaches in modern biology: from quantum chemistry to molecular simulations. Springer, Berlin
63. Hsiao YW, Drakenberg T, Ryde U (2005) NMR structure determination of proteins supplemented by quantum chemical calculations: detailed structure of the Ca^{2+} sites in the EGF34 fragment of protein S. J Biomol NMR 31:97–114
64. Lennartz C et al (2002) Enzymatic reactions of triosephosphate isomerase: a theoretical calibration study. J Phys Chem B 106:1758–1767
65. Jensen F (2007) Introduction to computational chemistry. Wiley, Chichester
66. Cramer CJ (2003) Essentials of computational chemistry. Wiley, Chichester
67. Koch W, Holthausen MC (2001) A chemist's guide to density functional theory. Wiley-VCH, Weinheim
68. Sousa SF, Fernandes PA, Ramos MJ (2007) General performance of density functionals. J Phys Chem A 111:10439–10452
69. Szabo A, Ostlund NS (1996) Modern quantum chemistry. Dover Publications, Inc, New York
70. Helgaker T, Jorgensen P, Olsen J (2000) Molecular electronic-structure theory. Wiley, Chichester
71. Schutz M, Manby FR (2003) Linear scaling local coupled cluster theory with density fitting. Part I: 4-external integrals. Phys Chem Chem Phys 5:3349–3358
72. Werner HJ, Manby FR, Knowles PJ (2003) Fast linear scaling second-order Moller-Plesset perturbation theory (MP2) using local and density fitting approximations. J Chem Phys 118:8149–8160

73. Schutz M (2002) A new, fast, semi-direct implementation of linear scaling local coupled cluster theory. Phys Chem Chem Phys 4:3941–3947
74. Werner HJ, Manby FR (2006) Explicitly correlated second-order perturbation theory using density fitting and local approximations. J Chem Phys 124:12
75. Claeyssens F et al (2006) High-accuracy computation of reaction barriers in enzymes. Angew Chem Int Ed 45:6856–6859
76. Mata RA et al (2008) Toward accurate barriers for enzymatic reactions: QM/MM case study on p-hydroxybenzoate hydroxylase. J Chem Phys 128:8
77. Mulholland AJ (2007) Chemical accuracy in QM/MM calculations on enzyme-catalysed reactions. Chem Cent J 1:5
78. Torrie GM, Valleau JP (1974) Monte-Carlo free-energy estimates using non-Boltzmann sampling - Application to subcritical Lennard-Jones fluid. Chem Phys Lett 28:578–581
79. Valleau JP, Torrie GMA (1977) A guide for Monte Carlo for statistical mechanics. In: Berne BJ (ed) Statistical mechanics. Plenum, New York
80. Ridder L et al (2002) Quantum mechanical/molecular mechanical free energy simulations of the glutathione S-transferase (M1-1) reaction with phenanthrene 9,10-oxide. J Am Chem Soc 124:9926–9936
81. Senn HM, Thiel S, Thiel W (2005) Enzymatic hydroxylation in p-hydroxybenzoate hydroxylase: a case study for QM/MM molecular dynamics. J Chem Theory Comput 1:494–505
82. Engels B, Peyerimhoff SD (1989) Theoretical-study of FC_2H_4. J Phys Chem-Us 93:4462–4470
83. Peric M, Engels B, Peyerimhoff SD (1995) Ab initio study of the Renner-Teller effect in the $X^2\Pi_u$ electronic-state of $B_2H_2^+$. J Mol Spectrosc 171:494–503
84. Engels B (1994) A detailed study of the configuration selected multireference configuration-interaction method combined with perturbation-theory to correct the wave-function. J Chem Phys 100:1380–1386
85. Muhlhauser M et al (1994) Ab-initio investigation of the stability of Si_3C_3 clusters and their structural and bonding features. Z Phys D Atom Mol Cl 32:113–123
86. Musch PW et al (2002) On the regioselectivity of the cyclization of enyne-ketenes: a computational investigation and comparison with the Myers-Saito and Schmittel reaction. J Am Chem Soc 124:1823–1828
87. Schmittel M et al (1998) Two novel thermal biradical cyclizations in theory and experiment: new synthetic routes to 6H-indolo 2,3-b quinolines and 2-amino-quinolines from enyne-carbodiimides. Angew Chem Int Ed 37:2371–2373
88. Schmittel M et al (2001) Ring size effects in the C^2-C^6 biradical cyclisation of enyne-allenes and the relevance for neocarzinostatin. J Chem Soc Perkin Trans 2 1331–1339
89. Engels B et al (1998) Regioselectivity of biradical cyclizations of enyne-allenes: influence of substituents on the switch from the Myers-Saito to the novel C^2-C^6 cyclization. Angew Chem Int Ed 37:1960–1963
90. Christl M, Engels B (2009) Stable five-membered-ring allenes with second-row elements only: not allenes, but zwitterions. Angew Chem Int Ed 48:1538–1539
91. Schoneboom JC et al (2003) Computational assessment of the electronic structure of 1-azacyclohexa-2,3,5-triene (3 delta(2)-1H-pyridine) and its benzo derivative (3 delta(2)-1H-quinoline) as well as generation and interception of 1-methyl-3 delta(2)-1H-quinoline. Chem-Eur J 9:4641–4649
92. Engels B et al (2002) Cycloallenes. Part 17. Computational assessment of the electronic structures of cyclohexa-1,2,4-triene, 1-oxacyclohexa-2,3,5-triene (3 delta(2)-pyran), their benzo derivatives, and cyclohexa-1,2-diene. An experimental approach to 3 delta(2)-pyran. J Am Chem Soc 124:287–297
93. Musch PW, Engels B (2001) The importance of the ene reaction for the C^2-C^6 cyclization of enyne-allenes. J Am Chem Soc 123:5557–5562

94. Shaik S et al (2010) P450 enzymes: their structure, reactivity, and selectivity-modeled by QM/MM calculations. Chem Rev 110:949–1017
95. Sit PHL et al (2010) Quantum mechanical and quantum mechanical/molecular mechanical studies of the iron-dioxygen intermediates and proton transfer in superoxide reductase. J Chem Theory Comput 6:2896–2909
96. Scherlis DA et al (2007) Simulation of heme using DFT+U: a step toward accurate spin-state energetics. J Phys Chem B 111:7384–7391
97. Cococcioni M, de Gironcoli S (2005) Linear response approach to the calculation of the effective interaction parameters in the LDA+U method. Phys Rev B 71:16
98. Kulik HJ et al (2006) Density functional theory in transition-metal chemistry: a self-consistent Hubbard U approach. Phys Rev Lett 97:4
99. Bikiel DE et al (2006) Modeling heme proteins using atomistic simulations. Phys Chem Chem Phys 8:5611–5628
100. Sit PHL, Cococcioni M, Marzari N (2007) Car-Parrinello molecular dynamics in the DFT+U formalism: structure and energetics of solvated ferrous and ferric ions. J Electroanal Chem 607:107–112
101. Toniolo A et al (2004) QM/MM connection atoms for the multistate treatment of organic and biological molecules. Theor Chem Acc 111:270–279
102. Toniolo A, Granucci G, Martinez TJ (2003) Conical intersections in solution: a QM/MM study using floating occupation semiempirical configuration interaction wave functions. J Phys Chem A 107:3822–3830
103. Martinez TJ (2006) Insights for light-driven molecular devices from ab initio multiple spawning excited-state dynamics of organic and biological chromophores. Acc Chem Res 39:119–126
104. Marques MAL, Rubio A (2009) Time-dependent density-functional theory. Phys Chem Chem Phys 11:4436
105. Dreuw A, Head-Gordon M (2005) Single-reference ab initio methods for the calculation of excited states of large molecules. Chem Rev 105:4009–4037
106. Caricato M et al (2009) Using the ONIOM hybrid method to apply equation of motion CCSD to larger systems: benchmarking and comparison with time-dependent density functional theory, configuration interaction singles, and time-dependent Hartree-Fock. J Chem Phys 131:12
107. Dinh PM, Reinhard PG, Suraud E (2010) Dynamics of clusters and molecules in contact with an environment. Phys Rep 485:43–107
108. Parac M et al (2010) QM/MM calculation of solvent effects on absorption spectra of guanine. J Comput Chem 31:90–106
109. Sanchez-Garcia E, Doerr M, Thiel W (2010) QM/MM Study of the absorption spectra of DsRed.M1 chromophores. J Comput Chem 31:1603–1612
110. Yanai T, Tew DP, Handy NC (2004) A new hybrid exchange-correlation functional using the Coulomb-attenuating method (CAM-B3LYP). Chem Phys Lett 393:51–57
111. Peach MJG et al (2006) Assessment of a Coulomb-attenuated exchange-correlation energy functional. Phys Chem Chem Phys 8:558–562
112. Rohrdanz MA, Herbert JM (2008) Simultaneous benchmarking of ground- and excited-state properties with long-range-corrected density functional theory. J Chem Phys 129:034107
113. Fan P-D, Valiev M, Kowalski K (2008) Large-scale parallel calculations with combined coupled cluster and molecular mechanics formalism: excitation energies of zinc-porphyrin in aqueous solution. Chem Phys Lett 458:205–209
114. Dreuw A, Head-Gordon M (2004) Failure of time-dependent density functional theory for long-range charge-transfer excited states: the zincbacteriochlorin-bacterlochlorin and bacteriochlorophyll-spheroidene complexes. J Am Chem Soc 126:4007–4016
115. Tozer DJ et al (1999) Does density functional theory contribute to the understanding of excited states of unsaturated organic compounds? Mol Phys 97:859–868

116. Moret ME et al (2005) Quantum mechanical/molecular mechanical (OM/MM) car-parrinello simulations in excited states. Chimia 59:493–498
117. Grimm S, Nonnenberg C, Frank I (2003) Restricted open-shell Kohn-Sham theory for pi-pi(*) transitions. I. Polyenes, cyanines, and protonated imines. J Chem Phys 119:11574–11584
118. Nonnenberg C, Grimm S, Frank I (2003) Restricted open-shell Kohn-Sham theory for pi-pi(*) transitions. II. Simulation of photochemical reactions. J Chem Phys 119:11585–11590
119. Rohrig UF et al (2003) QM/MM Car-Parrinello molecular dynamics study of the solvent effects on the ground state and on the first excited singlet state of acetone in water. Chemphyschem 4:1177–1182
120. Masson F et al (2009) A QM/MM investigation of thymine dimer radical anion splitting catalyzed by DNA photolyase. Chemphyschem 10:400–410
121. Langer H, Doltsinis NL (2003) Excited state tautomerism of the DNA base guanine: a restricted open-shell Kohn-Sham study. J Chem Phys 118:5400–5407
122. Ben-Nun M, Quenneville J, Martinez TJ (2000) Ab initio multiple spawning: photochemistry from first principles quantum molecular dynamics. J Phys Chem A 104:5161–5175
123. Ben-Nun M, Martinez TJ (2002) Ab initio quantum molecular dynamics. In: Prigogine I, Rice SA (eds) Advances in chemical physics. Wiley, New York
124. Manthe U, Koppel H (1990) Dynamics on potential-energy surfaces with a conical intersection - adiabatic, intermediate, and diabatic behavior. J Chem Phys 93:1658–1669
125. Manthe U, Koppel H, Cederbaum LS (1991) Dissociation and predissociation on coupled electronic potential-energy surfaces - a 3-dimensional wave packet dynamic study. J Chem Phys 95:1708–1720
126. Klessinger M, Michl J (1995) Excited states and photochemistry of organic molecules. VCH, New York
127. Robb MA, Bernardi F, Olivucci M (1995) Conical intersections as a mechanistic feature of organic-photochemistry. Pure Appl Chem 67:783–789
128. Yarkony DR (1996) Diabolical conical intersections. Rev Mod Phys 68:985–1013
129. Turro NJ (1991) Modern molecular photochemistry. University Science Books, Sausalito
130. Heller EJ (1981) Frozen Gaussians - a very simple semi-classical approximation. J Chem Phys 75:2923–2931
131. Virshup AM et al (2009) Photodynamics in complex environments: ab initio multiple spawning quantum mechanical/molecular mechanical dynamics. J Phys Chem B 113:3280–3291
132. Garcia JI et al (2007) QM/MM modeling of enantioselective pybox-ruthenium- and box-copper-catalyzed cyclopropanation reactions: scope, performance, and applications to ligand design. Chem-Eur J 13:4064–4073
133. Levine BG, Martinez TJ (2007) Isomerization through conical intersections. Annu Rev Phys Chem 58:613–634
134. Bearpark MJ, Larkin SM, Vreven T (2008) Searching for conical intersections of potential energy surfaces with the ONIOM method: application to previtamin D. J Phys Chem A 112:7286–7295
135. Sicilia F et al (2008) New algorithms for optimizing and linking conical intersection points. J Chem Theory Comput 4:257–266
136. Tokmachev AM et al (2010) Fluorescence of the perylene radical cation and an inaccessible D-0/D-1 conical intersection: an MMVB, RASSCF, and TD-DFT computational study. J Chem Phys 132:9
137. Dewar MJS, Thiel W (1977) Ground-states of molecules.38. MNDO method - approximations and parameters. J Am Chem Soc 99:4899–4907
138. Dewar MJS, Thiel W (1977) Ground-states of molecules. 39. MNDO results for molecules containing hydrogen, carbon, nitrogen, and oxygen. J Am Chem Soc 99:4907–4917
139. Dewar MJS et al (1985) The development and use of quantum-mechanical molecular-models. 76. AM1 - a new general-purpose quantum-mechanical molecular-model. J Am Chem Soc 107:3902–3909

140. Stewart JJP (1989) Optimization of parameters for semiempirical methods. 1. Method. J Comput Chem 10:209–220
141. Stewart JJP (1989) Optimization of parameters for semiempirical methods. 2. Applications. J Comput Chem 10:221–264
142. Stewart JJP (1991) Optimization of parameters for semiempirical methods. 3. Extension of Pm3 to Be, Mg, Zn, Ga, Ge, As, Se, Cd, In, Sn, Sb, Te, Hg, Tl, Pb, and Bi. J Comput Chem 12:320–341
143. Elstner M (2006) The SCC-DFTB method and its application to biological systems. Theor Chem Acc 116:316–325
144. Elstner M et al (1998) Self-consistent-charge density-functional tight-binding method for simulations of complex materials properties. Phys Rev B 58:7260–7268
145. Repasky MP, Chandrasekhar J, Jorgensen WL (2002) PDDG/PM3 and PDDG/MNDO: improved semiempirical methods. J Comput Chem 23:1601–1622
146. Weber W, Thiel W (2000) Orthogonalization corrections for semiempirical methods. Theor Chem Acc 103:495–506
147. Tuttle T, Thiel W (2008) OMx-D: semiempirical methods with orthogonalization and dispersion corrections. Implementation and biochemical application. Phys Chem Chem Phys 10:2159–2166
148. Silva-Junior MR, Thiel W (2010) Benchmark of electronically excited states for semiempirical methods: MNDO, AM1, PM3, OM1, OM2, OM3, INDO/S, and INDO/S2. J Chem Theory Comput 6:1546–1564
149. Sattelmeyer KW, Tubert-Brohman I, Jorgensen WL (2006) NO-MNDO: reintroduction of the overlap matrix into MNDO. J Chem Theory Comput 2:413–419
150. Rocha GB et al (2006) RM1: a reparameterization of AM1 for H, C, N, O, P, S, F, Cl, Br, and I. J Comput Chem 27:1101–1111
151. Feng F et al (2009) Can semiempirical quantum models calculate the binding energy of hydrogen bonding for biological systems? J Theor Comput Chem 8:691–711
152. Stewart JJP (2007) Optimization of parameters for semiempirical methods V: modification of NDDO approximations and application to 70 elements. J Mol Model 13:1173–1213
153. Danilov VI, Stewart JJP, van Mourik T (2007) A PM6 study of the "hydration shell" of nucleic acid 64 bases in small water clusters. J Biomol Struct Dyn 24:64
154. Kruger T et al (2005) Validation of the density-functional based tight-binding approximation method for the calculation of reaction energies and other data. J Chem Phys 122:5
155. Yang Y et al (2007) Extension of the self-consistent-charge density-functional tight-binding method: third-order expansion of the density functional theory total energy and introduction of a modified effective coulomb interaction. J Phys Chem A 111:10861–10873
156. Schaefer P, Riccardi D, Cui Q (2005) Reliable treatment of electrostatics in combined QM/MM simulation of macromolecules. J Chem Phys 123:014905
157. Riccardi D, Schaefer P, Cui Q (2005) pK_a calculations in solution and proteins with QM/MM free energy perturbation simulations: a quantitative test of QM/MM protocols. J Phys Chem B 109:17715–17733
158. Riccardi D et al (2006) Development of effective quantum mechanical/molecular mechanical (QM/MM) methods for complex biological processes. J Phys Chem B 110:6458–6469
159. Sattelmeyer KW, Tirado-Rives J, Jorgensen WL (2006) Comparison of SCC-DFTB and NDDO-based semiempirical molecular orbital methods for organic molecules. J Phys Chem A 110:13551–13559
160. Otte N, Scholten M, Thiel W (2007) Looking at self-consistent-charge density functional tight binding from a semiempirical perspective. J Phys Chem A 111:5751–5755
161. Seabra GD, Walker RC, Roitberg AE (2009) Are current semiempirical methods better than force fields? A study from the thermodynamics perspective. J Phys Chem A 113:11938–11948
162. McNamara JP et al (2004) Towards a quantum mechanical force field for carbohydrates: a reparametrized semi-empirical MO approach. Chem Phys Lett 394:429–436

163. Sattelle BM, Almond A (2010) Less is more when simulating unsulfated glycosaminoglycan 3D-structure: comparison of GLYCAM06/TIP3P, PM3-CARB1/TIP3P, and SCC-DFTB-D/TIP3P predictions with experiment. J Comput Chem 31:2932–2947
164. Shaik S, Hiberty PC (2008) A chemist's guide to valence bond theory. Wiley, Hoboken
165. Shaik S, Shurki A (1999) Valence bond diagrams and chemical reactivity. Angew Chem Int Ed 38:586–625
166. Shaik SS (1989) A Qualitative Valence Bond Approach to Organic Reactions. In: Bertrán J, Csizmadia GI (eds) New theoretical concepts for understanding organic reactions. Kluwer Academic Publishers, Dordrecht
167. Shaik SS, Hilberty PC (1991) Theoretical concepts for chemical bonding. Springer, Berlin
168. Hilberty PC, Shaik S (2002) BOVB - a valence bond method incorporating static and dynamic electron correlation effects. In: Cooper DL (ed) Valence bond theory. Elsevier, Amsterdam
169. Aqvist J, Warshel A (1993) Simulation of enzyme-reactions using valence-bond force-fields and other hybrid quantum-classical approaches. Chem Rev 93:2523–2544
170. Warshel A, Weiss RM (1980) An empirical valence bond approach for comparing reactions in solutions and in enzymes. J Am Chem Soc 102:6218–6226
171. Warshel A (1991) Modeling of chemical reactions in enzymes and solutions. Wiley, New York
172. Shurki A, Warshel A (2003) Protein simulations. Academic, San Diego
173. Warshel A (2003) Computer simulations of enzyme catalysis: methods, progress, and insights. Annu Rev Biophys Biomol Struct 32:425–443
174. Leach AR (2001) Molecular modelling. Pearson Education Limited, Harlow
175. Shurki A, Crown HA (2005) Hybrid ab initio VB/MM method - a valence bond ride through classical landscapes. J Phys Chem B 109:23638–23644
176. Bearpark MJ et al (1997) Benchmarking the molecular mechanics valence bond method: photophysics of styrene and indene. J Phys Chem A 101:8395–8401
177. Bearpark MJ, Boggio-Pasqua M (2003) Excited states of conjugated hydrocarbon radicals using the molecular mechanics - valence bond (MMVB) method. Theor Chem Acc 110:105–114
178. Bearpark MJ et al (1994) Molecular mechanics valence-bond methods for large active spaces - application to conjugated polycyclic-hydrocarbons. Chem Phys Lett 217:513–519
179. Blancafort L et al (2003) A valence-bond-based complete-active-space self-consistent-field method for the evaluation of bonding in organic molecules. Theor Chem Acc 110:92–99
180. Garavelli M et al (2003) A simple approach for improving the hybrid MMVB force field: application to the photoisomerization of s-cis butadiene. J Comput Chem 24:1357–1363
181. Durand P, Malrieu JP (2007) Effective Hamiltonians and pseudo-operators as tools for rigorous modelling. Adv Chem Phys 67:321–412
182. Bernardi F et al (1988) Parametrization of a Heitler-London valence bond Hamiltonian from complete-active-space self-consistent-field computations - an application to chemical-reactivity. J Chem Phys 89:6365–6375
183. Said M, Maynau D, Malrieu JP (1984) Excited-state properties of linear polyenes studied through a nonempirical Heisenberg Hamiltonian. J Am Chem Soc 106:580–587
184. Said M et al (1984) A nonempirical Heisenberg Hamiltonian for the study of conjugated hydrocarbons - ground-state conformational studies. J Am Chem Soc 106:571–579
185. Allinger NL (1976) Calculation of molecular structure and energy by force-field methods. Adv Phys Org Chem 13:1–82
186. Allinger NL (1977) Conformational-analysis.130. MM2 - hydrocarbon force-field utilizing V1 and V2 torsional terms. J Am Chem Soc 99:8127–8134
187. Bernardi F, Olivucci M, Robb MA (1992) Simulation of MC-SCF results on covalent organic multibond reactions - molecular mechanics with valence bond (MM-VB). J Am Chem Soc 114:1606–1616

188. Warshel A (1991) Computer modelling of chemical reactions in enzymes and solutions. Wiley, New York
189. Chang YT, Minichino C, Miller WH (1992) Classical trajectory studies of the molecular dissociation dynamics of formaldehyde: $H_2CO \rightarrow H_2 + CO$. J Chem Phys 96:4341–4355
190. Grochowski P et al (1996) Density functional based parametrization of a valence bond method and its applications in quantum classical molecular dynamics simulations of enzymatic reactions. Int J Quantum Chem 60:1143–1164
191. Albu TV, Corchado JC, Truhlar DG (2001) Molecular mechanics for chemical reactions: a standard strategy for using multiconfiguration molecular mechanics for variational transition state theory with optimized multidimensional tunneling. J Phys Chem A 105:8465–8487
192. Wei W, Zhong SJ, Shaik S (1998) VBDFT(s): a Huckel-type semi-empirical valence bond method scaled to density functional energies. Application to linear polyenes. Chem Phys Lett 292:7–14
193. Wu W, Shaik S (1999) VB-DFT: a nonempirical hybrid method combining valence bond theory and density functional energies. Chem Phys Lett 301:37–42
194. Wu W et al (2000) Using valence bond theory to understand electronic excited states: application to the hidden excited state (2^1A_g) of $C_{2n}H_{2n+2}$ (n = 2-14) polyenes. J Phys Chem A 104:8744–8758
195. Wu W et al (2001) VBDFT(s) - a semi-empirical valence bond method: application to linear polyenes containing oxygen and nitrogen heteroatoms. Phys Chem Chem Phys 3:5459–5465
196. Sharir-Ivry A et al (2010) VB/MM protein landscapes: a study of the S_N2 reaction in haloalkane dehalogenase. J Phys Chem B 114:2212–2218
197. Cornell WD et al (1995) A 2nd generation force-field for the simulation of proteins, nucleic-acids, and organic-molecules. J Am Chem Soc 117:5179–5197
198. Kollman P et al (1998) AMBER: a program for simulation of biological and organic molecules. In: Schleyer PV et al (eds) Encyclopedia of computational chemistry. Wiley, Chichester
199. Wang J, Cieplak P, Kollman PA (2000) How well does a restrained electrostatic potential (RESP) model perform in calculating conformational energies of organic and biological molecules? J Comput Chem 21:1049–1074
200. Duan Y et al (2003) A point-charge force field for molecular mechanics simulations of proteins based on condensed-phase quantum mechanical calculations. J Comput Chem 24:1999–2012
201. MacKerell AD et al (1998) All-atom empirical potential for molecular modeling and dynamics studies of proteins. J Phys Chem B 102:3586–3616
202. MacKerell ADJ et al (1998) Protein force fields. Wiley, Chichester
203. Foloppe N, MacKerell JAD (2000) All-atom empirical force field for nucleic acids: I. Parameter optimization based on small molecule and condensed phase macromolecular target data. J Comput Chem 21:86–104
204. MacKerell AD, Banavali NK (2000) All-atom empirical force field for nucleic acids: II. Application to molecular dynamics simulations of DNA and RNA in solution. J Comput Chem 21:105–120
205. MacKerell JAD (2001) Atomistic models and force fields. In: Becker OM et al (eds) Computational biochemistry and biophysics. Dekker, New York
206. van Gunsteren WF, Daura X, Mark AE (1998) GROMOS force field. In: Schleyer Pv et al (eds) Encyclopedia of computational chemistry. Wiley, Chichester
207. Scott WRP et al (1999) The GROMOS biomolecular simulation program package. J Phys Chem A 103:3596–3607
208. van Gunsteren WF et al (1996) Gromos – GROningen MOlecular Simulation computer program package (GROMOS96) available at: http://www.gromos.net/
209. Jorgensen WL, Maxwell DS, Tirado-Rives J (1996) Development and testing of the OPLS all-atom force field on conformational energetics and properties of organic liquids. J Am Chem Soc 118:11225–11236

210. Jorgensen WL (1998) OPLS force fields. In: Schleyer Pv et al (eds) Encyclopedia of computational chemistry. Wiley, Chichester
211. Kaminski GA et al (2001) Evaluation and reparametrization of the OPLS-AA force field for proteins via comparison with accurate quantum chemical calculations on peptides. J Phys Chem B 105:6474–6487
212. Allinger NL, Kok RA, Imam MR (1988) Hydrogen-bonding in MM2. J Comput Chem 9:591–595
213. Allinger NL, Yuh YH, Lii JH (1989) Molecular mechanics - the MM3 force-field for hydrocarbons. 1. J Am Chem Soc 111:8551–8566
214. Lii JH, Allinger NL (1989) Molecular mechanics - The MM3 force-field for hydrocarbons. 3. The vanderwaals potentials and crystal data for aliphatic and aromatic-hydrocarbons. J Am Chem Soc 111:8576–8582
215. Lii JH, Allinger NL (1989) Molecular mechanics - the MM3 force-field for hydrocarbons. 2. Vibrational frequencies and thermodynamics. J Am Chem Soc 111:8566–8575
216. Allinger NL, Chen KS, Lii JH (1996) An improved force field (MM4) for saturated hydrocarbons. J Comput Chem 17:642–668
217. Ma BY et al (1996) Systematic comparison of experimental, quantum mechanical, and molecular mechanical bond lengths for organic molecules. J Phys Chem-Us 100:8763–8769
218. Nevins N, Chen KS, Allinger NL (1996) Molecular mechanics (MM4) calculations on alkenes. J Comput Chem 17:669–694
219. Nevins N, Lii JH, Allinger NL (1996) Molecular mechanics (MM4) calculations on conjugated hydrocarbons. J Comput Chem 17:695–729
220. Lifson S, Warshel A (1968) Consistent force field for calculations of conformations vibrational spectra and enthalpies of cycloalkane and n-alkane molecules. J Chem Phys 49:5116
221. Warshel A, Levitt M, Lifson S (1970) Consistent force field for calculation of vibrational spectra and conformations of some amides and lactam rings. J Mol Spectrosc 33:84
222. Warshel A, Lifson S (1970) Consistent force field calculations. 2. Crystal structures, sublimation energies, molecular and lattice vibrations, molecular conformations, and enthalpies of alkanes. J Chem Phys 53:582
223. Liang CX et al (1994) Ab-initio studies of lipid model species. 2. Conformational-analysis of inositols. J Am Chem Soc 116:3904–3911
224. Maple JR et al (1994) Derivation of class-II force-fields. 1. Methodology and quantum force-field for the alkyl functional-group and alkane molecules. J Comput Chem 15:162–182
225. Halgren TA (1996) Merck molecular force field. 1. Basis, form, scope, parameterization, and performance of MMFF94. J Comput Chem 17:490–519
226. Halgren TA (1996) Merck molecular force field. 2. MMFF94 van der Waals and electrostatic parameters for intermolecular interactions. J Comput Chem 17:520–552
227. Halgren TA (1996) Merck molecular force field. 3. Molecular geometries and vibrational frequencies for MMFF94. J Comput Chem 17:553–586
228. Halgren TA (1996) Merck molecular force field. 5. Extension of MMFF94 using experimental data, additional computational data, and empirical rules. J Comput Chem 17:616–641
229. Halgren TA (1999) MMFF VII. Characterization of MMFF94, MMFF94s, and other widely available force fields for conformational energies and for intermolecular-interaction energies and geometries. J Comput Chem 20:730–748
230. Halgren TA (1999) MMFF VI. MMFF94s option for energy minimization studies. J Comput Chem 20:720–729
231. Halgren TA, Nachbar RB (1996) Merck molecular force field. 4. Conformational energies and geometries for MMFF94. J Comput Chem 17:587–615
232. Rappe AK et al (1992) UFF, a full periodic-table force-field for molecular mechanics and molecular-dynamics simulations. J Am Chem Soc 114:10024–10035
233. Casewit CJ, Colwell KS, Rappe AK (1992) Application of a universal force-field to organic-molecules. J Am Chem Soc 114:10035–10046

234. Mayo SL, Olafson BD, Goddard WA (1990) Dreiding - a generic force-field for molecular simulations. J Phys Chem-Us 94:8897–8909
235. Lindahl E, Hess B, van der Spoel D (2001) GROMACS 3.0: a package for molecular simulation and trajectory analysis. J Mol Model 7:306–317
236. van der Spoel D et al (2005) GROMACS: fast, flexible, and free. J Comput Chem 26:1701–1718
237. Clark M, Cramer RD, Vanopdenbosch N (1989) Validation of the general-purpose tripos 5.2 force-field. J Comput Chem 10:982–1012
238. Hagler AT, Dauber P, Lifson S (1979) Consistent force-field studies of inter-molecular forces in hydrogen-bonded crystals. 3. C=O. . .H-O hydrogen-bond and the analysis of the energetics and packing of carboxylic-acids. J Am Chem Soc 101:5131–5141
239. Hobza P et al (1997) Performance of empirical potentials (AMBER, CFF95, CVFF, CHARMM, OPLS, POLTEV), semiempirical quantum chemical methods (AM1, MNDO/M, PM3), and ab initio Hartree-Fock method for interaction of DNA bases: comparison with nonempirical beyond Hartree-Fock results. J Comput Chem 18:1136–1150
240. Hornak V et al (2006) Comparison of multiple amber force fields and development of improved protein backbone parameters. Proteins 65:712–725
241. Hu H, Elstner M, Hermans J (2003) Comparison of a QM/MM force field and molecular mechanics force fields in simulations of alanine and glycine "dipeptides" (Ace-Ala-Nme and Ace-Gly-Nme) in water in relation to the problem of modeling the unfolded peptide backbone in solution. Proteins 50:451–463
242. Gundertofte K, Liljefors T, Norrby PO (1996) A comparison of conformational energies calculated by several molecular mechanics methods. J Comput Chem 17:429–449
243. Ponder JW, Case DA (2003) Force fields for protein simulations. In: Richards FM, Eisendberg DS, Kuriyan J (eds) Protein simulations. Elsevier Academic, Amsterdam
244. MacKerell AD (2004) Empirical force fields for biological macromolecules: overview and issues. J Comput Chem 25:1584–1604
245. Okur A et al (2003) Using PC clusters to evaluate the transferability of molecular mechanics force fields for proteins. J Comput Chem 24:21–31
246. Wikipedia, the free encyclopedia: force field (chemistry) at http://en.wikipedia.org/wiki/Force_field_%28chemistry%29. Accessed: March 2011
247. Imberty A, Perez S (2000) Structure, conformation, and dynamics of bioactive oligosaccharides: theoretical approaches and experimental validations. Chem Rev 100:4567–4588
248. Kirschner KN et al (2008) GLYCAM06: a generalizable biomolecular force field. Carbohydrates. J Comput Chem 29:622–655
249. Tessier MB et al (2008) Extension of the GLYCAM06 biomolecular force field to lipids, lipid bilayers and glycolipids. Mol Simul 34:349–363
250. Hemmingsen L et al (2004) Evaluation of carbohydrate molecular mechanical force fields by quantum mechanical calculations. Carbohydr Res 339:937–948
251. Swope WC et al (2008) COMP 327-Comprehensive comparison and assessment of force fields for pharmaceutical applications by computation of hydration free energy. Abstr Pap Am Chem S 236
252. Vanommeslaeghe K, Acharya C, MacKerell AD (2008) COMP 6-development of parameters for the CHARMM general force field. Abstr Pap Am Chem S 236
253. Vanommeslaeghe K et al (2010) CHARMM general force field: a force field for drug-like molecules compatible with the CHARMM all-atom additive biological force fields. J Comput Chem 31:671–690
254. Sherrill CD et al (2009) Assessment of standard force field models against high-quality ab initio potential curves for prototypes of pi-pi, CH/pi, and SH/pi interactions. J Comput Chem 30:2187–2193
255. Jeziorski B, Moszynski R, Szalewicz K (1994) Perturbation-theory approach to intermolecular potential-energy surfaces of van-der-Waals complexes. Chem Rev 94:1887–1930

256. van der Avoird A et al (1980) Ab initio studies of the interactions in vanderwaals molecules. Top Curr Chem 93:1–51
257. Hesselmann A, Korona T (2011) On the accuracy of DFT-SAPT, MP2, SCS-MP2, MP2C, and DFT plus Disp methods for the interaction energies of endohedral complexes of the C_{60} fullerene with a rare gas atom. Phys Chem Chem Phys 13:732–743
258. Hobza P et al (2010) Stabilization and structure calculations for noncovalent interactions in extended molecular systems based on wave function and density functional theories. Chem Rev 110:5023–5063
259. Hohenstein EG, Sherrill CD (2010) Density fitting of intramonomer correlation effects in symmetry-adapted perturbation theory. J Chem Phys 133:014101
260. Jansen G et al (2008) Stacking energies for average B-DNA structures from the combined density functional theory and symmetry-adapted perturbation theory approach. J Am Chem Soc 130:1802
261. Jansen G, Tekin A (2007) How accurate is the density functional theory combined with symmetry-adapted perturbation theory approach for CH-pi and pi-pi interactions? A comparison to supermolecular calculations for the acetylene-benzene dimer. Phys Chem Chem Phys 9:1680–1687
262. Mooij WTM et al (1999) Transferable ab initio intermolecular potentials. 1. Derivation from methanol dimer and trimer calculations. J Phys Chem A 103:9872–9882
263. Chipot C et al (2009) Polarizable intermolecular potentials for water and benzene interacting with halide and metal ions. J Chem Theory Comput 5:3022–3031
264. Hloucha M, Sum AK, Sandler SI (2000) Computer simulation of acetonitrile and methanol with ab initio-based pair potentials. J Chem Phys 113:5401–5406
265. Jansen G, Torheyden M (2006) A new potential energy surface for the water dimer obtained from separate fits of ab initio electrostatic, induction, dispersion and exchange energy contributions. Mol Phys 104:2101–2138
266. Li X et al (2006) Interaction energies between glycopeptide antibiotics and substrates in complexes determined by X-ray crystallography: application of a theoretical databank of aspherical atoms and a symmetry-adapted perturbation theory-based set of interatomic potentials. Acta Crystallogr D 62:639–647
267. Misquitta AJ, Totton TS, Kraft M (2010) A first principles development of a general anisotropic potential for polycyclic aromatic hydrocarbons. J Chem Theory Comput 6:683–695
268. Mitchell JBO, Price SL (2000) A systematic nonempirical method of deriving model intermolecular potentials for organic molecules: application to amides. J Phys Chem A 104:10958–10971
269. van der Avoird A, Szalewicz K, Leforestier C (2009) Towards the complete understanding of water by a first-principles computational approach. Chem Phys Lett 482:1–14
270. Goodman JM, Paton RS (2009) Hydrogen bonding and pi-stacking: how reliable are force fields? A critical evaluation of force field descriptions of nonbonded interactions. J Chem Inf Model 49:944–955
271. Sponer J et al (2009) Balance of attraction and repulsion in nucleic-acid base stacking: CCSD (T)/complete-basis-set-limit calculations on uracil dimer and a comparison with the force-field description. J Chem Theory Comput 5:1524–1544
272. Sponer J et al (2010) Reference MP2/CBS and CCSD(T) quantum-chemical calculations on stacked adenine dimers. Comparison with DFT-D, MP2.5, SCS(MI)-MP2, M06-2X, CBS (SCS-D) and force field descriptions. Phys Chem Chem Phys 12:3522–3534
273. Zgarbova M et al (2010) Large-scale compensation of errors in pairwise-additive empirical force fields: comparison of AMBER intermolecular terms with rigorous DFT-SAPT calculations. Phys Chem Chem Phys 12:10476–10493
274. Corry B et al (2010) Molecular dynamics simulations of structure and dynamics of organic molecular crystals. Phys Chem Chem Phys 12:14916–14929

275. Hobza P et al (2010) On the reliability of the AMBER force field and its empirical dispersion contribution for the description of noncovalent complexes. Chemphyschem 11:2399–2408
276. Tateno M, Hagiwara Y (2009) Evaluation of stabilization energies in π–π and cation–π interactions involved in biological macromolecules by ab initio calculations. J Phys Condens Matter 21:064243
277. Wetmore SD, Rutledge LR (2010) The assessment of density functionals for DNA-protein stacked and T-shaped complexes. Can J Chem 88:815–830
278. Tafipolsky M, Engels B (2011) Accurate intermolecular potentials with physically grounded electrostatics. J Chem Theory Comput 7:1791–1803
279. Head-Gordon T et al (2010) Current status of the AMOEBA polarizable force field. J Phys Chem B 114:2549–2564
280. Ponder JW et al (2010) Tinker – software tools for molecular modelling (5.1) available at: http://dasher.wustl.edu/tinker
281. van der Avoird A et al (2010) Vibration-rotation-tunneling states of the benzene dimer: an ab initio study. Phys Chem Chem Phys 12:8219–8240
282. Spackman MA (2006) The use of the promolecular charge density to approximate the penetration contribution to intermolecular electrostatic energies. Chem Phys Lett 418:158–162
283. Spackman MA (1986) A simple quantitative model of hydrogen-bonding. J Chem Phys 85:6587–6601
284. Gordon MS, Slipchenko LV (2009) Damping functions in the effective fragment potential method. Mol Phys 107:999–1016
285. Piquemal JP et al (2008) Simple formulas for improved point-charge electrostatics in classical force fields and hybrid quantum mechanical/molecular mechanical embedding. Int J Quantum Chem 108:1905–1912
286. Pedersen LG et al (2010) Gaussian multipole model (GMM). J Chem Theory Comput 6:190–202
287. Wang B, Truhlar DG (2010) Including charge penetration effects in molecular modeling. J Chem Theory Comput 6:3330–3342
288. Singh UC, Kollman PA (1986) A combined ab initio quantum-mechanical and molecular mechanical method for carrying out simulations on complex molecular-systems - applications to the CH_3Cl+Cl^- exchange-reaction and gas-phase protonation of polyethers. J Comput Chem 7:718–730
289. Bakowies D, Thiel W (1996) Hybrid models for combined quantum mechanical and molecular mechanical approaches. J Phys Chem-Us 100:10580–10594
290. Gao J (1997) Energy components of aqueous solution: insight from hybrid QM/MM simulations using a polarizable solvent model. J Comput Chem 18:1061–1071
291. Gao JL, Byun K (1997) Solvent effects on the n->pi transition of pyrimidine in aqueous solution. Theor Chem Acc 96:151–156
292. Thompson MA (1996) QM/MMpol: a consistent model for solute/solvent polarization. Application to the aqueous solvation and spectroscopy of formaldehyde, acetaldehyde, and acetone. J Phys Chem-Us 100:14492–14507
293. Thompson MA, Schenter GK (1995) Excited-states of the bacteriochlorophyll-B dimer of *Rhodopseudomonas-viridis* - a QM/MM study of the photosynthetic reaction-center that includes MM polarization. J Phys Chem-Us 99:6374–6386
294. Cornell WD et al (1996) A second generation force field for the simulation of proteins, nucleic acids, and organic molecules (vol 117, pg 5179, 1995). J Am Chem Soc 118:2309
295. Kunz APE, Eichenberger AP, van Gunsteren WF (2011) A simple, efficient polarizable molecular model for liquid carbon tetrachloride. Mol Phys 109:365–372
296. Kunz APE, van Gunsteren WF (2009) Development of a nonlinear classical polarization model for liquid water and aqueous solutions: COS/D. J Phys Chem A 113:11570–11579

297. Geerke DP, Van Gunsteren WF (2007) The performance of non-polarizable and polarizable force-field parameter sets for ethylene glycol in molecular dynamics simulations of the pure liquid and its aqueous mixtures. Mol Phys 105:1861–1881
298. Grossfield A, Ren PY, Ponder JW (2003) Ion solvation thermodynamics from simulation with a polarizable force field. J Am Chem Soc 125:15671–15682
299. Maple JR et al (2005) A polarizable force field and continuum solvation methodology for modeling of protein-ligand interactions. J Chem Theory Comput 1:694–715
300. Oostenbrink C et al (2004) A biomolecular force field based on the free enthalpy of hydration and solvation: the GROMOS force-field parameter sets 53A5 and 53A6. J Comput Chem 25:1656–1676
301. Chang TM, Dang LX (2005) Liquid-vapor interface of methanol-water mixtures: a molecular dynamics study. J Phys Chem B 109:5759–5765
302. Patel SA, Brooks CL (2006) Revisiting the hexane-water interface via molecular dynamics simulations using nonadditive alkane-water potentials. J Chem Phys 124:204706
303. Warshel A, Kato M, Pisliakov AV (2007) Polarizable force fields: history, test cases, and prospects. J Chem Theory Comput 3:2034–2045
304. Harder E et al (2008) Understanding the dielectric properties of liquid amides from a polarizable force field. J Phys Chem B 112:3509–3521
305. Xie WS et al (2007) Development of a polarizable intermolecular potential function (PIPF) for liquid amides and alkanes. J Chem Theory Comput 3:1878–1889
306. Rick SW, Stuart SJ (2003) Potentials and algorithms for incorporating polarizability in computer simulations. In: Lipkowitz KB, Boyd DB (eds) Reviews in computational chemistry. Wiley, New York
307. Yu HB, van Gunsteren WF (2005) Accounting for polarization in molecular simulation. Comput Phys Commun 172:69–85
308. van Belle D et al (1987) Calculations of electrostatic properties in proteins - analysis of contributions from induced protein dipoles. J Mol Biol 198:721–735
309. Vesely FJ (1977) N-Particle dynamics of polarizable Stockmayer-type molecules. J Comput Phys 24:361–371
310. Straatsma TP, McCammon JA (1990) Molecular dynamics simulations with interaction potentials including polarization development of a noniterative method and application to water. Mol Simul 5:181–192
311. Drude P (1902) The theory of optics. Longmans, Green and Co, New York
312. Rick SW, Stuart SJ, Berne BJ (1994) Dynamical fluctuating charge force-fields - application to liquid water. J Chem Phys 101:6141–6156
313. Anisimov VM et al (2005) Determination of electrostatic parameters for a polarizable force field based on the classical Drude oscillator. J Chem Theory Comput 1:153–168
314. Cieplak P, Caldwell J, Kollman P (2001) Molecular mechanical models for organic and biological systems going beyond the atom centered two body additive approximation: aqueous solution free energies of methanol and N-methyl acetamide, nucleic acid base, and amide hydrogen bonding and chloroform/water partition coefficients of the nucleic acid bases. J Comput Chem 22:1048–1057
315. Cieplak P et al (2009) Polarization effects in molecular mechanical force fields. J Phys Condens Matter 21:21
316. Patel S, Brooks CL (2004) CHARMM fluctuating charge force field for proteins: I parameterization and application to bulk organic liquid simulations. J Comput Chem 25:1–15
317. Patel S, Mackerell AD, Brooks CL (2004) CHARMM fluctuating charge force field for proteins: II Protein/solvent properties from molecular dynamics simulations using a nonadditive electrostatic model. J Comput Chem 25:1504–1514
318. Vorobyov IV, Anisimov VM, MacKerell AD (2005) Polarizable empirical force field for alkanes based on the classical drude oscillator model. J Phys Chem B 109:18988–18999

319. Wang ZX et al (2006) Strike a balance: optimization of backbone torsion parameters of AMBER polarizable force field for simulations of proteins and peptides. J Comput Chem 27:781–790
320. Banks JL et al (1999) Parametrizing a polarizable force field from ab initio data. I. The fluctuating point charge model. J Chem Phys 110:741–754
321. Kaminski GA et al (2004) Development of an accurate and robust polarizable molecular mechanics force field from ab initio quantum chemistry. J Phys Chem A 108:621–627
322. Kaminski GA et al (2002) Development of a polarizable force field for proteins via ab initio quantum chemistry: first generation model and gas phase tests. J Comput Chem 23:1515–1531
323. Xie WS, Gao JL (2007) Design of a next generation force field: the X-POL potential. J Chem Theory Comput 3:1890–1900
324. Cho AE et al (2005) Importance of accurate charges in molecular docking: quantum mechanical/molecular mechanical (QM/MM) approach. J Comput Chem 26:915–931
325. Friesner RA (2006) Modeling polarization in proteins and protein-ligand complexes: methods and preliminary results. Adv Protein Chem 72:79
326. Illingworth CJR et al (2006) Classical polarization in hybrid QM/MM methods. J Phys Chem A 110:6487–6497
327. Kaminski S et al (2010) Vibrational Raman spectra from the self-consistent charge density functional tight binding method via classical time-correlation functions. J Chem Theory Comput 6:1240–1255
328. Lopes PEM, Roux B, MacKerell AD (2009) Molecular modeling and dynamics studies with explicit inclusion of electronic polarizability: theory and applications. Theor Chem Acc 124:11–28
329. Geerke DP, van Gunsteren WF (2007) Calculation of the free energy of polarization: quantifying the effect of explicitly treating electronic polarization on the transferability of force-field parameters. J Phys Chem B 111:6425–6436
330. Lin ZX, Schmid N, van Gunsteren WF (2011) The effect of using a polarizable solvent model upon the folding equilibrium of different -peptides. Mol Phys 109:493–506
331. Illingworth CJR et al (2008) Toward a consistent treatment of polarization in model QM/MM calculations. J Phys Chem A 112:12151–12156
332. Swope WC, Horn HW, Rice JE (2010) Accounting for polarization cost when using fixed charge force fields. II. Method and application for computing effect of polarization cost on free energy of hydration. J Phys Chem B 114:8631–8645
333. Biswas PK, Gogonea V (2008) A polarizable force-field model for quantum-mechanical-molecular-mechanical Hamiltonian using expansion of point charges into orbitals. J Chem Phys 129:154108
334. Pliego JR (2011) Shells theory of solvation and the long-range born correction. Theor Chem Acc 128:275–283
335. Jiang W et al (2011) High-performance scalable molecular dynamics simulations of a polarizable force field based on classical drude oscillators in NAMD. J Phys Chem Lett 2:87–92
336. Stillinger FH, Rahman A (1974) Improved simulation of liquid water by molecular-dynamics. J Chem Phys 60:1545–1557
337. Phillips JC et al (2005) Scalable molecular dynamics with NAMD. J Comput Chem 26:1781–1802
338. Zhang Y, Lin H (2008) Flexible-boundary quantum-mechanical/molecular-mechanical calculations: partial charge transfer between the quantum-mechanical and molecular-mechanical subsystems. J Chem Theory Comput 4:414–425
339. Zhang Y, Lin H, Truhlar DG (2007) Self-consistent polarization of the boundary in the redistributed charge and dipole scheme for combined quantum-mechanical and molecular-mechanical calculations. J Chem Theory Comput 3:1378–1398

340. Hamad S, Woodley SM, Catlow CRA (2009) Experimental and computational studies of ZnS nanostructures. Mol Simul 35:1015–1032
341. Catlow CRA et al (2008) Zinc oxide: a case study in contemporary computational solid state chemistry. J Comput Chem 29:2234–2249
342. To J et al (2008) Hybrid QM/MM investigations into the structure and properties of oxygen-donating species in TS-1. J Phys Chem C 112:7173–7185
343. Goumans TPM et al (2008) Hydrogenation of CO on a silica surface: an embedded cluster approach. J Chem Phys 128:6
344. Goumans TPM, Catlow CRA, Brown WA (2008) Catalysis of addition reactions by a negatively charged silica surface site on a dust grain. J Phys Chem C 112:15419–15422
345. Adriaens DA et al (2010) Computational study of carbonyl sulphide formation on model interstellar dust grains. J Phys Chem C 114:1892–1900
346. Goumans TPM et al (2009) An embedded cluster study of the formation of water on interstellar dust grains. Phys Chem Chem Phys 11:5431–5436
347. Goumans TPM et al (2009) Formation of H_2 on an olivine surface: a computational study. Mon Not R Astron Soc 393:1403–1407
348. Olsen JM, Aidas K, Kongsted J (2010) Excited states in solution through polarizable embedding. J Chem Theory Comput 6:3721–3734
349. Slipchenko LV (2010) Solvation of the excited states of chromophores in polarizable environment: orbital relaxation versus polarization. J Phys Chem A 114:8824–8830
350. Mata RA, Cabral BJC (2010) QM/MM approaches to the electronic spectra of hydrogen-bonding systems with connection to many-body decomposition schemes. In: Sabin JR, Brandas, E, Canuto S (eds) Advances in quantum chemistry. Elsevier Academic, San Diego
351. Yoo S et al (2008) Solvent effects on optical properties of molecules: a combined time-dependent density functional theory/effective fragment potential approach. J Chem Phys 129:144112
352. Fujimoto K, Yang WT (2008) Density-fragment interaction approach for quantum-mechanical/molecular-mechanical calculations with application to the excited states of a Mg(2+)-sensitive dye. J Chem Phys 129:054102
353. Fux S et al (2010) Accurate frozen-density embedding potentials as a first step towards a subsystem description of covalent bonds. J Chem Phys 132:164101
354. Neugebauer J et al (2010) A subsystem TDDFT approach for solvent screening effects on excitation energy transfer couplings. J Chem Theory Comput 6:1843–1851
355. Neugebauer J et al (2005) An explicit quantum chemical method for modeling large solvation shells applied to aminocoumarin C151. J Phys Chem A 109:7805–7814
356. Neugebauer J et al (2005) The merits of the frozen-density embedding scheme to model solvatochromic shifts. J Chem Phys 122:094115
357. Neugebauer J et al (2005) Modeling solvent effects on electron-spin-resonance hyperfine couplings by frozen-density embedding. J Chem Phys 123:114101
358. Ranaghan KE, Mulholland AJ (2010) Investigations of enzyme-catalysed reactions with combined quantum mechanics/molecular mechanics (QM/MM) methods. Int Rev Phys Chem 29:65–133
359. Maseras F, Morokuma K (1995) IMOMM - a new integrated ab-initio plus molecular mechanics geometry optimization scheme of equilibrium structures and transition-states. J Comput Chem 16:1170–1179
360. Matsubara T, Sieber S, Morokuma K (1996) A test of the new "integrated MO + MM" (IMOMM) method for the conformational energy of ethane and n-butane. Int J Quantum Chem 60:1101–1109
361. Froese RDJ, Morokuma K (1999) IMOMO-G2MS approaches to accurate calculations of bond dissociation energies of large molecules. J Phys Chem A 103:4580–4586
362. Humbel S, Sieber S, Morokuma K (1996) The IMOMO method: integration of different levels of molecular orbital approximations for geometry optimization of large systems: test for n-butane conformation and S_N2 reaction: RCl + Cl. J Chem Phys 105:1959–1967

363. Froese RDJ, Morokuma K (1996) The IMOMO and IMOMM methods for excited states. A study of the adiabatic S0->T1, T2 excitation energies of cyclic alkenes and enones. Chem Phys Lett 263:393–400
364. Svensson M et al (1996) ONIOM: a multilayered integrated MO+MM method for geometry optimizations and single point energy predictions. A test for Diels-Alder reactions and $Pt(P(t\text{-}Bu)_3)_2 + H_2$ oxidative addition. J Phys Chem-Us 100:19357–19363
365. Dapprich S et al (1999) A new ONIOM implementation in Gaussian98. Part I. The calculation of energies, gradients, vibrational frequencies and electric field derivatives. J Mol Struct-Theochem 461:1–21
366. Vreven T et al (2006) Combining quantum mechanics methods with molecular mechanics methods in ONIOM. J Chem Theory Comput 2:815–826
367. Vreven T et al (2003) Geometry optimization with QM/MM, ONIOM, and other combined methods. I. Microiterations and constraints. J Comput Chem 24:760–769
368. Ryde U (1996) The coordination of the catalytic zinc ion in alcohol dehydrogenase studied by combined quantum-chemical and molecular mechanics calculations. J Comput Aided Mol Des 10:153–164
369. Ryde U, Olsson MHM (2001) Structure, strain, and reorganization energy of blue copper models in the protein. Int J Quantum Chem 81:335–347
370. Zhang YK, Lee TS, Yang WT (1999) A pseudobond approach to combining quantum mechanical and molecular mechanical methods. J Chem Phys 110:46–54
371. Nicoll RM et al (2001) Quantum mechanical/molecular mechanical methods and the study of kinetic isotope effects: modelling the covalent junction region and application to the enzyme xylose isomerase. Theor Chem Acc 106:105–112
372. Reuter N et al (2000) Frontier bonds in QM/MM methods: a comparison of different approaches. J Phys Chem A 104:1720–1735
373. Hall RJ et al (2000) Aspects of hybrid QM/MM calculations: the treatment of the QM/MM interface region and geometry optimization with an application to chorismate mutase. J Comput Chem 21:1433–1441
374. Amara P, Field MJ (2003) Evaluation of an ab initio quantum mechanical/molecular mechanical hybrid-potential link-atom method. Theor Chem Acc 109:43–52
375. Lin H, Truhlar DG (2005) Redistributed charge and dipole schemes for combined quantum mechanical and molecular mechanical calculations. J Phys Chem A 109:3991–4004
376. Konig PH et al (2005) A critical evaluation of different QM/MM frontier treatments with SCC-DFTB as the QM method. J Phys Chem B 109:9082–9095
377. Assfeld X, Rivail JL (1996) Quantum chemical computations on parts of large molecules: the ab initio local self consistent field method. Chem Phys Lett 263:100–106
378. Pu JZ, Gao JL, Truhlar DG (2004) Generalized hybrid orbital (GHO) method for combining ab initio Hartree-Fock wave functions with molecular mechanics. J Phys Chem A 108:632–650
379. Jung J et al (2007) New implementation of a combined quantum mechanical and molecular mechanical method using modified generalized hybrid orbitals. J Chem Phys 127:204102
380. Bessac F et al (2003) Effective group potentials: a powerful tool for hybrid QM/MM methods? J Mol Struct-Theochem 632:43–59
381. Day PN et al (1996) An effective fragment method for modeling solvent effects in quantum mechanical calculations. J Chem Phys 105:1968–1986
382. Adamovic I, Freitag MA, Gordon MS (2003) Density functional theory based effective fragment potential method. J Chem Phys 118:6725–6732
383. Adamovic I, Gordon MS (2006) Methanol-water mixtures: a microsolvation study using the effective fragment potential method. J Phys Chem A 110:10267–10273
384. Netzloff HM, Gordon MS (2004) The effective fragment potential: small clusters and radial distribution functions. J Chem Phys 121:2711–2714
385. Poteau R et al (2001) Effective group potentials. 1. Method. J Phys Chem A 105:198–205

386. Poteau R et al (2001) Effective group potentials. 2. Extraction and transferability for chemical groups involved in covalent or donor-acceptor bonds. J Phys Chem A 105:206–214
387. Exner TE, Mezey PG (2003) Ab initio quality properties for macromolecules using the ADMA approach. J Comput Chem 24:1980–1986
388. Exner TE, Mezey PG (2005) Evaluation of the field-adapted ADMA approach: absolute and relative energies of crambin and derivatives. Phys Chem Chem Phys 7:4061–4069
389. Eckard S, Exner TE (2006) Generalized hybrid orbitals in the FA-ADMA method. Z Phys Chem 220:927–944
390. DiLabio GA, Hurley MM, Christiansen PA (2002) Simple one-electron quantum capping potentials for use in hybrid QM/MM studies of biological molecules. J Chem Phys 116:9578–9584
391. Moon S, Christiansen PA, DiLabio GA (2004) Quantum capping potentials with point charges: a simple QM/MM approach for the calculation of large-molecule NMR shielding tensors. J Chem Phys 120:9080–9086
392. Jardillier N, Goursot A (2008) One-electron quantum capping potential for hybrid QM/MM studies of silicate molecules and solids. Chem Phys Lett 454:65–69
393. Ohnishi YY et al (2008) Frontier orbital consistent quantum capping potential (FOC-QCP) for bulky ligand of transition metal complexes. J Phys Chem A 112:1946–1955
394. Komin S, Sebastiani D (2009) Optimization of capping potentials for spectroscopic parameters in hybrid quantum mechanical/mechanical modeling calculations. J Chem Theory Comput 5:1490–1498
395. Wang B, Truhlar DG (2010) Combined quantum mechanical and molecular mechanical methods for calculating potential energy surfaces: tuned and balanced redistributed-charge algorithm. J Chem Theory Comput 6:359–369
396. DiLabio GA, Wolkow RA, Johnson ER (2005) Efficient silicon surface and cluster modeling using quantum capping potentials. J Chem Phys 122:5
397. Goedecker S, Teter M, Hutter J (1996) Separable dual-space Gaussian pseudopotentials. Phys Rev B 54:1703–1710
398. Hartwigsen C, Goedecker S, Hutter J (1998) Relativistic separable dual-space Gaussian pseudopotentials from H to Rn. Phys Rev B 58:3641–3662
399. Schiffmann C, Sebastiani D (2011) Artificial bee colony optimization of capping potentials for hybrid QM/MM calculations. J Chem Theory Comput 7:1307–1315
400. Brown SP, Spiess HW (2001) Advanced solid-state NMR methods for the elucidation of structure and dynamics of molecular, macromolecular, and supramolecular systems. Chem Rev 101:4125–4155
401. Schulz-Dobrick M et al (2005) Determining the geometry of hydrogen bonds in solids with picometer accuracy by quantum chemical calculations and NMR spectroscopy. Chemphyschem 6:315–327
402. Spiess HW (2003) Nuclear magnetic resonance spectroscopy in macromolecular science. Macromol Chem Phys 204:340–346
403. Press WH et al (1992) Numerical recipes. Cambridge University Press, Cambridge, UK
404. Karaboga D, Akay B (2009) A survey: algorithms simulating bee swarm intelligence. Artif Intell Rev 31:61–85
405. Karaboga D, Basturk B (2007) A powerful and efficient algorithm for numerical function optimization: artificial bee colony (ABC) algorithm. J Global Optim 39:459–471
406. Karaboga D, Basturk B (2008) On the performance of artificial bee colony (ABC) algorithm. Appl Soft Comput 8:687–697
407. Moon S, Patchkovskii S, Salahub DR (2003) QM/MM calculations of EPR hyperfine coupling constants in blue copper proteins. J Mol Struct-Theochem 632:287–295
408. Kerdcharoen T, Liedl KR, Rode BM (1996) A QM/MM simulation method applied to the solution of Li^+ in liquid ammonia. Chem Phys 211:313–323
409. Hofer TS et al (2005) Structure and dynamics of solvated Sn(II) in aqueous solution: an ab initio QM/MM MD approach. J Am Chem Soc 127:14231–14238

410. Schwenk CF, Loeffler HH, Rode BM (2003) Structure and dynamics of metal ions in solution: QM/MM molecular dynamics simulations of Mn^{2+} and V^{2+}. J Am Chem Soc 125:1618–1624
411. Rode BM, Schwenk CF, Tongraar A (2004) Structure and dynamics of hydrated ions-new insights through quantum mechanical simulations. J Mol Liq 110:105–122
412. Kerdcharoen T, Morokuma K (2002) ONIOM-XS: an extension of the ONIOM method for molecular simulation in condensed phase. Chem Phys Lett 355:257–262
413. Kerdcharoen T, Morokuma K (2003) Combined quantum mechanics and molecular mechanics simulation of Ca^{2+}/ammonia solution based on the ONIOM-XS method: octahedral coordination and implication to biology. J Chem Phys 118:8856–8862
414. Morokuma K (2003) ONIOM and its applications to material chemistry and catalyses. Bull Korean Chem Soc 24:797–801
415. Heyden A, Lin H, Truhlar DG (2007) Adaptive partitioning in combined quantum mechanical and molecular mechanical calculations of potential energy functions for multiscale simulations. J Phys Chem B 111:2231–2241
416. Zhang Y, Lin H (2010) Flexible-boundary QM/MM calculations: II. Partial charge transfer across the QM/MM boundary that passes through a covalent bond. Theor Chem Acc 126:315–322
417. Nielsen SO et al (2010) Recent progress in adaptive multiscale molecular dynamics simulations of soft matter. Phys Chem Chem Phys 12:12401–12414
418. Hofer TS et al (2010) Simulations of liquids and solutions based on quantum mechanical forces. In: vanEldik R, Harvey J (eds) Advances in inorganic chemistry: theoretical and computational inorganic chemistry, Vol 62. Elsevier Academic, San Diego
419. Darden T, York D, Pedersen L (1993) Particle mesh Ewald - an N.log(N) method for Ewald sums in large systems. J Chem Phys 98:10089–10092
420. York DM, Darden TA, Pedersen LG (1993) The effect of long-range electrostatic interactions in simulations of macromolecular crystals - a comparison of the Ewald and truncated list methods. J Chem Phys 99:8345–8348
421. Essmann U et al (1995) A smooth particle mesh Ewald method. J Chem Phys 103:8577–8593
422. Nam K, Gao JL, York DM (2005) An efficient linear-scaling Ewald method for long-range electrostatic interactions in combined QM/MM calculations. J Chem Theory Comput 1:2–13
423. Walker RC, Crowley MF, Case DA (2008) The implementation of a fast and accurate QM/MM potential method in Amber. J Comput Chem 29:1019–1031
424. Laino T et al (2005) An efficient real space multigrid OM/MM electrostatic coupling. J Chem Theory Comput 1:1176–1184
425. Laino T et al (2006) An efficient linear-scaling electrostatic coupling for treating periodic boundary conditions in QM/MM simulations. J Chem Theory Comput 2:1370–1378
426. Berkowitz M, McCammon JA (1982) Molecular-dynamics with stochastic boundary-conditions. Chem Phys Lett 90:215–217
427. Brunger A, Brooks CL, Karplus M (1984) Stochastic boundary-conditions for molecular-dynamics simulations of St2 water. Chem Phys Lett 105:495–500
428. Brooks CL, Karplus M (1983) Deformable stochastic boundaries in molecular-dynamics. J Chem Phys 79:6312–6325
429. Lee FS, Warshel A (1992) A local reaction field method for fast evaluation of long-range electrostatic interactions in molecular simulations. J Chem Phys 97:3100–3107
430. Tironi IG et al (1995) A generalized reaction field method for molecular-dynamics simulations. J Chem Phys 102:5451–5459
431. Beglov D, Roux B (1994) Finite representation of an infinite bulk system - solvent boundary potential for computer-simulations. J Chem Phys 100:9050–9063
432. Benighaus T, Thiel W (2011) Long-range electrostatic effects in QM/MM studies of enzymatic reactions: application of the solvated macromolecule boundary potential. J Chem Theory Comput 7:238–249

433. Im W, Berneche S, Roux B (2001) Generalized solvent boundary potential for computer simulations. J Chem Phys 114:2924–2937
434. Thiel W, Benighaus T (2008) Efficiency and accuracy of the generalized solvent boundary potential for hybrid QM/MM simulations: implementation for semiempirical Hamiltonians. J Chem Theory Comput 4:1600–1609
435. Thiel W, Benighaus T (2009) A general boundary potential for hybrid QM/MM simulations of solvated biomolecular systems. J Chem Theory Comput 5:3114–3128
436. Wales DJ (2003) Energy landscapes. Cambridge University Press, Cambridge
437. Moult J et al (2009) Critical assessment of methods of protein structure prediction—round VIII. Proteins Struct Funct Bioinf 77:1–4
438. Klahn M et al (2005) On possible pitfalls in ab initio quantum mechanics/molecular mechanics minimization approaches for studies of enzymatic reactions. J Phys Chem B 109:15645–15650
439. Christen M, van Gunsteren WF (2008) On searching in, sampling of, and dynamically moving through conformational space of biomolecular systems: a review. J Comput Chem 29:157–166
440. Oakley MT et al (2008) Search strategies in structural bioinformatics. Curr Protein Pept Sci 9:260–274
441. van Gunsteren WF et al (2006) Biomolecular modeling: goals, problems, perspectives. Angew Chem Int Ed 45:4064–4092
442. Chen IJ, Foloppe N (2011) Is conformational sampling of drug-like molecules a solved problem? Drug Dev Res 72:85–94
443. Chen IJ, Foloppe N (2010) Drug-like bioactive structures and conformational coverage with the ligprep/confgen suite: comparison to programs MOE and catalyst. J Chem Inf Model 50:822–839
444. Chen IJ, Foloppe N (2008) Conformational sampling of druglike molecules with MOE and catalyst: implications for pharmacophore modeling and virtual screening. J Chem Inf Model 48:1773–1791
445. Bruccoleri RE, Karplus M (1987) Prediction of the folding of short polypeptide segments by uniform conformational sampling. Biopolymers 26:137–168
446. Gippert GP, Wright PE, Case DA (1998) Distributed torsion angle grid search in high dimensions: a systematic approach to NMR structure determination. J Biomol NMR 11:241–263
447. Sadowski J, Bostrom J (2006) MIMUMBA revisited: torsion angle rules for conformer generation derived from X-ray structures. J Chem Inf Model 46:2305–2309
448. Smellie A et al (2003) Conformational analysis by intersection: CONAN. J Comput Chem 24:10–20
449. Chandrasekhar J, Saunders M, Jorgensen WL (2001) Efficient exploration of conformational space using the stochastic search method: application to beta-peptide oligomers. J Comput Chem 22:1646–1654
450. Chen JH, Im W, Brooks CL (2005) Application of torsion angle molecular dynamics for efficient sampling of protein conformations. J Comput Chem 26:1565–1578
451. Glen RC, Payne AWR (1995) A genetic algorithm for the automated generation of molecules within constraints. J Comput Aided Mol Des 9:181–202
452. Scheraga HA et al (1999) Surmounting the multiple-minima problem in protein folding. J Global Optim 15:235–260
453. Bohm G (1996) New approaches in molecular structure prediction. Biophys Chem 59:1–32
454. Floudas CA, Klepeis JL, Pardalos PM (1999) Global optimization approaches in protein folding and peptide docking. American Mathematical Society, New Jersey
455. Leach AR (1991) A survey of methods for searching the conformational space of small and medium-sized molecules. In: Lipkowitz KB, Boyd DB (eds) Reviews in computational chemistry. VCH, New York

456. Neumaier A (1997) Molecular modeling of proteins and mathematical prediction of protein structure. Siam Rev 39:407–460
457. Li ZQ, Laidig KE, Daggett V (1998) Conformational search using a molecular dynamics-minimization procedure: applications to clusters of coulombic charges, Lennard-Jones particles, and waters. J Comput Chem 19:60–70
458. Vengadesan K, Gautham N (2005) A new conformational search technique and its applications. Curr Sci India 88:1759–1770
459. Kostrowicki J, Scheraga HA (1992) Application of the diffusion equation method for global optimization to oligopeptides. J Phys Chem-Us 96:7442–7449
460. Chang G, Guida WC, Still WC (1989) An internal coordinate Monte-Carlo method for searching conformational space. J Am Chem Soc 111:4379–4386
461. Morales LB, Gardunojuarez R, Romero D (1991) Applications of simulated annealing to the multiple-minima problem in small peptides. J Biomol Struct Dyn 8:721–735
462. Wilson SR et al (1991) Applications of simulated annealing to the conformational-analysis of flexible molecules. J Comput Chem 12:342–349
463. Grubmuller H (1995) Predicting slow structural transitions in macromolecular systems: conformational flooding. Phys Rev E Stat Phys Plasmas Fluids Relat Interdiscip Topics 52:2893–2906
464. Huber T, Torda AE, van Gunsteren WF (1994) Local elevation: a method for improving the searching properties of molecular dynamics simulation. J Comput Aided Mol Des 8:695–708
465. Iannuzzi M, Laio A, Parrinello M (2003) Efficient exploration of reactive potential energy surfaces using Car-Parrinello molecular dynamics. Phys Rev Lett 90:238302
466. Yang YD, Liu HY (2006) Genetic algorithms for protein conformation sampling and optimization in a discrete backbone dihedral angle space. J Comput Chem 27:1593–1602
467. Nanias M et al (2005) Protein structure prediction with the UNRES force-field using replica-exchange Monte Carlo-with-minimization; comparison with MCM, CSA, and CFMC. J Comput Chem 26:1472–1486
468. Grebner C et al (2011) Efficiency of tabu-search-based conformational search algorithms. J Comput Chem 32:2245–2253
469. Chu CM, Alsberg BK (2010) A knowledge-based approach for screening chemical structures within de novo molecular evolution. J Chemom 24:9
470. Sakae Y et al (2011) New conformational search method using genetic algorithm and knot theory for proteins. Pac Symp Biocomput 217–228
471. Watts KS et al (2010) ConfGen: a conformational search method for efficient generation of bioactive conformers. J Chem Inf Model 50:534–546
472. Ling S, Gutowski M (2011) SSC: a tool for constructing libraries for systematic screening of conformers. J Comput Chem 32:2047–2054, Published online in Wiley Online Library (wileyonlinelibrary.com; DOI 10.1002/jcc.21774)
473. Goldstein M, FredJ E, Gerber RB (2011) A new hybrid algorithm for finding the lowest minima of potential surfaces: approach and application to peptides. J Comput Chem 32:1785–1800, Published online in Wiley Online Library (wileyonlinelibrary.com; DOI 10.1002/jcc.21775)
474. Wales DJ, Doye JPK (1997) Global optimization by basin-hopping and the lowest energy structures of Lennard-Jones clusters containing up to 110 atoms. J Phys Chem A 101:5111–5116
475. Grebner C, Engels B (2012) A new tabu-search-based algorithm for solvation of proteins (in preparation)
476. Henkelman G, Jónsson H (1999) A dimer method for finding saddle points on high dimensional potential surfaces using only first derivatives. J Chem Phys 111:7010–7022
477. Kästner J, Sherwood P (2008) Superlinearly converging dimer method for transition state search. J Chem Phys 128:014106

478. Heyden A, Bell AT, Keil FJ (2005) Efficient methods for finding transition states in chemical reactions: comparison of improved dimer method and partitioned rational function optimization method. J Chem Phys 123:224101
479. Honda S et al (2004) 10 residue folded peptide designed by segment statistics. Structure 12:1507–1518
480. Satoh D et al (2006) Folding free-energy landscape of a 10-residue mini-protein, chignolin. FEBS Lett 580:3422–3426
481. Suenaga A et al (2007) Folding dynamics of 10-residue beta-hairpin peptide chignolin. Chem Asian J 2:591–598
482. Henkelman G, Jóhannesson G, Jónsson H (2000) Methods for finding saddle points and minimum energy paths. In: Schwartz SD (ed) Progress in theoretical chemistry and physics. Kluwer Academic, New York, page 269–3000
483. Baker J (1986) An algorithm for the location of transition-states. J Comput Chem 7:385–395
484. Banerjee A et al (1985) Search for stationary-points on surface. J Phys Chem-Us 89:52–57
485. Cerjan CJ, Miller WH (1981) On finding transition-states. J Chem Phys 75:2800–2806
486. Simons J et al (1983) Walking on potential-energy surfaces. J Phys Chem-Us 87:2745–2753
487. Henkelman G, Jónsson H (2000) Improved tangent estimate in the nudged elastic band method for finding minimum energy paths and saddle points. J Chem Phys 113:9978–9985
488. Quapp W, Bofill JM (2010) A comment to the nudged elastic band method. J Comput Chem 31:2526–2531
489. Sheppard D, Terrell R, Henkelman G (2008) Optimization methods for finding minimum energy paths. J Chem Phys 128:134106
490. Peters B et al (2004) A growing string method for determining transition states: comparison to the nudged elastic band and string methods. J Chem Phys 120:7877–7886
491. Woodcock HL et al (2003) Exploring the quantum mechanical/molecular mechanical replica path method: a pathway optimization of the chorismate to prephenate Claisen rearrangement catalyzed by chorismate mutase. Theor Chem Acc 109:140–148
492. Henkelman G, Uberuaga BP, Jónsson H (2000) A climbing image nudged elastic band method for finding saddle points and minimum energy paths. J Chem Phys 113:9901–9904
493. Goodrow A, Bell AT, Head-Gordon M (2008) Development and application of a hybrid method involving interpolation and ab initio calculations for the determination of transition states. J Chem Phys 129:174109
494. Goodrow A, Bell AT, Head-Gordon M (2009) Transition state-finding strategies for use with the growing string method. J Chem Phys 130:244108
495. Goodrow A, Bell AT, Head-Gordon M (2010) A strategy for obtaining a more accurate transition state estimate using the growing string method. Chem Phys Lett 484:392–398
496. Shang C, Liu ZP (2010) Constrained Broyden minimization combined with the dimer method for locating transition state of complex reactions. J Chem Theory Comput 6:1136–1144
497. Schwartz SD, Schramm VL (2009) Enzymatic transition states and dynamic motion in barrier crossing. Nat Chem Biol 5:552–559
498. Peter C et al (2004) Estimating entropies from molecular dynamics simulations. J Chem Phys 120:2652–2661
499. Zhang Y, Liu H, Yang W (2000) Free energy calculation on enzyme reactions with an efficient iterative procedure to determine minimum energy paths on a combined ab initio QM/MM potential energy surface. J Chem Phys 112:3483–3492
500. Torrie GM, Valleau JP (1977) Nonphysical sampling distributions in Monte Carlo free-energy estimation: umbrella sampling. J Comput Phys 23:187–199
501. Laio A, Parrinello M (2002) Escaping free-energy minima. Proc Natl Acad Sci USA 99:12562–12566
502. Hu H, Lu Z, Yang W (2007) QM/MM minimum free-energy path: methodology and application to triosephosphate isomerase. J Chem Theory Comput 3:390–406
503. Jorgensen WL (1989) Free energy calculations: a breakthrough for modeling organic chemistry in solution. Acc Chem Res 22:184–189

504. Rod TH, Ryde U (2005) Accurate QM/MM free energy calculations of enzyme reactions: methylation by catechol O-methyltransferase. J Chem Theory Comput 1:1240–1251
505. Valiev M et al (2007) Hybrid approach for free energy calculations with high-level methods: application to the SN2 reaction of CHCl3 and OH- in water. J Chem Phys 127:051102
506. Zwanzig RW (1954) High-temperature equation of state by a perturbation method. I. Nonpolar gases. J Chem Phys 22:1420–1426
507. Hori K et al (2011) A free-energy perturbation method based on Monte Carlo simulations using quantum mechanical calculations (QM/MC/FEP method): application to highly solvent-dependent reactions. J Comput Chem 32:778–786
508. Kästner J et al (2006) QM/MM free-energy perturbation compared to thermodynamic integration and umbrella sampling: application to an enzymatic reaction. J Chem Theory Comput 2:452–461
509. Senn HM et al (2009) Finite-temperature effects in enzymatic reactions - insights from QM/MM free-energy simulations. Can J Chem 87:1322–1337
510. Maurer P, Iftimie R (2010) Combining ab initio quantum mechanics with a dipole-field model to describe acid dissociation reactions in water: first-principles free energy and entropy calculations. J Chem Phys 132:074112
511. Sheppard AN, Acevedo O (2009) Multidimensional exploration of valley-ridge inflection points on potential-energy surfaces. J Am Chem Soc 131:2530–2540
512. Kirkwood JG (1935) Statistical mechanics of fluid mixtures. J Chem Phys 3:300
513. Sharma R et al (2008) A computational study of the intramolecular deprotonation of a carbon acid in aqueous solution. Phys Chem Chem Phys 10:2475–2487
514. Xie H-B et al (2010) Reaction mechanism of monoethanolamine with CO2 in aqueous solution from molecular modeling. J Phys Chem A 114:11844–11852
515. Yonezawa Y et al (2009) Intra- and intermolecular interaction inducing pyramidalization on both sides of a proline dipeptide during isomerization: an ab initio QM/MM molecular dynamics simulation study in explicit water. J Am Chem Soc 131:4535–4540
516. Yonezawa Y, Standley DM, Nakamura H (2011) Degree of pyramidality governs the height and peak position of the free-energy-barrier for the cis-trans isomerization of N-Methylacetamide. Chem Phys Lett 503:139–144
517. Alfonso-Prieto M et al (2009) The molecular mechanism of the catalase reaction. J Am Chem Soc 131:11751–11761
518. Petersen L et al (2009) Mechanism of cellulose hydrolysis by inverting GH8 endoglucanases: a QM/MM metadynamics study. J Phys Chem B 113:7331–7339
519. Stanton CL et al (2007) QM/MM metadynamics study of the direct decarboxylation mechanism for orotidine-5-monophosphate decarboxylase using two different QM regions: acceleration too small to explain rate of enzyme catalysis. J Phys Chem B 111:12573–12581
520. Ayala PY, Schlegel HB (1997) A combined method for determining reaction paths, minima, and transition state geometries. J Chem Phys 107:375
521. Zeng XC et al (2009) Calculating solution redox free energies with ab initio quantum mechanical/molecular mechanical minimum free energy path method. J Chem Phys 130:164111
522. Hu H, Yang W (2010) Elucidating solvent contributions to solution reactions with ab initio QM/MM methods. J Phys Chem B 114:2755–2759
523. Hu H, Boone A, Yang W (2008) Mechanism of OMP decarboxylation in orotidine 5'-monophosphate decarboxylase. J Am Chem Soc 130:14493–14503
524. Kirkilionis M (2010) Exploration of cellular reaction systems. Brief Bioinform 11:153–178
525. Simonson T (2008) Dielectric relaxation in proteins: the computational perspective. Photosynth Res 97:21–32
526. Jensen JH et al (2005) Prediction and rationalization of protein pK_a values using QM and QM/MM methods. J Phys Chem A 109:6634–6643
527. Buback V et al (2009) Rational design of improved aziridine-based inhibitors of cysteine proteases. J Phys Chem B 113:5282–5289

528. Helten H, Schirmeister T, Engels B (2004) Model calculations about the influence of protic environments on the alkylation step of epoxide, aziridine, and thiirane based cysteine protease inhibitors. J Phys Chem A 108:7691–7701
529. Paasche A et al (2009) Origin of the reactivity differences of substituted aziridines: CN vs CC bond breakages. J Org Chem 74:5244–5249
530. Vicik R et al (2006) Rational design of aziridine-containing cysteine protease inhibitors with improved potency: studies on inhibition mechanism. ChemMedChem 1:1021–1028
531. Reuter W, Engels B, Peyerimhoff SD (1992) Reaction of singlet and triplet methylene with ethene - a multireference configuration-interaction study. J Phys Chem-Us 96:6221–6232
532. Barone V, Cossi M (1998) Quantum calculation of molecular energies and energy gradients in solution by a conductor solvent model. J Phys Chem A 102:1995–2001
533. Klamt A, Eckert F, Arlt W (2010) COSMO-RS: an alternative to simulation for calculating thermodynamic properties of liquid mixtures. In: Prausnitz JM, Doherty MF, Segalman MA (eds) Annual review of chemical and biomolecular engineering, Vol 1 Annual Reviews, Palo Alto
534. Klamt A et al (1998) Refinement and parametrization of COSMO-RS. J Phys Chem A 102:5074–5085
535. Klamt A, Schuurmann G (1993) COSMO – a new approach to dielectric screening in solvents with explicit expressions for the screening energy and its gradient. J Chem Soc Perkin Trans 2 799–805
536. Ruiz-Lopez MF (2008) The multipole moment expansion solvent continuum model: a brief review. In: Canuto S (ed) Solvation effects on molecules and biomolecules: computational methods and applications. Springer
537. Schafer A et al (2000) COSMO implementation in TURBOMOLE: extension of an efficient quantum chemical code towards liquid systems. Phys Chem Chem Phys 2:2187–2193
538. Tomasi J (2004) Thirty years of continuum solvation chemistry: a review, and prospects for the near future. Theor Chem Acc 112:184–203
539. Tomasi J, Mennucci B, Cammi R (2005) Quantum mechanical continuum solvation models. Chem Rev 105:2999–3093
540. Zhan CG (2011) Development and application of first-principles electronic structure approach for molecules in solution based on fully polarizable continuum model. Acta Phys Chim Sin 27:1–10
541. Barone V, Biczysko M, Brancato G (2010) Extending the range of computational spectroscopy by QM/MM approaches: time-dependent and time-independent routes. In: Sabin JR, Brandas E, Canuto S (eds) Advances in quantum chemistry. Elsevier Academic, San Diego
542. Barone V, Improta R, Rega N (2008) Quantum mechanical computations and spectroscopy: from small rigid molecules in the gas phase to large flexible molecules in solution. Acc Chem Res 41:605–616
543. Barone V, Polimeno A (2007) Integrated computational strategies for UV/vis spectra of large molecules in solution. Chem Soc Rev 36:1724–1731
544. Pedone A, Biczysko M, Barone V (2010) Environmental effects in computational spectroscopy: accuracy and interpretation. Chemphyschem 11:1812–1832
545. Curutchet C et al (2009) Electronic energy transfer in condensed phase studied by a polarizable QM/MM model. J Chem Theory Comput 5:1838–1848
546. Difley S et al (2010) Electronic properties of disordered organic semiconductors via QM/MM simulations. Acc Chem Res 43:995–1004
547. Endres F (2010) Physical chemistry of ionic liquids. Phys Chem Chem Phys 12:1648
548. Fanfrlik J et al (2008) Interpretation of protein/ligand crystal structure using QM/MM calculations: case of HIV-1 protease/metallacarborane complex. J Phys Chem B 112:15094–15102
549. Helten H, Schirmeister T, Engels B (2005) Theoretical studies about the influence of different ring substituents on the nucleophilic ring opening of three-membered heterocycles and

possible implications for the mechanisms of cysteine protease inhibitors. J Org Chem 70:233–237
550. Peters MB, Raha K, Merz KM (2006) Quantum mechanics in structure-based drug design. Curr Opin Drug Discov Devel 9:370–379
551. Raha K et al (2007) The role of quantum mechanics in structure-based drug design. Drug Discov Today 12:725–731
552. LaPointe SM, Weaver DF (2007) A review of density functional theory quantum mechanics as applied to pharmaceutically relevant systems. Curr Comput Aided Drug Des 3:290–296
553. Cavalli A, Carloni P, Recanatini M (2006) Target-related applications of first principles quantum chemical methods in drug design. Chem Rev 106:3497–3519
554. Mladenovic M et al (2007) The importance of the active site histidine for the activity of epoxide- or aziridine-based inhibitors of cysteine proteases. ChemMedChem 2:120–128
555. Mladenovic M et al (2008) Atomistic insights into the inhibition of cysteine proteases: first QM/MM calculations clarifying the stereoselectivity of epoxide-based inhibitors. J Phys Chem B 112:11798–11808
556. Mladenovic M et al (2008) Atomistic insights into the inhibition of cysteine proteases: first QM/MM calculations clarifying the regiospecificity and the inhibition potency of epoxide- and aziridine-based inhibitors. J Phys Chem B 112:5458–5469
557. Mladenovic M et al (2009) Environmental effects on charge densities of biologically active molecules: do molecule crystal environments indeed approximate protein surroundings? J Phys Chem B 113:5072–5082
558. Warren JG et al (2010) Conformational preferences of pro line analogues with a fused benzene ring. J Phys Chem B 114:11761–11770
559. Gleeson MP, Gleeson D (2009) QM/MM calculations in drug discovery: a useful method for studying binding phenomena? J Chem Inf Model 49:670–677
560. Horowitz G (1998) Organic field-effect transistors. Adv Mater 10:365–377
561. Forrest SR (2004) The path to ubiquitous and low-cost organic electronic appliances on plastic. Nature 428:911–918
562. Gratzel M (2003) Dye-sensitized solar cells. J Photochem Photobiol C 4:145–153
563. Gregg BA, Hanna MC (2003) Comparing organic to inorganic photovoltaic cells: theory, experiment, and simulation. J Appl Phys 93:3605–3614
564. Bredas JL et al (2009) Molecular understanding of organic solar cells: the challenges. Acc Chem Res 42:1691–1699
565. May V, Kühn O (2004) Charge and energy transfer dynamics in molecular systems. Wiley-VCH, Weinheim
566. Forrest SR (1997) Ultrathin organic films grown by organic molecular beam deposition and related techniques. Chem Rev 97:1793–1896
567. Pullerits T, Sundstrom V (1996) Photosynthetic light-harvesting pigment-protein complexes: toward understanding how and why. Acc Chem Res 29:381–389
568. Grimsdale AC, Mullen K (2005) The chemistry of organic nanomaterials. Angew Chem Int Ed 44:5592–5629
569. Poulsen L et al (2007) Three-dimensional energy transport in highly luminescent host-guest crystals: a quantitative experimental and theoretical study. J Am Chem Soc 129:8585–8593
570. Herbst W, Hunger K (1997) Industrial organic pigments: production, properties, applications. Wiley-VCH, Weinheim
571. Klebe G et al (1989) Crystallochromy as a solid-state effect - correlation of molecular-conformation, crystal packing and color in perylene-3,4-9,10-bis(dicarboximide) pigments. Acta Crystallogr B 45:69–77
572. Graser F, Hadicke E (1984) Crystal-structure and color of perylene-3,4-9,10-bis (dicarboximide) pigments. 2. Liebigs Ann Chem 483–494
573. Forster T (1948) Zwischenmolekulare Energiewanderung Und Fluoreszenz. Ann Phys-Berlin 2:55–75

574. Forster T (1949) Experimentelle Und Theoretische Untersuchung Des Zwischenmolekularen Übergangs Von Elektronenanregungsenergie. Z Naturforsch A 4:321–327
575. Forster T (1969) Excimers. Angew Chem Int Ed 8:333
576. Eisenschlitz R, London F (1930) Über das Verhältnis der van der Waalschen Kräfte zu den Homöopolaren Bindungskräften. Zeitschr f Physik 60:491–527
577. Beljonne D et al (2011) Electronic processes at organic-organic interfaces: insight from modeling and implications for opto-electronic devices. Chem Mater 23:591–609
578. Bredas JL et al (2004) Charge-transfer and energy-transfer processes in pi-conjugated oligomers and polymers: a molecular picture. Chem Rev 104:4971–5003
579. Hennebicq E et al (2005) Exciton migration in rigid-rod conjugated polymers: an improved Forster model. J Am Chem Soc 127:4744–4762
580. Cornil J et al (2001) Interchain interactions in organic pi-conjugated materials: impact on electronic structure, optical response, and charge transport. Adv Mater 13:1053–1067
581. Hwang I, Scholes GD (2011) Electronic energy transfer and quantum-coherence in pi-conjugated polymers. Chem Mater 23:610–620
582. Olaya-Castro A, Scholes GD (2011) Energy transfer from Forster-Dexter theory to quantum coherent light-harvesting. Int Rev Phys Chem 30:49–77
583. Scholes GD (2003) Long-range resonance energy transfer in molecular systems. Annu Rev Phys Chem 54:57–87
584. Scholz R et al (2005) Investigation of molecular dimers in alpha-PTCDA by ab initio methods: binding energies, gas-to-crystal shift, and self-trapped excitons. Phys Rev B 72:18
585. Hoffmann M et al (2000) The lowest energy Frenkel and charge-transfer excitons in quasi-one-dimensional structures: application to MePTCDI and PTCDA crystals. Chem Phys 258:73–96
586. Gisslen L, Scholz R (2009) Crystallochromy of perylene pigments: interference between Frenkel excitons and charge-transfer states. Phys Rev B 80:23
587. Fink RF et al (2008) Ab initio configuration interaction description of excitation energy transfer between closely packed molecules. Chem Phys 343:353–361
588. Fink RF et al (2008) Assessment of quantum chemical methods and basis sets for excitation energy transfer. Chem Phys 346:275–285
589. Fink RF et al (2008) Exciton trapping in pi-conjugated materials: a quantum-chemistry-based protocol applied to perylene bisimide dye aggregates. J Am Chem Soc 130:12858
590. Zhao HM et al (2009) Understanding ground- and excited-state properties of perylene tetracarboxylic acid bisimide crystals by means of quantum chemical computations. J Am Chem Soc 131:15660–15668
591. Burquel A et al (2006) Pathways for photoinduced charge separation and recombination at donor-acceptor heterojunctions: the case of oligophenylenevinylene-perylene bisimide complexes. J Phys Chem A 110:3447–3453
592. Guthmuller J, Zutterman F, Champagne B (2009) Multimode simulation of dimer absorption spectra from first principles calculations: application to the 3,4,9,10-perylenetetracarboxylic diimide dimer. J Chem Phys 131:8
593. Beljonne D et al (2000) Interchain interactions in conjugated materials: the exciton model versus the supermolecular approach. J Chem Phys 112:4749–4758
594. Liu W et al (2011) Assessment of TD-DFT- and TD-HF-based approaches for the prediction of exciton coupling parameters, potential energy curves and electronic characters of electronically excited aggregates. J Comput Chem 32:1971–1981
595. Marcus Y (1988) Ionic-radii in aqueous-solutions. Chem Rev 88:1475–1498
596. Marcus Y (2009) Effect of ions on the structure of water: structure making and breaking. Chem Rev 109:1346–1370
597. Ohtaki H, Radnai T (1993) Structure and dynamics of hydrated ions. Chem Rev 93:1157–1204
598. Feig M (2010) Modelling solvent environments: applications to simulations of biomolecules. Wiley-VCH, Weinheim

599. Bernal JD (1937) An attempt at a molecular theory of liquid structure. Trans Faraday Soc 33:27–40
600. Bennetto HP, Caldin EF (1971) Solvent effects on kinetics of reactions of nickel(II) and cobalt(II) ions with 2,2′-bipyridyl and 2,2′,2″-terpyridyl. J Chem Soc A 2191
601. Bennetto HP, Caldin EF (1971) Kinetics of solvent exchange and ligand substitution reactions of metal ions in relation to structural properties of solvent. J Chem Soc A 2198
602. Bennetto HP, Caldin EF (1971) Kinetics of reaction of nickel(II) ions with 2,2′-bipyridyl in water-methanol mixtures. J Chem Soc A 2207
603. Frank HS, Wen W-Y (1957) Ion-solvent interaction. Structural aspects of ion-solvent interaction in aqueous solutions: a suggested picture of water structure. Discuss Faraday Soc 24:133–140
604. Tongraar A, Liedl KR, Rode BM (1997) Solvation of Ca^{2+} in water studied by Born-Oppenheimer ab initio QM/MM dynamics. J Phys Chem A 101:6299–6309
605. Tongraar A, Liedl KR, Rode BM (1998) Born-Oppenheimer ab initio QM/MM dynamics simulations of Na^+ and K^+ in water: from structure making to structure breaking effects. J Phys Chem A 102:10340–10347
606. Tongraar A, Liedl KR, Rode BM (1998) The hydration shell structure of Li^+ investigated by Born-Oppenheimer ab initio QM/MM dynamics. Chem Phys Lett 286:56–64
607. Tongraar A et al (2010) Structure of the hydrated Ca^{2+} and Cl^-: combined X-ray absorption measurements and QM/MM MD simulations study. Phys Chem Chem Phys 12:10876–10887
608. Azam SS, ul Zaheer H, Fatmi MQ (2010) Classical and QM/MM MD simulations of sodium (I) and potassium(I) ions in aqueous solution. J Mol Liq 153:95–100
609. Bucher D et al (2010) Coordination numbers of K^+ and Na^+ ions inside the selectivity filter of the KcsA potassium channel: insights from first principles molecular dynamics. Biophys J 98: L47–L49
610. Truong TN, Stefanovich EV (1996) Development of a perturbative approach for Monte Carlo simulations using a hybrid ab initio QM/MM method. Chem Phys Lett 256:348–352
611. Tongraar A, Hannongbua S (2008) Solvation structure and dynamics of ammonium (NH_4^+) in liquid ammonia studied by HF/MM and B3LYP/MM molecular dynamics simulations. J Phys Chem B 112:885–891
612. Intharathep P, Tongraar A, Sagarik K (2005) Structure and dynamics of hydrated NH_4^+: an ab initio QM/MM molecular dynamics simulation. J Comput Chem 26:1329–1338
613. Intharathep P, Tongraar A, Sagarik K (2006) Ab initio QM/MM dynamics of H_3O^+ in water. J Comput Chem 27:1723–1732
614. Takenaka N, Koyano Y, Nagaoka M (2010) Microscopic hydration mechanism in the ammonia dissolution process: importance of the solute QM polarization. Chem Phys Lett 485:119–123
615. Mohammed AM et al (2005) Quantum mechanical/molecular mechanical molecular dynamic simulation of zinc(II) ion in water. J Mol Liq 119:55–62
616. Vchirawongkwin V et al (2007) Ti(I) - the strongest structure-breaking metal ion in water? A quantum mechanical/molecular mechanical simulation study. J Comput Chem 28:1006–1016
617. Vchirawongkwin V et al (2007) Quantum mechanical/molecular mechanical simulations of the T1(III) ion in water. J Comput Chem 28:1057–1067
618. Fatmi MQ et al (2005) An extended ab initio QM/MM MD approach to structure and dynamics of Zn(II) in aqueous solution. J Chem Phys 123:054514
619. Fatmi MQ et al (2007) Stability of different zinc(II)-diamine complexes in aqueous solution with respect to structure and dynamics: a QM/MM MD study. J Phys Chem B 111:151–158
620. Fatmi MQ, Hofer TS, Rode BM (2010) The stability of $Zn(NH_3)_4^{2+}$ in water: a quantum mechanical/molecular mechanical molecular dynamics study. Phys Chem Chem Phys 12:9713–9718
621. Pham VT et al (2010) The solvent shell structure of aqueous iodide: X-ray absorption spectroscopy and classical, hybrid QM/MM and full quantum molecular dynamics simulations. Chem Phys 371:24–29

622. Tongraar A, Hannongbua S, Rode BM (2010) QM/MM MD simulations of iodide ion (I^-) in aqueous solution: a delicate balance between ion-water and water-water H-bond interactions. J Phys Chem A 114:4334–4339
623. Yagasaki T, Saito S, Ohmine I (2010) Effects of nonadditive interactions on ion solvation at the water/vapor interface: a molecular dynamics study. J Phys Chem A 114:12573–12584
624. Hinteregger E et al (2010) Structure and dynamics of the chromate ion in aqueous solution. An ab initio QMCF-MD simulation. Inorg Chem 49:7964–7968
625. Pribil AB et al (2008) Structure and dynamics of phosphate ion in aqueous solution: an ab initio QMCF MD study. J Comput Chem 29:2330–2334
626. Pribil AB et al (2008) Quantum mechanical simulation studies of molecular vibrations and dynamics of oxo-anions in water. Chem Phys 346:182–185
627. Tongraar A, Rode BM (2003) The hydration structures of F^- and Cl^- investigated by ab initio QM/MM molecular dynamics simulations. Phys Chem Chem Phys 5:357–362
628. Tongraar A, Tangkawanwanit P, Rode BM (2006) A combined QM/MM molecular dynamics simulations study of nitrate anion (NO_3^-) in aqueous solution. J Phys Chem A 110:12918–12926
629. Kubozono Y et al (1994) An EXAFS investigation of local-structure around Rb^+ in aqueous-solution. Z Naturforsch A 49:727–729
630. Munozpaez A et al (1995) EXAFS investigation of the 2nd hydration shell of metal-cations in dilute aqueous-solutions. Physica B 208:395–397
631. Munozpaez A, Pappalardo RR, Marcos ES (1995) Determination of the 2nd hydration shell of Cr^{3+} and Zn^{2+} in aqueous-solutions by extended X-ray-absorption fine-structure. J Am Chem Soc 117:11710–11720
632. Yaita T, Ito D, Tachimori S (1998) La-139 NMR relaxation and chemical shift studies in the aqueous nitrate and chloride solutions. J Phys Chem B 102:3886–3891
633. Chizhik VI et al (2002) Microstructure and dynamics of electrolyte solutions containing polyatomic ions by NMR relaxation and molecular dynamics simulation. J Mol Liq 98–9:173–182
634. Kaatze U (1983) Dielectric effects in aqueous-solutions of 1-1, 2-1, and 3-1 valent electrolytes - kinetic depolarization, saturation, and solvent relaxation. Z Phys Chem Neue Fol 135:51–75
635. Bopp P, Jancsó G, Heinzinger K (1983) An improved potential for non-rigid water molecules in the liquid phase. Chem Phys Lett 98:129–133
636. Jancso G, Bopp P, Heinzinger K (1984) Molecular dynamics study of high-density liquid water using a modified central-force potential. Chem Phys 85:377–387
637. Jorgensen WL et al (1983) Comparison of simple potential functions for simulating liquid water. J Chem Phys 79:926–935
638. Matsuoka O, Clementi E, Yoshimine M (1976) CI study of water dimer potential surface. J Chem Phys 64:1351–1361
639. Rowlinson JS (1951) The lattice energy of ice and the 2nd virial coefficient of water vapour. Trans Faraday Soc 47:120–129
640. Stillinger FH, Rahman A (1978) Revised central force potentials for water. J Chem Phys 68:666–670
641. Aguilar CM, De Almeida WB, Rocha WR (2008) Solvation and electronic spectrum of Ni^{2+} ion in aqueous and ammonia solutions: a sequential Monte Carlo/TD-DFT study. Chem Phys 353:66–72
642. Beret EC et al (2009) Opposite effects of successive hydration shells on the aqua ion structure of metal cations. Mol Simul 35:1007–1014
643. Eilmes A, Kubisiak P (2010) Relative complexation energies for Li^+ ion in solution: molecular level solvation versus polarizable continuum model study. J Phys Chem A 114:973–979

644. Mallik BS, Semparithi A, Chandra A (2008) A first principles theoretical study of vibrational spectral diffusion and hydrogen bond dynamics in aqueous ionic solutions: D_2O in hydration shells of Cl^- ions. J Chem Phys 129:194512
645. Men CJ, Tao FM (2007) Hydration and dissociation of calcium hydroxide in water clusters: a quantum chemical study. J Theor Comput Chem 6:595–609
646. Xenides D, Randolf BR, Rode BM (2006) Hydrogen bonding in liquid water: an ab initio QM/MM MD simulation study. J Mol Liq 123:61–67
647. Armunanto R, Schwenk CF, Rode BM (2005) Ab initio QM/MM simulation of Ag^+ in 18.6% aqueous ammonia solution: structure and dynamics investigations. J Phys Chem A 109:4437–4441
648. Santosh MS et al (2010) Molecular dynamics investigation of dipeptide - transition metal salts in aqueous solutions. J Phys Chem B 114:16632–16640
649. Marchi M, Sprik M, Klein ML (1990) Solvation and ionization of alkali-metals in liquid-ammonia - a path integral Monte-Carlo study. J Phys Condens Matter 2:5833–5848
650. Andzelm J, Kolmel C, Klamt A (1995) Incorporation of solvent effects into density-functional calculations of molecular-energies and geometries. J Chem Phys 103:9312–9320
651. Cossi M et al (2002) New developments in the polarizable continuum model for quantum mechanical and classical calculations on molecules in solution. J Chem Phys 117:43–54
652. Eckert F, Klamt A (2002) Fast solvent screening via quantum chemistry: COSMO-RS approach. AIChE J 48:369–385
653. Acevedo O, Jorgensen WL (2006) Solvent effects on organic reactions from QM/MM simulations. In: David CS (ed) Annual reports in computational chemistry. Elsevier, New Haven
654. Vayner G et al (2004) Steric retardation of S_N2 reactions in the gas phase and solution. J Am Chem Soc 126:9054–9058
655. Acevedo O, Jorgensen WL (2005) Influence of inter- and intramolecular hydrogen bonding on Kemp decarboxylations from QM/MM simulations. J Am Chem Soc 127:8829–8834
656. Acevedo O, Jorgensen WL (2006) Medium effects on the decarboxylation of a biotin model in pure and mixed solvents from QM/MM simulations. J Org Chem 71:4896–4902
657. Acevedo O, Jorgensen WL (2004) Solvent effects and mechanism for a nucleophilic aromatic substitution from QM/MM simulations. Org Lett 6:2881–2884
658. Chen X et al (2009) Steric and solvation effects in ionic S_N2 reactions. J Am Chem Soc 131:16162–16170
659. Geerke DP et al (2007) Combined QM/MM molecular dynamics study on a condensed-phase S_N2 reaction at nitrogen: the effect of explicitly including solvent polarization. J Chem Theory Comput 3:1499–1509
660. Singleton DA et al (2003) Mechanism of ene reactions of singlet oxygen. A two-step no-intermediate mechanism. J Am Chem Soc 125:1319–1328
661. Thompson JD, Cramer CJ, Truhlar DG (2003) Parameterization of charge model 3 for AM1, PM3, BLYP, and B3LYP. J Comput Chem 24:1291–1304
662. Acevedo O, Squillacote ME (2008) A new solvent-dependent mechanism for a triazolinedione ene reaction. J Org Chem 73:912–922
663. Acevedo O, Jorgensen WL (2006) Cope elimination: elucidation of solvent effects from QM/MM simulations. J Am Chem Soc 128:6141–6146
664. Acevedo O, Jorgensen WL (2007) Understanding rate accelerations for Diels-Alder reactions in solution using enhanced QM/MM methodology. J Chem Theory Comput 3:1412–1419
665. Acevedo O, Jorgensen WL, Evanseck JD (2007) Elucidation of rate variations for a Diels-Alder reaction in ionic liquids from QM/MM simulations. J Chem Theory Comput 3:132–138
666. Chandrasekhar J, Shariffskul S, Jorgensen WL (2002) QM/MM simulations for Diels-Alder reactions in water: contribution of enhanced hydrogen bonding at the transition state to the solvent effect. J Phys Chem B 106:8078–8085
667. Jorgensen WL et al (1994) Investigation of solvent effects on pericyclic-reactions by computer-simulations. J Chem Soc Faraday Trans 90:1727–1732

668. Thomas LL, Tirado-Rives J, Jorgensen WL (2010) Quantum mechanical/molecular mechanical modeling finds Diels-Alder reactions are accelerated less on the surface of water than in water. J Am Chem Soc 132:3097–3104
669. Gunaydin H et al (2007) Computation of accurate activation barriers for methyl-transfer reactions of sulfonium and ammonium salts in aqueous solution. J Chem Theory Comput 3:1028–1035
670. Lebrero MCG, Estrin DA (2007) QM-MM investigation of the reaction of peroxynitrite with carbon dioxide in water. J Chem Theory Comput 3:1405–1411
671. Alexandrova AN, Jorgensen WL (2007) Why urea eliminates ammonia rather than hydrolyzes in aqueous solution. J Phys Chem B 111:720–730
672. Estiu G, Merz KM (2004) Enzymatic catalysis of urea decomposition: elimination or hydrolysis? J Am Chem Soc 126:11832–11842
673. Jung YS, Marcus RA (2007) On the theory of organic catalysis on water. J Am Chem Soc 129:5492–5502
674. Jung YS, Marcus RA (2010) Protruding interfacial OH groups and 'on-water' heterogeneous catalysis. J Phys Condens Matter 22:284117
675. Narayan S et al (2005) "On water": unique reactivity of organic compounds in aqueous suspension. Angew Chem Int Ed 44:3275–3279
676. Zheng YY, Zhang JP (2010) Catalysis in the oil droplet/water interface for aromatic Claisen rearrangement. J Phys Chem A 114:4325–4333
677. Acevedo O, Armacost K (2010) Claisen rearrangements: insight into solvent effects and "on water" reactivity from QM/MM simulations. J Am Chem Soc 132:1966–1975
678. Marcus RA (2010) Spiers memorial lecture interplay of theory and computation in chemistry-examples from on-water organic catalysis, enzyme catalysis, and single-molecule fluctuations. Faraday Discuss 145:9–14
679. Radak BK et al (2009) Modeling reactive scattering of F(^{2}P) at a liquid squalane interface: a hybrid QM/MM molecular dynamics study. J Phys Chem A 113:7218–7226
680. Sambasivarao SV, Acevedo O (2009) Development of OPLS-AA force field parameters for 68 unique ionic liquids. J Chem Theory Comput 5:1038–1050
681. Gao JL (1991) A priori computation of a solvent-enhanced S_N2 reaction profile in water - the Menshutkin reaction. J Am Chem Soc 113:7796–7797
682. Arantes GM, Ribeiro MCC (2008) A microscopic view of substitution reactions solvated by ionic liquids. J Chem Phys 128:114503
683. Aggarwal A et al (2002) The role of hydrogen bonding in controlling the selectivity of Diels-Alder reactions in room-temperature ionic liquids. Green Chem 4:517–520
684. Ananikov VP, Musaev DG, Morokuma K (2010) Real size of ligands, reactants and catalysts: studies of structure, reactivity and selectivity by ONIOM and other hybrid computational approaches. J Mol Catal A-Chem 324:104–119
685. Qin S et al (2008) Computational investigation on stereochemistry in titanium-salicylaldehydes-catalyzed cyanation of benzaldehyde. J Org Chem 73:4840–4847
686. Drudis-Sole G et al (2008) DFT/MM study on copper-catalyzed cyclopropanation - enantioselectivity with no enthalpy barrier. Eur J Org Chem 5614–5621
687. Curet-Arana MC et al (2008) Quantum chemical determination of stable intermediates for alkene epoxidation with Mn-porphyrin catalysts. J Mol Catal A-Chem 285:120–127
688. Brookes NJ et al (2009) The influence of peripheral ligand bulk on nitrogen activation by three-coordinate molybdenum complexes - a theoretical study using the ONIOM method. J Comput Chem 30:2146–2156
689. Balcells D, Maseras F, Ujaque G (2005) Computational rationalization of the dependence of the enantioselectivity on the nature of the catalyst in the vanadium-catalyzed oxidation of sulfides by hydrogen peroxide. J Am Chem Soc 127:3624–3634
690. Drudis-Sole G et al (2005) A QM/MM study of the asymmetric dihydroxylation of terminal aliphatic n-alkenes with $OsO_4(DHQD)_2PYDZ$: enantioselectivity as a function of chain length. Chem-Eur J 11:1017–1029

691. Feldgus S, Landis CR (2000) Large-scale computational modeling of $[Rh(DuPHOS)]^+$-catalyzed hydrogenation of prochiral enamides: reaction pathways and the origin of enantioselection. J Am Chem Soc 122:12714–12727
692. Feldgus S, Landis CR (2001) Origin of enantioreversal in the rhodium-catalyzed asymmetric hydrogenation of prochiral enamides and the effect of the alpha-substituent. Organometallics 20:2374–2386
693. French SA et al (2004) Active sites for heterogeneous catalysis by functionalisation of internal and external surfaces. Catal Today 93–95:535–540
694. Santra S et al (2009) Adsorption of dioxygen to copper in CuHY zeolite. Phys Chem Chem Phys 11:8855–8866
695. Sklenak S et al (2009) Aluminium siting in the ZSM-5 framework by combination of high resolution Al-27 NMR and DFT/MM calculations. Phys Chem Chem Phys 11:1237–1247
696. Zeng XC et al (2008) Ab initio quantum mechanical/molecular mechanical simulation of electron transfer process: fractional electron approach. J Chem Phys 128:124510
697. Shavitt I (1985) Geometry and singlet-triplet energy-gap in methylene - a critical-review of experimental and theoretical determinations. Tetrahedron 41:1531–1542
698. Harrison JF (1974) Structure of methylene. Acc Chem Res 7:378–384
699. Borden WT, Davidson ER (1979) Singlet-triplet energy separations in some hydrocarbon diradicals. Annu Rev Phys Chem 30:125–153
700. Leopold DG et al (1985) Methylene - a study of the x $^3B_1$ and a $^1A_1$ states by photoelectron-spectroscopy of CH_2^- and CD_2. J Chem Phys 83:4849–4865
701. Schaefer HF (1986) Methylene - a paradigm for computational quantum-chemistry. Science 231:1100–1107
702. Hayashi S, Taikhorshid E, Schulten K (2009) Photochemical reaction dynamics of the primary event of vision studied by means of a hybrid molecular simulation. Biophys J 96:403–416
703. Roca-Sanjuan D et al (2009) DNA nucleobase properties and photoreactivity: modeling environmental effects. Pure Appl Chem 81:743–754
704. Rossle SC, Frank I (2009) First-principles simulation of photoreactions in biological systems. Front Biosci 14:4862–4877
705. Wanko M et al (2006) Computational photochemistry of retinal proteins. J Comput Aided Mol Des 20:511–518
706. Ryde U (2007) Accurate metal-site structures in proteins obtained by combining experimental data and quantum chemistry. Dalton Trans 607-625
707. Hersleth HP et al (2006) Structures of the high-valent metal-ion haem-oxygen intermediates in peroxidases, oxygenases and catalases. J Inorg Biochem 100:460–476
708. Kallrot N et al (2005) Theoretical study of structure of catalytic copper site in nitrite reductase. Int J Quantum Chem 102:520–541
709. Nilsson K et al (2004) The protonation status of compound II in myoglobin, studied by a combination of experimental data and quantum chemical calculations: quantum refinement. Biophys J 87:3437–3447
710. Nilsson K, Ryde U (2004) Protonation status of metal-bound ligands can be determined by quantum refinement. J Inorg Biochem 98:1539–1546
711. Rulisek L, Ryde U (2006) Structure of reduced and oxidized manganese superoxide dismutase: a combined computational and experimental approach. J Phys Chem B 110:11511–11518
712. Ryde U, Nilsson K (2003) Quantum refinement - a combination of quantum chemistry and protein crystallography. J Mol Struct-Theochem 632:259–275
713. Ryde U, Nilsson K (2003) Quantum chemistry can locally improve protein crystal structures. J Am Chem Soc 125:14232–14233
714. Ryde U, Olsen L, Nilsson K (2002) Quantum chemical geometry optimizations in proteins using crystallographic raw data. J Comput Chem 23:1058–1070

715. Soderhjelm P, Ryde U (2006) Combined computational and crystallographic study of the oxidised states of NiFe hydrogenase. J Mol Struct-Theochem 770:199–219
716. Ryde U, Greco C, De Gioia L (2010) Quantum refinement of FeFe hydrogenase indicates a dithiomethylamine ligand. J Am Chem Soc 132:4512
717. Ryde U et al (2007) Identification of the peroxy adduct in multicopper oxidases by a combination of computational chemistry and extended X-ray absorption fine-structure measurements. J Am Chem Soc 129:726–727
718. Hsiao YW et al (2006) EXAFS structure refinement supplemented by computational chemistry. Phys Rev B 74:214101
719. Hsiao Y-W, Ryde U (2006) Interpretation of EXAFS spectra for sitting-atop complexes with the help of computational methods. Inorg Chim Acta 359:1081–1092
720. Yu N et al (2006) Assigning the protonation states of the key aspartates in beta-secretase using QM/MM X-ray structure refinement. J Chem Theory Comput 2:1057–1069
721. Hudecova J et al (2010) Side chain and flexibility contributions to the Raman optical activity spectra of a model cyclic hexapeptide. J Phys Chem A 114:7642–7651
722. Bour P et al (2008) Vibrational circular dichroism and IR spectral analysis as a test of theoretical conformational modeling for a cyclic hexapeptide. Chirality 20:1104–1119
723. Gauss J (1992) Calculation of NMR chemical-shifts at 2nd-order many-body perturbation-theory using gauge-including atomic orbitals. Chem Phys Lett 191:614–620
724. Gauss J (1993) Effects of electron correlation in the calculation of nuclear-magnetic-resonance chemical-shifts. J Chem Phys 99:3629–3643
725. Buehl M et al (1999) The DFT route to NMR chemical shifts. J Comput Chem 20:91–105
726. Malkina OL et al (1998) Spin-orbit corrections to NMR shielding constants from density functional theory. How important are the two-electron terms? Chem Phys Lett 296:93–104
727. Pickard CJ, Mauri F (2001) All-electron magnetic response with pseudopotentials: NMR chemical shifts. Phys Rev B 63:245101
728. Vaara J et al (2001) Study of relativistic effects on nuclear shieldings using density-functional theory and spin-orbit pseudopotentials. J Chem Phys 114:61–71
729. Arnold WD, Oldfield E (2000) The chemical nature of hydrogen bonding in proteins via NMR: J-couplings, chemical shifts, and AIM theory. J Am Chem Soc 122:12835–12841
730. Autschbach J, Ziegler T (2000) Nuclear spin-spin coupling constants from regular approximate relativistic density functional calculations. II. Spin-orbit coupling effects and anisotropies. J Chem Phys 113:9410–9418
731. Benedict H et al (2000) Nuclear scalar spin-spin couplings and geometries of hydrogen bonds. J Am Chem Soc 122:1979–1988
732. Helgaker T, Jaszunski M, Ruud K (1999) Ab initio methods for the calculation of NMR shielding and indirect spin-spin coupling constants. Chem Rev 99:293–352
733. Helgaker T, Watson M, Handy NC (2000) Analytical calculation of nuclear magnetic resonance indirect spin-spin coupling constants at the generalized gradient approximation and hybrid levels of density-functional theory. J Chem Phys 113:9402–9409
734. Beer M, Kussmann J, Ochsenfeld C (2011) Nuclei-selected NMR shielding calculations: a sublinear-scaling quantum-chemical method. J Chem Phys 134:15
735. Kussmann J, Ochsenfeld C (2007) Linear-scaling method for calculating nuclear magnetic resonance chemical shifts using gauge-including atomic orbitals within Hartree-Fock and density-functional theory. J Chem Phys 127:16
736. Ochsenfeld C, Kussmann J, Koziol F (2004) Ab initio NMR spectra for molecular systems with a thousand and more atoms: a linear scaling method. Angew Chem Int Ed 43:4485–4489
737. Ciofini I (2004) Use of continuum models in magnetic resonance parameter calculation. In: Kaupp M, Buehl M, Malkin VG (eds) Calculation of NMR and EPR parameters. Wiley VCH Verlag GmbH & Co. KGaA, Weinheim
738. Pickard CJ, Mauri F (2004) Calculations of magnetic resonance parameters in solids and liquids using periodic boundary conditions. In: Kaupp M, Buehl M, Malkin VG (eds)

Calculation of NMR and EPR parameters. Wiley VCH Verlag GmbH & Co. KGaA, Weinheim
739. Johnson ER, DiLabio GA (2009) Convergence of calculated nuclear magnetic resonance chemical shifts in a protein with respect to quantum mechanical model size. J Mol Struct-Theochem 898:56–61
740. Pedone A et al (2008) Accurate first-principle prediction of ^{29}Si and ^{17}O NMR parameters in SiO_2 polymorphs: the cases of zeolites sigma-2 and ferrierite. J Chem Theory Comput 4:2130–2140
741. Heine T et al (2001) Performance of DFT for ^{29}Si NMR chemical shifts of silanes. J Phys Chem A 105:620–626
742. van Wüllen C (2004) Chemical shifts with Hartree-Fock and density functional methods. In: Kaupp M, Buehl M, Malkin VG (eds) Calculation of NMR and EPR parameters. Wiley VCH Verlag GmbH & Co. KGaA, Weinheim
743. Gauss J, Stanton JF (2004) Electron-correlated methods for the calculation of NMR chemical shifts. In: Kaupp M, Buehl M, Malkin VG (eds) Calculation of NMR and EPR parameters. Wiley VCH Verlag GmbH & Co. KGaA, Weinheim
744. Helgaker T, Pecul M (2004) Spin-spin coupling constants with HF and DFT methods. In: Kaupp M, Buehl M, Malkin VG (eds) Calculations of NMR and EPR parameters. Wiley VCH, Weinheim
745. Bjornsson R, Fruchtl H, Buehl M (2011) ^{51}V NMR parameters of $VOCl_3$: static and dynamic density functional study from the gas phase to the bulk. Phys Chem Chem Phys 13:619–627
746. Geethalakshmi KR et al (2009) ^{51}V NMR chemical shifts calculated from QM/MM models of peroxo forms of vanadium haloperoxidases. J Phys Chem B 113:4456–4465
747. Gester RM et al (2009) NMR chemical shielding and spin-spin coupling constants of liquid NH3: a systematic investigation using the sequential QM/MM method. J Phys Chem A 113:14936–14942
748. Harriman JE (1978) Theoretical foundations of electronic spin resonance. Academic, New York
749. Kaupp M, Buehl M, Malkin VG (2004) Calculation of NMR and EPR parameters. Wiley VCH Verlag GmbH & Co. KGaA, Weinheim
750. Weltner W (1983) Magnetic atoms and molecules. Van Nostrand Reinhold Company Inc., New York
751. Goldfarb D (2009) Modern EPR spectroscopy: beyond the EPR spectrum. Phys Chem Chem Phys 11:6553–6554
752. McWeeny R (1970) Spins in chemistry. Academic, New York
753. Lushington GH (2000) Small closed-form CI expansions for electronic g-tensor calculations. J Phys Chem A 104:2969–2974
754. Lushington GH, Bundgen P, Grein F (1995) Ab-initio study of molecular g-tensors. Int J Quantum Chem 55:377–392
755. Lushington GH, Grein F (1997) Multireference configuration interaction calculations of electronic g-tensors for NO_2, H_2O^+, and CO^+. J Chem Phys 106:3292–3300
756. Schreckenbach G, Ziegler T (1997) Calculation of the G-tensor of electron paramagnetic resonance spectroscopy using gauge-including atomic orbitals and density functional theory. J Phys Chem A 101:3388–3399
757. Malkina OL et al (2000) Density functional calculations of electronic g-tensors using spin-orbit pseudopotentials and mean-field all-electron spin-orbit operators. J Am Chem Soc 122:9206–9218
758. Kaupp M et al (2002) Calculation of electronic g-tensors for transition metal complexes using hybrid density functionals and atomic meanfield spin-orbit operators. J Comput Chem 23:794–803
759. Bolvin H (2006) An alternative approach to the g-matrix: theory and applications. Chemphyschem 7:1575–1589

760. Brownridge S et al (2003) Efficient calculation of electron paramagnetic resonance g-tensors by multireference configuration interaction sum-over-state expansions, using the atomic mean-field spin-orbit method. J Chem Phys 118:9552–9562
761. Delabie A et al (2002) The siting of Cu(II) in mordenite: a theoretical spectroscopic study. Phys Chem Chem Phys 4:134–145
762. Gilka N, Tatchen J, Marian CM (2008) The g-tensor of AlO: principal problems and first approaches. Chem Phys 343:258–269
763. Neese F (2007) Analytic derivative calculation of electronic g-tensors based on multireference configuration interaction wavefunctions. Mol Phys 105:2507–2514
764. Neyman KM et al (2002) Calculation of electronic g-tensors using a relativistic density functional Douglas-Kroll method. J Phys Chem A 106:5022–5030
765. Vahtras O, Engstrom M, Schimmelpfennig B (2002) Electronic g-tensors obtained with the mean-field spin-orbit Hamiltonian. Chem Phys Lett 351:424–430
766. Vancoillie S, Malmqvist P-Å, Pierloot K (2007) Calculation of EPR g tensors for transition-metal complexes based on multiconfigurational perturbation theory (CASPT2). Chemphyschem 8:1803–1815
767. van Lenthe E, Wormer PES, van der Avoird A (1997) Density functional calculations of molecular g-tensors in the zero-order regular approximation for relativistic effects. J Chem Phys 107:2488–2498
768. Gauss J, Kallay M, Neese F (2009) Calculation of electronic g-tensors using coupled cluster theory. J Phys Chem A 113:11541–11549
769. Arbuznikov AV et al (2002) Validation study of meta-GGA functionals and of a model exchange-correlation potential in density functional calculations of EPR parameters. Phys Chem Chem Phys 4:5467–5474
770. Arbuznikov AV, Kaupp M (2004) Unrestricted open-shell Kohn-Sham scheme with local hybrid exchange-correlation potentials: improved calculation of electronic g-tensors for transition-metal complexes. Chem Phys Lett 391:16–21
771. Arbuznikov AV, Kaupp M (2005) Localized hybrid exchange-correlation potentials for Kohn-Sham DFT calculations of NMR and EPR parameters. Int J Quantum Chem 104:261–271
772. Engels B, Peyerimhoff SD, Davidson ER (1987) Calculation of hyperfine coupling-constants - an ab initio MRD CI study for nitrogen to analyze the effects of basis-sets and CI parameters. Mol Phys 62:109–127
773. Knight LB et al (1987) Electron-spin-resonance and ab initio theoretical-studies of the cation radicals $^{14}N^{4+}$ and $^{15}N^{4+}$ - the trapping of ion neutral reaction-products in neon matrices at 4-K. J Chem Phys 87:885–897
774. Feller D, Davidson ER (1984) Ab initio configuration-interaction calculations of the hyperfine-structure in small radicals. J Chem Phys 80:1006–1017
775. Chipman DM (1983) Theoretical-study of the properties of methyl radical. J Chem Phys 78:3112–3132
776. Suter HU, Huang MB, Engels B (1994) A multireference configuration-interaction study of the hyperfine-structure of the molecules CCO, CNN, and NCN in their triplet ground-states. J Chem Phys 101:7686–7691
777. Engels B et al (1992) Study of the hyperfine coupling-constants (^{14}N And ^{1}H) of the NH_2 molecules in the X^2B_1 ground-state and the A^2A_1 excited-state. J Chem Phys 96:4526–4535
778. Engels B, Peyerimhoff SD (1988) Study of the 1s and 2s shell contributions to the isotropic hyperfine coupling-constant in nitrogen. J Phys B-At Mol Opt Phys 21:3459–3471
779. Engels B et al (1988) The hyperfine coupling-constants of the 5 lowest states of CH - an ab initio MRDCI study. Chem Phys Lett 152:397–401
780. Barone V et al (2009) Magnetic interactions in phenyl-bridged nitroxide diradicals: conformational effects by multireference and broken symmetry DFT approaches. J Phys Chem A 113:15150–15155

781. Svistunenko DA, Jones GA (2009) Tyrosyl radicals in proteins: a comparison of empirical and density functional calculated EPR parameters. Phys Chem Chem Phys 11:6600–6613
782. Munzarova M, Kaupp M (1999) A critical validation of density functional and coupled-cluster approaches for the calculation of EPR hyperfine coupling constants in transition metal complexes. J Phys Chem A 103:9966–9983
783. Munzarova ML, Kubacek P, Kaupp M (2000) Mechanisms of EPR hyperfine coupling in transition metal complexes. J Am Chem Soc 122:11900–11913
784. Arbuznikov AV, Vaara J, Kaupp M (2004) Relativistic spin-orbit effects on hyperfine coupling tensors by density-functional theory. J Chem Phys 120:2127–2139
785. Suter HU et al (1994) Difficulties in the calculation of electron-spin-resonance parameters using density-functional methods. Chem Phys Lett 230:398–404
786. Fangstrom T et al (1997) Structure and dynamics of the silacyclobutane radical cation, studied by ab initio and density functional theory and electron spin resonance spectroscopy. J Chem Phys 107:297–306
787. Huang MB et al (1995) Multireference configuration-interaction and density-functional study of the azetidine radical-cation and the neutral azetidin-1-Yl radical. J Phys Chem-Us 99:9724–9729
788. Suter HU, Engels B (1996) An ab initio determination of the magnetic hyperfine structure of C_2 in the four lowest triplet states. Chem Phys Lett 261:644–650
789. Cimino P et al (2010) Interplay of stereo-electronic, environmental, and dynamical effects in determining the EPR parameters of aromatic spin-probes: INDCO as a test case. Phys Chem Chem Phys 12:3741–3746
790. Engels B, Suter HU, Peric M (1996) Ab initio investigation of vibrational effects on magnetic hyperfine coupling constants in the $X^3\Sigma_g^-$ state of B_2H_2. J Phys Chem-Us 100:10121–10122
791. Peric M, Engels B (1992) Ab initio calculation of the vibronically averaged values for the hyperfine coupling-constants in NH_2, NHD, and ND_2. J Chem Phys 97:4996–5006
792. Staikova M et al (1993) Ab-initio calculations of the vibronically averaged hyperfine coupling-constants in the $1^2\Pi_u$ (X^2B_1, A^2A_1) state of the water cation. Mol Phys 80:1485–1497
793. Pavone M et al (2007) Interplay of intrinsic, environmental, and dynamic effects in tuning the EPR parameters of nitroxides: further insights from an integrated computational approach. J Phys Chem B 111:8928–8939
794. Funken K et al (1990) Study of the hyperfine coupling-constants of the molecules NH_2, NHD and ND_2. Chem Phys Lett 172:180–186
795. Peric M, Engels B, Peyerimhoff SD (1991) Ab initio investigation of the vibronic structure of the C_2H spectrum - calculation of the hyperfine coupling-constants for the 3 lowest-lying electronic states. J Mol Spectrosc 150:56–69
796. Peric M, Engels B, Peyerimhoff SD (1991) Ab initio investigation of the vibronic structure of the C_2H SPECTRUM - computation of the vibronically averaged values for the hyperfine coupling-constants. J Mol Spectrosc 150:70–85
797. Brancato G et al (2005) A mean field approach for molecular simulations of fluid systems. J Chem Phys 122:154109
798. Brancato G, Rega N, Barone V (2006) Reliable molecular simulations of solute-solvent systems with a minimum number of solvent shells. J Chem Phys 124:214505
799. Brancato G, Rega N, Barone V (2007) Unraveling the role of stereo-electronic, dynamical, and environmental effects in tuning the structure and magnetic properties of glycine radical in aqueous solution at different pH values. J Am Chem Soc 129:15380–15390
800. Brancato G, Rega N, Barone V (2008) A hybrid explicit/implicit solvation method for first-principle molecular dynamics simulations. J Chem Phys 128:144501
801. Rega N, Brancato G, Barone V (2006) Non-periodic boundary conditions for ab initio molecular dynamics in condensed phase using localized basis functions. Chem Phys Lett 422:367–371

802. Cossi M et al (1996) Ab initio study of solvated molecules: a new implementation of the polarizable continuum model. Chem Phys Lett 255:327–335
803. Naumov S, Reinhold J, Beckert D (2003) Investigation of the molecular structure of the radical anions of some pyrimidine-type bases in aqueous solution by comparison of calculated hyperfine coupling constants with EPR results. Phys Chem Chem Phys 5:64–72
804. Cances E, Mennucci B (2001) Comment on "reaction field treatment of charge penetration". J Chem Phys 114:4744–4745
805. Cossi M et al (2001) Polarizable dielectric model of solvation with inclusion of charge penetration effects. J Chem Phys 114:5691–5701
806. Cossi M et al (2003) Energies, structures, and electronic properties of molecules in solution with the C-PCM solvation model. J Comput Chem 24:669–681
807. Lu JM et al (2001) A Fourier transform EPR study of uracil and thymine radical anions in aqueous solution. Phys Chem Chem Phys 3:952–956
808. Houriez C et al (2009) Further insights into the environmental effects on the computed hyperfine coupling constants of nitroxides in aqueous solution. J Phys Chem B 113:15047–15056
809. Houriez C et al (2010) Structure and spectromagnetic properties of the superoxide radical adduct of DMPO in water: elucidation by theoretical investigations. J Phys Chem B 114:11793–11803
810. Adamo C et al (1999) Tuning of structural and magnetic properties of nitronyl nitroxides by the environment. A combined experimental and computational study. J Phys Chem A 103:3481–3488
811. Barone V et al (1998) Assessment of a combined QM/MM approach for the study of large nitroxide systems in vacuo and in condensed phases. J Am Chem Soc 120:7069–7078
812. Barone V, Cimino P (2009) Validation of the B3LYP/N07D and PBE0/N07D computational models for the calculation of electronic g-tensors. J Chem Theory Comput 5:192–199
813. Barone V et al (1993) Ab-initio configuration-interaction calculation of isotropic spin-densities in nitronyl and iminonitroxides. New J Chem 17:545–549
814. Beyer M et al (2003) Synthesis of novel aromatic nitroxides as potential DNA intercalators. An EPR spectroscopical and DFT computational study. J Org Chem 68:2209–2215
815. Cirujeda J et al (2000) Spin density distribution of a-nitronyl aminoxyl radicals from experimental and ab initio calculated ESR isotropic hyperfine coupling constants. J Am Chem Soc 122:11393–11405
816. di Matteo A et al (1999) Intrinsic and environmental effects in the physico-chemical properties of nitroxides. The case of 2-phenyl-4,4,5,5-tetramethyl-4,5-dihydro-1H-imidazol-1-oxyl 3-oxide. Chem Phys Lett 310:159–165
817. Mattar SM, Stephens AD (2000) UB1LYP hybrid density functional studies of the 2,2,6,6-tetramethyl-4-piperidone-oxyl (TEMPONE) hyperfine tensors. Chem Phys Lett 319:601–610
818. Stipa P (2006) A multi-step procedure for evaluating the EPR parameters of indolinonic aromatic aminoxyls: a combined DFT and spectroscopic study. Chem Phys 323:501–510
819. Zheludev A et al (1994) Spin-density in a nitronyl nitroxide free-radical - polarized neutron-diffraction investigation and ab-initio calculations. J Am Chem Soc 116:2019–2027
820. Colombo MC et al (2008) Copper binding sites in the C-terminal domain of mouse prion protein: a hybrid (QM/MM) molecular dynamics study. Proteins 70:1084–1098
821. Sinnecker S, Neese F (2006) QM/MM calculations with DFT for taking into account protein effects on the EPR and optical spectra of metalloproteins. Plastocyanin as a case study. J Comput Chem 27:1463–1475
822. Bernini C et al (2011) EPR parameters of amino acid radicals in P. eryngii versatile peroxidase and its W164Y variant computed at the QM/MM level. Phys Chem Chem Phys 13:5078–5098
823. Neese F (2003) A spectroscopy oriented configuration interaction procedure. J Chem Phys 119:9428–9443

824. Mattar SM, Durelle J (2010) Calculation of the 4,5-dihydro-1,3,2-dithiazolyl radical g-tensor components by the coupled-perturbed Kohn-Sham hybrid density functional and configuration interaction methods: a comparative study. Magn Reson Chem 48:S122–S131
825. Engels B (1991) Estimation of the influence of the configurations neglected within truncated multireference CI wave-functions on molecular-properties. Chem Phys Lett 179:398–404
826. Mattar SM (1999) Calculation of the ^{1}H ^{13}C, ^{14}N and ^{33}S hyperfine tensors of the 1,3,2-dithiazol-2-yl radical using hybrid density functionals. Chem Phys Lett 300:545–552
827. Arrondo JLR et al (1993) Quantitative studies of the structure of proteins in solution by Fourier-transform infrared-spectroscopy. Prog Biophys Mol Biol 59:23–56
828. Elliot A, Ambrose EJ (1950) Structure of synthetic polypeptides. Nature 165:921–922
829. Bour P, Keiderling TA (1993) Ab-initio simulations of the vibrational circular-dichroism of coupled peptides. J Am Chem Soc 115:9602–9607
830. Berova N, Nakanishi K, Woody RW (2000) Circular dichroism principles and applications. Wiley VCH, New York
831. Barron LD, Hecht L, Bell AD (1996) Vibrational Raman optical activity of biomolecules. In: Fasman GD (ed) Circular dichroism and the conformational analysis of biomolecules. Plenum, New York
832. Keiderling TA, Kubelka J, Hilario J (2006) Vibrational circular dichroism of biopolymers. Summary of methods and applications. In: Braiman MS, Gregoriou VG (eds) Vibrational spectroscopy of biological and polymeric materials. CRC, New York
833. Barron LD, Buckingham AD (1971) Rayleigh and Raman scattering from optically active molecules. Mol Phys 20:1111–1119
834. Barron LD, Buckingham AD (1975) Rayleigh and Raman optical-activity. Annu Rev Phys Chem 26:381–396
835. Barron LD, Buckingh AD (1973) Raman circular intensity differential observations on some monoterpenes. J Chem Soc Chem Commun 152–153
836. Nafie LA, Keiderling TA, Stephens PJ (1976) Vibrational circular-dichroism. J Am Chem Soc 98:2715–2723
837. Polavarapu PL (1990) Ab initio vibrational Raman and Raman optical-activity spectra. J Phys Chem-Us 94:8106–8112
838. Jalkanen KJ et al (2003) Vibrational analysis of various isotopomers of L-alanyl-L-alanine in aqueous solution: vibrational absorption, vibrational circular dichroism, Raman, and Raman optical activity spectra. Int J Quantum Chem 92:239–259
839. Stephens PJ et al (1994) Ab-initio calculation of vibrational absorption and circular-dichroism spectra using density-functional force-fields. J Phys Chem-Us 98:11623–11627
840. Jeon J, Cho M (2010) Direct quantum mechanical/molecular mechanical simulations of two-dimensional vibrational responses: N-methylacetamide in water. New J Phys 12:065001
841. Poully JC, Gregoire G, Schermann JP (2009) Evaluation of the ONIOM method for interpretation of infrared spectra of gas-phase molecules of biological interest. J Phys Chem A 113:8020–8026
842. Misra N et al (2010) Vibrational analysis of boldine hydrochloride using QM/MM approach. Spectrosc-Int J 24:483–499
843. Amadei A et al (2010) Theoretical-computational modelling of infrared spectra in peptides and proteins: a new frontier for combined theoretical-experimental investigations. Curr Opin Struct Biol 20:155–161
844. Daidone I et al (2010) On the origin of IR spectral changes upon protein folding. Chem Phys Lett 488:213–218
845. Horspool W, Armesto D (1992) Organic photochemistry: a comprehensive treatment. Ellis Horwood Limited, West Sussex
846. Dutoi AD et al (2010) Tracing molecular electronic excitation dynamics in real time and space. J Chem Phys 132:144302
847. Moret ME et al (2010) Electron localization dynamics in the triplet excited state of $[Ru(bpy)_3]^{2+}$ in aqueous solution. Chem-Eur J 16:5889–5894

848. Abel S et al (2011) Molecular simulations of dodecyl-beta-maltoside micelles in water: influence of the headgroup conformation and force field parameters. J Phys Chem B 115:487–499
849. Kistler KA, Matsika S (2009) Solvatochromic shifts of uracil and cytosine using a combined multireference configuration interaction/molecular dynamics approach and the fragment molecular orbital method. J Phys Chem A 113:12396–12403
850. Kistler KA, Matsika S (2010) Photophysical pathways of cytosine in aqueous solution. Phys Chem Chem Phys 12:5024–5031
851. Olsen JM et al (2010) Solvatochromic shifts in uracil: a combined MD-QM/MM study. J Chem Theory Comput 6:249–256
852. Oncak M, Lischka H, Slavicek P (2010) Photostability and solvation: photodynamics of microsolvated zwitterionic glycine. Phys Chem Chem Phys 12:4906–4914
853. Loos PF et al (2008) Theoretical investigation of the geometries and UV-vis spectra of poly (L-glutamic acid) featuring a photochromic azobenzene side chain. J Chem Theory Comput 4:637–645
854. Grimme S, Waletzke M (1999) A combination of Kohn-Sham density functional theory and multi-reference configuration interaction methods. J Chem Phys 111:5645–5655
855. Eckert-Maksic M et al (2010) Matrix-controlled photofragmentation of formamide: dynamics simulation in argon by nonadiabatic QM/MM method. Phys Chem Chem Phys 12: 12719–12726
856. Ruckenbauer M et al (2010) Azomethane: nonadiabatic photodynamical simulations in solution. J Phys Chem A 114:12585–12590
857. Koch DM et al (2006) Nonadiabatic trajectory studies of $NaI(H_2O)_n$ photodissociation dynamics. J Phys Chem A 110:1438–1454
858. Malaspina T, Coutinho K, Canuto S (2008) Analyzing the n ->pi* electronic transition of formaldehyde in water. A sequential Monte Carlo/time-dependent density functional theory. J Braz Chem Soc 19:305–311
859. Nielsen CB et al (2007) Density functional self-consistent quantum mechanics/molecular mechanics theory for linear and nonlinear molecular properties: applications to solvated water and formaldehyde. J Chem Phys 126:154112
860. Lin YL, Gao J (2007) Solvatochromic shifts of the n $\rightarrow$ π* transition of acetone from steam vapor to ambient aqueous solution: a combined configuration interaction QM/MM simulation study incorporating solvent polarization. J Chem Theory Comput 3:1484–1493
861. Wallqvist A, Ahlstrom P, Karlstrom G (1990) A new intermolecular energy calculation scheme - applications to potential surface and liquid properties of water. J Phys Chem-Us 94:1649–1656
862. Hermida-Ramon JM, Ohrn A, Karlstrom G (2009) Aqueous solvent effects on structure and lowest electronic transition of methylene peroxide in an explicit solvent model. Chem Phys 359:118–125

Top Curr Chem (2014) 351: 103–124
DOI: 10.1007/128_2011_193

Published online: 28 July 2011

Electronic Stress as a Guiding Force for Chemical Bonding

Alfredo Guevara-García, Paul W. Ayers, Samantha Jenkins, Steven R. Kirk, Eleonora Echegaray, and Alejandro Toro-Labbe

Abstract In the electron-preceding picture of chemical change, the paramount problem is identifying favorable changes in electronic structure. The electronic stress tensor provides this information; its eigenvectors represent electronic normal modes, pointing the way towards energetically favorable (or unfavorable) chemical rearrangements. The resulting method is well founded in both density functional theory and the quantum theory of atoms in molecules (QTAIM). Stress tensor analysis is a natural way to extend the QTAIM to address chemical reactivity. The definition and basic properties of the electronic stress tensor are reviewed and the inherent ambiguity of the stress tensor is discussed. Extending previous work in which the stress tensor was used to analyze hydrogen-bonding patterns, this work focuses on chemical bonding patterns in organic reactions. Other related material (charge-shift bonding, links to the second-density-derivative tensor) is summarized and reviewed. The stress tensor provides a multifaceted characterization of bonding and can be used to predict and describe bond formation and migration.

Keywords Chemical reaction prediction, Conceptual density functional theory, Ehrenfest force, Electronic stress tensor, Reaction force partitioning, Quantum theory of atoms in molecules

A. Guevara-García and P.W. Ayers (✉)
Department of Chemistry and Chemical Biology, McMaster University, Hamilton, ON, Canada
e-mail: ayers@mcmaster.ca

S. Jenkins and S.R. Kirk
College of Chemistry and Chemical Engineering, Hunan Normal University, Changsha, Hunan 410081, China

Department of Engineering, University West, Trollhättan 461 29, Sweden

E. Echegaray and A. Toro-Labbe
Laboratorio de Química Teórica Computacional (QTC), Facultad de Química, Pontificia Universidad Católica de Chile, Casilla 306, Correo 22, Santiago, Chile

Contents

1 The Electron-Preceding Picture

Chemical reactions are usually pictured as changes in a molecule's structure, as defined by the positions of its atomic nuclei. In this electron-following picture [1, 2], the rearrangement of the atomic nuclei is the essential feature of a chemical process, and the most favorable types of rearrangement can be revealed by normal mode analysis of the Hessian or the compliance matrix [3–5].

An alternative viewpoint considers the rearrangement of chemical bonds to be the essential feature of a chemical process. This is the electron-preceding picture, where the rearrangement of a molecule's electronic structure is considered to be the characteristic feature of chemical reactions [1, 2, 6, 7]. If one visualizes molecules with the classic "balls-and-springs" model, the electron-following picture represents structural transformations as changes in the atomic positions (balls), and the bonds (springs) stretch and deform as required by the change in the atomic positions. In the electron-preceding picture, one shifts the bonds (by tugging on the springs), and the atomic positions (balls) follow.

In the Born–Oppenheimer approximation, changes in the positions of the atomic nuclei and changes in molecular electronic structure occur in lockstep, so the electron-preceding and electron-following pictures are mathematically equivalent. The electron-following picture is much more widely used, however, mainly because there are standard methods for finding the normal vibrational modes from the Hessian or the compliance matrix. By contrast, it is not clear how one should define, much less compute, normal electronic modes.

We claim that the eigenvectors of the electronic stress tensor can be used to represent the normal modes of electronic rearrangement. Here we review previous work on this topic and pursue the key ideas further, focusing on the application of the electronic stress tensor to organic reactivity.

2 Background

2.1 The Electronic Stress Tensor

We were motivated to study the electronic stress tensor because it is an electronic quantity that is closely analogous to the vibrational Hessian used in the electron-following picture. The elements of the Hessian represent the change in a component of the force ($i = 1,2,3$; corresponding to the three Cartesian directions) on the αth nucleus in response to a change in the position of the βth nucleus in the j direction:

$$H_{\alpha i,\beta j} = -\frac{\partial F_{\alpha,i}}{\partial R_{\beta,j}}. \tag{1}$$

The eigenvectors of the Hessian matrix, **H**, correspond to the normal modes. Eigenvectors with positive eigenvalues indicate bound motions of the nuclei; eigenvalues with negative eigenvalues indicate unbound "dissociative" motions.

In the electron-preceding picture, we need to represent how the forces on a volume element of electron density respond to a shift in electron density. Imagine a small cube of constant electron density, centered at **r** with volume d**r**. Imagine deforming the cube of density by expanding or contracting its faces. The change in a component of the force on a face of the cube in response to a change in the area of the face defines an element of the stress tensor:

$$\sigma_{ij}(\mathbf{r}) = \frac{\partial F_i(\mathbf{r})}{\partial A_j}. \tag{2}$$

We use the eigenvectors of the stress tensor, $\vec{\sigma}(\mathbf{r})$, to represent the normal electronic modes. Eigenvectors with positive eigenvalues represent tensile modes; in these directions it is favorable to stretch the cube of electron density. Eigenvectors with negative eigenvalues represent compressive modes; in these directions it is favorable to squeeze the electron density. Near the center of a chemical bond, the stress tensor usually has one tensile mode (representing the attraction of the electrons at **r** towards the atomic nuclei) and two compressive modes (representing the attraction of electrons away from the bond axis towards the center of the chemical bond). Near the center of a ring of atoms in a molecule like benzene, the stress tensor usually has two tensile modes (representing the attraction of the electrons toward the atomic nuclei on the periphery of the ring) and one compressive mode (representing the fact that electrons are attracted into the plane of the ring). In the center of a cage of atoms, the stress tensor usually has three tensile modes [8–10].

2.2 Quantum Theory of Atoms in Molecules

The electronic stress tensor is defined at every point in space, but this is too much information to be routinely useful for qualitative studies of chemical bonding and molecular reactivity. Recalling that our goal is to understand how changes of the electrons in chemical bonds induce changes in atomic positions, it seems reasonable to focus not on the values of the stress tensor in atoms, but the values of the stress tensor in bonds. It is particularly interesting to consider the center of the bonding region, where the electron density cannot be assigned to either of the atoms that compose the bond. In this location the stress tensor provides "pure" information about the stresses on the electrons in the chemical bond, uncontaminated by the individual atomic contributions to the stress. For this reason, we focus our attention on the critical points in the electron density, i.e., places where the gradient of the electron density is zero, $\nabla\rho(\mathbf{r}_{\mathrm{cp}}) = 0$.

Critical points of the electron density are a key feature in the QTAIM propounded by Bader and coworkers [11, 12]. In QTAIM, interacting atoms are connected by a bond path, a ridgeline of high electron density. The only point on the bond path that is not assigned to one of the atoms is the saddle point on the ridgeline, which is called a bond critical point (bcp). Similarly, the center of a ring of atoms is defined by the ring critical point (rcp), which is the only point in the ring that is neither assigned to an atom nor to a pair of bonded atoms. At the center of a cage of atoms there is a cage critical point (ccp), which is the unique intersection point of all the atomic regions that form the cage. The critical points of the electron density are the only locations in space that unambiguously characterize a bond, ring, or cage of atoms, rather than one (possibly several, in the case of rings and cages) of the comprising atoms. By analyzing the stress tensor at the critical points of the electron density, we can understand how bonds, rings, and cages of atoms shift and deform during chemical processes.

QTAIM provides a topological description of molecular structure. This topological description is summarized in a "molecular graph" of atoms (maxima in the electron density) connected by bond paths (passing through bcps), together with higher-order features like rings (characterized by rcps) and cages (characterized by ccps) of atoms [13–16]. Chemical changes are often associated with catastrophes in which new bond paths are formed or existing bond paths disappear [17, 18]. The Poincaré–Hopf relation relates the number of electron-density-maxima (usually, but not always, located at the atomic nuclei) to the number and type of critical points:

$$n(\mathrm{max}) - n(\mathrm{bcp}) + n(\mathrm{rcp}) - n(\mathrm{ccp}) = 1. \tag{3}$$

In molecules there is an effective critical point at infinity because $\nabla\rho(\mathbf{r}) \to 0$ far away from the molecule. Taking this into account leads to the analogous formula for periodic solids, the Euler–Poincaré relation:

$$n(\mathrm{max}) - n(\mathrm{bcp}) + n(\mathrm{rcp}) - n(\mathrm{ccp}) = 0. \tag{4}$$

One implication of these formulae is that formation of a new bond path [increasing n(bcp) by one] coincides with creation of a ring of atoms (or occasionally a new maximum). Similarly, if one breaks a ring [n(rcp) decreases by one], a bond path (occasionally a cage) disappears [19].

The different types of critical points in the electron density can be classified based on the second derivative matrix of the electron density:

$$\left[\nabla\nabla^T\rho(\mathbf{r})\right]_{ij} = \frac{\partial^2\rho(\mathbf{r}_{ij})}{\partial r_i \partial r_j}. \tag{5}$$

The matrix $\nabla\nabla^T\rho(\mathbf{r})$ has one positive eigenvalue at a bcp, two at an rcp, and three at a ccp. Notice that this eigenstructure is exactly what one usually observes in the stress tensor. Thus, at a bcp, there is a "tensile" eigenvector of $\nabla\nabla^T\rho(\mathbf{r})$ that is tangent to the bond path, representing the attraction of the electrons in a volume element centered at the bcp towards the atomic nuclei at the termini of the bond. Also at a bcp, there are two "compressive" eigenvectors of $\nabla\nabla^T\rho(\mathbf{r})$ that are perpendicular to the bond path; these represent the attraction of electrons away from the bond path to the center of the bonding region.

Historically, eigenvector analysis of $\nabla\nabla^T\rho(\mathbf{r})$ has been very useful for describing structural changes in solids [17, 20–28]. We believe this is because the eigenvectors of $\nabla\nabla^T\rho(\mathbf{r})$ approximate the eigenvectors of the stress tensor. Indeed, at the critical points of the electron density in a one-electron system, the eigenvectors of the stress tensor and $\nabla\nabla^T\rho(\mathbf{r})$ are identical. Similarly, for a critical point of the electron density in a nearly uniform electron gas (where the second-order gradient expansion of the stress tensor is appropriate), the eigenvectors of $\overleftrightarrow{\sigma}(\mathbf{r})$ and $\nabla\nabla^T\rho(\mathbf{r})$ coincide [28, 29]. The suggestion that $\overleftrightarrow{\sigma}(\mathbf{r})$ might be approximated by $\nabla\nabla^T\rho(\mathbf{r})$ in QTAIM is already present in the first work of Bader on the electronic stress tensor [30]. Our experience shows, however, that analysis of electronic structure based on the stress tensor usually gives more reliable results.

We will not discuss the eigenvectors of $\nabla\nabla^T\rho(\mathbf{r})$, or their similarity to those of the stress tensor, any further in this work; the interested reader is referred to our recent publications for mathematical details and numerical comparisons of the two approaches [28, 31, 32].

3 The Electronic Stress Tensor

3.1 History

The use of the correspondence principle to define a quantum mechanical analog of the stress tensor in classical mechanics goes back to Schrödinger and Pauli [33, 34]. The interest of electronic structure theorists in the stress tensor has been episodic, starting with the rise of computational density functional theory in the

late 1970s and early 1980s [15, 30, 35–42]. After this work, the field was largely dormant for over a decade, until 2001, when Tachibana began to use the stress tensor to characterize chemical bonds and predict the chemical reactivity of materials [8–10, 43–51]. Physicists independently rediscovered the utility of the stress tensor for visualizing and characterizing electronic structure soon after [52–55]. Until recently, little of this work went beyond "proof of principle" computations. This is probably partly because computing the electronic stress tensor accurately is very difficult, requiring triple-zeta (and ideally larger) basis sets [46]. Whether the stress tensor can be accurately represented with the pseudopotential plane-wave calculations that are popular in condensed-matter physics is an open question.

3.2 Properties

3.2.1 Link to the Electronic Wavefunction

Although the electronic stress tensor can be computed directly from the N-electron wavefunction, Ψ, it is most convenient to write the equation for the stress tensor in terms of the one-electron density matrix:

$$\gamma(\mathbf{r},\mathbf{r}) = N \iint \cdots \int \Psi^*(\mathbf{r}',\mathbf{r}_2,\mathbf{r}_3,\ldots\mathbf{r}_N)\Psi(\mathbf{r},\mathbf{r}_2,\mathbf{r}_3,\ldots,\mathbf{r}_N)\mathrm{d}\mathbf{r}_2\mathrm{d}\mathbf{r}_3\ldots\mathrm{d}\mathbf{r}_N. \quad (6)$$

The diagonal element of the one-electron density matrix is the electron density, the probability of observing an electron at the point $\mathbf{r}$:

$$\rho(\mathbf{r}) = \gamma(\mathbf{r},\mathbf{r}). \quad (7)$$

The stress tensor, as defined by Schrödinger, Pauli, Epstein, and Bader, is then defined as [30, 33–35]:

$$\overleftrightarrow{\sigma}(\mathbf{r}) = -\frac{1}{4}\left[\left(\frac{\partial^2}{\partial r_i \partial r_j'} + \frac{\partial^2}{\partial r_i' \partial r_j} - \frac{\partial^2}{\partial r_i \partial r_j} - \frac{\partial^2}{\partial r_i' \partial r_j}\right)\gamma(\mathbf{r},\mathbf{r}')\right]_{\mathbf{r}=\mathbf{r}'}, \quad (8)$$

where

$$r_1 = x \quad r_2 = y \quad r_3 = z. \quad (9)$$

It follows directly from this definition that:

- The stress tensor is a real symmetric matrix:

$$\overleftrightarrow{\sigma}(\mathbf{r}) = \left(\overleftrightarrow{\sigma}(\mathbf{r})\right)^* \qquad \sigma_{ij}(\mathbf{r}) = \sigma_{ij}^*(\mathbf{r}), \quad (10)$$

$$\overleftrightarrow{\sigma}(\mathbf{r}) = \left(\overleftrightarrow{\sigma}(\mathbf{r})\right)^T \qquad \sigma_{ij}(\mathbf{r}) = \sigma_{ji}(\mathbf{r}). \tag{11}$$

- The trace of the stress tensor defines a kinetic energy density:

$$t(\mathbf{r}) = -\frac{1}{2}\mathrm{Tr}\left[\overleftrightarrow{\sigma}(\mathbf{r})\right]. \tag{12}$$

- The integrated trace of the stress tensor is proportional to the total kinetic energy:

$$T = -\frac{1}{2}\int \mathrm{Tr}\left[\overleftrightarrow{\sigma}(\mathbf{r})\right]\mathrm{d}\mathbf{r}. \tag{13}$$

3.2.2 Link to the Forces on Electrons

Recall that the stress tensor is defined as the change in force on the surface of a volume element from a differential change in the area of that element (2). On the other hand, (12) and (13) indicate that the stress tensor is linked not only to the electronic potential energy (which defines the force on the electrons), but also to the kinetic energy. The stress tensor is thus revealed as the key component in the differential virial theorem [30, 35, 56, 57]:

$$\mathbf{F}(\mathbf{r}) = -\nabla \cdot \overleftrightarrow{\sigma}(\mathbf{r}). \tag{14}$$

The force, $\mathbf{F}(\mathbf{r})$ in (14) is usually called the Ehrenfest or tension force; it is the average force that an electron in a molecule feels due its attraction to the atomic nuclei its repulsion from the $N-1$ other electrons [30, 58]:

$$\mathbf{F}(\mathbf{r}) = N\left\langle \Psi \middle| \nabla_{\mathbf{r}} \left(\sum_{\alpha=1}^{N_{\text{atoms}}} \frac{-Z_\alpha}{|\mathbf{r}-\mathbf{R}_\alpha|} + \sum_{i=2}^{N} \frac{1}{|\mathbf{r}-\mathbf{r}_i|} \right) \middle| \Psi \right\rangle. \tag{15}$$

Equation (14) is called the differential virial theorem because if one takes the dot product of both sides of (14) with $\mathbf{r}$ and integrates over all space one obtains [35, 56]

$$\int \mathbf{r}\cdot\mathbf{F}(\mathbf{r})\mathrm{d}\mathbf{r} = \int \nabla\cdot\overleftrightarrow{\sigma}(\mathbf{r})\cdot\mathbf{r}\mathrm{d}\mathbf{r} = -2T. \tag{16}$$

It is useful to define a potential that generates the Ehrenfest force:

$$\mathbf{F}(\mathbf{r}) = -\nabla \mathcal{V}(\mathbf{r}). \tag{17}$$

Although this potential is not uniquely defined by the defining equation (17), it can be uniquely defined by requiring that the potential energy of interaction for an electron far from a molecule is zero:

$$\underbrace{\lim}_{|\mathbf{r}|\to\infty} \mathcal{V}(\mathbf{r}) = 0. \tag{18}$$

The potential $\mathcal{V}(\mathbf{r})$ is closely related to the average potential defined by Slater [59, 60]; we call it the Ehrenfest potential. For Ehrenfest potentials that are homogeneous of degree minus one in $\mathbf{r}$, (16) gives the usual Coulombic virial relation between the total potential energy and the total kinetic energy, $-V = 2T$.

3.2.3 Inherent Ambiguity

Any definition of $\overleftrightarrow{\sigma}(\mathbf{r})$ whose divergence gives the correct Ehrenfest force is acceptable. That is, the stress tensor is an inherently ambiguous quantity. In particular, every possible divergence-free tensor, $\nabla \cdot \overleftrightarrow{\mathbf{G}}(\mathbf{r}) = 0$, provides an alternative definition of the stress tensor, namely:

$$\overleftrightarrow{\sigma}(\mathbf{r}) + \overleftrightarrow{\mathbf{G}}(\mathbf{r}). \tag{19}$$

That is, when one defines the stress tensor, one must make a choice of gauge [55, 61–67]. This ambiguity is closely related to the well-known ambiguity in the definition of the local kinetic energy [64, 68–71] and arises because there are infinitely many ways to define quantum mechanical operators that correspond to a given classical observable in the $\hbar \to 0$ limit [72, 73]. In practice, all of the definitions of the stress tensor that have been used in the literature belong to a very restricted two-parameter family of stress tensors [64]:

$$\sigma_{ij}^{(\alpha,\beta)}(\mathbf{r}) = -\frac{1}{2}\left[\alpha\left(\frac{\partial^2}{\partial r_i \partial r'_j} + \frac{\partial^2}{\partial r'_i \partial r_j}\right) - (1-\alpha)\left(\frac{\partial^2}{\partial r_i \partial r_j} + \frac{\partial^2}{\partial r'_i \partial r'_j}\right)\gamma(\mathbf{r},\mathbf{r}')\right]_{\mathbf{r}=\mathbf{r}'} + \frac{1}{2}\beta\delta_{ij}\nabla^2\rho(\mathbf{r}). \tag{20}$$

Other definitions are certainly possible, however [64]. The most common definition in the literature, by far, is (8), which is the special case of (20) where $\alpha = ½$ and $\beta = 0$.

4 Applications of the Stress Tensor

4.1 Computational Methods

All the computational results here used density functional theory (B3LYP [74–77]) and the *Gaussian* program (*G03* in Sect. 4.2; *G09* elsewhere) to find a Slater-determinant wavefunction [78, 79]. The electron density, stress tensor, and other properties were evaluated using AIMALL [80]. In all calculations, large polarized basis sets were used. Further computational details may be found in our other papers on this topic [31, 32].

4.2 Chemical Bond Characterization

Analyzing the stress tensor at the bcp, $\overleftrightarrow{\sigma}(\mathbf{r}_{\mathrm{bcp}})$, provides information about the stresses that electrons in the chemical bond feel. With rare exceptions, at the bcp the stress tensor has one tensile mode (which is nearly tangent to the bond path) and two compressive modes (which are nearly perpendicular to the bond path). The typical pattern of eigenvalues for the stress tensor at a bcp is then $\lambda_1 \leq \lambda_2 < 0 < \lambda_3$. The relative strength of these modes, as measured by their eigenvalues, can be used to characterize the bonding. In particular, the ratio of strength of the tensile mode (λ_3) to the average strength of the compressive modes, $(-1/2(\lambda_1 + \lambda_2))$,

$$\Xi = -\frac{\lambda_3}{\frac{1}{2}(\lambda_1 + \lambda_2)}, \tag{21}$$

can be used to characterize the transition from conventional covalent bonding (e.g., the carbon–carbon bond in ethane) to charge-shift bonding (the bond in F_2) [31, 81]. In Table 1 the eigenvalues of the stress tensor and the tensile/compressive ratio are tabulated for the paradigmatic series of molecules with increasing charge-shift-bonding character [81–83]. As the charge-shift nature of the bond increases, Ξ increases [31].

In a conventional covalent bond like the carbon–carbon bond in ethane (Fig. 1), the electron density at the bcp is greater than the sum of the electron densities of the

Table 1 The eigenvalues of the electronic stress tensor (λ_1, λ_2, λ_3) and the tensile to compressive ratio defined in (21), computed at the bcp of the indicated bond

	λ_1	λ_2	λ_3	Ξ
$H_3C–CH_3$	–0.172	–0.172	0.070	0.407
$H_2N–NH_2$	–0.253	–0.236	0.131	0.535
HO–OH	–0.294	–0.280	0.191	0.665
F–F	–0.362	–0.362	0.270	0.745

All calculations were performed at the B3LYP/cc-pVQZ level. This data is excerpted from [31]; further discussion can be found there

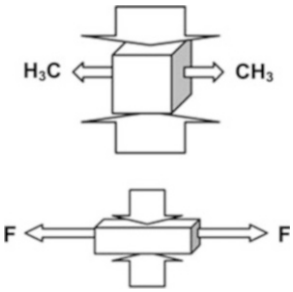

Fig. 1 A cartoon representation of volume element of the electron density at the bond critical point (bcp) and associated tensile and compressive modes of the stress tensor in ethane and the fluorine dimer. The *rectangular prism* represents the volume element at the bcp; it is deformed in a way that reveals the relative importance of tensile (stretching) and compressive (squeezing) forces on the bond

isolated fragments. That is, electron density accumulates in the central region of the chemical bond and the deformation density at the bcp is positive [81, 82, 84, 85]. In a charge-shift bond like the fluorine–fluorine bond in F_2 (Fig. 1), the electron density at the bcp is less than the sum of the electron densities of the isolated fragments; the deformation density at the bcp is negative [81, 82, 85]. In the valence-bond picture, the dominant energetic contribution to the charge-shift bond strength is the resonance energy with the ionic structures $F^+F^- \leftrightarrow F^-F^+$.

Analyzing the electronic stress tensor shows that the "mechanics" of electrons in covalent and charge-shift bonds is different. In a charge-shift bond, the tensile mode is stronger, relative to the compressive modes, than it is in a covalent bond. That is, in a charge-shift bond, the attraction of electrons to the nuclei is relatively high, which favors depletion of the electron density along the bond path. By contrast, in a covalent bond the compressive modes are relatively powerful, favoring accumulation of electron density along the bond path. Note that the compressive modes are actually stronger in F_2 than they are in ethane, even though F_2 is not a conventional covalently-bound molecule. The key feature is not the absolute strengths of the compressive and tensile modes, as this quantity is sensitive to the bond length and variations in the amplitude of the total electron density at the bcp. What matters is whether the tensile mode is stronger or weaker than usual, compared to the compressive mode.

4.3 Fracture, Migration, and Formation of Chemical Bonds

A weak compressive mode of the stress tensor at a bcp indicates that the compressive stresses that hold the bond path in place are weak. It is relatively easy, then, to move the bond path in the direction of the least compressive mode. Figure 2 shows a schematic representation of this effect in enol to aldehyde tautomerization of acetaldehyde.

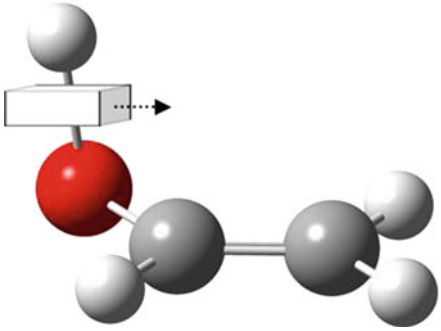

Fig. 2 A cartoon representation of the volume element of the electron density at the bond critical point (bcp) and the associated stress tensor in ethenol. The least compressive mode indicates the most facile direction in which to nudge the bond path. This motion, indicated by the *dotted arrow*, indicates the migration pathway of the hydrogen atom in the tautomerization reaction of ethenol to acetaldehyde

To explore more fully the predictive and interpretative power of the stress tensor in organic reactivity, one can use the stress-tensor in the context of reaction force analysis [86–90]. The reaction force is defined as minus one times the derivative of the potential energy curve with respect to the reaction coordinate:

$$F(\xi) = -\frac{\mathrm{d}U}{\mathrm{d}\xi} = -\left(\frac{\partial V_{\mathrm{nn}}}{\partial \xi} + \frac{\partial E}{\partial \xi}\right), \tag{22}$$

where V_{nn} is the nuclear–nuclear repulsion energy and E is the electronic energy. At stationary points of the potential energy curve – reactions, products, transition states, and reactive intermediates – the reaction force is zero. When $\mathrm{d}F(\xi)/\mathrm{d}\xi < 0$, this usually indicates that the dominant contributions to the energy come from changes in the molecular geometry; when $\mathrm{d}F(\xi)/\mathrm{d}\xi > 0$, changes in electronic structure usually dominate.

The eigenvectors of the electronic stress tensor, evaluated at critical points of the electron density and important structures along the reaction pathway for acetaldehyde tautomerization, are shown in Fig. 3.

As an example of how QTAIM, reaction force analysis, and the eigenvectors of the stress tensor at the critical points of the electron density can be used to elucidate the mechanical forces that drive chemical reactions, consider the ethenol to aldehyde tautomerization reaction. The key information needed for our analysis is in Fig. 3. In the reactant structure, the migrating hydrogen atom is connected by a bond path to the alcohol/aldehyde oxygen atom. Shifting the bond path requires perturbing the electron density, and the Hohenberg–Kohn variational principle indicates that shifting the electron density will cause the energy to increase. However, the amount of force that is required to nudge the bond away from its preferred pathway is least in the direction of the least-compressive eigenvector, $\hat{\mathbf{e}}_2$. Adjusting the bond path in the $\hat{\mathbf{e}}_2$ direction closes the OHC angle and reduces the

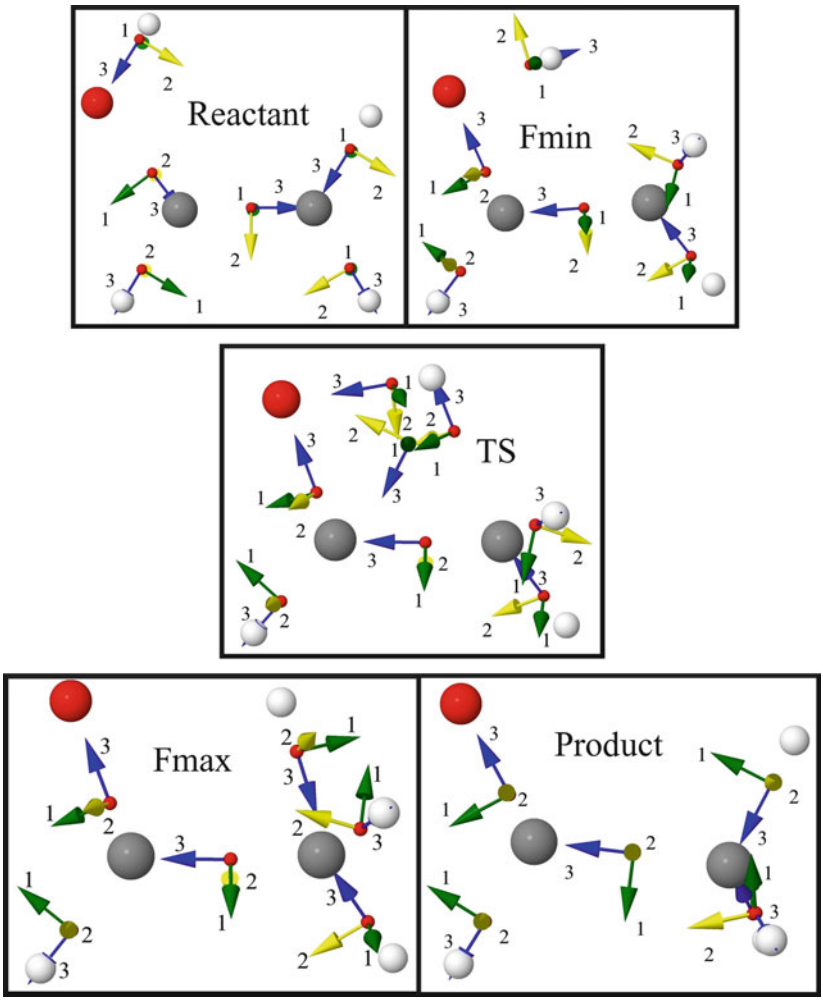

Fig. 3 Stress tensor analysis along the reaction path from the enol to the aldehyde form of acetaldehyde. The eigenvectors of the stress tensor at the critical points of the electron density are shown, labeled by their eigenvalues in increasing order, $\lambda_1 < \lambda_2 < \lambda_3$. The stress tensor was computed at the B3LYP/6-311G(d,p) level. Further details can be found in the paper of Guevara-García et al. [32]

HC bond distance, where C denotes the carbon atom in the $=CH_2$ group. The least compressive mode of the stress tensor "points the way" to chemical reactivity.

As one marches along the reaction coordinate, the reaction force decreases until it reaches a minimum value; the molecular conformation where the reaction force is minimized is called the force minimum (Fmin). The portion of the reaction coordinate between the reactant and the force minimum can be termed the "reactant region." In most reactions, the reaction region is dominated by geometric preparation;

large qualitative changes in electronic structure do not occur. This is true for this example also: the topology of the electron density (that is, the connectivity pattern of maxima and bond paths) does not change during this portion of the reaction path. The least compressive eigenvector, $-\hat{\mathbf{e}}_2$, associated with the OH bcp still points in the direction of favorable hydrogen migration. (Remember that the sign of the eigenvector is arbitrary.)

Starting at the force minimum, the reaction force increases, passing through zero (for the transition state) and finally reaching a maximum. This portion of the reaction path can be labeled as the transition-state region. The transition-state region is where most of the qualitative changes in electronic structure associated with the reaction normally occur, and this is also true in this example. Between the force minimum and the transition state, a new bond path and ring are formed. [Both are formed simultaneously, in accord with the Poincaré–Hopf relation (3)]. Between the transition state and the force maximum, the rcp and the bcp coalesce and annihilate each other, so that the only bond path in the force maximum structure is the one between the accepting carbon atom and the migrating hydrogen atom.

In the transition state, the motion of the hydrogen atom is along the tensile modes of the OH and CH bcps. Neither the OH nor the CH chemical bond is very strong in this region, so the tensile mode is relatively weak – it is easy to shift charge along these bond paths. It becomes difficult to discern how the bonds will rearrange based on the analysis of the stress tensor at the bcps, so we shift our focus to the rcp, which has one compressive eigenvector (with eigenvalue $\lambda_1 < 0$) and two tensile eigenvectors ($0 < \lambda_2 < \lambda_3$). The most "crushable" axis of the ring is associated with the smallest tensile mode. This mode corresponds to closing the OHC angle, which is the type of motion one expects to lead to the products of the reaction.

Starting at the force maximum, the reaction force decreases until it is again zero in the product structure. This portion of the reaction coordinate can be termed the product region, and it is ordinarily associated mostly with geometric relaxation, rather than qualitative changes in electronic structure. This is also true here: the topology of the electron density is qualitatively similar in the force maximum and product structures no new critical points are formed in the product region of the reaction coordinate.

In the force maximum and the product structures, it is the most compressive eigenvector, $\hat{\mathbf{e}}_1$, rather than the least compressive eigenvector, $\hat{\mathbf{e}}_2$, of the CH bcp that points the way to the reactants. Although this may seem counterintuitive, the least compressive eigenvector is in fact providing an accurate prediction of the easiest direction for CH bond migration: it points in the direction associated with methyl rotation.

Although the details of QTAIM, reaction force analysis, and stress tensor analysis differ from reaction to reaction, this same general pattern of reasoning is often fruitful [32]. In Fig. 4 the eigenvectors of the stress tensor are plotted for two interesting C–H bcps in 5-methylcyclopentadiene. Notice that the least compressive eigenvector points the way to the more stable isomer, 1-methylcyclopentadiene. In particular, the uppermost hydrogen atom in the figure moves out of the plane of the paper, away from the donor carbon atom, and towards the acceptor donor atom; the other hydrogen atom on the donor atom moves behind the plane of the ring.

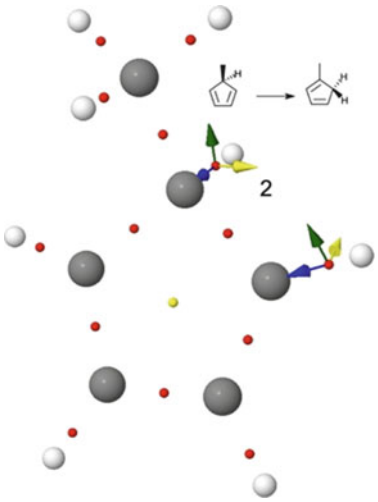

Fig. 4 Stress tensor analysis of the reactant in the 1,5-sigmatropic hydrogen shift reaction from 5-methylcyclopentadiene to 1-methylcyclopentadiene. The eigenvectors of the stress tensor at the bcps of the two active C–H bonds are shown. The stress tensor was computed at the B3LYP/6-311G(d,p) level. Further details can be found in the paper of Guevara-García et al. [32]

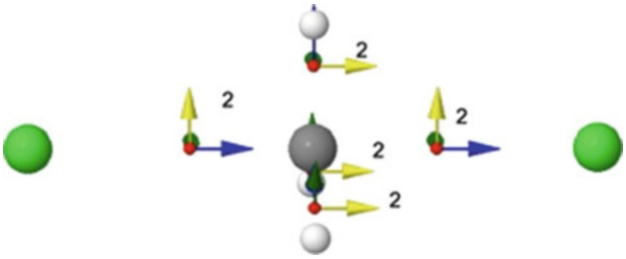

Fig. 5 The eigenvectors of the stress tensor at the bcps in the transition state of the symmetric S_N2 reaction of methyl chloride with Cl^-. The stress tensor was computed with B3LYP/6-311G(d,p)

Our limited experience with the stress tensor suggests that it usually gives reliable predictions and useful insight into chemical reactivity as long as the chemical reaction is associated with a change in the topology of the electron density. This is not always true: bond paths are not chemical bonds [91–96], and in some reactions there is no change in the topology of the electron density. For example, no new critical points are formed in the intramolecular hydrogen-migration in malonaldehyde [32]. Similarly, in the gas-phase symmetric S_N2 reaction of methyl chloride with Cl^-, there is a bond path connecting the nucleophilic Cl^- and the electrophilic carbon atom even in the reactant, and no new bond paths are formed throughout the entire energy profile. While the least-compressive eigenvectors of the C–Cl bcps do not provide any insight into the reaction mechanism, if one plots the stress tensor eigenvectors at the bcps of the C–H bonds in the transition state (Fig. 5), one observes that the least

compressive modes correspond to the out-of-plane motion that pushes the transition-state structure towards the tetrahedral product state.

4.4 Ehrenfest-Force Partitioning

Traditionally, the most important application of the electronic stress tensor has been for the visualization of the electronic structure and chemical binding in molecules and materials. For example, Tao et al. [52] use the trace of the stress tensor to locate electron-pair regions, in a manner reminiscent of the electron localization function [97–99]. It is not surprising that the stress tensor works well for this purpose: for any stress tensor in the family defined by (20), the trace of the stress tensor is a sum of the positive-definite local kinetic energy (the so-called localized orbital locator) and the electron-density Laplacian; both quantities are very effective for finding electron-pair regions [100–103]. The trace of the stress tensor, per electron, $\mathrm{Tr}\left[\overleftrightarrow{\sigma}(\mathbf{r})\right]/\rho(\mathbf{r})$, is proportional to the nighness indicator, which also locates electron-pair regions [71].

The stress tensor does provide other types of new interpretative information. For example, a characteristic feature of covalent binding is that the region in space where $\lambda_3 > 0$ forms a "spindle" [8, 44, 47].

Perhaps the most interesting information that one gleans is obtained from the Ehrenfest force, $\mathbf{F}(\mathbf{r}) = -\nabla \cdot \overleftrightarrow{\sigma}(\mathbf{r}) = -\nabla \mathcal{V}(\mathbf{r})$. $\mathbf{F}(\mathbf{r})$ is singular at a point-charge atomic nucleus because the Ehrenfest potential is singular there. The Ehrenfest force does not suffer from the same ambiguities as the underlying stress tensor (cf. Sect. 3.2.3), and arguably provides a better physical and mathematical foundation for further analysis.

In conventional QTAIM, one uses the gradient of the electron density, $\nabla\rho(\mathbf{r})$, to define atomic regions. Starting at the atomic nuclei (maxima in the electron density), following all possible gradient descent paths fills the volume of the atomic basin (cf. Fig. 6a). Critical points of the electron density lie on the boundaries between two or more atoms, and are not assigned to any one atomic basin. In QTAIM, to determine what atom a point in space is most closely associated with, one follows the ascending gradient path from that atom until the gradient path terminates at an atomic nucleus. One must be cautious, however, because of the occasional presence of nonnuclear maxima in the electron density.

One can perform a QTAIM-like analysis based on the Ehrenfest force, since $\mathbf{F}(\mathbf{r})$ also defines a vector field with a (divergent) maximum at the nucleus. For any given point in space, $\mathbf{r}_0$, one can follow the force-ascent lines to a nucleus, and decide that this atom exerts more force on the point $\mathbf{r}_0$ than the other atoms in the system. One must be cautious, however, because of the occasional presence of nonnuclear minima in the Ehrenfest potential [9, 10]. That is, in the same way that one may draw analogies between the stress tensor and the second derivative of the density, $\overleftrightarrow{\sigma}(\mathbf{r}) \sim \nabla\nabla^T\rho(\mathbf{r})$, one may draw analogies between the Ehrenfest force and the

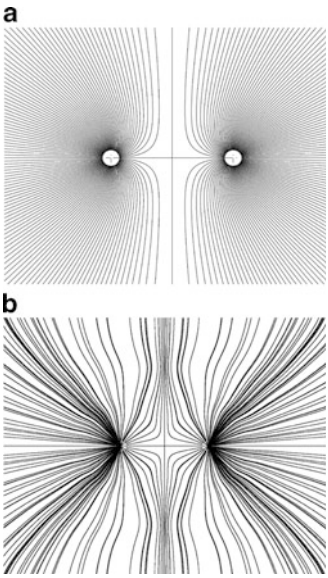

Fig. 6 The partitioning of the hydrogen molecule into atomic regions based on the gradient of the electron density (*top panel*) and the Ehrenfest force (*bottom panel*). The stress tensor and electron density were computed with B3LYP/6-311 ++G(d,p). The *vertical lines* in these figures were added to show the interatomic surface more clearly

gradient of the density, $\mathbf{F}(\mathbf{r}) \sim \nabla\rho(\mathbf{r})$, and between the Ehrenfest potential and the electron density, $\mathcal{V}(\mathbf{r}) \sim -\rho(\mathbf{r})$. Basins in the Ehrenfest potential define the region in which there are stable classical "orbits" around an atomic nucleus. Points where $\mathbf{F}(\mathbf{r}) = 0$ are called Lagrange points; at such points all the forces on an electron are balanced. Lagrange points lie on the boundaries between two basins of the Ehrenfest potential, and are analogous to critical points in QTAIM.

The gradient paths of the electron density and the Ehrenfest-force-descent curves are plotted for H_2 and H_2O in Figs. 6 and 7, respectively. The Ehrenfest-force partitioning is qualitatively similar to the usual QTAIM partitioning based on $\nabla\rho(\mathbf{r})$, but it is clear that the Ehrenfest force is much more sensitive to numerical noise than $\nabla\rho(\mathbf{r})$. (Recall that the Ehrenfest force is based on the third derivative of the one-electron reduced density matrix.) There are often extra regions (which we believe are spurious artifacts, perhaps from the diffuse functions in the basis set) far from the atomic centers. Based only on our preliminary results, we cannot say whether Ehrenfest-force-partitioning will eventually acquire the same practical utility as QTAIM, but we find the fundamental idea of partitioning a molecular system based on the forces that the atoms exert on an electron at a given point conceptually appealing. The main difference one sees between the electron-density-gradient partitioning (Fig. 7, top panel) and Ehrenfest-force partitioning (bottom panel) is that the hydrogen atoms in the force partitioning method are significantly larger. Recall that the Coulomb attraction to an atomic nucleus has a long r^{-1} tail, while atomic electron densities decay exponentially, like e^{-r}. It is perhaps not too surprising, then, that partitioning the water molecule using $\mathbf{F}(\mathbf{r}) = -\nabla\mathcal{V}(\mathbf{r})$ gives larger hydrogen basins than partitioning using $\nabla\rho(\mathbf{r})$.

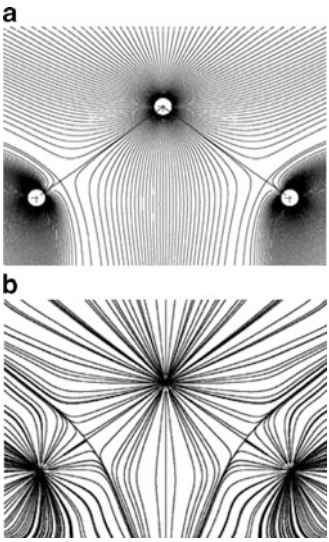

Fig. 7 The partitioning of the water molecule into regions based on the gradient of the electron density (*top panel*) and the Ehrenfest force (*bottom panel*). The stress tensor and electron density were computed with B3LYP/6-311++G(d,p). The spurious basins are believed to be an artifact of the basis set. In the *top panel*, interatomic " *bond lines*" were added for clarity

5 Past, Present, and Future

In 1980, Richard Bader wrote a paper entitled "Quantum Topology of Molecular Charge Distributions: The Mechanics of an Atom in a Molecule" in which he proposed that the electronic stress tensor, which he defined using (8), is the key quantity for understanding molecular electronic structure in a "mechanical" way. In the last decade we, together with other researchers, have been pursuing this suggestion. It is now clear that stress-tensor analysis can provide both quantitative assessment and qualitative insight about the nature of the chemical bond [8, 10, 43, 44, 52]. As one example, we showed how the relative strength of the tensile and compressive modes of the stress tensor, evaluated at the bcp, measure the extent of charge-shift bonding.

The fact that the stress tensor provides a *dynamical* picture of electrons moving under the influence of forces is arguably even more interesting. Traditionally, the QTAIM has been concerned with the qualitative description and taxonomy of molecular structures, while density-based tools for predicting and describing the most favorable modes of chemical reactivity have traditionally been taken from the field of conceptual DFT [104–109]. We provided a conceptual argument that the eigenvectors of the stress tensor, evaluated at the critical points of the electron density, represent the normal electronic modes of chemical reactivity in the electron-preceding picture [28]. By combining principles from QTAIM (most notably, the emphasis on the electronic stress tensor and the focus on critical points of the electron density) with the reaction-path partitioning method called reaction force analysis, we showed that the normal modes of the electronic stress tensor can not only describe but, in favorable cases, predict, the mechanism of a chemical reaction. The key feature of this analysis is that it allows one to discuss chemical

reactions using the classical–mechanical language of stress and force. We have already seen some limitations of this approach, most notably in cases where chemical reactions occur without any change in the topology in the electron density. In the future we hope to explore the scope of stress-tensor analysis for chemical reactions more thoroughly, and we are currently compiling a database of several hundred reaction pathways for this purpose.

In Sect. 4.4, we presented preliminary results on the Ehrenfest-force-partitioning of molecules into subsystems. It seems sensible to us to define regions in molecules based on the Ehrenfest force that electrons feel or, equivalently, based on the Ehrenfest potential that defines this force. In this picture, molecules are divided into subsystems, and the key "critical points" between the subsystems are the Lagrange points, where all the forces on the electrons are balanced and $\mathbf{F}(\mathbf{r}) = 0$. In Ehrenfest-force partitioning, Lagrange points lie on the boundary between atomic regions, which is reasonable if one considers that at a Lagrange point the forces on an electron from two (or more) atoms is balanced. We believe this approach is attractive conceptually and it is arguably the most natural way to define molecular subsystems if one wishes to use the electron-density stress as the key quantity for describing molecular electronic structure and reactivity. Whether the numerical difficulties we have encountered can be overcome is an important question for the future.

Acknowledgments PWA thanks the Canada Research Chairs and NSERC for funding. Computational facilities were provided by Sharcnet. AG-G was supported by a fellowship from CONACYT (Mexico). The Knowledge Foundation (grant number 2004/0284) and the Hundred Talents Foundation of Hunan Province are gratefully acknowledged for the support of SJ and SRK. EE and ATL acknowledge financial support from Fondecyt through project No. 1090460

References

1. Nakatsuji H (1974) Common nature of the electron cloud of a system undergoing change in nuclear configuration. J Am Chem Soc 96:24–30
2. Nakatsuji H (1974) Electron-cloud following and preceding and the shapes of molecules. J Am Chem Soc 96:30–37
3. Nichols J, Taylor H, Schmidt P, Simons J (1990) Walking on potential-energy surfaces. J Chem Phys 92:340–346
4. Decius JC (1963) Compliance matrix and molecular vibrations. J Chem Phys 38:241–248
5. Swanson BI, Satija SK (1977) Molecular vibrations and reaction pathways: minimum energy coordinates and compliance constants for some tetrahedral and octahedral complexes. J Am Chem Soc 99:987–991
6. Nalewajski RF (2000) Coupling relations between molecular electronic and geometrical degrees of freedom in density functional theory and charge sensitivity analysis. Comput Chem 24:243–257
7. Nalewajski RF (2006) Probing the interplay between electronic and geometric degrees-of-freedom in molecules and reactive systems. Adv Quantum Chem 51:235–305
8. Tachibana A (2005) A new visualization scheme of chemical energy density and bonds in molecules. J Mol Model 11:301–311

9. Szarek P, Tachibana A (2007) The field theoretical study of chemical interaction in terms of the rigged QED: new reactivity indices. J Mol Model 13:651–663
10. Szarek P, Sueda Y, Tachibana A (2008) Electronic stress tensor description of chemical bonds using nonclassical bond order concept. J Chem Phys 129:094102
11. Bader RFW (1990) Atoms in molecules: a quantum theory. Clarendon, Oxford
12. Popelier PLA (2000) Atoms in molecules: an introduction. Pearson, Harlow
13. Bader RFW, Nguyendang TT, Tal Y (1979) Quantum topology of molecular charge-distributions. 2. Molecular-structure and its change. J Chem Phys 70(9):4316–4329
14. Bader RFW, Tal Y, Anderson SG, Nguyen-Dang TT (1980) Quantum topology: theory of molecular structure and its change. Isr J Chem 19:8–29
15. Bader RFW, Nguyendang TT (1981) Quantum-theory of atoms in molecules: Dalton revisited. Adv Quantum Chem 14:63–124
16. Tal Y, Bader RFW, Nguyendang TT, Ojha M, Anderson SG (1981) Quantum topology. 4. Relation between the topological and energetic stabilities of molecular structures. J Chem Phys 74:5162–5167
17. Bone RGA, Bader RFW (1996) Identifying and analyzing intermolecular bonding interactions in van der Waals molecules. J Phys Chem 100:10892–10911
18. Bader RFW, Laidig KE (1991) The prediction and calculation of properties of atoms in molecules. Theochem 80:75–94
19. Collard K, Hall GG (1977) Orthogonal trajectories of the electron density. Int J Quantum Chem 12:623–637
20. Jenkins S, Morrison I (1999) Characterization of various phases of ice on the basis of the charge density. J Phys Chem B 103:11041–11049
21. Jenkins S, Heggie MI (2000) Quantitative analysis of bonding in 90 degrees partial dislocation in diamond. J Phys Condens Matter 12:10325–10333
22. Jenkins S, Morrison I (2000) The chemical character of the intermolecular bonds of seven phases of ice as revealed by ab initio calculation of electron densities. Chem Phys Lett 317:97–102
23. Jenkins S, Morrison I (2001) The dependence on structure of the projected vibrational density of states of various phases of ice as calculated by ab initio methods. J Phys Condens Matter 13:9207–9229
24. Jenkins S, Kirk SR, Ayers PW (2006) Topological transitions between ice phases. In: Kuhs WF (ed) Physics and chemistry of ice (PCI-2006). Royal Society of Chemistry, pp 249–256
25. Jenkins S, Kirk SR, Ayers PW (2006) The importance of O-O bonding interactions in various phases of ice. In: Kuhs WF (ed) Physics and chemistry of ice (PCI-2006). Royal Society of Chemistry, pp 257–263
26. Jenkins S, Kirk SR, Ayers PW (2006) The chemical character of very high pressure ice phases. In: Kuhs WF (ed) Physics and chemistry of ice (PCI-2006). Royal Society of Chemistry, pp 265–272
27. Jenkins S, Kirk SR, Ayers PW (2006) Real-space study of mechanical instability of ice XI on a 'bond-by-bond' basis. In: Kuhs WF (ed) Physics and chemistry of ice (PCI-2006). Royal Society of Chemistry, pp 273–280
28. Ayers PW, Jenkins S (2009) An electron-preceding perspective on the deformation of materials. J Chem Phys 130:154104
29. Holas A, March NH (1995) Exact theorems concerning noninteracting kinetic-energy density functional in D dimensions and their implications for gradient expansions. Int J Quantum Chem 56:371–383
30. Bader RFW (1980) Quantum topology of molecular charge-distributions. 3. The mechanics of an atom in a molecule. J Chem Phys 73:2871–2883
31. Jenkins S et al. (2011) The mechanics of charge-shift bonds: A perspective from the electronic stress tensor. Chem Phys Lett 510:18–20
32. Guevara-García A et al. (2011) Pointing the way to the products? Comparison of the stress tensor and the second-derivative tensor of the electron density. J Chem Phys 134:234106

33. Schrödinger E (1927) Der energieimpulssatz der materiewellen. Ann Phys 387:265–272
34. Pauli W (1958) Handbuch der physik. Springer, Berlin
35. Epstein ST (1975) Coordinate invariance, the differential force law, and the divergence of the stress-energy tensor. J Chem Phys 63:3573–3574
36. Bartolotti LJ, Parr RG (1980) The concept of pressure in density functional theory. J Chem Phys 72:1593–1596
37. Deb BM, Bamzai AS (1978) Internal stresses in molecules. 1. One-electron systems. Mol Phys 35:1349–1367
38. Deb BM, Bamzai AS (1979) Internal stresses in molecules. 2. Local view of chemical-binding in the H2 molecule. Mol Phys 38:2069–2097
39. Deb BM, Ghosh SK (1979) Some local force densities and stress tensors in molecular quantum mechanics. J Phys B At Mol Opt Phys 12:3857–3871
40. Ghosh SK, Berkowitz M (1985) A classical fluid-like approach to the density-functional formalism of many-electron systems. J Chem Phys 83:2976–2983
41. Nielsen OH, Martin RM (1983) 1st-Principles calculation of stress. Phys Rev Lett 50:697–700
42. Nielsen OH, Martin RM (1985) Quantum-mechanical theory of stress and force. Phys Rev B 32:3780–3791
43. Tachibana A (2001) Electronic energy density in chemical reaction systems. J Chem Phys 115:3497–3518
44. Tachibana A (2004) Spindle structure of the stress tensor of chemical bond. Int J Quantum Chem 100:981–993
45. Ichikawa K, Tachibana A (2009) Stress tensor of the hydrogen molecular ion. Phys Rev A 80:062507
46. Ichikawa K, Wagatsuma A, Kusumoto M, Tachibana A (2010) Electronic stress tensor of the hydrogen molecular ion: comparison between the exact wave function and approximate wave functions using Gaussian basis sets. J Mol Struct Theochem 951:49–59
47. Tachibana A (2010) Energy density concept: a stress tensor approach. J Mol Struct Theochem 943:138–151
48. Henry DJ et al (2011) Reactivity and regioselectivity of aluminum nanoclusters: insights from regional density functional theory. J Phys Chem C 115:1714–1723
49. Fukushima A, Senami M, Tsuchida Y, Tachibana A (2010) Local dielectric property of cubic hafnia. Jpn J Appl Phys 49:111504
50. Ichikawa K et al (2009) A theoretical study on a reaction of iron(III) hydroxide with boron trichloride by ab initio calculation. J Mol Struct Theochem 915:1–10
51. Szarek P et al. (2009) Regional DFT: electronic stress tensor study of aluminum nano-structures for hydrogen storage. In: Wei DQ, Wang XJ (eds) Theory and applications of computational chemistry – 2008, AIP conference proceedings, vol 1102, pp 299–305
52. Tao JM, Vignale G, Tokatly IV (2008) Quantum stress focusing in descriptive chemistry. Phys Rev Lett 100:206405
53. Tokatly IV (2005) Quantum many-body dynamics in a Lagrangian frame: I. Equations of motion and conservation laws. Phys Rev B 71:165104
54. Maranganti R, Sharma P (2010) Revisiting quantum notions of stress. Proc R Soc A Math Phys Eng Sci 466:2097–2116
55. Maranganti R, Sharma P, Wheeler L (2007) Quantum notions of stress. J Aerospace Eng 20:22–37
56. Holas A, March NH (1995) Exact exchange-correlation potential and approximate exchange potential in terms of density matrices. Phys Rev A 51:2040–2048
57. Nagy A, March NH (1997) Differential and local virial theorem. Mol Phys 91:597–602
58. Ehrenfest P (1927) Bemerkung über die angenäherte Gültigkeit der klassischen Mechanik innerhalb der Quantenmechanik. Z Phys A 45:455–457
59. Slater JC (1951) A simplification of the Hartree-Fock method. Phys Rev 81(3):385–390
60. Yang ZZ, Davidson ER (1997) Evaluation of a characteristic atomic radius by an ab initio method. Int J Quantum Chem 62(1):47–53

61. Rogers CL, Rappe AM (2002) Geometric theory of stress fields for quantum systems at finite temperature. In: Landau DP, Lewis SP, Schuttler HB (eds) Computer simulation studies in condensed-matter physics xiv, Springer Proceedings in Physics, vol 89, pp 209–213
62. Rogers CL, Rappe AM (2002) Geometric formulation of quantum stress fields. Phys Rev B 65:224117
63. Godfrey MJ (1988) Stress-field in quantum systems. Phys Rev B 37:10176–10183
64. Anderson JSM, Ayers PW, Hernandez JIR (2010) How ambiguous is the local kinetic energy? J Phys Chem A 114:8884–8895
65. Morante S, Rossi GC, Testa M (2006) The stress tensor of a molecular system: an exercise in statistical mechanics. J Chem Phys 125:034101
66. Nelson DF, Lax M (1976) Asymmetric total stress tensor. Phys Rev B 13:1770–1776
67. Das A (1978) Stress tensor in a class of gauge theories. Phys Rev D 18:2065–2067
68. Cohen L (1979) Local kinetic energy in quantum mechanics. J Chem Phys 70:788–789
69. Cohen L (1984) Representable local kinetic energy. J Chem Phys 80:4277–4279
70. Cohen L (1996) Local values in quantum mechanics. Phys Lett A 212:315–319
71. Ayers PW, Parr RG, Nagy A (2002) Local kinetic energy and local temperature in the density-functional theory of electronic structure. Int J Quantum Chem 90:309–326
72. Cohen L (1966) Generalized phase-space distribution functions. J Math Phys 7:781–786
73. Cohen L (1966) Can quantum mechanics be formulated as classical probability theory. Philos Sci 33:317–322
74. Becke AD (1988) Density-functional exchange-energy approximation with correct asymptotic-behavior. Phys Rev A 38:3098–3100
75. Becke AD (1993) Density-functional thermochemistry. 3. The role of exact exchange. J Chem Phys 98:5648–5652
76. Lee C, Yang W, Parr RG (1988) Development of the Colle-Salvetti correlation-energy formula into a functional of the electron density. Phys Rev B 37:785–789
77. Miehlich B, Savin A, Stoll H, Preuss H (1989) Results obtained with the correlation-energy density functionals of Becke and Lee, Yang and Parr. Chem Phys Lett 157(3):200–206
78. Frisch MJ et al (2004) Gaussian03, Revision D.01. Gaussian Inc., Wallingford, CT
79. Frisch MJ et al (2009) Gaussian 09, Revision A.1. Gaussian Inc., Wallingford CT
80. Keith TA (2010) AIMAll. aim.tkgristmill.com, 10.09.12.
81. Shaik S, Danovich D, Wu W, Hiberty PC (2009) Charge-shift bonding and its manifestations in chemistry. Nat Chem 1:443–449
82. Shaik S, Maitre P, Sini G, Hiberty PC (1992) The charge-shift bonding concept: electron-pair bonds with very large ionic-covalent resonance energies. J Am Chem Soc 114:7861–7866
83. Zhang LX, Ying FM, Wu W, Hiberty PC, Shaik S (2009) Topology of electron charge density for chemical bonds from valence bond theory: a probe of bonding types. Chem Eur J 15:2979–2989
84. Hirshfeld FL (1977) Theor Chim Act 44:129–138
85. Hiberty PC, Ramozzi R, Song LC, Wu W, Shaik S (2007) The physical origin of large covalent-ionic resonance energies in some two-electron bonds. Faraday Discuss 135:261–272
86. Toro-Labbe A (1999) Characterization of chemical reactions from the profiles of energy, chemical potential and hardness. J Phys Chem A 103:4398–4403
87. Bulat FA, Toro-Labbe A (2003) An extension of the Hammond postulate. Structural effects on the classification of chemical reactions. J Phys Chem A 107:3987–3994
88. Toro-Labbé A, Gutierrerez-Oliva S, Murray JS, Politzer P (2007) A new perspective on chemical and physical processes: the reaction force. Mol Phys 105:2619–2625
89. Toro-Labbe A, Gutierrerez-Oliva S, Politzer P, Murray JS (2009) The reaction force: a rigorously defined approach to analyzing chemical and physical processes. In: Chattaraj PK (ed) Chemical reactivity theory: a density functional view. CRC, Boca Raton, pp 293–302
90. Politzer P et al (2005) The reaction force: three key points along an intrinsic reaction coordinate. J Chem Sci 117:467–472

91. Wang SG, Qiu YX, Schwarz WHE (2010) Antibond breaking – the formation and decomposition of He@Adamantane: descriptions, explanations, and meaning of concepts. Chem Eur J 16:9107–9116
92. Bader RFW (2009) Bond paths are not chemical bonds. J Phys Chem A 113:10391–10396
93. Wang SG, Qiu YX, Schwarz WHE (2009) Bonding or nonbonding? Description or explanation? "Confinement bonding" of He@adamantane. Chem Eur J 15:6032–6040
94. Grimme S et al (2009) When do interacting atoms form a chemical bond? Spectroscopic measurements and theoretical analyses of dideuteriophenanthrene. Angew Chem Int Ed 48:2592–2595
95. Cerpa E, Krapp A, Flores-Moreno R, Donald KJ, Merino G (2009) Influence of endohedral confinement on the electronic interaction between He atoms: a He-2@C20H20 case study. Chem Eur J 15:1985–1990
96. Cerpa E, Krapp A, Vela A, Merino G (2008) The implications of symmetry of the external potential on bond paths. Chem Eur J 14:10232–10234
97. Becke AD, Edgecombe KE (1990) A simple measure of electron localization in atomic and molecular systems. J Chem Phys 92:5397–5403
98. Savin A, Nesper R, Wengert S, Fassler TF (1997) ELF: the electron localization function. Angew Chem 36:1809–1832
99. Savin A et al (1991) A new look at electron localization. Angew Chem 30:409–412
100. Gillespie RJ, Bytheway I, Dewitte RS, Bader RFW (1994) Trigonal bipyramidal and related molecules of the main-group elements: investigation of apparent exceptions to the VSEPR model through the analysis of the Laplacian of the electron density. Inorg Chem 33:2115–2121
101. Bader RFW, Gillespie RJ, Macdougall PJ (1988) A physical basis for the VSEPR model of molecular geometry. J Am Chem Soc 110:7329–7336
102. Schmider HL, Becke AD (2002) Two functions of the density matrix and their relation to the chemical bond. J Chem Phys 116(8):3184–3193
103. Schmider HL, Becke AD (2000) Chemical content of the kinetic energy density. Theochem J Mol Struct 527:51–61
104. Parr RG, Yang W (1989) Density-functional theory of atoms and molecules. Oxford University Press, New York
105. Geerlings P, De Proft F, Langenaeker W (2003) Conceptual density functional theory. Chem Rev 103:1793–1873
106. Ayers PW, Anderson JSM, Bartolotti LJ (2005) Perturbative perspectives on the chemical reaction prediction problem. Int J Quantum Chem 101:520–534
107. Gazquez JL (2008) Perspectives on the density functional theory of chemical reactivity. J Mex Chem Soc 52:3–10
108. Cohen MH, Ganduglia-Pirovano MV, Kudrnovsky J (1995) Reactivity kernels, the normal modes of chemical reactivity, and the hardness and softness spectra. J Chem Phys 103:3543–3551
109. Nalewajski RF (1995) Chemical reactivity concepts in charge sensitivity analysis. Int J Quantum Chem 56(5):453–476

Top Curr Chem (2014) 351: 125–148
DOI: 10.1007/128_2011_155

Published online: 26 May 2011

Controlling Supramolecular Assembly Using Electronic Effects

Christer B. Aakeröy and Kanishka Epa

Abstract Through systematic structural studies using custom designed probe molecules, it has been shown that the balance between hydrogen-bonds in the context of supramolecular chemistry and crystal engineering can be understood and guided by a semiquantitative thermodynamic assessment that integrates theoretical and experimental views of solution-based molecular recognition events. Although pK_a values can be used for ranking hydrogen-bond donors/acceptors within a family of compounds, they do not offer reliable information when comparing different functional groups. However, against a backdrop of a simple electrostatic interpretation of hydrogen bonds coupled with a focus on the primary non-covalent interactions, molecular electrostatic potential surfaces can be employed for guiding the synthesis of binary- and ternary co-crystals with the desired connectivity and dimensionality.

Keywords Cocrystals · Crystal engineering · Hydrogen bonds

Contents

C.B. Aakeröy (✉) and K. Epa
Department of Chemistry, Kansas State University, Manhattan, KS 66506, USA
e-mail: aakeroy@k-state.edu

1 Introduction

1.1 Fundamental Challenges in Supramolecular Synthesis

Intermolecular forces are ultimately responsible for the way in which discrete molecular building blocks are assembled into infinite architectures within crystalline materials, and for providing the necessary specificity and selectivity in complex biological systems in solution phase. Although it is important to acknowledge that every crystal structure and host–guest interaction is the result of a subtle balance between a multitude of non-covalent forces, the hydrogen bond is the crucial element in supramolecular chemistry. In fact, the strength and directionality of the hydrogen bond [1–8], as compared to other intermolecular forces, account for its significance and have made it the most robust and effective non-covalent synthetic vector available to us.

The term "synthesis" normally refers to the construction of new species by bringing together discrete entities, accompanied by the breaking and making of covalent bonds [9]. The fact that conventional synthesis utilizes the stability, strength, and irreversibility (when compared to most intermolecular interactions) of covalent bonds, means that we can devise assembly processes composed of several independent steps performed in a sequential manner, e.g. protection, functional-group transformation, coupling-reaction, deprotection, etc.

In supramolecular synthesis, on the other hand, different entities are held together via dynamic and reversible intermolecular interactions and, therefore, most synthetic procedures have to take place via a one-pot process. A supramolecular "intermediate" can rarely be prepared, isolated, and purified, and then added to another reactant in solution in order to perform sequential, assembly-line type synthesis, and herein lies a daunting challenge. How can we devise sophisticated and reliable synthetic routes for heteromeric supramolecular structures if we are limited to one-step reactions?

A possible solution to the problem of making one-pot synthesis "sequential" could be to develop modular assembly processes that take advantage of a hierarchy of intermolecular interactions that operate in parallel with limited structural interference between multiple molecular recognition events. If we are able to rank the relative importance of hydrogen bonds, which are employed regularly and successfully as structure-directing forces in both natural [10] and synthetic supramolecular systems [11], it may be possible to refine supramolecular synthesis and target more complex architectures composed of several different molecular building-blocks.

1.2 The Hydrogen Bond [12]

Since electrons are responsible for all chemical bonding, it is helpful to discuss hydrogen bonds in quantities that directly describe electron densities rather than with

concepts like σ- and π-bonding, electronegativity, etc.[1] The total interaction energy of a hydrogen bond can be partitioned into several constituents [13], the sum of which represents the total energy difference, ΔE_{HB}, between the hydrogen-bonded system at equilibrium and the total energy of the isolated, unperturbed components. The *electrostatic* contribution represents the energy change that would take place if two isolated components, D–H and A, were positioned in such a way that the geometry represents the hydrogen-bonded complex, D–H $\cdots$ A, but without perturbing their respective charge distribution and without any electron exchange taking place. The *polarization* energy represents the energy gain that would arise if the charge distributions of the isolated components were deformed to resemble the charge distribution of the hydrogen-bonded complex (without allowing charge transfer between D–H and A). The *charge transfer* represents the energy change that would result from electron transfer between D–H and A. The notion of "covalency" in a hydrogen bond is related to the latter term; charge transfer results in a build-up of charge in the overlap region, where it is shared between the original components D–H and A. The *dispersion* energy (another stabilizing component) results from the correlated motion of electrons on D–H and A. The only destabilizing term, the *exchange* energy between D–H and A, essentially corresponds to the repulsion that arises when too many electrons are located within the same region of space – this component also prevents the system from collapsing.

1.3 From Molecular to Supramolecular

It is well known that site-specific molecular reactivity can be guided via substituent-effected modulation of the electronic environment (Scheme 1).

Furthermore, the importance and variability of hydrogen-bond interactions in solution-based host–guest chemistry have been recognized in several model

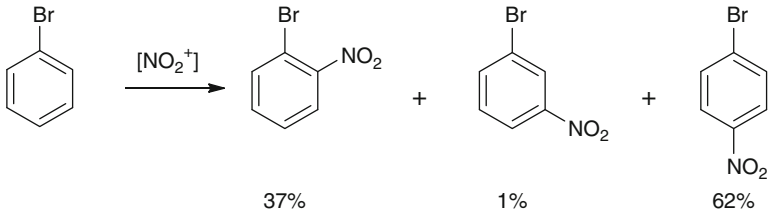

Scheme 1 An example of product distribution affected by substituent effects

[1]For an up-to-date discussion of hydrogen-bond nomenclature, see the IUPAC Project: "Categorizing hydrogen bonding and other intermolecular interactions," http://www.iupac.org/web/ins/2004-026-2-100.

systems [14, 15]. For example, the hydrogen-bond strength between pyridine moieties and phenols has been modified with the aid of, e.g. -Cl and -NMe_2 substituents, resulting in large differences in complex stability [16]. Wilcox and co-workers have employed molecular substituent effects to probe the nature of, and balance between, electrostatic and dispersion forces in certain protein folding motifs [17], and they have used ab initio calculations to show that local electric field strengths can be valuable indicators for molecular recognition phenomena [18]. Electron substituent effects have also been utilized to control the rate coefficient for proton removal in some resorcinol derivatives [19].

Excellent examples of how electron withdrawing and donating substituents influence molecular structure in the solid state are furnished by the hydroxypyridine–pyridone tautomers. The balance between tautomers is determined by the basicity of the nitrogen atom which can be altered via substituents on the ring [20]. The parent *ortho* compound exists as the pyridone in the solid state [21] (Scheme 2a), but by decreasing the basicity of the nitrogen atom with an electron withdrawing substituent [22] (Scheme 2b), the balance is shifted to the pyridine tautomer. With electron donating groups adjacent to the nitrogen atom, the basicity is increased and the balance is shifted to the 4-pyridone (Scheme 2c) [23]. Finally, the compelling neutron diffraction study of a co-crystal between 2-pyridone and 6-chloro-2-hydroxypyridine (1:1) (Scheme 2d) [21], shows the presence of two different tautomers in the same structure, with the balance again controlled by the electronic influence of the substituents.

In crystal engineering, however, the focus is on site-specific interactions of an *intermolecular* nature (in this context, an intriguing analogy between covalent and supramolecular synthesis has been formulated with the introduction of the term "intermolecular synthon" – a robust, transferable connector that can be used for linking molecules (not molecular fragments as in covalent synthesis) into predictable aggregates [24]). The question is, can we use tools and principles forged in synthetic organic chemistry to construct supramolecular architectures? More specifically, can we use substituent effects to "switch" *inter*molecular interactions on and off by altering the local electrostatic environment of individual molecules?

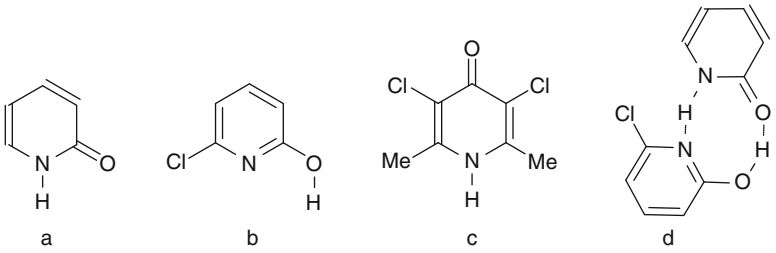

Scheme 2 Schematic representations of the molecular structures found in crystal structures of some pyridine/pyridones

1.4 Methodologies

1.4.1 Co-Crystallizations for Probing Intermolecular Interactions

Since the hydrogen bond is inherently electrostatic in nature, its strength is affected by the local electron density. Consequently, if we can modulate the electrostatic potential in the vicinity of a specific hydrogen-bond acceptor/donor, we may be able to control its willingness to participate in intermolecular hydrogen bonds, thereby dialing-in the supramolecular assembly in a precise manner. If we can electronically "activate" and "deactivate" an influential hydrogen-bond acceptor through substituent effects, a transition from *molecular* structure to *supramolecular* synthesis is accomplished, thereby providing an important tool for directing molecular recognition and crystal engineering.

One way of identifying correlations between molecular and supramolecular synthesis can be supplied by co-crystallization experiments. Co-crystals provide access to additional compounds, which allows us to compare the relative occurrence of different motifs.

The rules formulated by Etter [25, 26] provide an empirical guideline for establishing a hydrogen-bond based hierarchy of these intermolecular interactions. A few examples of commonly occurring synthons comprising complementary homomeric and heteromeric pairs are shown in Scheme 3.

In order to test Etter's guidelines [25, 26] *"the best proton donor and acceptor remaining after intramolecular hydrogen-bond formation will form an intermolecular hydrogen-bond"* and to continue developing a hierarchy of interactions, a collection of supramolecular reagents have been designed and synthesized in our laboratories in recent years, and they have subsequently been utilized in systematic

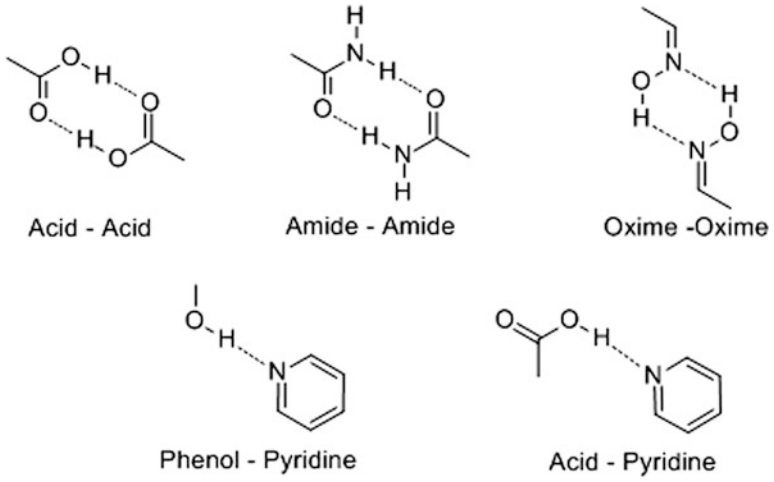

Scheme 3 Examples of hydrogen-bond based synthons

co-crystallization reactions in order to establish the possible existence of hydrogen-bond based structural preferences.

1.4.2 Theoretical Foundation

Hydrogen bond abilities and free energies of complexation have been correlated with pK_a values, and within closely related classes of compounds such comparisons frequently yield correct qualitative results [27–29]. However, in our own systematic studies we have also employed the elegant approach recently developed by Hunter [30], which allows for an extrapolation from experimental (or calculated) thermodynamic data on individual molecules to estimates of relative strengths of intermolecular interactions in the solid state. Even though the interaction energy between two molecules is commonly partitioned into several components, it is generally accepted that, for molecules reasonably close to van der Waals contacts, the electrostatic component is dominant. Thus, the association constant for a hydrogen-bonded supramolecular complex, A–B, can be described by a simple equation [31]:

$$\log K = c_1 \alpha_2^{\mathrm{H}} \beta_2^{\mathrm{H}} + c_2, \tag{1}$$

where c_1 and c_2 are constants that depend on the solvent, and $\alpha_2{}^{\mathrm{H}}$ and $\beta_2{}^{\mathrm{H}}$ are functional-group constants [32] determined by the hydrogen-bond donor/acceptor capabilities of the molecules. The latter terms are directly related to the positive and negative charges, respectively, on the two atoms H and A in a D–H $\cdots$ A hydrogen bond. c_1 increases when the polarity of the solvent decreases (as expected for electrostatic interactions), and c_2 is -1.0 ± 0.1. Equation (1) has been modified to account for the fact that the original work used carbon tetrachloride as a standard for a non-hydrogen bonding solvent [30]. Thus, (2) is more versatile as it allows for the examination of complexation in any solvent, as well as a ranking of weaker hydrogen-bond donors such as C–H moieties:

$$\Delta\Delta G_{\mathrm{H-bond}}\left(\mathrm{kJ\ mol^{-1}}\right) = -(\alpha\beta + \alpha_s\beta_s) + (\alpha\beta_s + \alpha_s\beta) = -(\alpha - \alpha_s)(\beta - \beta_s). \tag{2}$$

The normalized hydrogen-bond donor/acceptor constants can be obtained via (3) and (4) if experimental values for $\alpha_2{}^{\mathrm{H}}$ and $\beta_2{}^{\mathrm{H}}$ are available, but they can also be estimated from AM1 calculated molecular electrostatic potential (MEP) surfaces ($E_{\max}$ or $E_{\min}$):

$$\alpha = 4.1(\alpha_2^{\mathrm{H}} + 0.33) = E_{\max}/52\,\mathrm{kJ\,mol^{-1}}, \tag{3}$$

$$\beta = 10.3(\beta_2^{\mathrm{H}} + 0.06) = -E_{\min}/52\,\mathrm{kJ\,mol^{-1}}. \tag{4}$$

The results obtained from the thermodynamic calculations on HB strength and molecular association have been matched against extensive structural data, and this two-pronged approach can allow us to draw important conclusions about how much supramolecular control/predictability we can expect from thermodynamic means. We recognize that there are more sophisticated methods [33] for determining interaction energies than those adopted herein, but in this study we hope to find theoretical tools that are (1) able to handle large systems, (2) readily accessible, and (3) capable of producing reliable *trends* for establishing a hierarchy of hydrogen bonds.

2 Case Studies

2.1 *Relating Supramolecular Yield to the Charge on the Hydrogen-Bond Donor*

Oximes are known to form O–H · · · N hydrogen bonds with pyridines [34], which demonstrates that the interaction between the pyridine nitrogen atom and the oxime proton is viable even in competition with plausible alternative motifs such as oxime · · · oxime dimers, tetramers, and polymers. However, if the oxime moiety and the N-heterocycle belong to different molecular fragments, what will happen? Is an oxime O–H · · · N (N-heterocycle) hydrogen bond strong enough to bring about the formation of co-crystals? The oxime functional group displays pK_a values in an intermediate range between that of carboxylic acids and amides. In addition, the acidity and the precise electrostatic nature of the oxime proton can be altered without making dramatic steric modifications in close proximity of the –OH donor site (Scheme 4).

A systematic structural and spectroscopic examination of the products resulting from co-crystallization reactions between three types of phenyloximes R–C=N–OH (where R = H, Me, or CN) and a series of N-heterocyclic

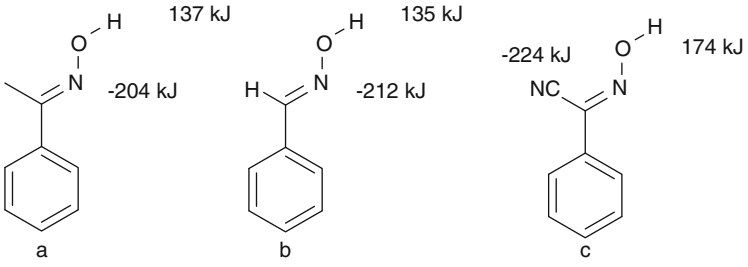

Scheme 4 The magnitude of the maxima and minima (in kJ/mol) on the electrostatic potential surface; in both acetyloxime and benzaldoxime, **a** and **b**, respectively, the imine nitrogen is the location of the minimum value in the electrostatic potential

Table 1 Supramolecular yields for each family of oxime

	Cyanooximes	Acetyloximes	Aldoximes
Attempted co-crystallizations	16	24	24
Co-crystals formed	16	2	1
Supramolecular yield	100%	8%	4%

hydrogen-bond acceptors have shown that the acidity of the oxime –OH hydrogen-bond donor is crucial to the efficacy of the supramolecular assembly process [35]. The supramolecular yield for each family of oxime is given in Table 1. Note that the term "supramolecular yield" is clearly distinct from the regular usage of the term "yield" (specific to one particular reaction). It is meant to give a sense of how frequently one can expect a desired supramolecular synthon to appear if two specific functional groups (in this case, hydrogen-bond donor and hydrogen-bond acceptor) are present together in a significant number of different reactions.

Despite the fact that each oxime was allowed to react with the same set of hydrogen-bond acceptors, the results are dramatically different. The more acidic cyanooximes were extremely effective, 16/16, at forming co-crystals, whereas the less acidic acetyloximes/aldoximes only produced co-crystals in 3 out of a total of 48 attempts. Cyanooximes are comparable to carboxylic acids, in terms of success rate, whereas the much less acidic CH_3- and H- substituted analogs are not effective at generating co-crystals despite close similarities in steric and geometric parameters. The importance and validity of using experimental pK_a-values (within a functional group class) and calculated electrostatic potential surfaces as a basis for predicting the supramolecular yield of an O–H $\cdots$ N interaction for driving the formation of co-crystals is unambiguously established.

2.2 *Relating Supramolecular Yield to the Charge on the Hydrogen-Bond Acceptor*

2.2.1 Pyrazoles Versus Methyl-Substituted Pyrazoles [36]

N-heterocycles such as pyridines and imidazoles/benzimidoles are known to form co-crystals with carboxylic acids, driven by O–H $\cdots$ N hydrogen bonds [37–44]. The negative electrostatic potential of the nitrogen atoms in these compounds represents an attractive binding site for an approaching carboxylic acid. Pyrazole and 3,5-dimethyl pyrazole are two additional examples of hydrogen-bond acceptors containing N-heterocycles sites and 3,5-dimethylpyrazole is more basic than pyrazole due to the electronic influence of the two electron-donating substituents. If the strength of an O–H $\cdots$ N hydrogen bond were a measure of how easily co-crystals could be obtained with a range of hydrogen-bond donors, one would expect a greater success rate with 3,5-dimethylpyrazole than with pyrazole.

Scheme 5 pK_a values and calculated electrostatic potential values on **1** and **2**

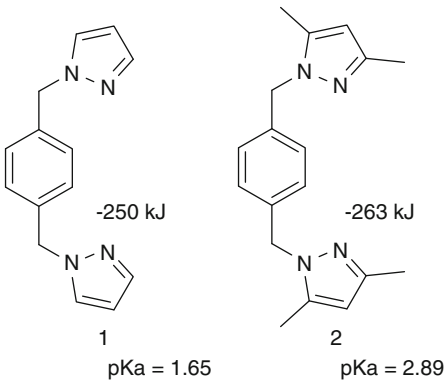

In order to test this hypothesis we synthesized two ditopic symmetric ligands, 1,4-bis[(pyrazole-1-yl)methyl]benzene, **1** and 1,4-bis[(3,5-dimethyl-1-yl)methyl] benzene, **2** [45], (calculated MEPs and pK_a values are shown in Scheme 5).[2,3] In addition, the two compounds have similar solubilities, and the presence of the methyl groups in **2** does not constitute any steric hindrance for a potential hydrogen-bond donor.

Each compound, **1**, **2**, was combined in a 1:2 ligand-acid ratio with 30 different carboxylic acids. All products were characterized by infrared spectroscopy to determine if a co-crystal had formed. The presence of two broad bands at ca. 2,500 cm^{-1} and 1,900 cm^{-1}, characteristic of an O–H $\cdots$ N (acid $\cdots$ N-heterocycle) hydrogen-bond interaction, was taken as evidence for co-crystal formation since these bands would not appear in any of the individual compounds.

Crystals suitable for single-crystal structure determination of three representative compounds showed that the expected intermolecular interactions and stoichiometries were present. The crystal structure determination of **1a**, obtained from the reaction between **1** and 3,5-dinitrobenzoic acid, shows the expected 1:2 co-crystal. The assembly is facilitated by an O–H $\cdots$ N hydrogen bond between the O–H group on the carboxylic acid and the pyrazol-1-yl nitrogen atom (Fig. 1).

The crystal structure determination of the solid obtained from the reaction between **2** and 2,6-difluorobenzoic acid shows a co-crystal assembled via an O–H $\cdots$ N hydrogen interaction between the carboxylic acid and the available nitrogen atoms on **2** (Fig. 2).

[2]The two ligands shown in Scheme 5 were constructed using Spartan '04 (Wavefunction. Inc Irvine, CA). Their molecular geometries were optimized using AM1, and the maxima and minima in the molecular electrostatic potential surface. (0.002 e/au isosurface) were determined using a positive point charge in vacuum as the probe.

[3]pK_a values were obtained through calculations of the conjugate acids. The calculations were carried out using ACD/Solaris version 476, Advanced Chemistry Development, Inc. Toronto, ON, Canada, www.acdlabs.com, 1994–2005.

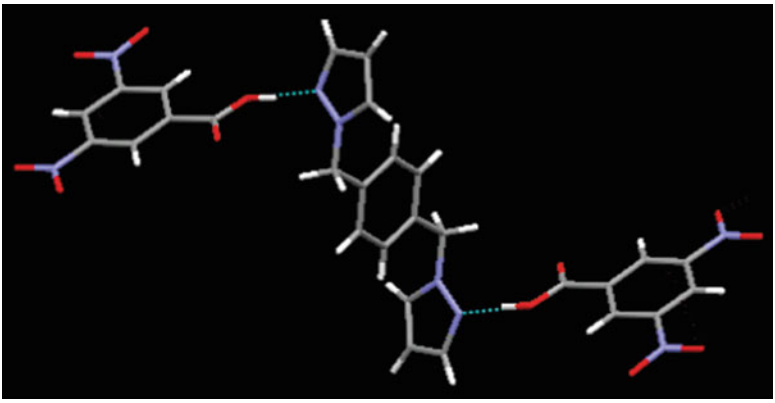

Fig. 1 Primary intermolecular interactions in the crystal structure of **1a**

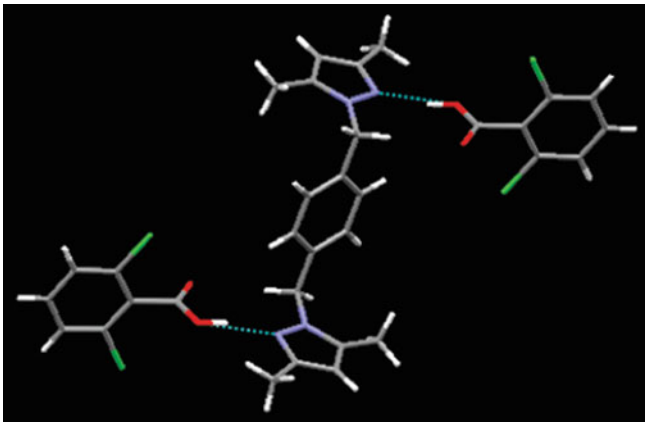

Fig. 2 Main intermolecular interactions in the 1:2 binary co-crystal of **2** and 2,6-difluorobenzoic acid

2b is a co-crystal composed of **2** and pentamethylbenzoic acid in the expected 1:2 ratio. In this case there are two inequivalent supermolecules constructed through heteromeric O–H · · · N hydrogen bonds (Fig. 3). Both heterocyclic compounds are located about inversion centers.

Based on the spectroscopic data (supported by three single-crystal structure determinations) it is shown that the more basic 3,5-dimethylpyrazole-based compound produces many more co-crystals than the corresponding (and less basic) pyrazole ligand, 20/30 (67%) vs 11/30 (37%). The presence of the methyl groups in **2** have increased the magnitude of the negative electrostatic potential on the nitrogen atoms which is also reflected in the basicity of **2**.

Since **1** and **2** display many chemical similarities, it is reasonable to ascribe the superiority of **2** as a co-crystallizing agent to the increased strength of the O–H · · · N

Fig. 3 Hydrogen bonds in the two unique supermolecules in the crystal structure of **2** and pentamethylbenzoic acid

hydrogen bond that it can form with a range of carboxylic acids. These observations mirror the results [35] that connected the relative acidity/positive electrostatic potential of oxime moieties to the supramolecular yield of oxime · · · N-heterocycle co-crystals. Consequently, simple changes in molecular structure can alter hydrogen-bonding capability in a controlled manner which, in turn, provides a handle for fine-tuning supramolecular reactivity. It is reasonable to assume that this observation can be translated into a tool that can facilitate practical hydrogen-bond based supramolecular synthesis of co-crystals involving a wide range of components. Furthermore, by applying these ideas to more complicated supramolecular building blocks with inequivalent hydrogen-bond acceptor sites, it may be easier to construct predictable, multi-component supramolecular systems with much greater structural and chemical complexity.

2.2.2 Balancing Synthons: The Supramolecular Selectivity of *Iso*-Nicotinamide [46]

The next study focuses on three commonly occurring hydrogen-bonding moieties – carboxylic acid, primary amide, and pyridine – to establish the preference of hydrogen bonding interactions between them. The molecule of choice for this study was *iso*-nicotinamide which contains the two latter hydrogen bonding moieties. A co-crystallization of *iso*-nicotinamide with carboxylic acids can in principle result in the three possible heterosynthons shown in Scheme 6.

In order to explore the balance between these intermolecular interactions and possibly to extract reliable data for ranking the synthons in the context of the

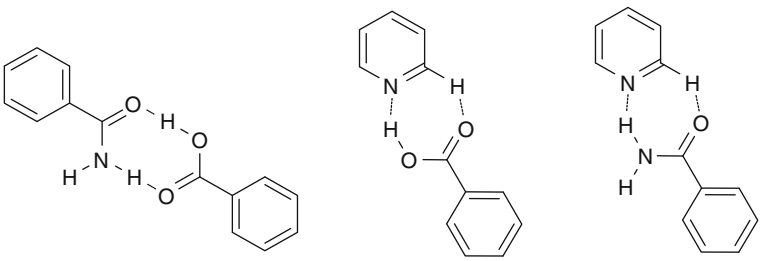

Scheme 6 Possible heterosynthons involving *iso*-nicotinamide and carboxylic acids

Table 2 Co-crystal screen of *iso*-nicotinamide and carboxylic acids

#	Carboxylic acid	Ratio of *iso*-nicotinamide: acid
1	Cinnamic acid	1:1
2	3-Hydroxybenzoic acid	1:1
3	3-*N*,*N*-Dimethylbenzoic acid	1:1
4	3,5-Bis(trifluoromethyl)benzoic acid	1:1
5	D,L-Mandelic acid	1:1
6	Chloroacetic acid	1:1
7	Fumaric acid monoethylester	1:1
8	12-Bromododecanoic acid	2:1
9	Fumaric acid	2:1
10	Succinic acid	2:1
11	4-Ketopimelic acid	2:1
12	Thiodiglycolic acid	2:1

Scheme 7 Dominating synthons in *iso*-nicotinamide: carboxylic acid co-crystals

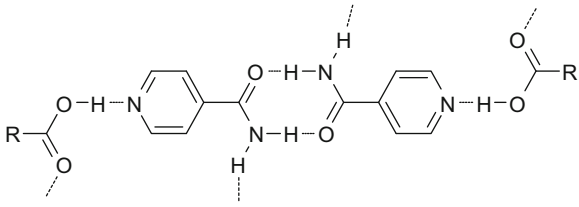

best-donor/best-acceptor concept, *iso*-nicotinamide was co-crystallized with a diverse selection of carboxylic acids, comprising both aliphatic and aromatic acids. The different acids and ratios used are shown in Table 2. All the co-crystals obtained were characterized using single-crystal X-ray diffraction in order to establish the precise intermolecular interactions that take place in each sample.

All 12 structures obtained displayed the very same primary intermolecular interactions: (1) the pyridine–carboxylic acid interaction and (2) the self-complementary amide–amide dimer (Scheme 7).

The carboxylic acid is well known to form stronger hydrogen bonds than the -NH_2 moiety on the amide, and the best donor clearly displays a strong preference for the pyridine moiety, the best acceptor site. Once these functionalities have found each other via an acid · · · py synthon, it is left to the amide to interact with itself (typically across an inversion center) via a classic homomeric amide · · · amide dimer. In order to determine whether these structures are representative of co-crystals of acids and nicotinamide, we performed an additional analysis of all relevant data found in the Cambridge Structural Database [47]. The search, which included all nicotinamide and *iso*-nicotinamide co-crystals with carboxylic acids, but excluded other potentially competing moieties such as –OH, yielded 32 hits. In every single case, the pyridine – carboxylic acid synthon was present, which emphasizes that these intermolecular interactions are very selective, remarkably reliable, and robust, despite the fact that we are dealing with readily reversible non-covalent interactions. The consistency of the motifs can be explained in the context of best donor–best acceptor scenario underpinned by electrostatic considerations.

2.2.3 The Supramolecular Balance Between N-Heterocycles and an Amide

Iso-nicotinamide is a relatively simple molecule with two distinctly different binding sites and, as shown above, carboxylic acids clearly prefer the pyridine nitrogen atom, the "best acceptor." The question is, is the selectivity limited to *iso*-nicotinamide and does the electrostatic argument hold for related molecules?

If the electrostatic argument is to stand up to scrutiny, when an amide is combined with a more basic N-heterocycle on the same molecular scaffolding, an incoming carboxylic acid should still bind preferentially to the latter site, leaving the amide to form a homomeric dimer again.

A disadvantage of using *iso*-nicotinamide in this context is that, even though it has two different functional groups, any covalent modification made on the molecule affects both groups. Therefore it was necessary to "decouple" electrostatically the N-heterocycle from the amide moiety. We decided to replace pyridine with a benzimidazole moiety, a stronger base, and a more powerful hydrogen bond acceptor, and we separated the amide from the heterocycle by placing them on different aromatic rings bridged by a "non-conducting" methylene-linker. All in all, six different [(benzimidazol-1-yl)methyl]-benzamides were synthesized (Scheme 8), and subsequently co-crystallized with a wide variety of carboxylic acids [48, 49].

A total of six crystal structures were obtained and in each case the same connectivity as was observed in the study on *iso*-nicotinamide was found. For example, the co-crystal of 3-[(benzimidazol-1-yl)methyl]-benzamide with 3-nitrobenzoic acid yielded the expected result. The –OH group of the acid binds to the aromatic nitrogen of the benzimidazole and the amide forms a homomeric dimer (Fig. 4, top). If the system is saturated with acid, a 2:1 co-crystal is obtained with the carboxylic acid interacting with both the benzimidazole site and with the amide moiety (Fig. 4, bottom). The latter structure does offer important additional information because it shows that the acid is capable of interacting with both sites so

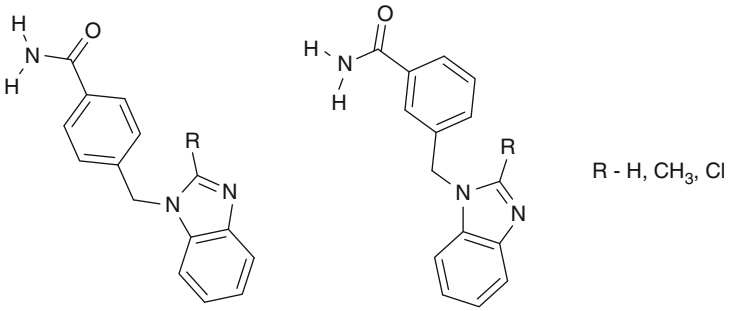

Scheme 8 Six [(benzimidazol-1-yl)methyl]-benzamide based supramolecular reagents

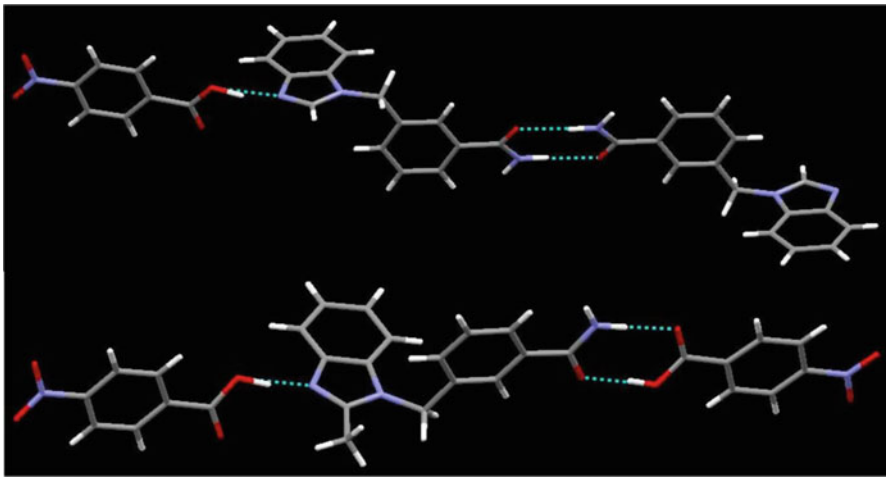

Fig. 4 Primary hydrogen bonds in the co-crystals of 3-[(benzimidazol-1-yl)methyl]-benzamide (*top*) and 3-[(2-methylbenzimidazol-1-yl)methyl]-benzamide with 3-nitrobenzoic acid (*bottom*)

there is no inherent geometric problem for the acid to form a heteromeric synthon with the amide.

As expected, by using a stronger hydrogen bond acceptor than the pyridine moiety, the acid again opts for the aromatic nitrogen atom (which is now an even better acceptor) over the amide group. This strengthens the argument that the best donor selects the best acceptor (where ranking is based upon charge).

To verify that this is purely based on the hydrogen-bond strength of the donors and acceptors, it is important to establish whether the balance between an aromatic N-heterocycle and an amide can be reversed by lowering sufficiently the hydrogen-bond accepting property of the aromatic nitrogen atom. With this in mind, we synthesized a set of ditopic supramolecular reagents that combined an amide moiety with a very weak base, pyrazole. The idea was that if the basicity of the

heterocycle is instrumental in determining the balance between the amide and heterocycle, then at some point an incoming carboxylic acid should abandon the base, if it is too weak, and instead opt for a heteromeric acid · · · amide synthon [50]. In Scheme 9 the three different generic ditopic ligands compared in this study are listed together with pK_a values and MEP-based charges.

Again, the amide and the N-heterocyclic moiety were placed on different parts of the molecular scaffold, and separated by a methylene bridge (Scheme 10).

Four crystal structures have been obtained to date and they include co-crystals of 4-[(pyrazol-1-yl)methyl]-benzamide with oxalic acid (Fig. 5), succinic acid, benzoic acid (Fig. 6), and 2-fluorobenzoic acid, respectively. In all four cases, the

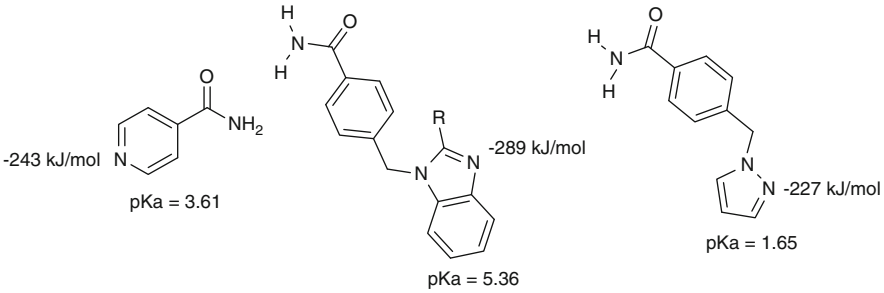

Scheme 9 Comparison of pK_a values and electrostatic potential values of different N-heterocycles

Scheme 10 Postulated connectivity in co-crystals of acids and amide-pyrazoles

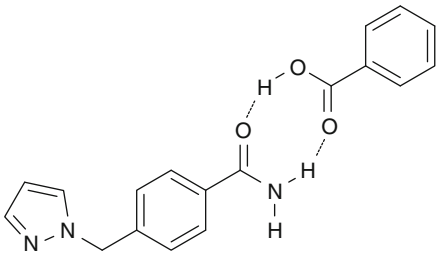

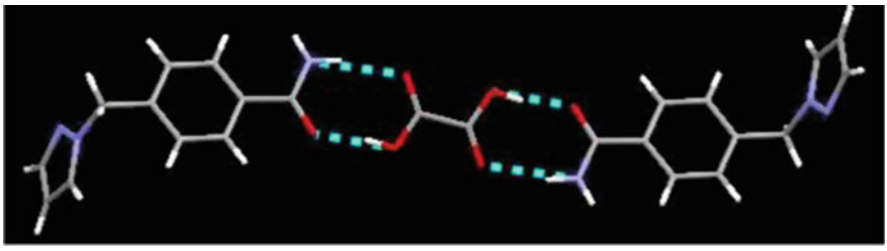

Fig. 5 Primary hydrogen bonds in 4-[(pyrazol-1-yl)methyl]-benzamide oxalic acid (2:1)

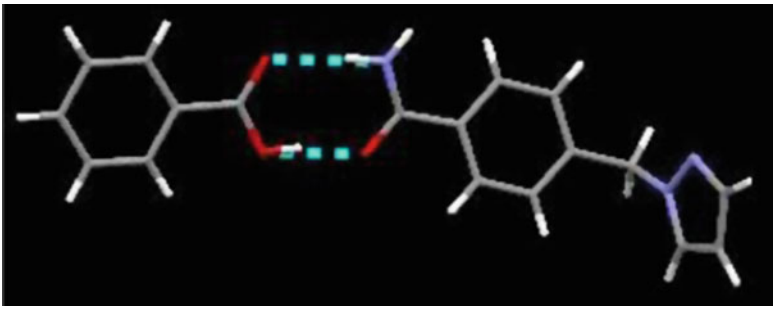

Fig. 6 Primary hydrogen bonds in 4-[(pyrazol-1-yl)methyl]-benzamide benzoic acid (1:1)

N-heterocycle, the pyrazole moiety, a very weak base, is no longer competitive with the amide for the attention of the carboxylic acid and now the amide $\cdots$ acid interaction is dominant. Again, this offers further evidence that charge plays a key role in controlling, and even in switching, intermolecular interactions involving hydrogen bonds.

In summary, carboxylic acid prefers to bind to an N-heterocyclic moiety in preference to an amide moiety as long as the base is sufficiently strong (e.g. pyridine, imidazole, and benzimidazole). However, if the basicity of the heterocycle is lowered enough, as was the case with 4-[(pyrazol-1-yl)methyl]-benzamide, the acid prefers to interact with the amide. We can therefore conclude that electrostatic charges provide a useful tool in establishing robust hydrogen-bond hierarchies that can be forged into effective supramolecular synthetic tools.

3 Synthesis of Ternary Co-Crystals

An improved understanding of non-covalent interactions gives the supramolecular chemist the ability to build complex multi-component heteromeric structures like binary and ternary co-crystals. The above studies have shown that hydrogen bonding takes place according to a hierarchy of donors and acceptors where the best donor binds to the best acceptor and the second best donor to the second best acceptor. The hierarchy of donors and acceptors can be determined by their pK_a values (as long as the same type of functionality is being considered) or electrostatic charges.

Iso-nicotinamide has two distinct functional groups – the pyridyl nitrogen and the amide group. The above study (Sect. 2.2.2) shows that carboxylic acids have a very strong preference for the pyridyl nitrogen. Binary co-crystals between *iso*-nicotinamide and a carboxylic acid usually comprise an acid – pyridyl nitrogen heterosynthon – and an amide – amide homosynthon. It was also observed that, if pyridine was replaced by a nitrogen heterocycle of higher pK_a, the acid forms a hydrogen bond with the amide. We therefore postulated that it may be possible to combine *iso*-nicotinamide with two acids of different pK_a- values thereby constructing an exceptionally rare ternary co-crystal, Scheme 11 [51].

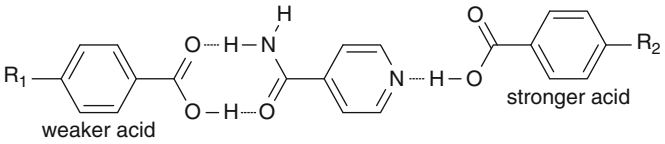

Scheme 11 Template for a ternary co-crystal

Table 3 pK_a values of acids used in the synthesis of ternary co-crystals with *iso*-nicotinamide

	Stronger acid	pK_a	Weaker acid	*p*K$_a$
1	3,5-Dinitrobenzoic acid	2.8	3-Methylbenzoic acid	4.3
2	3,5-Dinitrobenzoic acid	2.8	4-(Dimethylamino)benzoic acid	6.5
3	3,5-Dinitrobenzoic acid	2.8	4-Hydroxy-3-methoxycinnamic acid	4.4

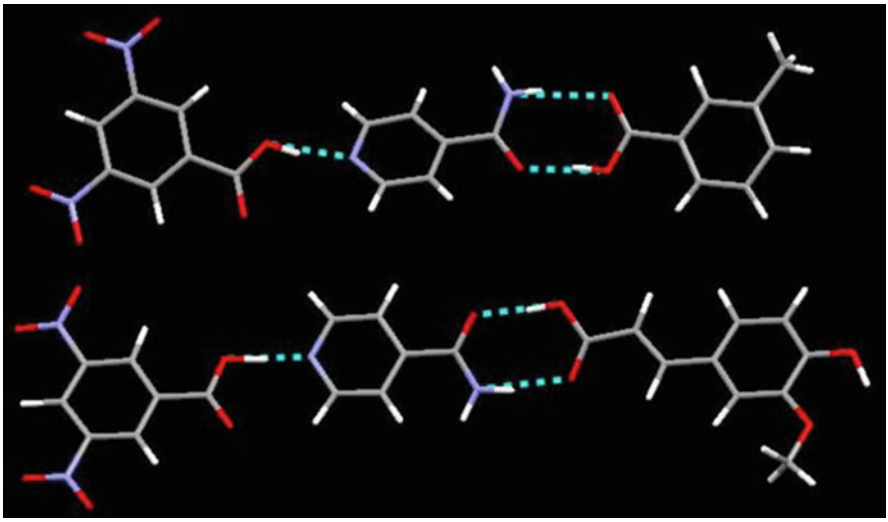

Fig. 7 Primary hydrogen bonds in two ternary co-crystals

If the best donor binds to the best acceptor and the second best donor to the second best acceptor, then this strategy should yield ternary co-crystals. The experimental setup used is shown in Table 3.

The products of these reactions were again characterized by single-crystal X-ray diffraction, and, remarkably, ternary co-crystals with the postulated connectivity were obtained in all three cases. The stronger acid, 3,5-dinitro benzoic acid, formed a hydrogen bond with the pyridyl group, the best acceptor. The weaker acid formed an acid–amide dimer with the amide group, the second best acceptor site (Fig. 7).

4 Electrostatic Potential Is Better than pK_a

As demonstrated, pK_a values can be used to rank hydrogen-bond donating/accepting ability as long as the study is limited to the same family of molecules. When considering different functional groups, pK_a values often provide misleading data. For example, 4-hydroxybenzoic acid has two hydrogen bond donor groups: –COOH and –OH. The pK_a of the two groups are 4.47 and 9.06, respectively and, according to this criterion, the carboxylic acid would be the best and the –OH group the second best donor. In the co-crystal formed between 4-hydroxybenzoic acid and nicotinamide, the best donor or the carboxylic acid group should bind to the pyridine nitrogen atom, which is the best acceptor (Scheme 12).

The experimental outcome of the above co-crystallization, however, produced the opposite connectivity [52]. As shown in Fig. 8, the phenol –OH binds to the pyridyl nitrogen.

However, the observed results are readily explained within the context of Hunter's work based on AM1 calculated based electrostatic potential surfaces. A calculation on 4-hydroxybenzoic acid shows that the phenol –OH is a stronger hydrogen-bond donor than the carboxylic acid (Scheme 13).

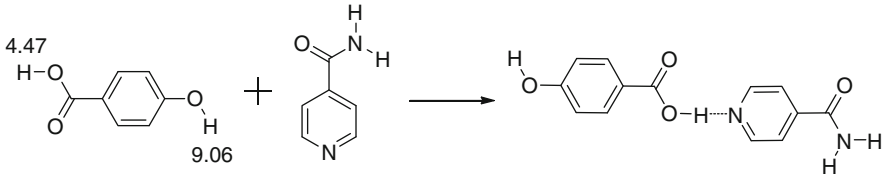

Scheme 12 Expected intermolecular connectivity based on pK_a values

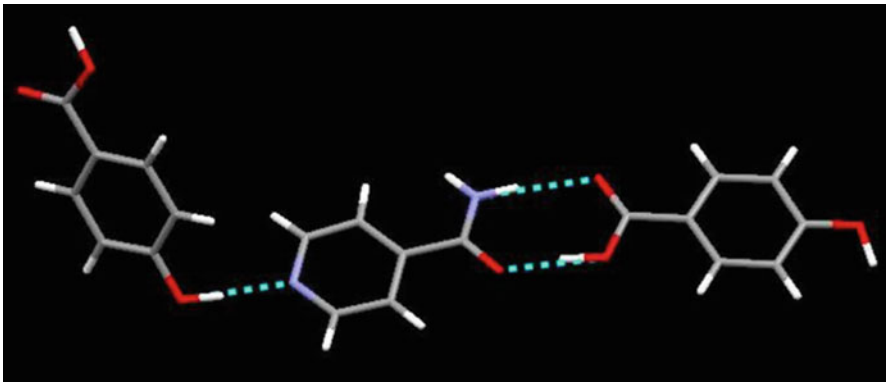

Fig. 8 Primary hydrogen-bonds in the co-crystal of 4-hydroxybenzoic acid and *iso*-nicotinamide [52]

Scheme 13 MEP values for 4-hydroxybenzoic acid

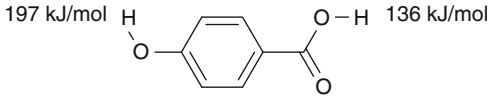

Table 4 AM1-based MEP surface values of donor and acceptor functional groups

	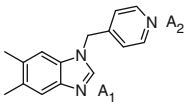	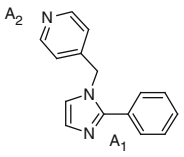	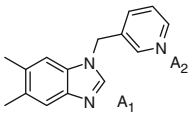	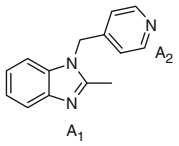
A_1	−299	−311	−301	−299
A_2	−274	−271	−255	−269
	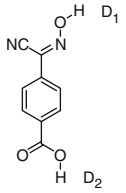	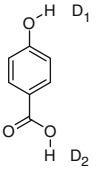	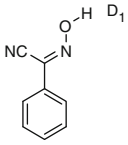	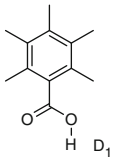
D_1	+190	+197	+171	+129
D_2	+152	+136	–	–

We recently examined the usefulness of MEP surfaces for rationalizing and predicting intermolecular connectivities in co-crystals on the assumption that hydrogen bonds are primarily electrostatic interactions. To test this hypothesis, monotopic and ditopic molecules with different charges were synthesized as shown in Table 4 [53].

If the MEP arguments hold then the best donors (D_1) with the highest potential values will bind to the best acceptors (A_1) with the highest negative potential value and the second best donors (D_2) will bind to the second best acceptors (Scheme 14).

Similarly, with the single point donors it should be possible to assemble ternary systems as shown in Scheme 15, where the cyanooxime with the higher charge is expected to bind to the acceptor with the highest negative potential (A_1) and the tetramethylbenzoic acid with the lower potential value should bind to the second best acceptor site (A_2).

Single crystal X-ray crystallography shows that hydrogen bonding does take place as predicted in both cases (Figs. 9 and 10).

These structures demonstrate that the MEP calculation approach is a more effective and versatile method for establishing a hierarchy of hydrogen bonding donors and acceptors as it is not confined to comparing groups in the same family like pK_a values. The hydrogen bond is essentially an electrostatic attraction force

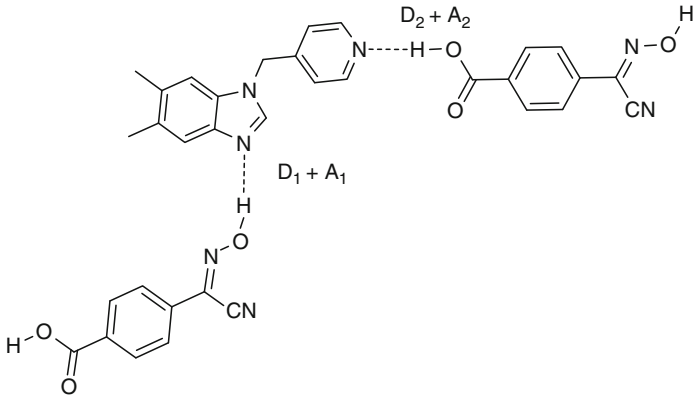

Scheme 14 Expected result based on MEP surface calculations

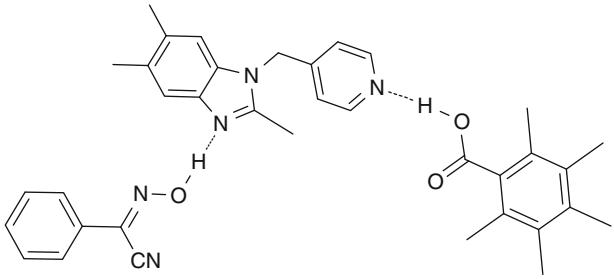

Scheme 15 Postulated outcome for a ternary co-crystal based on MEP surface calculations

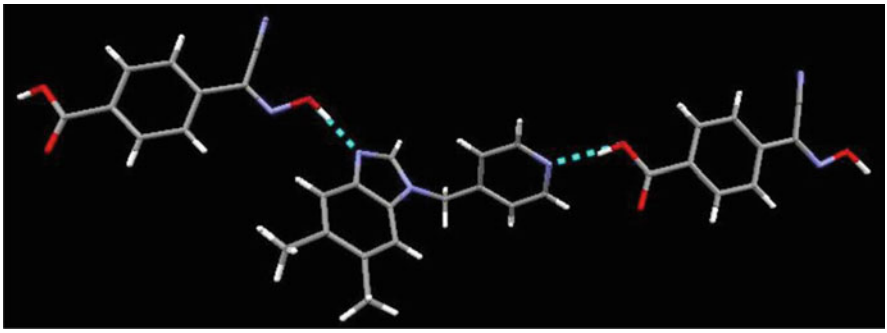

Fig. 9 Primary hydrogen bonds in a binary co-crystal of (Z)-4-(cyano(hydroxyimino)methyl) benzoic acid and ditopic hydrogen-bond acceptor

between two dipoles. pK_a on the other hand is a measure of the ionizability of a given group which does not make it an effective scale for ranking hydrogen-bond forming ability. In the case of acids, the pK_a value is essentially a measure of how

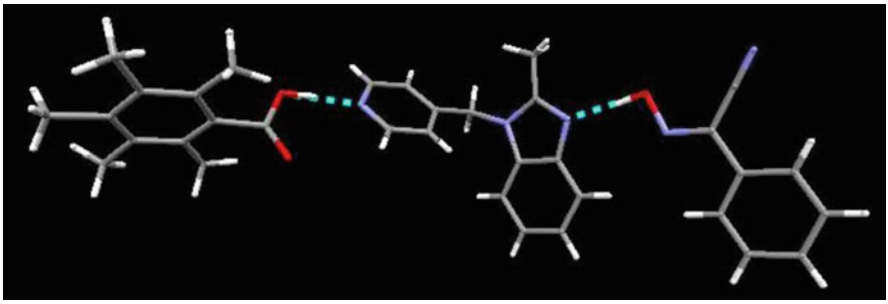

Fig. 10 The two most important hydrogen-bond interactions in a ternary co-crystal of *N*-hydroxybenzimidoyl cyanide, pentamethylbenzoic acid, and a ditopic hydrogen-bond acceptor

easily the acid can be deprotonated, which can be used to compare a group of acids. When comparing an acid and a phenol, the acid has a higher pK_a but experimentally, the phenol is a better hydrogen bond donor. The MEP calculations give values corresponding to the charges at each group and the data obtained fit better with experimental observations. Therefore, MEP calculations are better suited for establishing a hierarchy of different hydrogen bonding groups.

5 Conclusions

A main goal of this review has been to summarize a series of systematic structural studies in order to determine whether the assembly of binary and ternary co-crystals can be understood and guided by a semiquantitative thermodynamic assessment that integrates theoretical and experimental views of solution-based molecular recognition events [54, 55]. The kinetic aspects of crystallization clearly play an important role in the transition from solution-phase assemblies to solid-state structure. However, it would be extremely useful, from a supramolecular synthesis perspective, if there was a link between the relative strength/ importance of a series of related supramolecular synthons (as determined by readily accessible thermodynamic parameters) and the frequency of occurrence of such motifs in the solid state. Note that this undertaking is only concerned with the structural importance and consequences of the primary intermolecular interactions; we do not propose to attempt crystal-structure prediction. From the evidence that we have gathered, it is clear that covalent handles can be used to dial-in supramolecular selectivity and reactivity and that this behavior can be understood against a backdrop of a simple electrostatic interpretation of hydrogen bonds coupled with a focus on the primary non-covalent interactions. By addressing specific questions about how relatively simple molecules prefer to bind to each other, we may now acquire the ability (1) to position molecules where we want them to be, (2) to construct heteromolecular architectures with desirable metrics, and (3) to translate intermolecular communication into blueprints for materials design and for constructing viable biological

mimics, which represent highly significant long-term goals of interest to a wide range of scientists.

References

1. Hadži D, Thompson WH (eds) (1959) Hydrogen bonding. Pergamon Press, Oxford
2. Pimentell GC, McClellan AL (1960) The hydrogen bond. W H Freeman, San Francisco
3. Pauling L (1963) The nature of the chemical bond. Cornell University Press, Ithaca
4. Hamilton WC, Ibers JA (1968) Hydrogen bonding in solids. Benjamin, New York
5. Emsley JE (1980) Chem Soc Rev 9:91
6. Tuck DG (1968) Progr Inorg Chem 9:161
7. Speakman JC (1972) Struct Bond 16:141
8. Steiner T (2002) Angew Chem Int Ed 41:48
9. Aakeröy CB, Salmon DJ (2005) CrystEngComm 7:439
10. Jeffrey GA, Saenger W (1991) Hydrogen bonding in biological structures. Springer, Berlin
11. Lehn JM (1995) Supramolecular chemistry. VCH, Weinheim
12. Scheiner S (1987) Hydrogen bonding. A theoretical perspective. Oxford University Press, Oxford
13. Umeyama H, Morokuma K (1977) J Am Chem Soc 99:1316
14. Rebek J Jr (1990) Angew Chem Int Ed Engl 29:245
15. Lehn JM (1990) Angew Chem Int Ed Engl 29:1304
16. Neder KM, Whitlock HW Jr (1990) J Am Chem Soc 112:9412
17. Kim EI, Paliwal S, Wilcox CS (1998) J Am Chem Soc 120:11192
18. Wilcox CS, Kim EI, Romano D, Kuo LH, Burt AL, Curran DP (1995) Tetrahedron 51:621
19. Coker A, Hibber F (1995) J Chem Soc Perkin Trans 2:1
20. Elguero J, Marzin C, Katritzky AR, Linda P (1976) Advances in heterocyclic chemistry: supplement 1. Academic, New York
21. Almlöf J, Kvick Å, Olovsson I (1971) Acta Crystallogr B 27:1201
22. Kvick Å, Olovsson I (1968) Ark Kem 30:71
23. Boer FP (1972) Acta Crystallogr 28:3200
24. Desiraju GR (1995) Angew Chem Int Ed Engl 34:2311
25. Etter MC (1991) J Phys Chem 95:4601
26. Etter MC (1990) Acc Chem Res 23:120
27. Abraham MH (1993) Chem Soc Rev 22:73
28. Shan S, Loh S, Herschlag D (1996) Science 272:97
29. Chen DL, McLaughlin LW (2000) J Org Chem 65:7468
30. Hunter CA (2004) Angew Chem Int Ed 43:5310
31. Abraham MA, Platts JA (2001) J Org Chem 66:3484
32. Hansch C, Leo A, Taft RW (1991) Chem Rev 91:165
33. Lu YX, Zou JW, Fan JC, Zhao WN, Jiang YJ, Yu QS (2009) J Comput Chem 30:725
34. Aakeröy CB, Beatty AM, Leinen DS (2000) Cryst Growth Des 1:47
35. Aakeröy CB, Salmon DJ, Smith MM, Desper J (2006) Cryst Growth Des 6:1033
36. Aakeröy CB, Fasulo ME, Desper J (2006) CrystEngComm 8:586
37. Aakeröy CB, Desper J, Leonard B, Urbina JF (2005) CrystEngComm 5:865
38. Aakeröy CB, Hussain I, Desper J (2006) Cryst Growth Des 6:474
39. Bhogala BR, Basavoju S, Nangia A (2005) Cryst Growth Des 5:1683
40. Curtis SM, Le N, Fowler FW, Lauher JW (2005) Cryst Growth Des 5:2313
41. Saha BK, Nangia A, Jaskolski M (2005) CrystEngComm 7:355
42. Vishweshwar P, McMahon JA, Peterson ML, Hickey MB, Shattock TR, Zaworotko MJ (2005) Chem Commun 4601
43. Hosseini MW (2004) CrystEngComm 6:318

44. Desiraju GR (2002) Acc Chem Res 35:565
45. Hartshorn CM, Steel PJ (1995) Aust J Chem 48:1587
46. Aakeröy CB, Beatty AM, Helfrich BH (2002) J Am Chem Soc 124:14425
47. Allen FH (2002) Acta Cryst B 58:380
48. Aakeröy CB, Desper J, Urbina JF (2005) Chem Commun 2820
49. Aakeröy CB, Desper J, Leonard B, Urbina JF (2005) Cryst Growth Des 5:865
50. Aakeröy CB, Desper J, Scott BMT (2006) Chem Commun 1445
51. Aakeröy CB, Beatty AM, Helfrich BA (2001) Angew Chem Int Ed Engl 40:3240
52. Vishweshwar P, Nangia A, Lynch VM (2003) CrystEngComm 5:164
53. Aakeröy CB, Desper J, Smith MM (2007) Chem Commun 3936
54. Abraham MH (1993) Pure Appl Chem 65:2503
55. Schneider HJ (2003) Methods Princ Med Chem 19 (Protein-Ligand Interactions) 21:50

Top Curr Chem (2014) 351: 149–188
DOI: 10.1007/128_2013_485

Published online: 25 October 2013

A Theoretical and Experimental Chemist's Joint View on Hydrogen Bonding in Ionic Liquids and Their Binary Mixtures

Annegret Stark, Martin Brehm, Marc Brüssel, Sebastian B.C. Lehmann, Alfonso S. Pensado, Matthias Schöppke, and Barbara Kirchner

Abstract A combined experimental and theoretical approach including quantum chemistry tools and computational simulation techniques can provide a holistic description of the nature of the interactions present in ionic liquid media. The nature of hydrogen bonding in ionic liquids is an especially intriguing aspect, and it is affected by all types of interactions occurring in this media. Overall, these interactions represent a delicate balance of forces that influence the structure and dynamics, and hence the properties of ionic liquids. An understanding of the fundamental principles can be achieved only by a combination of computations and experimental work. In this contribution we show recent results shedding light on the nature of hydrogen bonding, for certain cases the formation of a three-dimensional network of hydrogen bonding, and its dynamics by comparing 1-ethyl-3-methylimidazolium based acetate, chloride and thiocyanate ionic liquids.

A particularly interesting case to study hydrogen bonding and other interactions is the investigation of binary mixtures of ionic liquids of the type [cation1][anion1]/[cation1][anion2]. In these mixtures, competing interactions are to be expected. We

A. Stark (✉)
Institute for Chemical Technology, Universität Leipzig, Linnéstr. 3-4, 04103 Leipzig, Germany
e-mail: annegret.stark@uni-leipzig.de

M. Brehm, M. Brüssel, S.B.C. Lehmann, and M. Schöppke
Wilhelm-Ostwald-Institute for Physical and Theoretical Chemistry, Universität Leipzig, Linnéstr. 2, 04103 Leipzig, Germany

A.S. Pensado
Wilhelm-Ostwald-Institute for Physical and Theoretical Chemistry, Universität Leipzig, Linnéstr. 2, 04103 Leipzig, Germany

Mulliken Center for Theoretical Chemistry, Institute for Physical and Theoretical Chemistry, Universität Bonn, Beringstr. 4+6, 53115 Bonn, Germany

B. Kirchner
Mulliken Center for Theoretical Chemistry, Institute for Physical and Theoretical Chemistry, Universität Bonn, Beringstr. 4+6, 53115 Bonn, Germany

present both a thorough property meta-analysis of the literature and new data covering a wide range of anions, i.e., mixtures of 1-ethyl-3-methylimidazolium acetate with either trifluoroacetate, tetrafluoroborate, methanesulfonate, or bis (trifluoromethanesulfonyl)imide. In most cases, ideal mixing behavior is found, a surprising result considering the multitude of interactions present. However, ideal mixing behavior allows for the prediction of properties such as density, refractive index, surface tension, and, in most cases, viscosity as function of molar composition. Furthermore, we show that the prediction of properties such as the density of binary ionic liquid mixtures is possible by making use of group contribution methods which were originally developed for less complex non-ionic molecules. Notwithstanding this ideal mixing behavior, several exciting applications are discussed where preferential solvation via hydrogen bonding gives rise to non-additive effects leading to performance improvements. The assessment of the excess properties and ^{1}H NMR spectroscopic studies provide information on these structural changes and preferential interactions occurring in binary mixtures of ionic liquid, that clearly support the conclusions drawn from the computational studies.

Keywords Ab initio methods · Binary ionic liquid mixtures · Hydrogen bonding · Meta-analysis and physicochemical properties · Molecular simulation · Structure-affecting interactions

Contents

Abbreviations

$[C_n\text{mim}]^+$	1-Alkyl-3-methylimidazolium cation
$[C_n\text{mpy}]^+$	*N*-Alkyl-3-methylpyridinium cation
$[C_n\text{mpyr}]^+$	*N*-Alkyl-*N*-methylpyrrolidinium cation
$[EtNH_3]^+$	Ethylammonium cation
$[NTf_2]^-$	Bis(trifluoromethanesulfonyl)imide anion

$[OAc]^-$	Acetate anion
$[SCN]^-$	Thiocyanate anion
AIMD	Ab initio molecular dynamics
CDF	Combined distribution function
DFT	Density functional theory
IR	Infra red
MD	Molecular dynamics
MP2	Møller–Plesset perturbation theory
NMR	Nuclear magnetic resonance
u	Uncertainty

1 Introduction

The high interest in ionic liquids over the few last years is reflected in the large number of articles that has appeared in the scientific literature. Ionic liquids are promising candidates for a number of industrial applications [1], such as lithium batteries [2–4], dye-sensitized solar cells [5–8], electrochemistry [9, 10], lubricants [11–13], catalysis [14–17], or synthesis [18–20], to name just a few.

The nature of the interactions present in ionic liquids is quite complex. Long-range Coulomb interactions are the strongest interactions amongst the forces between ions [21–31], but short-range dispersion interactions also play an important role in explaining the physicochemical properties of ionic liquids. The low melting point and wide liquid range of ionic liquids is in fact due to the balance between the Coulomb and dispersion interactions. However, another type of interaction is also often present in ionic liquids: specific atomic features of the ions lead to secondary structure-directing effects in the liquid phase, known as hydrogen bonding [31–33].

The nature of hydrogen bonding still represents an intriguing issue in charged complexes and systems consisting of ions because its classification appears to be rather difficult [34]. The task group established by IUPAC recommended a definition for hydrogen bonding [35]: "The hydrogen bond is an attractive interaction between an hydrogen atom from a molecule or a molecular fragment X–H in which X is more electronegative than H, and an atom or a group of atoms in the same or a different molecule, in which there is evidence of bond formation." A typical hydrogen bond may be depicted as X–H···Y. Experimental or theoretical results, or ideally a combination of both, may provide evidence for hydrogen bond formation. The task group [35] suggested some useful criteria to establish whether a hydrogen bond occurs. Hydrogen bonding is referred to as a mainly electrostatic interaction, whereas its dispersion character arising from electron correlation effects also plays a significant role. The chemical structure of individual species in a hydrogen-bonded complex appears to dictate its nature; nevertheless the electronegativity of the elements could change depending on the chemical environment, an important aspect for organometallic and other highly polarizable systems.

Therefore, it is recommended that a structure in which the hydrogen atom does not carry a partial positive charge in X–H···Y cannot be considered as containing a hydrogen bond. Historically, a distance X–Y less than the sum of the van der Waals radii of X and Y was considered an infallible indicator of hydrogen bonding, implying an orbital overlap between the orbitals on both atoms that results in a net transfer of charge between the electronegative atoms. Although this situation arises for strong hydrogen bonds, it should not be considered as a necessary criterion in general. For some ionic liquid systems, e.g., those studied by Lehmann et al. [31], this criterion holds true. The X–H···Y hydrogen bond angle tends towards 180°. Deviations of 70° are nevertheless accepted to define a hydrogen bond. The closer the angle is to 180°, the stronger the hydrogen bond.

Given the complexity of defining when a hydrogen bond is present or not, a large number of experimental and computational techniques should be employed. Spectroscopy in every region of the electromagnetic spectrum has contributed to the knowledge of hydrogen bonding [36, 37]. IR and Raman spectroscopy played important roles in the early days of hydrogen bond investigations, and NMR spectroscopy also provides evidence of hydrogen bond formation, as in general the proton magnetic resonance of XH moves toward lower field compared to non-hydrogen-bonded XH. The pK_a of X–H and pK_b of Y–Z in a given solvent correlate strongly with the energy of the hydrogen bond formed between them, providing additional experimental evidence of the strength of the hydrogen bonding. Computational chemistry is one of the most powerful tools to study hydrogen bonded systems [36]. Quantum mechanics methods consider each system and geometry individually, and constitute a widely used tool to explore hydrogen bonding, even if these methods may provide results that do not correlate well with experiments: the experimental distances between the atoms involved in the hydrogen bond are vibrational averages, which differ from distances calculated from potential energy minimization. Therefore, dynamic techniques as classical molecular dynamics [38, 39] or ab initio molecular dynamics (AIMD) [40, 41] can shed light on describing hydrogen bonds. Quantum calculations provide structural data, a complete description of the potential energy surface, vibrational spectra, NMR chemical shifts, and coupling constants. Theoretical analysis of electron density topology [42] is a widely used technique to explore hydrogen-bonded systems.

The importance of hydrogen bonding in 1-alkyl-3-methylimidazolium ionic liquids was first highlighted by Seddon and coworkers [43] back in 1986. Since then, the determination of the nature of hydrogen bonding in imidazolium based ionic liquids represents a hot topic of research. Computational tools, such as quantum chemistry calculations on systems containing a few ion pairs, AIMD, or classical molecular simulations, can help to rationalize the effect of hydrogen bonding on the physicochemical properties of imidazolium based ionic liquids. Experimentally, the nature of hydrogen bonding in ionic liquids was studied intensively [25, 31, 39, 44–65] using a wide number of techniques, such as X-ray diffraction and mid-infrared and NMR spectroscopy, among others.

The existence of extended hydrogen bond networks in the liquid phase has been related to both the structure and the solvent properties of ionic liquids [66–69]. Dupont et al. regarded pure imidazolium ionic liquids as hydrogen-bonded polymeric supramolecules [67, 68]. Antonietti et al. stated that these supramolecular solvent structures could be interesting for molecular recognition and self-organization processes [69]. However, in these examples it is assumed that hydrogen bonds enhance the structuring of ionic liquids leading to similar behavior as known for molecular liquids. This is a hypothesis that cannot always hold, since the other dispersion and Coulomb interactions also need to be taken into account.

For example, the first evidence of the effect of eliminating a hydrogen bond donor site of the imidazolium cation on the thermodynamic properties was provided by Bonhôte et al. [70] They observed that the methylation of the C2 position of 1-alkyl-3-methylimidazolium based ionic liquids, and hence elimination of the C2–H2···X hydrogen bond leads to a material with higher viscosity and melting point, which is counterintuitive and against the above hypothesis [34]. Since then, much effort was made to rationalize the effect of hydrogen bonding on the physicochemical properties of imidazolium based ionic liquids. Thus, Hunt [71], using different DFT calculations of ionic liquids based on the 1-butyl-3-methylimidazolium and 1-butyl-2,3-dimethylimidazolium cations, concluded that the loss of hydrogen bonding is accompanied by a decrease in entropy (the presence of a methyl group on the C2 position decreases the mobility of the anion, as was also stated by Zahn et al. [29]), as the number of possible conformations that the anion can explore is much lower. The "entropy model" of Hunt assumes that hydrogen bonding stabilizes imidazolium based ionic liquids. Endo et al. [72], in a recent study, also support the "entropy model," as they conclude that the melting and freezing points of imidazolium based ionic liquids increase with the methylation on position C2 of the imidazolium ring due to an overcompensation of the phase transition entropy decrease for the enthalpy reduction. A different approach to explain the relationship between molecular structure and macroscopic properties for imidazolium based ionic liquids was proposed by Ludwig's group [46–48, 58]. The authors suggest that the hydrogen bonds represent a set of "defects" on the Coulomb network of the ionic liquids, and their influence, by increasing the dynamics of the cations and anions, is towards fluidizing the ionic liquid leading to lower melting points and viscosities. They also show from the vibrational shifts towards higher wavenumbers in the far infrared and terahertz spectra that the interactions between cation and anion in imidazolium based ionic liquids are more intense due to the presence of hydrogen bonding. Hydrogen bonding leads to characteristic shifts in the NMR and IR spectra reflecting the changes in the chemical environment of the imidazolium cation [59]. Both the IR and the NMR spectroscopic properties reveal a similar type of electronic perturbation caused by hydrogen bonding and the increase of the length of the C2–H2 bond. The hydrogen bond does not interrupt the ion pair or dominate it; however it perturbs the ion pairing in such a way that it can stabilize a transition state between two ion pair conformations, facilitating a higher mobility of the counter ions [31].

Noack et al. [53] studied the effect on the cation–anion interaction by including a methyl group in the C2 position of two different 1-alkyl-3-methylimidazolium cations, one with an ethyl side chain and the other with a butyl side chain, both containing the bis(trifluoromethanesulfonyl)imide anion. Their spectroscopic work suggests that electron density changes lead to changes in the position and strength of interionic interactions and reduced configurational variations, so a conjunction of both the "defect model" and the "entropy model" leads to a good description of the ionic liquid system. It is possible to conclude that hydrogen bonding is present in imidazolium based ionic liquids, and its presence affects the physicochemical properties of the ionic liquids. To date, the understanding of hydrogen bonding in ionic liquids is still evolving, and no theory or model can satisfactorily explain its fundamental nature in ionic liquids.

The aim of this chapter is to summarize the state-of-the-art on hydrogen bonding in ionic liquids, in particular imidazolium based ionic liquids, based on a combination of theoretical and experimental findings. In the first part, we summarize the understanding of hydrogen bonding interactions in ionic liquids from a theoretical chemist's point of view, using static quantum chemical calculations and AIMD. Then we show recent results of combined distribution function (CDF) analysis of three anions, i.e., acetate, chloride, and thiocyanate, indicating that the strength of the hydrogen bonds decreases in this order. More importantly, a dynamic hydrogen bond network is formed in acetate- and chloride-based ionic liquids.

In the second part of this chapter, hydrogen bonding interactions are assessed from an experimental chemist's point of view. In particular, we focus on binary mixtures of ionic liquids. These mixtures have only recently moved into the areas of interest of some research groups, but already it becomes clear that they represent unique systems in which one structural aspect (type and structure of ion or ion substituent, concentration of ion) at a time can be altered and hence studied, while keeping all other aspects constant. After giving some examples where the performance of an ionic liquid in an application may be improved by using binary ionic liquid mixtures exhibiting preferential solvation effects by hydrogen bonding, the physicochemical properties of binary ionic liquid mixtures are meta-analyzed, making use of the literature and new experimental data. Due to ideal mixing behavior in most cases, the prediction of properties by group contribution methods is possible, as shown for the first time for the density and the refractive index of such mixtures. Notwithstanding the ideal mixing behavior, the analysis of the excess properties shows that structural rearrangements occur in such mixtures as function of compositions, but these are not yet understood on a molecular level. An NMR spectroscopic study, however, shows that preferential hydrogen bonding interactions occur, in agreement with a recent molecular dynamics study on similar binary mixtures of ionic liquids. The results of the combined study lead to the conclusion that ionic liquids are complex materials in which already small changes in structure or composition can tremendously affect the balance between Coulomb, dispersion, and hydrogen bond interactions and hence the properties.

2 Hydrogen Bonding and Other Structure Affecting Interactions from a Theoretical Chemist's Point of View

In the following section we would like to summarize some relevant studies describing the interactions in imidazolium based ionic liquids from a theoretical point of view. To represent accurately the interactions present in systems containing ionic liquids, the use of methods such as density functional theory (DFT) or second-order Møller–Plesset perturbation theory (MP2), where the electronic structure of the molecules is explicitly considered, seems mandatory. The drawback of these techniques is that the calculations are usually performed with just a few molecules, then being not so representative for the liquid phase. On the other hand, classical molecular simulation, a well-known method to represent the structure and physicochemical properties of ionic liquids, applying mostly pairwise additive potentials, has some drawbacks, as it sometimes underestimates the strength of the hydrogen bonding [39, 73–76]. AIMD is a method that combines an explicit electronic structure calculation using a DFT method with the sampling of a molecular dynamics trajectory. AIMD methods are very reliable; nevertheless, they obey the "no free lunch theory": one has to pay with computer time and limitations on the size of the studied system for reliable accuracy, but they can provide important information about the hydrogen bonding in ionic liquids.

2.1 Static Quantum Chemical Calculations

In 2006, Hunt et al. [77] provided in a thorough study a set of explanations for several theoretical and experimental controversies on the variations in hydrogen bond donor and acceptor abilities of imidazolium based ionic liquids. Using the example of the ionic liquid [C_4mim][Cl], the relative acidity of the three hydrogen atoms in the imidazolium ring and their preferential interaction with the anions were compared. The authors conclude that all hydrogen atoms carry a positive charge. However, only the carbon atom C2 carries a positive charge, whereas the carbon atoms C4 and C5 are essentially neutral, explaining the most acidic behavior observed for the proton bound to the C2 position [77]. Hydrogen bonding is primarily ionic with a moderate covalent character, as an orbital analysis showed [77]. Two possible conformations (on-top and in-plane) are almost degenerate. Only the in-plane conformation resembles a standard hydrogen bond, while for the on-top conformation no hydrogen bond can be established.

Lehmann et al. [31] presented a comprehensive static quantum chemical study of several ion pairs (see Fig. 1). They observed several co-conformations between cation and anion, as for example in 1-ethyl-3-methylimidazolium bis(trifluoromethanesulfonyl)imide ([C_2mim][NTf_2]), where the most acidic proton (H2) interacted via the oxygen or via the nitrogen with the anion. As the energetic difference was small between the different conformers, they selected only one

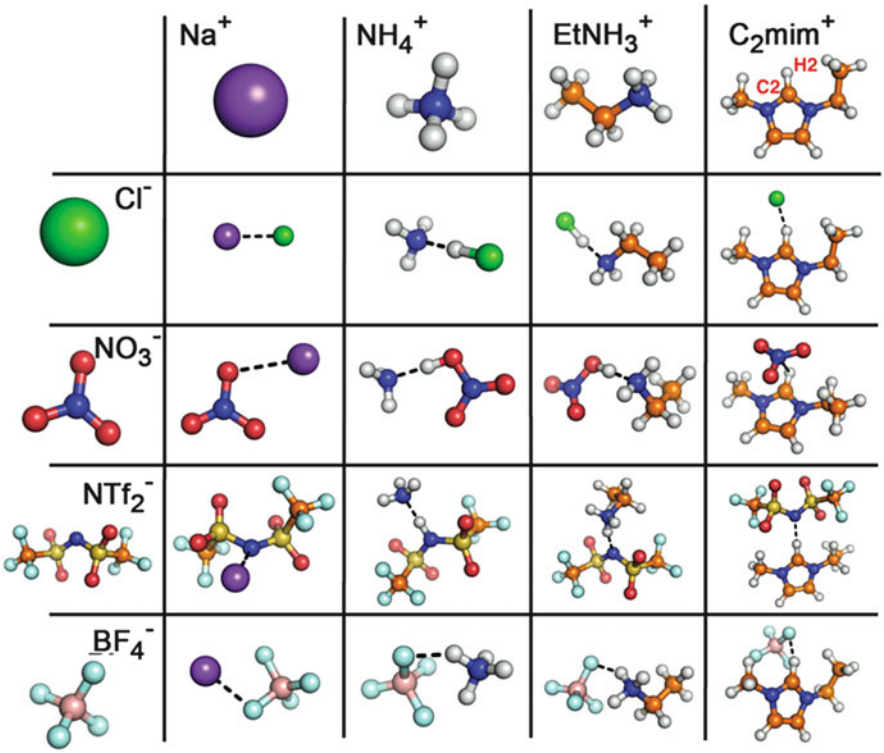

Fig. 1 Ion pairs investigated to analyze the effect of the cation and anion on the strength of the hydrogen bond [31]

co-conformer of the different ion pairs, except for the [C_2mim][Cl], where a complete conformational analysis was performed. The authors [31] observed that all interaction energies exceed the binding energy value of a normal hydrogen bond due to the strong electrostatic interaction. Weaker binding energies were obtained for the larger anions, as expected. This rough trend is observed for complexes with constant cations as well as for complexes with constant anions. As an example, sodium chloride possesses the strongest binding energy and with increasing the anion size, the binding energy decreases.

When changing the cation while maintaining a constant anion, for example chloride, the same effect can be observed. This energetic discussion is not simply reflected in the geometry of the hydrogen bond, but also in the donor–acceptor distance, showing that although a hydrogen bond might be present, it is still not the most important interaction. Tsuzuki et al. [78] come to a similar conclusion, as they found small angles (lacking of directionality) in energetically more stable conformers than in those with linear arrangement. Therefore they conclude that hydrogen bonding is not essential for the attraction between ion pairs. The question

arises: does hydrogen bonding play a role at all in ionic liquids? We will try to answer this question in this chapter.

Lehmann et al. [31] found ion pairs that display a wide range of hydrogen bond angles α(XHY). Some ion pairs in the on-top conformation (anion lies on top of the imidazolium ring) show very small angles. For example, $[C_2mim][NO_3]$ and $[C_2mim][Cl]$ (on-top) exhibit angles of less than 90°. Every ion pair with the $[BF_4]^-$ anion shows a hydrogen bond angle of 140° and the $[C_2mim][Cl]$ (in-plane) as well as $[NTf_2]^-$ based ionic liquids possess larger angles of approximately 160°. A complete conformational analysis for the ionic liquid $[C_2mim][Cl]$ ion pair indicates that the on-top conformers show large deviations from a hydrogen bond geometry while the in-plane conformers provide structures resembling more typical hydrogen bond geometries, exhibiting quite small energy differences between both equilibrium structures [31].

Some aspects are remarkable: On the example of some dialkylimidazolium bis-(trifluoromethylsulfonyl)imides Ludwig and coworkers [46, 58] also found that an agreement between calculated vibrational spectra and experimental data can only be obtained if conformers which hold absolute interaction energies smaller than the global minimum are chosen. Thus, the unique importance of the global minimum structure for the condensed phase is questionable. Another example highlights the limitation of the calculations performed with isolated molecules in the gas phase to represent the structure of ionic liquids in the liquid phase. Given the high gas phase basicities of the $[Cl]^-$ and $[NO_3]^-$ anions, the calculations in the gas phase show that the proton is transferred from the cation to the anion (for two ethylammonium based salts as well as for the three ion pairs $[NH_4][Cl]$, $[NH_4][NO_3]$, and $[NH_4][NTf_2]$), hence forming two neutral molecules which strongly hydrogen bond in an almost linear arrangement. This behavior (proton transfer) is not observed in the liquid phase, and highlights again that the results of calculations performed with isolated molecules to explain the behavior of a liquid phase should be carefully analyzed.

The frequency analysis reveals whether the hydrogen bond donor XH participates in a bond contact with the hydrogen bond acceptor Y. In the case that a regular hydrogen bond-like contact is given, the C2–H2 stretch vibration will show a red-shift and increase in intensity, otherwise no shift or even a blue-shift will be observed. In the case of an ionic liquid ion pair, this effect should be even larger than in a neutral hydrogen-bonded liquid due to the stronger Coulombic interaction. For ionic liquids based on the imidazolium cation, the extent of the red-shift and the intensity increase depends only slightly on (1) the participating groups and their ability to distribute the charge transferred upon hydrogen bond formation, and (2) the group electronegativities which dictate the quality of resonance within the hydrogen bond and therefore the bond length alteration. Therefore, Lehmann et al. [31] obtained for all presumably hydrogen bonding ion pairs large red-shifts for the C2–H2 stretch vibrations, i.e., the frequency of the C2–H2 stretch vibration of the isolated cations occurs at larger wavenumbers than those of the ion pairs. The vibrational spectra show a large red-shift and an increase in the intensity of the C2–H2 stretch frequency (ν C2–H2) for the in-plane compared to the on-top

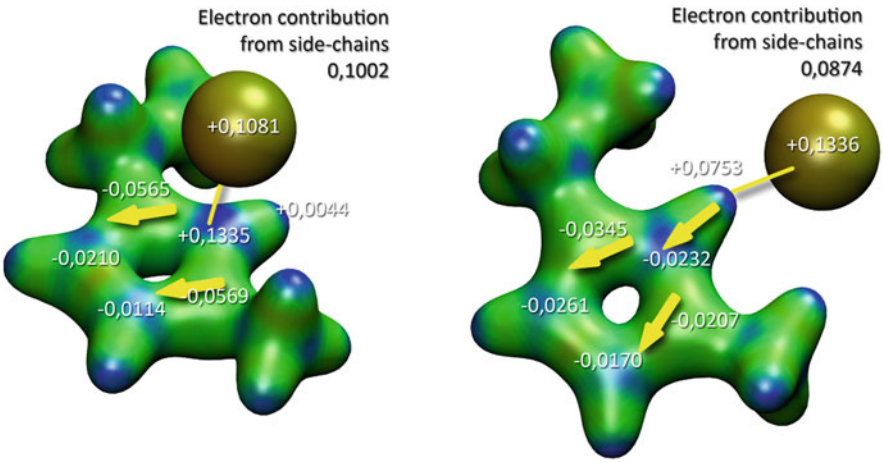

Fig. 2 The numbers depict the magnitude of the charge transfer for the on-top (*left*) and in-plane (*right*) conformers of [C_2mim][Cl] when related to the single isolated ions

conformation. Furthermore, a blue-shift and an intensity increase of the C2–H2 bending frequency of the on-top in contrast to the in-plane conformation as well as an increase in intensity of the out-of-plane bending ring vibrations in case of the on-top conformation of [C_2mim][Cl] is observed. Hunt and Gould [79] found the same behavior for the vibrational frequencies (red and blue shifts for the in-plane and on-top conformers) for the system [C_4mim][Cl]. The vibrational analysis clearly shows that the in-plane conformation exhibits hydrogen bonding capabilities, while the on-top conformation does not allow for the assumption that hydrogen bonding takes place within this non-directional structure.

Charge transfer is one of the most important features of hydrogen bonding. However, charge transfer is not an observable and depends on the population analysis as well as on the method and basis sets applied. A natural bond orbital population analysis for two different conformers of [C_2mim][Cl] was performed, and the results are depicted in Fig. 2, where we present the magnitude of the charge transfer between the conformers and the isolated ions. For this particular ion pair, in both the on-top and in-plane conformers, the carbon atom C2 and the hydrogen atom H2 carry a positive charge. For the in-plane conformer (the conformer with a hydrogen bond-type geometry), there is a transfer of electron density from the H2 to the C2, whereas the anion carries a less negative charge when compared with the on-top conformer.

2.2 Ab Initio Molecular Dynamics

AIMD is a method that can be used to study condensed phases with an explicit electronic structure calculation. This technique circumvents the limitations

presented in the previous section for static calculations performed with isolated molecules, and does not rely on empirical potentials as classical molecular dynamics, where the results are dependent on the quality of the potential [39]. AIMD is a tool that in combination with other available tools (experimental data, classical MD, and static quantum chemistry) can provide insight on the role of hydrogen bonds in ionic liquids. Brehm et al. [40, 80] simulated 36 ion pairs of the ionic liquid $[C_2mim][OAc]$ at 350 K. The electronic structure was calculated with DFT utilizing the BLYP-D functional [81, 82], which includes the empirical dispersion correction (D2) from Grimme [83]. Brüssel et al. [84, 85], using the same method, simulated 32 ion pairs of the ionic liquids $[C_2mim][Cl]$, 32 ion pairs of the ionic liquid $[C_2mim][SCN]$, and an equimolar binary mixture of both at 398 K.

Comparison of the different strengths of the hydrogen bonds present in ionic liquids will provide important information about the dependence of this kind of interaction on the type of anion. The high ability of $[C_2mim][OAc]$ to form a hydrogen bond network (see Fig. 3a) is reflected by its ability to dissolve strongly hydrogen bonding biomolecules such as cellulose. A first step towards understanding the solvation process is characterizing the hydrogen bonding network of the solvent [54]. $[C_2mim][Cl]$ is also capable of dissolving cellulose (even if the solubility of cellulose is lower than in the acetate based ionic liquid) while $[C_2mim][SCN]$ is not. Several authors state that the ability of several ionic liquids to dissolve cellulose is related to the strength of the respective hydrogen bonds present in the different ionic liquids [62, 86–88].

We present in Fig. 3 a set of CDFs for the three considered ionic liquids, where the *X* axis is the distance from the carbon atom C2 of the $[C_2mim]^+$ cation to an oxygen atom O of the $[OAc]^-$ anion (Fig. 3a), the chloride anion $[Cl]^-$ (Fig. 3b), the nitrogen atom N (Fig. 3c) or the sulfur atom S (Fig. 3d) of the $[SCN]^-$ anion, respectively. The *Y* axis is the angle defined by the vector which goes from the H2 atom to the C2 atom of the cation and the vector connecting the atom H2 and the selected atom of the anion. A value of this angle of 180° indicates that the atoms C2, H2, and the considered atom of the anion are aligned (the hydrogen bond would be perfectly linear).

An intense peak in the region around 350 pm/150–180° is present for the four combinations studied, decreasing in intensity in the order $[OAc]^- > [Cl]^- > N[SCN]^- > S[SCN]^-$. This intense peak is related to the hydrogen bond donated by the H2 atom of the $[C_2mim]^+$ cation and accepted by the anion. A second distinct peak is present in the region of 500 pm/30° (more intense for the ionic liquid $[C_2mim][Cl]$, and more diffuse for the ionic liquid $[C_2mim][SCN]$) that arises for the anion coordination with the hydrogen atoms on C4 and C5 of the imidazolium ring. We observe for $[C_2mim][OAc]$ a very narrow distribution of the oxygen atoms of the anion around the carbon atom C2 of the cation. The intensity of the peak in the CDF is slightly lower for $[C_2mim][Cl]$, and a smoother and wider distribution of the $[Cl]^-$ anion around the cation is also observed. For $[C_2mim][SCN]$, weak peaks (smeared and widely distributed) are observed in the CDF. We define a geometrical criterion to allow us to clarify the concept of hydrogen bonding in ionic liquids and to quantify its presence in the different ionic liquids. The adopted definition

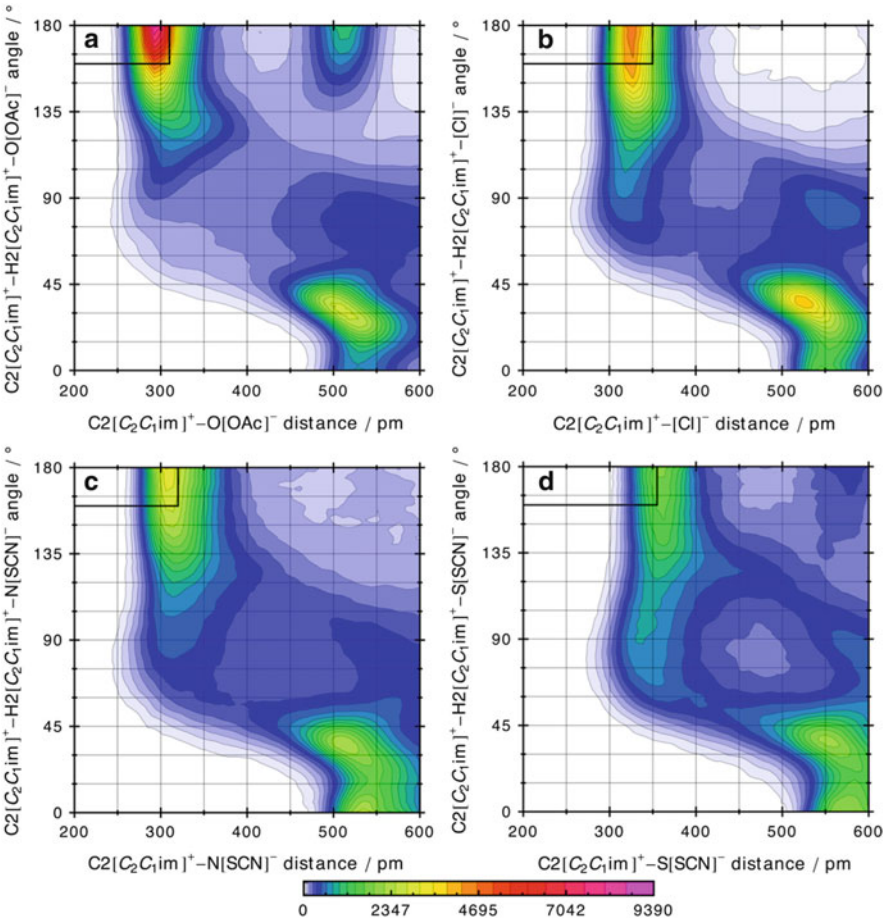

Fig. 3 Combined distribution functions showing the hydrogen bond geometry between the atom C2 of the $[C_2mim]^+$ cation and the (**a**) oxygen atoms of the $[OAc]^-$ anion, (**b**) $[Cl]^-$ anion, (**c**) nitrogen atom of the $[SCN]^-$ anion, and (**d**) sulfur atom of the $[SCN]^-$ anion. The *black area* defines the regions where the criteria to form a hydrogen bond used in this publication are fulfilled, i.e., the distance C2–Y is lower than the sum of the Van der Waals radii and the angle α(C2–H2–Y) is larger than 160°

considers that the distance between the carbon atom C2 of the cation and the oxygen atom of the $[OAc]^-$ anion, the $[Cl]^-$ anion, or the nitrogen or sulfur atom of the $[SCN]^-$ anion should be lower than the sum of the Van der Waals radii. Furthermore, the angle defined by the atoms C2 and H2 of the imidazolium cation and the considered atom of the anion should be between 160° and 180° (see black rectangles in Fig. 3). The IUPAC definition of hydrogen bonding [35] indicates that the hydrogen bond angle tends towards 180° and should preferable be greater than 110°. Skarmoutsos et al. [39] analyzed hydrogen bonding in the ionic liquids

[C_4mim][Cl] and [C_2mim][Cl] using classical MD. They observed that an angular cutoff of 30° may be too restrictive, as it does not include the bulk of the angle distribution for interactions which satisfy the distance criteria (the first minima of the atom–atom radial distribution function), and it does not reproduce the generally accepted picture of hydrogen bonding within these ionic liquids. Therefore, they suggest the use of an angle of 60° as an alternative cutoff for imidazolium based ionic liquids. However, it is then necessary to determine whether the large angle definition is a hydrogen interaction or a hydrogen bond. For this contribution, we have analyzed a large angular criterion, and found comparable results for the studied systems. Therefore, as the main goal of this analysis is to compare the hydrogen-bonding network on the three different ionic liquids, our criteria to define the hydrogen bond seem to be justified.

Using these criteria, we observe that in [C_2mim][OAc], more conformations with a hydrogen bonding geometry are observed. The presence of hydrogen bonding conformations decreases in the order $[OAc]^- > [Cl]^- > [SCN]^-$. It is interesting to notice that this observed trend correlates with the solubility of cellulose in these ionic liquids [87, 88].

A second step is analyzing the morphology of the hydrogen bonding network present in the three ionic liquids. The question that arises is whether there are just ions connected by a hydrogen bond or whether a three-dimensional dynamic network is present in the studied liquids. One aspect is the coordination of a single anion simultaneously to two different cations, and evaluating the probability of the occurrence of this event.

Figure 4 depicts CDFs for two distances applying the above-mentioned hydrogen bonding criteria for each ionic liquid. The *X* axis represents the distance between one oxygen atom of the $[OAc]^-$ anion, the $[Cl]^-$ anion or the nitrogen or sulfur atom of the $[SCN]^-$ anion, and one hydrogen atom of the imidazolium ring of the cation, respectively. The *Y* axis depicts the distance between the other oxygen atom of the $[OAc]^-$ anion, the $[Cl]^-$ anion or the sulfur or nitrogen atom of the $[SCN]^-$ anion, and a second cation. Strong peaks are observed for the ionic liquids [C_2mim][OAc] and [C_2mim][Cl] with short distances between the anions and the hydrogen atoms. We observe in Fig. 4a a more located and intense probability at the "hydrogen bonding positions" in the case of the [C_2mim][OAc] system. Similar behavior is found for the [C_2mim][Cl] system (Fig. 4b). Regarding Fig. 4c, showing the [C_2mim][SCN] system, a smeared out distribution of "hydrogen bond spots" can be seen, reflecting the lower ability of this ionic liquid to build a hydrogen bond network.

We also investigated the coordination of two different anions to the same cation via the different hydrogen atoms of the imidazolium ring, when the angular criterion to form a hydrogen bond is fulfilled. The CDFs depicted in Fig. 5 show on the *X* axis the distance between the hydrogen atom H2 of the imidazolium ring and an oxygen atom of the $[OAc]^-$ anion, the $[Cl]^-$ anion or the nitrogen or sulfur atom of the $[SCN]^-$ anion. The *Y* axis represents the distance between the rear hydrogen atoms H4 and H5 of the imidazolium ring of the same cation and the considered atoms of a second anion. We observe strong peaks at distances lower

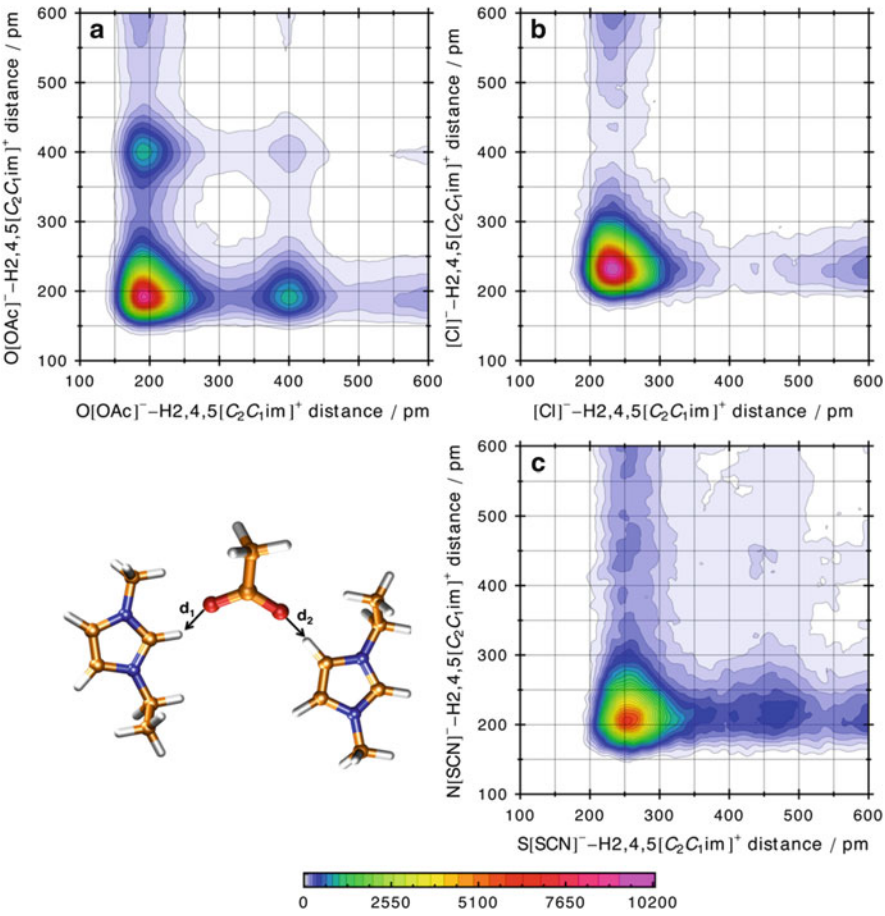

Fig. 4 Combined distribution functions showing the bridging behavior of the anion with two different cations: (a) two oxygen atoms of [OAc]-, (b) the [Cl]- anion, (c) the sulfur atom and the nitrogen atom of the [SCN]- anion [80]

than 250 pm for [C_2mim][OAc] and [C_2mim][Cl] (Fig. 5a, b), and a diffuse distribution for [C_2mim][SCN] (Fig. 5c). The results suggest that conformations that fulfill the criteria defined as hydrogen bonding are highly probable in the ionic liquids [C_2mim][OAc] and [C_2mim][Cl]. In these liquids a dynamic network exists that evolves through the bulk liquid and which connects several ions with each other. For [C_2mim][SCN], the distribution does not support the idea of a stable hydrogen bond network, in comparison with the other ionic liquids studied.

Even if the morphology of the hydrogen bonding network is similar for the ionic liquids based on the acetate and chloride anions, some differences arise. The acetate anion is bidentate, and both oxygen atoms can construct simultaneously two different hydrogen bonds, as can be seen in the localized spots in the CDFs

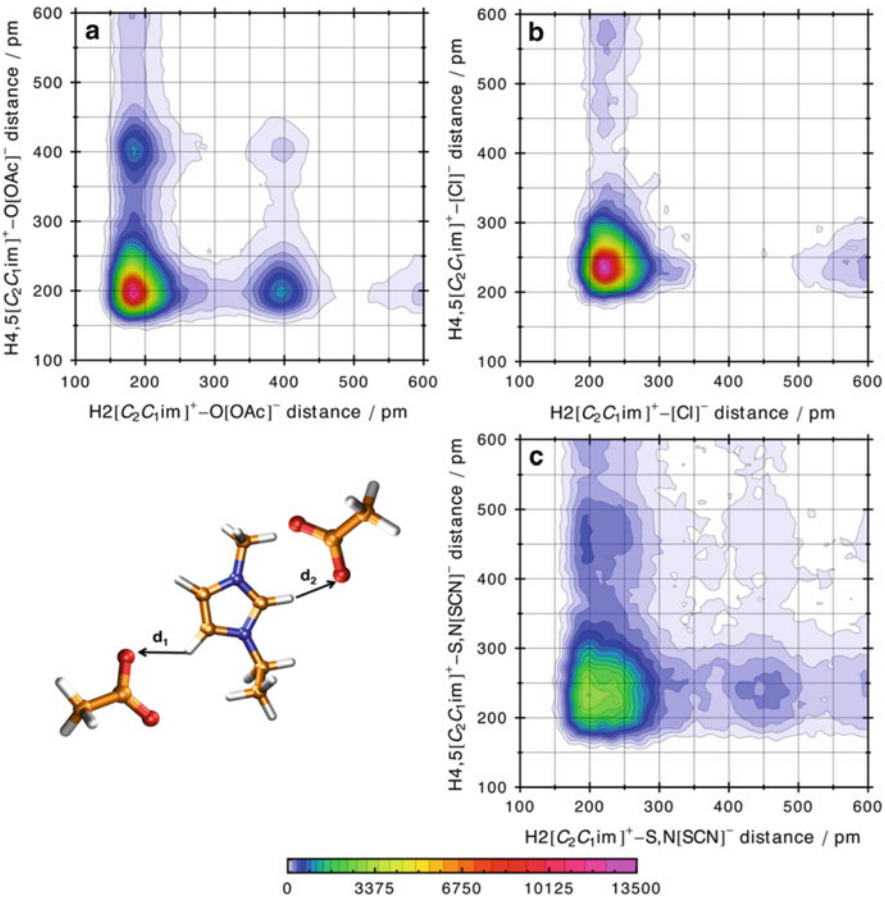

Fig. 5 Combined distribution functions showing the bridging behavior of one imidazolium cation via the H2,4,5 ring protons to two different anions: (a) an oxygen of two [OAc]- anions, (b) two [Cl]- anions and (c) a sulfur or a nitrogen atom of two [SCN]- anions [80]

presented in Figs. 4 and 5. Other than the acetate system, the chloride system shows slightly broader spots, reflecting a less structured hydrogen bonding network. From the results presented in Sect. 2.1, where a net charge transfer was observed from the $[Cl]^-$ anion to the imidazolium cation when a hydrogen bond conformation was formed, and the analysis of the morphology of the three-dimensional network present in $[C_2mim][Cl]$, where a single $[Cl]^-$ anion can be simultaneously involved in two hydrogen bonds, it seems reasonable to conclude that the hydrogen bond network is weaker than that observed in $[C_2mim][OAc]$.

To analyze the strength of the hydrogen bond network, we compute the hydrogen bond dynamics by using autocorrelation functions. $C_{in}(t) = 1$ if a hydrogen bond between a particular acceptor atom and the hydrogen atom exists, otherwise $C_{in}(t) = 0$. This hydrogen bond must be present at $t = 0$. The subscript "in" implies

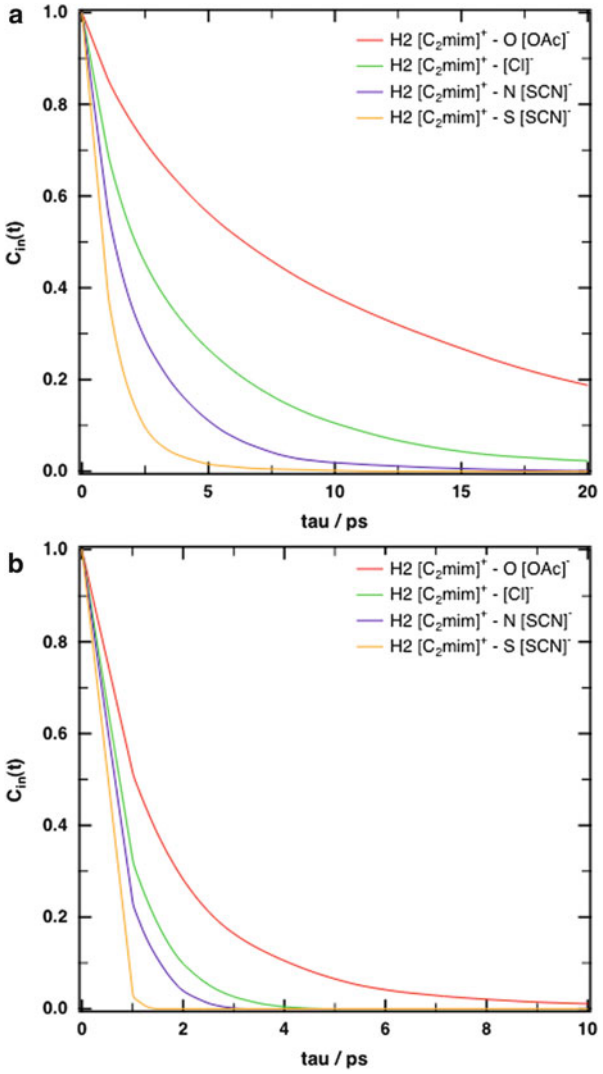

Fig. 6 Intermittent $C_{in}(t)$ hydrogen bond autocorrelation functions obtained from calculations (**a**) with the hydrogen bond criteria that the distance of the hydrogen bond donor and acceptor atom is lower than the sum of the Van der Waals radii and the angle α(C2-H2-Y) is larger than 160° and (**b**) with the distance criterion reduced to 90% of the sum of the Van der Waals radii

that the reformation of a hydrogen bond is allowed if it occurs in an interval of 1 ps after it is broken. This definition seems to be the most accurate to describe the hydrogen bond dynamics in ionic liquids [89]. Figure 6 depicts the results of the intermittent hydrogen bond dynamics for the hydrogen atom H2 of the imidazolium ring. Figure 6a shows the dynamic behavior of the systems when the hydrogen bonding criteria, depicted in Fig. 3, are considered. In Fig. 6b we reduce the distance criterion to 90% of the sum of the Van der Waals radii of the hydrogen bond donor and acceptor atoms. This definition is comparable to a strong hydrogen bond criterion for known molecular hydrogen bonding liquids such as water or HF [90–92].

We observe that the lifetime of a hydrogen bond follows the trend [C_2mim][OAc] $\gg$ [C_2mim][Cl] $>$ N of [C_2mim][SCN] $>$ S of [C_2mim][SCN]. Therefore, the hydrogen bond network is a more dominant feature on the structure of the ionic liquid [C_2mim][OAc], and is stronger because a given conformation of an anion and a cation that fulfills the hydrogen bond criteria lives much longer than when compared with the other ionic liquids studied.

The hydrogen bonds present in [C_2mim][SCN] exhibit short life times, and after 10 ps the correlation is lost. These results suggest that the correct description of the hydrogen bond interactions in ionic liquids requires the analyzing of both the structure and its dynamics. Therefore, we can conclude that for the [C_2mim][SCN] system there is no explicit hydrogen bonding network in the neat liquid observable. The [C_2mim][Cl] system reveals a weak hydrogen bonding network, while for [C_2mim][OAc] a complex and strong network is observable.

3 Hydrogen Bonding and Structure Affecting Interactions from an Experimentalist's Point of View

From the above discussion, the question arises as to how the relative arrangement of the ions, and the relative contributions of the diverse long and short range interactions between anions and cations, in particular hydrogen bond network formation, affect the physical and chemical properties of the bulk ionic liquid. In certain cases, specific and preferential interactions have indeed been made responsible for improvements in chemical applications (see below).

When using an ionic liquid in a reaction, we are interested in affecting the reactivity of a reactant by specific interactions to evoke organo-catalytic effects. Depending on the nature of the reactant and the type of reaction it is supposed to undergo, either the hydrogen bond donating or accepting ability of an ionic liquid may be of interest. For example, in order to study the hydrogen bond donating ability of the ionic liquid, one might want to look at the hydrogen bond acceptor ability (basicity) of a reactant, choose a model acceptor solute such as an amine H_2N-R, add it to the ionic liquid, and study its behavior spectroscopically. If the solute is present at infinite dilution, it may be permissible to presume that the effect of the remaining structural moiety R of the solute on the solvating environment (solute–solute or solute–anion interactions) is nil. At higher concentrations this will certainly not be the case. Hence, we choose an anion as hydrogen bond acceptor model and place it in different ionic liquid environments. This then gives rise to unique binary systems where the effect of the remaining structural moiety vanishes, independent of its concentration, as it is the same cation as the solvating ionic liquid.

Considering the sheer number of single ionic liquids, i.e., those comprised of one anion and one cation, which has been estimated to be in the order of 10^{18} [93], it is not surprising that at present the number of investigations dealing with binary ionic

liquid mixtures is still low. Herein, binary ionic liquid mixtures are defined as materials derived from the combination of two ionic liquids with either the same anion ([cation1][anion1]/[cation2][anion1]) or the same cation ([cation1][anion1]/[cation1][anion2]). Mixtures consisting of both different cations and different anions ([cation1][anion1]/[cation2][anion2]), i.e., reciprocal binary mixtures [94], have as yet been paid almost no attention [95].

3.1 Examples of Preferential Interactions in Binary Ionic Liquid Mixtures

For example, in our own research, we were interested in determining the capacity of cellulose-dissolving ionic liquids – in other words, how many ionic liquid anions per hydroxyl group of cellulose must be present to achieve dissolution? This research question is based on the currently accepted dissolution model of cellulose with ionic liquids: the strong intra- and intermolecular hydrogen bond network of cellulose hydroxyl groups is broken when a basic ionic liquid anion is introduced into the system which competes as hydrogen bond acceptor for interaction with the hydroxyl groups. The anion must be sufficiently basic, and cellulose-dissolving ionic liquid anions include acetate, chloride, diethylphosphate etc. (known as "dissolving ionic liquids") [87, 96, 97]. Less basic anions, such as bromide, may migrate into the cellulose network and lead to swelling, but they do not lead to physical dissolution (known as "non-dissolving ionic liquids") [87, 96, 97].

However, from a technical point of view, there is a dilemma involved in a process based on a basic ionic liquid for cellulose dissolution: It is well known that in 1,3-dialkylimidazolium based ionic liquids, hydrogen bonding between the H2 and the anion is a prominent structural feature. The resulting directed interaction leads (in general) to high melting points, in particular when the anion is basic [87]. In other words, ionic liquids which qualify as "dissolving ionic liquids" often exhibit high melting points and high viscosities, leading to slow dissolution kinetics, often accompanied by some decomposition of the polymer chains [98–100].

Hence, we postulated that it should be possible to use binary mixtures consisting of a little (but sufficient) cellulose-dissolving ionic liquid (e.g., [C_2mim][OAc]) and an excess of a "non-dissolving ionic liquid" (e.g., [C_2mim][Br]). In fact, an extensive experimental study demonstrated that only equimolar amounts of acetate anion (relative to cellulose hydroxyl moieties) need to be present to achieve dissolution, and the second ionic liquid, which has no cellulose-dissolving ability on its own, provides the fluid medium and does not lead to precipitation of the cellulose even if present in tenfold excess (at 100°C) [87, 88].

This study, and a ^{1}H NMR study conducted in parallel on single ionic liquids with ethanol as cellulose model, clearly demonstrated that as halide anions exhibit strong and preferential interactions with the H2 of the 1,3-dialkylimidazolium cation rather than with the cellulose (or ethanol) hydroxyl group, the cellulose-dissolving anion

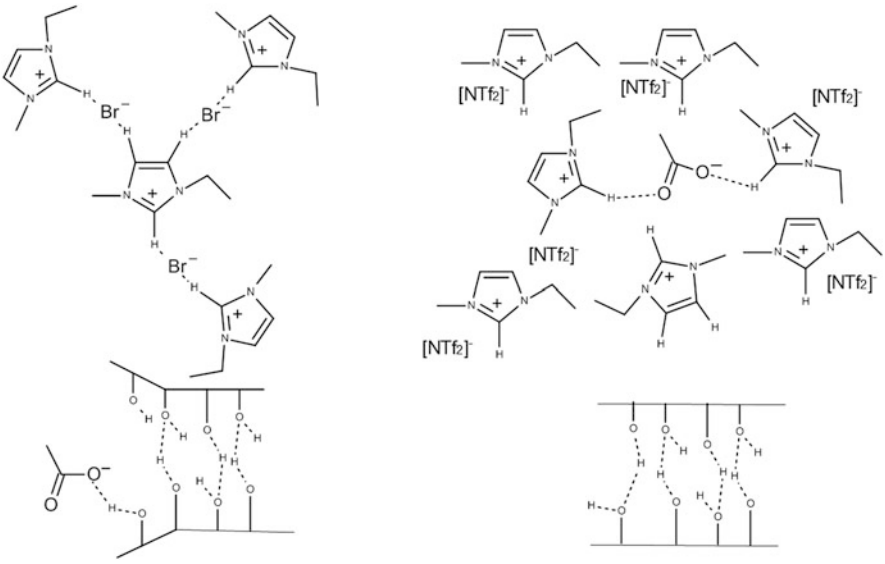

Fig. 7 Representation of the preferential interactions between bromide and H2 of the imidazolium cation, liberating acetate for dissolving interaction with cellulose (*left*), and non-specific interactions of $[NTf_2]^-$, leading to cation-acetate rather than dissolving acetate-cellulose interactions (*right*)

(acetate) is liberated for undergoing interactions with these hydroxyl groups. In contrast to this is the case of binary mixtures of an acetate based, cellulose-dissolving ionic liquid and a non-dissolving ionic liquid that does not feature strong preferential interactions with the cation via hydrogen bonding, such as tetrafluoroborate or bis-(trifluoromethanesulfonyl)imide: In these instances, the solubility of cellulose is dramatically decreased, since competition exists between the hydrogen bond donors (cation, hydroxyl groups) to interact with the hydrogen bond accepting anion (Fig. 7).

Overall, it can be stated that the more basic the "non-dissolving ionic liquid", the less "dissolving ionic liquid" is required.

Additionally, this study showed another interesting aspect of hydrogen bonding: water (or other hydrogen bond donors such as methanol) is generally used to precipitate cellulose from the ionic liquid after processing. When water is added, the anion establishes hydrogen bonds with water rather than maintaining the dissolving interactions with cellulose. Simultaneously, the cellulose polymer chains aggregate by reestablishing inter- and intramolecular cellulosic hydrogen bonds, hence leading to precipitation. In an ionic liquid, the critical amount of water that can be added before precipitation occurs is dependent upon the concentration of the cellulose dissolved and the type of anion. Concentration dependent experiments showed that in $[C_2mim][OAc]$, a large excess of about 2 equiv. of water can be accommodated at quasi-infinitely diluted cellulose. Overall, in this ionic liquid, the maximum ratio for maintaining a solution was (H_2O + cell. OH-group):$[C_2mim][OAc] = 2{:}1$. For $[C_2mim][Cl]$, the maximum ratio for maintaining a solution was

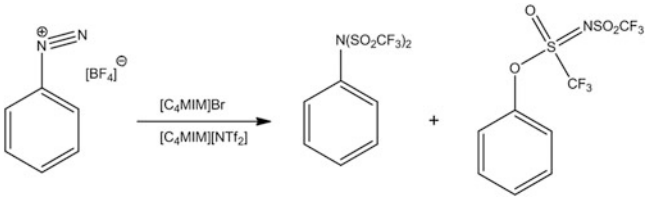

Scheme 1 Proposed reaction scheme of dediazoniation of $[PhN_2][BF_4]$ in $[C_4mim]Br/[C_4mim][NTf_2]$ binary mixtures [101]

(H_2O + cell. OH-group):$[C_2mim][Cl] = 0.5:1$, impressively demonstrating the higher capacity of acetate based ionic liquids, which must be related to their high hydrogen bonding ability (see also the discussion in Sect. 2.2). The structural motifs are, however, not yet known but they are under investigation in our groups [40, 80].

Another impressive example, where preferential interactions have led to surprising changes in the apparent nucleophilicity of the anions, has been presented by Chiappe's group [101]. In the nucleophilic dediazoniation carried out in binary mixtures of $[C_4mim][NTf_2]$ and $[C_4mim][Br]$ (or $[C_4mim][Cl]$), it was not the bromide (or chloride) but the bis(trifluoromethanesulfonyl)imide anion that was the stronger nucleophile. Hence, the expected halobenzene was not formed, but two unusual $[NTf_2]$-derivatives were obtained instead (Scheme 1). Again, this phenomenon is due to the strong and preferential hydrogen bond interaction between the cation's H2 and bromide, [88] which decreases its activity for the nucleophilic attack. The less coordinated $[NTf_2]^-$ anion is then able to substitute the diazo-group.

Other areas of application for binary ionic liquid mixtures may also be found in separation science, as shown in some pioneering work on the examples of aromatics/alkanes or gases [102, 103].

3.2 *Bulk Physicochemical Properties of Binary Ionic Liquid Mixtures*

Before looking in detail into the physicochemical properties of binary ionic liquid mixtures, it is worth mentioning that, up to now, two strategies have been established by ionic liquid chemists to tune the properties, i.e.:

1. Altering the cation and/or the cation's substitution pattern to affect the physical properties (e.g., viscosity, density, surface tension, conductivity, solubility), while maintaining the prevailing chemical properties by using the same anion.
2. Adding a co-solvent, e.g., to decrease the viscosity and hence improve issues such as mass transfer. This strategy, however, is often accompanied by technical disadvantages such as increased volatility and flammability of the mixtures.

With the advent of binary mixture applications, a third strategy is now added to the toolbox. The application examples discussed above show that the resulting properties are not necessarily the sum of their constituents, but non-additive effects

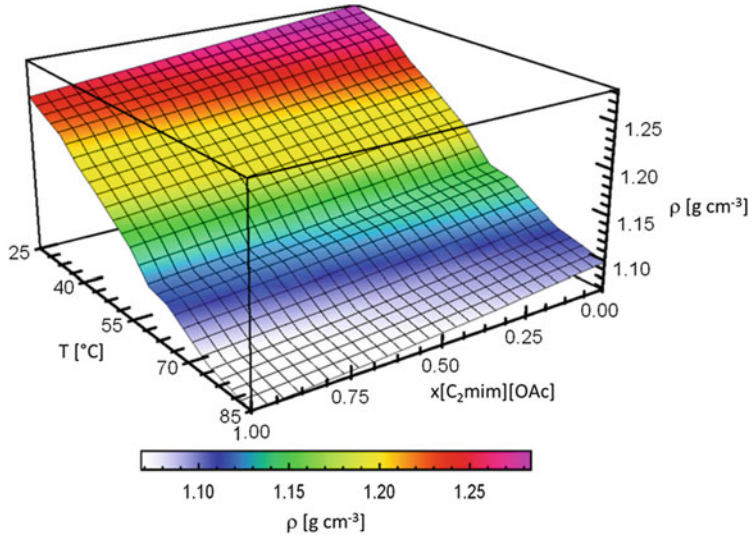

Fig. 8 Density-molar fraction-temperature plots of $[C_2mim][BF_4]/[C_2mim][OAc]$-mixtures ($u(\rho) \approx \pm 0.002$ g cm^{-1}) [115]

may be expected. However, the limits of this strategy are as yet unknown, and only a few reports have started to appear which discuss the behavior of ionic liquid binary mixtures from a physicochemical point of view [94]. However, due to the large number of ionic liquids available, the number of successional studies employing the same ionic liquid binary combination with several characterization techniques is low. We therefore investigated binary ionic liquid mixtures of $[C_2mim][OAc]$ with several related ionic liquids in which the basicity of the second anion decreased ($[CH_3SO_3]^- > [CF_3CO_2]^- > [BF_4]^- > [NTf_2]^-$ [104, 105]) with regards to the effect of the molar composition on the density, viscosity, refractive index, and surface tension. In addition, a ^{1}H NMR spectroscopic study was conducted.

The density was found to be a linear function of both composition and temperature (Fig. 8). Even the dependence of the density on the composition of mixtures containing very different anions such as $[OAc]^-$ and $[NTf_2]^-$ can be modeled by linear equations (Table 1). In fact, a meta-analysis of the literature shows that ideal mixing behavior, i.e., a linear dependence of both temperature and molar composition, is found with regards to the density of most binary ionic liquid mixtures investigated to date [84, 106–113]. It is therefore possible to predict some very important properties from tabulated data of the pure components, which will facilitate transfer of complex binary ionic liquid mixtures into applications.

The refractive index of binary ionic liquid mixtures can be interpreted in terms of electron polarizability: if the density is a linear function of the mixtures' composition, the refractive index is also linearly related to the molar refraction by the Lorentz–Lorenz equation. Our data show that the refractive index increases linearly for all ionic liquids with the mole fraction of $[C_2mim][OAc]$ (Fig. 9). Linear relationships were also found for $[C_4mpy][(CN)_2N]/[C_4mpy][BF_4]$,

Table 1 Equations for the prediction of the density of various ionic liquid-[C_2mim][OAc]-mixtures as function of temperature and composition

Density data of pure ionic liquids as function of temperature[a]	
[C_2mim][OAc]	$\rho = -5.510{*}10^{-4}{*}T$[K] + 1.2615 ($R^2 = 0.9995$)
[C_2mim][CF_3CO_2]	$\rho = -7.198{*}10^{-4}{*}T$[K] + 1.5055 ($R^2 = 0.9996$)
[C_2mim][NTf_2]	$\rho = -8.786{*}10^{-4}{*}T$[K] + 1.7773 ($R^2 = 0.9978$)
[C_2mim][BF_4]	$\rho = -6.697{*}10^{-4}{*}T$[K] + 1.4836 ($R^2 = 0.9999$)
[C_2mim][CH_3SO_3]	$\rho = -6.116{*}10^{-4}{*}T$[K] + 1.4241 ($R^2 = 0.9956$)
Density data of mixtures of ionic liquids as function of x([C_2mim][OAc])	
[C_2mim][CF_3CO_2]	ρ(298 K) = −0.1929 × x([C_2mim][OAc]) + 1.2919 ($R^2 = 0.9995$)
	ρ(358 K) = −0.1830 × x([C_2mim][OAc]) + 1.2483 ($R^2 = 0.9996$)
[C_2mim][NTf_2]	ρ(298 K) = −0.201 × x([C_2mim][OAc])^2 − 0.2105 × x([C_2mim][OAc]) + 1.51 ($R^2 = 0.9998$)
	ρ(358 K) = −0.191 × x([C_2mim][OAc])^2 − 0.2007 × x([C_2mim][OAc]) + 1.4583 ($R^2 = 0.9997$)
[C_2mim][BF_4]	ρ(298 K) = −0.1853 × x([C_2mim][OAc]) + 1.2825 ($R^2 = 0.9998$)
	ρ(358 K) = −0.1761 × x([C_2mim][OAc]) + 1.242 ($R^2 = 0.9997$)
[C_2mim][CH_3SO_3]	ρ(298 K) = −0.1421 × x([C_2mim][OAc]) + 1.2404 ($R^2 > 0.9999$)
	ρ(358 K) = −0.138x + 1.2085 ($R^2 = 0.9999$)

[a]Determined between 298.15 and 358.15 K

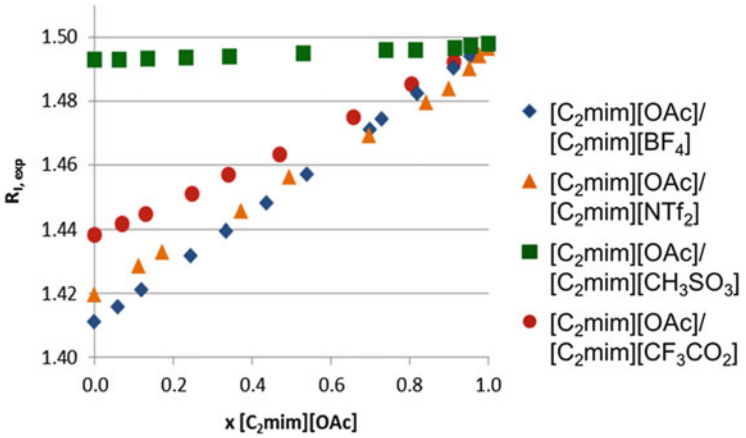

Fig. 9 Refractive index of binary ionic liquid mixtures at 26.5°C ($u \approx \pm$ 0.001; 589.3 nm Na-D-line)

[C_4mpy][BF_4]/[C_8mpy][BF_4] [111], and [C_4py][BF_4]/[C_4py][NTf_2] [112] binary mixtures. Hence, in the mixtures investigated to date, the electron polarizability is not exceedingly affected by the composition.

The surface tension is also a linear function of the composition. However, due to the fact that clean surfaces are difficult to obtain, the deviations are rather large (Fig. 10). A thorough literature review on surface tension data of ionic liquids has

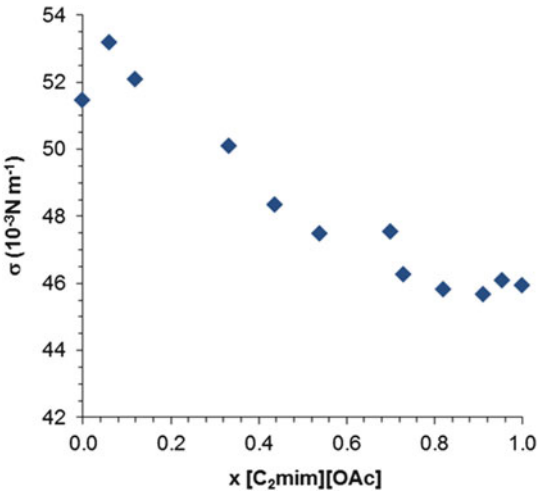

Fig. 10 Surface tension of the binary ionic liquid mixture $[C_2mim][OAc]/[C_2mim][BF_4]$ at 25°C ($u \approx \pm\ 0.5 \times 10^{-3}$ N m^{-1})

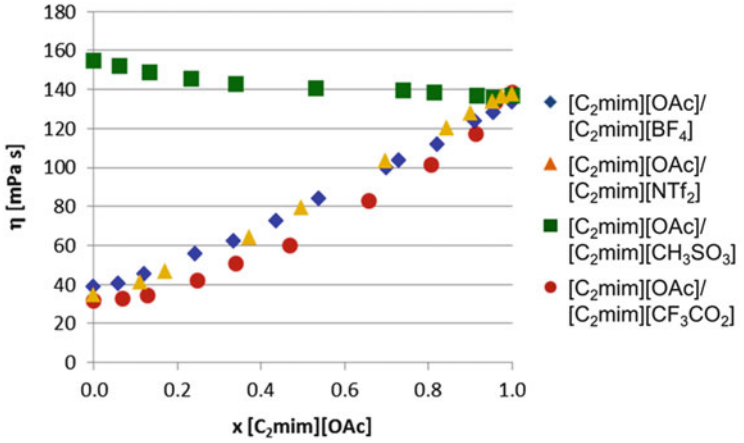

Fig. 11 Viscosity of binary ionic liquid mixtures at 25°C ($u \approx \pm\ 0.5$ mPa s)

just been published, where this issue and differences between measurement techniques have been discussed in detail [114].

The complex balance of Coulomb, van der Waals, and hydrogen bond interactions is reflected in the viscosity of a medium. The temperature-dependent dynamic viscosity measurements showed no linear correlation. However, although the dynamic viscosity is a non-molar quantity (as it is a measure of the inner friction between neighboring liquid layers moving with different velocities), it depends linearly on the molar composition of the mixture. The only exception in our current work (Fig. 11) is the mixture $[C_2mim][OAc]/[C_2mim][CF_3CO_2]$.

Overall, our results tie in with those presented in the literature in that only rarely do deviations from ideality occur [109, 110, 112, 116, 117; Stark A, Ramzan M (2012) unpublished work]. However, as stated above, many ion combinations remain to be studied, in particular those where the structural make-up of the constituents features large differences regarding hydrogen bond acceptor/donor strengths.

3.3 *Predicting Physicochemical Properties of Binary Ionic Liquid Mixtures*

These often ideal dependencies are surprising, because one could have expected a very complex mixing behavior affecting the properties, considering that binary ionic liquid mixtures consist of three chemical moieties (i.e., number of ion types). Shimizu et al. [118] argued that the ideal mixing behavior observed for many binary ionic liquid mixtures may be explained by the fact that most interaction modi are already present in the pure ionic liquids, and hence new types of interaction are not formed on mixing. Therefore, a pronounced effect is only observed if either the anions or the cations are very unlike, e.g., if a short and a long alkyl chain exist in binary mixtures containing only one anion type but different cations, or if the basicity of the anions in binary mixtures containing only one cation type but different anions are chosen.

From an application point of view, linear relationships allow for the simple prediction of the physical bulk properties from linear equations (see above). Moreover, they should allow for the prediction of many properties from group contribution methods. For single (pure) ionic liquids, this approach has been impressively shown by Deetlefs et al. [119]. For example, the parachor P, [120, 121] which correlates surface tension σ to density ρ irrespective of temperature, can be obtained experimentally (1) or from a group contribution approach [122]. It can be used to predict either σ or ρ from existing data collections (M = molar mass):

$$P = M\sigma^{1/4}/\rho \tag{1}$$

Table 2 shows that the parachors of pure ionic liquids calculated from density and surface tension data and the parachors estimated by the group contribution method agree very well [122]. Similarly, the molar refraction $R_{\mathrm{m,est}}$ was estimated and used to determine the refractive index $R_{\mathrm{I,est}}$ by (2) (Lorentz–Lorenz equation), which is also compared to $R_{\mathrm{I,exp}}$ in Table 2 [123]:

$$R_{\mathrm{m}} = \left(\frac{M}{\rho}\right)\left(\frac{R_{\mathrm{I}}^2 - 1}{R_{\mathrm{I}}^2 + 2}\right) \tag{2}$$

The percentage errors between the experimental and estimated parachors as well as experimental and estimated refractive indices are surprisingly low (between

Table 2 Experimental data used for estimations by group contribution methods, estimated parachor and refractive index of pure ionic liquids, as well as relative errors (experimental density taken at 25°C, experimental refractive index taken at 26.5°C)

Ionic liquid	M (g mol^{-1})	σ_{exp} (10^{-3} N m^{-1})	ρ_{exp} (g cm^{-3})	$P_{exp.}$[a]	$P_{est.}$[b]	$\%E$ (P)[c]	$R_{m,\ est}$[d]	$R_{I,\ exp}$	$R_{I,est}$[e]	$\%E$ (RI)[c]
[C_2mim][OAc]	170.21	45.94	1.099	403.3	403.8	0.13	49.3	1.4973	1.5489	3.44
[C_2mim][CH_3SO_3]	206.27	50.90 [125]	1.24	444.2	450.4	1.39	52.5	1.4928	1.5444	3.46
[C_2mim][CF_3CO_2]	224.18	nda[f]	1.291	nda[f]	439.8	nda[f]	49.4	1.4384	1.4809	2.95
[C_2mim][BF_4]	197.97	51.44	1.284	412.9	393.7	4.63	47.1	1.4109	1.5236	7.99
[C_2mim][NTf_2]	391.31	41.62 [126]	1.513	656.6	638.9	2.69	70.4	1.4198	1.4573	2.65

[a]Experimental parachor P calculated from surface tension and density data using (1)
[b]Estimated parachor [119, 122]
[c]$\%E$ = value (exp.-calc.)/value (exp.) × 100%
[d]Estimated molar refraction [123]
[e]Estimated refractive index, calculated using (2) (with R_M and R_I)
[f]No literature data available

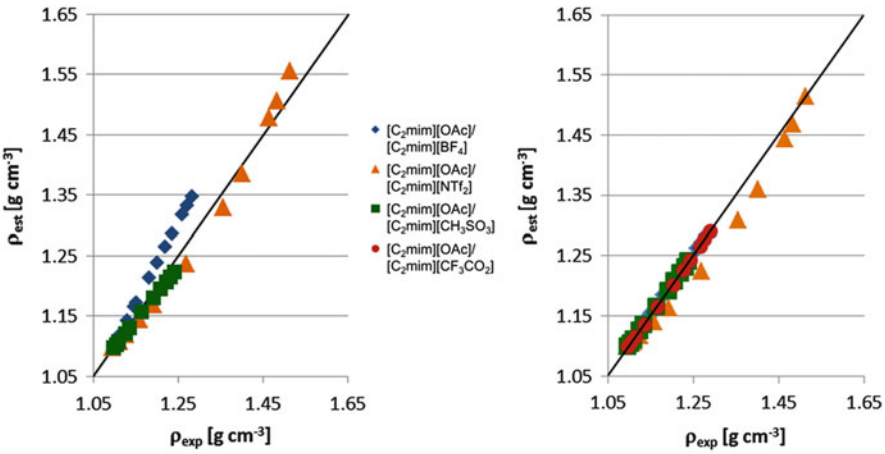

Fig. 12 Predicted and experimentally determined densities of binary ionic liquid mixtures. *Left*: from parachor [122] at 25°C (3), *right*: from molar refraction [123] at 26.5°C (4);*black line*: $x = y$

0.13% and 4.63%, 2.65% and 7.99%, respectively), considering that the estimated values are based on molecular non-ionic moieties, hence neglecting Coulomb interactions and hydrogen bonding. This is in accordance with reported results [119]. In order to determine whether the additivity concept can be extended to binary ionic liquid mixtures [112, 124], the densities of binary ionic liquids of varying compositions were calculated either from P_{est} and the surface tensions of the pure components (3), or from R_{m} and the refractive indices R_{I} of the pure components (4):

$$\rho = \mathrm{x}_1 \left(\frac{M_1 \sigma_1^{1/4}}{P_1} \right) + (1 - \mathrm{x}_1) \left(\frac{M_2 \sigma_2^{1/4}}{P_2} \right) \tag{3}$$

$$\rho = \mathrm{x}_1 \left(\frac{M_1}{R_{\mathrm{m},1}} \right) \left(\frac{R_{\mathrm{I},1}^2 - 1}{R_{\mathrm{I},1}^2 + 2} \right) + (1 - \mathrm{x}_1) \left(\frac{M_2}{R_{\mathrm{m},2}} \right) \left(\frac{R_{\mathrm{I},2}^2 - 1}{R_{\mathrm{I},2}^2 + 2} \right) \tag{4}$$

Figure 12, left, shows that the correlation between experimental and estimated density values is excellent at high molar ratios of [C_2mim][OAc] (i.e., low density), due to the low percentage error of P_{est} of this ionic liquid. The densities of all compositions of [C_2mim][CH_3SO_3] in the acetate based ionic liquid give very good correlations, indicating that the moieties used for the calculation of the parachor [122] represent the overall interactions quite well. At low molar ratios (i.e., low densities) of [C_2mim][NTf_2] in the mixture, this is also the case, but at high molar ratios (and also for [C_2mim][BF_4]) the parachor overestimates the contribution of these ionic liquids. Although for most engineering applications the error is sufficiently small, it is clear that the more "unlike" the ionic liquid anions (e.g., with respect to their respective density), the lower the quality of predictions based on the parachor.

Similarly, Fig. 12, right, shows the comparison between the experimental and estimated densities obtained via calculating the molar refraction from a group contribution method [123], for which only knowledge of the refractive indices of the pure components is necessary. This method provides density data, which deviates less than 0.3% from the experimental values, except for $[C_2mim][NTf_2]$, where the maximum error is 3.6%. Considering the low experimental effort and the small sample size (a drop) for obtaining refractive indices, this method of estimating densities should prove very useful for finding a suitable ionic liquid binary mixture for a given application.

However, the predictive power of group contribution methods is too low to be able to obtain information on underlying reorientation processes occurring in the mixtures. Hence, experimental data are necessary to detect pronounced deviations in the excess properties. To understand underlying structural changes and the resulting effects on their properties, further detailed investigations of physicochemical properties are necessary.

3.4 A Closer Look: Excess Properties of Binary Ionic Liquid Mixtures

A more detailed look at the excess properties leads to a better understanding about reorientation processes occurring in a mixture. The excess property (e.g., excess molar volume) is the difference between the experimental value of a given mixture and the ideal value [(5) for the excess molar volume V_E]. For V_E, positive values indicate that the mixture requires more space than the ideal mixture, indicating less effective packing, the loss of interaction, or the occurrence of repulsive forces:

$$V_E = V_{m,exp} - V_{m,id} \tag{5}$$

The meta-analysis of the combined literature and this new data on excess molar volumes V_E leads to the following conclusions (Table 3):

1. V_E are generally small (<0.1%), indicating little structural rearrangements occurring upon addition of a second ionic liquid. Somewhat larger deviations (0.1–0.5%) are obtained if the cations or anions are very unlike.
2. V_E are often positive, indicating that the packing is less efficient in the binary mixture than expected from the molar volumes of the neat ionic liquids. For example, V_E increases in binary ionic liquid mixtures consisting of a common anion ($[NTf_2]^-$) if the alkyl chain length difference between two 1-alkyl-3-methylimidazolium substituents becomes larger [106], or the cation types are very different ($[C_{6,6,6,14}P][NTf_2]$/$[C_3mpyr][NTf_2]$) [117]. In some instances, polar and apolar domains can form, as witnessed in a combined molecular dynamics/ATR-IR spectroscopic study on the example of $[C_3mpyr][BF_4]$/$[C_8mpyr][BF_4]$ binary mixtures [111]. V_E also increases for mixtures with very

Table 3 Meta-analysis of the literature on the excess molar volume (V_E) and the deviation of the viscosity data from ideal mixing behavior ($\Delta\eta$)

Examples of positive V_E	Deviation[a]	Examples of negative $\Delta\eta$	Deviation
$[C_4mim][BF_4]/[C_4mim][PF_6]$ [107]	<0.07% (25°C)	$[C_2mim][SCN]/[C_2mim][Cl]$ (Stark A, Ramzan M (2012) unpublished work)	75% (70°C)
$[C_2mim][(CN)_2N]/[C_2mim][BF_4]$ [109]	<0.1% (25°C)	$[C_4mim][BF_4]/[C_6mim][BF_4]$ [116]	5% (25°C)
$[C_nmim][NTf_2]/C_mmim][NTf_2]$ (n, m = 2–10) [106]	<0.1% (25°C)	$[C_2mim][BF_4]/[C_6mim][BF_4]$ [116]	27% (25°C)
$[C_4mim][BF_4]/[C_4mim][NTf_2]$ [106]	<0.1% (25°C)	$[C_4mim][BF_4]/[C_4mim][CH_3SO_4]$ [116]	1% (25°C)
$[C_2mim][OAc]/[C_2mim][CF_3CO_2]$ [108]	0.3% (100°C) 0.24% (25°C)[b]	$[C_4mim][BF_4]/[C_4mim][PF_6]$ [116]	16% (25°C)
$[C_2mim][OAc]/[C_2mim][CH_3SO_3]$	0.24% (25°C)[b]	$[C_2mim][OAc]/[C_2mim][CH_3SO_3]$	6% (65°C)[a]
$[C_2mim][OAc]/[C_2mim][BF_4]$	0.22% (25°C)[b]	$[C_2mim][OAc]/[C_2mim][BF_4]$	12% (45°C)[a]
$[C_2mim][OAc]/[C_2mim][NTf_2]$	0.20% (25°C)[b]	$[C_2mim][OAc]/[C_2mim][NTf_2]$	12% (25°C)[a]
$[C_6mim][PF_6]/[C_6mim][Cl]$ [97]	0.05% (50°C)	$[C_2mim][OAc]/[C_2mim][CF_3CO_2]$	30% (25°C)[a]
$[C_6mim][BF_4]/[C_6mim][Cl]$ [110]	0.04% (50°C)	$[C_2mim][(CN)_2N]/[C_2mim][BF_4]$ [109]	–
$[C_8mim][BF_4]/[C_8mim][Cl]$ [110]	0.02% (50°C)	$[C_6mim][BF_4]/[C_6mim][Cl]$ [110]	65% (60°C)
$[C_{6,6,6,14}P][NTf_2]/[C_3mpyr][NTf_2]$ [117]	0.5% (20°C)	$[C_8mim][BF_4]/[C_8mim][Cl]$ [110]	60% (60°C)
$[C_2mim][NTf_2]/[C_3mpyr][NTf_2]$ [117]	0.06% (20°C)	$[C_6mpyr][NTf_2]/[C_3mpyr][NTf_2]$ [117]	–
$[C_6mpyr][NTf_2]/[C_3mpyr][NTf_2]$ [117]	0.02% (20°C)	$[C_2mim][NTf_2]/[C_3mpyr][NTf_2]$ [117]	–
$[C_4mpyr][(CN_2)N]/[C_3mpyr][NTf_2]$ [117]	0.2% (20°C)	$[C_4mpyr][(CN)_2N]/[C_3mpyr][NTf_2]$ [117]	–
Examples of negative V_E	Deviation	$[C_4py][BF_4]/[C_4py][NTf_2]$ [112]	17% (30°C)
$[C_2mim][BF_4]/[C_6mim][BF_4]$ [107]	<0.03% (25°C)	Examples of positive ($\Delta\eta$)	Deviation
$[C_4mim][BF_4]/[C_4mim][CH_3SO_4]$ [107]	0.03% (25°C)	$[C_{6,6,6,14}P][NTf_2]/[C_3mpyr][NTf_2]$ [117]	–
$[C_4mim][BF_4]/[C_6mim][BF_4]$ [107]	0.03% (25°C)		

[a]Note that due to the low experimental error of density measurements (generally <0.2%) and the conversion to molar volumes, these deviations are indeed statistically significant
[b]This work

"unlike" anions, e.g., $[C_2mim][OAc]/[C_2mim][CF_3CO_2]$ [108] mixtures show a maximum deviation of 0.3%. Also, in the study of $[C_4mim][PF_6]/[C_4mim][BF_4]$, $[C_4mim][PF_6]/[C_4mim][NTf_2]$, and $[C_4mim][BF_4]/[C_4mim][NTf_2]$, the deviation found for the $[BF_4]^-/[NTf_2]^-$ mixture was largest [106]. Similarly, $[C_6mim][PF_6]/[C_6mim][Cl]$ binary mixtures showed larger deviations of V_E than $[C_6mim][BF_4]/[C_6mim][Cl]$ [110].

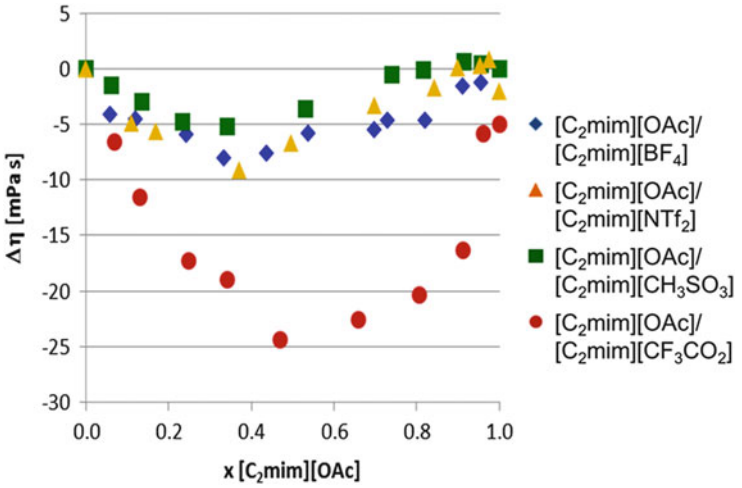

Fig. 13 Deviation from ideal viscosity of binary ionic liquid mixtures at 25°C

However, negative V_E were found occasionally (Table 3), indicating more efficient packing. How this relates to the structure is not yet obvious from the little data available.

In certain instances, unsymmetrical and sometimes sinusoidal functions were observed, e.g., with increasing amounts of $[C_2mim][SCN]$ in $[C_2mim][Cl]$, with $\Delta_{max} = 0.11\ cm^3mol^{-1}$ at $x([C_2mim][SCN]) = 0.5$ and $\Delta_{min} = -0.08\ cm^3mol^{-1}$ at $x([C_2mim][SCN]) = 0.85$ (at 70°C), with a maximum deviation of 0.08% [84]. Such behavior has also been found for binary ionic liquid mixtures such as $[C_8mim][BF_4]/[C_8mim][Cl]$, with negative V_E at low chloride ratios [110].

3. V_E increases in magnitude with increasing temperature [110, 112, 117].

Although fundamentally, ideal and excess quantities are only defined for thermodynamic properties, this concept has been extended to other properties. Figure 13 shows typical deviations from ideal viscosity of various binary ionic liquid mixtures at 25°C.

The meta-analysis of the viscosity data revealed the following trends:

1. Most mixtures investigated to date show large negative deviation from ideality indicating reduced friction, i.e., the addition of the second ionic liquid acts as a lubricant on the first (see Table 3). In many cases, the functions are not symmetrical, and may even be sinusoidal (e.g., for $[C_2mim][OAc]/[C_2mim][NTf_2]$ and $[C_2mim][OAc]/[C_2mim][CH_3SO_3]$).
2. With regards to the cation, the deviation from ideal appears to be larger if the alkyl substituents are more "unlike." Hence, the deviation is less for $[C_4mim][BF_4]/[C_6mim][BF_4]$ binary mixtures than for $[C_2mim][BF_4]/[C_6mim][BF_4]$ [116]. With regards to the effect of the anion, it is not possible to extract a

trend from the data (Table 3). However, it is clear that both the cation and the anion combinations can be responsible for reduced friction.

3. The viscosity of binary mixtures approaches the ideal behavior with increasing temperature [112; Stark A, Ramzan M (2012) unpublished work]. However, for sinusoidal functions such as [C_2mim][OAc]/[C_2mim][CH_3SO_3] (see Fig. 13), this trend is not clearly discernible.

Overall, the available viscosity data does not allow one to draw a conclusive picture of the structural changes that lead (in most instances) to a lower viscosity than predicted. Combined conductivity measurements could show if this "lubrication" is connected to increased ion conductivity or not. Only a few conductivity studies have been carried out with binary ionic liquid mixtures. It is known that, like the viscosity, the conductivity is not always linearly dependent on the composition of the binary ionic liquid mixture [113, 117]. Every et al. [127], who studied binary ionic liquid mixtures of [C_2mim][CF_3SO_3]/[C_2mim][NTf_2] as early as 2000, found by combining results from density, conductivity, and diffusion measurements that the enormous increase of conductivity in binary mixtures of about 40% (determined at 90°C) must be due to a suppression of ion aggregation, i.e., a lower ordering than in the respective pure ionic liquids. A conductivity increasing effect (albeit of only 4%) was also found for [C_2mim][$(CN)_2$N]/[C_2mim][BF_4] at 25°C [109]. One could expect that if mixtures existed which possess lower than ideal mixture viscosity, their conductivity might be higher, which could be beneficially exploited in electrochemical applications. However, one study showed that in the case of [C_8mim][BF_4]/[C_8mim][Cl] mixtures, both the viscosity and the molar conductivity deviated negatively from ideality, meaning that although the friction within these binary mixtures is less than expected, the conductivity does not increase accordingly. This could indicate stable ion pair formation or nano-segregation leading to both reduced ion mobility and lower interactions with the neighboring aggregates, hence reducing the viscosity [110]. Clearly, more detailed experiments are required before conclusions can be drawn.

Extreme deviations from ideal mixing behavior indicate de-mixing phenomena [117], as witnessed by the fact that ionic liquids are not necessarily miscible over the full molar range of compositions. For example, the corresponding chloride salt precipitates from dry mixtures of [C_4mim][Cl]/[C_4mim][BF_4], [C_4mim][Cl]/[C_4mim][NO_3] [128], or [C_2mim][Cl]/[C_2mim][SCN] [84]. In 2006, Arce et al. reported the mutual immiscibility of binary ionic liquid mixtures based on trihexyltetradecylphosphonium ($[C_{6,6,6,14}P]^+$) and $[C_n\text{mim}]^+$ (where $n < 6$) chlorides or bis(trifluoromethanesulfonyl)imides. While for the [$C_{6,6,6,14}$P][NTf_2]/[C_2mim][NTf_2] (and in later work [$C_{6,6,6,14}$P][NTf_2]/[C_2py][NTf_2] [129] and [$C_{6,6,6,14}$P][NTf_2]/[C_3mpyr][NTf_2] [117]) binary mixture, a strong temperature dependence was found, the solubility of the corresponding [$C_{6,6,6,14}$P][Cl]/[$C_n$mim][Cl] mixtures was less affected by the temperature, and decreased with increasing alkyl chain on the imidazolium cation. The analysis of the composition of the phases showed that preferential ion association occurs via hydrogen bonding. This preferential interaction leads to even higher separation selectivities in

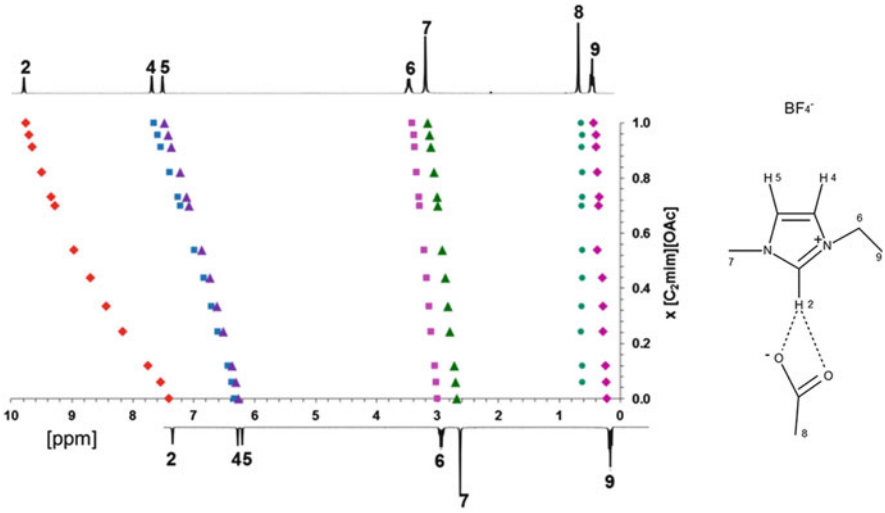

Fig. 14 ^{1}H NMR chemical shifts extracted from spectra of binary mixtures of $[C_2mim][OAc]$ and $[C_2mim][BF_4]$ as function of molar ratio (measurements performed in the non-diluted mixtures at 20°C with a coaxial insert containing acetone-δ_6).

liquid–liquid systems, when two anion- and cation types are used, e.g., $[C_{6,6,6,14}P]^+$ is coextracted with the $[NTf_2]^-$, while $[C_2mim]^+$ is preferentially extracted with $[CH_3SO_3]^-$ [130].

3.5 *^{1}H NMR Spectroscopic Results*

Specific interactions between the cations and anions of binary ionic liquid mixtures can be understood when analyzing ^{1}H NMR spectroscopic data as functions of the molar ratio. Figure 14 shows the chemical shifts extracted from spectra of mixtures where the addition of $[C_2mim][OAc]$ to $[C_2mim][BF_4]$ leads to a tremendous downfield shift of the ring protons, while the chemical shift of the *N*-alkyl substituents and the acetate's methyl moiety are much less affected. This downfield shift can be explained by the stronger hydrogen bond acceptor strength of acetate vs tetrafluoroborate, which is hence capable of interacting with the acidic ring protons. However, it also appears as if this interaction was much more focused on the H2 interaction, i.e., with the most acidic ring proton, in particular at low acetate concentrations. This can be interpreted as preferential interaction of the more basic acetate with this position.

In order to scrutinize this finding in more detail, we investigated the "percentage maximum positive or negative ^{1}H NMR chemical shift deviation" Δ_{max} and Δ_{min}, respectively, i.e., the difference between the experimentally determined values and the respective value of a linear function connecting the shift values of the pure

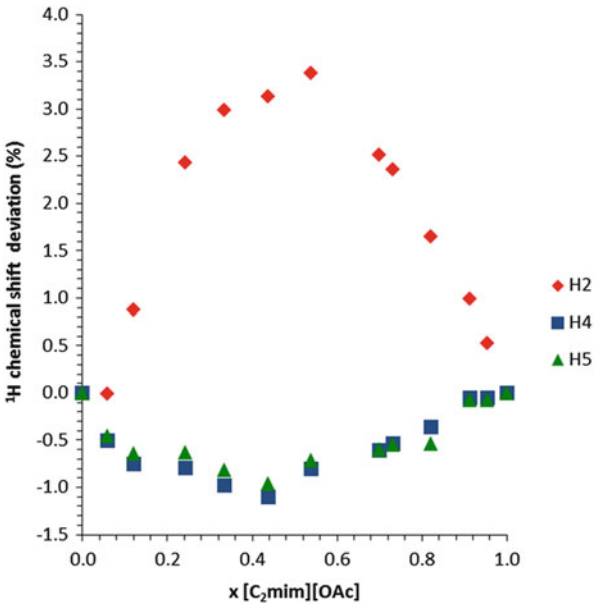

Fig. 15 Maximum percentage ^{1}H NMR chemical shift deviation on the example of binary mixtures of [C_2mim][OAc] and [C_2mim][BF_4] at 20°C

components. This treatment gives further evidence to the above interpretation, as the excess H2 shift was positive (indicating stronger interactions being formed upon addition of [C_2mim][OAc]) for all ionic liquids, in particular mixtures containing [C_2mim][NTf_2] or [C_2mim][BF_4] (Fig. 15). On the other hand, both the H4 and H5 shifts were negative. Table 4 gives the maximum deviations found. The data show that mixtures containing the least basic anions bis(trifluoromethansulfonyl)imide and tetrafluoroborate, i.e., those that are most dissimilar to the acetate, give the largest deviations. The more alike the anions become, the less this is the case. Table 4 demonstrates that the methanesulfonate anion should be less basic than the trifluoroacetate according to this argument, which is in disagreement with the order of basicity established using solvatochromic dyes, and shows that hydrogen bonding is not the only structure influencing interaction [104, 105]. Additionally, the results obtained from mixtures containing either $[CH_3SO_3]^-$ or $[CF_3CO_2]^-$ are less symmetric, also indicating even more complex reorientations taking place.

Prior to these results, AIMD studies carried out at 398 K with binary mixtures of [C_2mim][Cl]/[C_2mim][SCN] had already suggested that, upon addition of the chloride based ionic liquid, the interaction strength between thiocyanate and H2 is reduced while the H2–chloride interaction becomes more prominent due to the higher basicity of chloride [84, 85]. Furthermore, in the absence of chloride, the preferred site of interaction is between the H2 and the nitrogen atom of thiocyanate, while for H4 and H5, the main interaction site is with its sulfur atom. Addition of chloride not only reduces the interaction of thiocyanate with the H2, but also changes its interaction in H4 and H5 from sulfur to the nitrogen atom. The structural arrangement is hence mostly governed by the competition of the anions for

Table 4 Maximum positive and negative deviations of the ^{1}H NMR shifts in % relative to the ideal chemical shift at 20°C (molar ratios x[C_2mim][OAc] in brackets)

	Δ_{max} H2	Δ_{min} H2	Δ_{min} H4($\approx\Delta_{min}$ H5)
[C_2mim][NTf_2]/[C_2mim][OAc]	5.9% ($x = 0.5$)	–	−2.0% ($x = 0.4$)
[C_2mim][BF_4]/[C_2mim][OAc]	3.4% ($x = 0.5$)	–	−1.0% ($x = 0.5$)
[C_2mim][CH_3SO_3]/[C_2mim][OAc][a]	1.0% ($x = 0.6$)	−1.0% ($x = 0.9$)	−1.0% ($x = 0.9$)
[C_2mim][CF_3CO_2]/[C_2mim][OAc][a]	0.5% ($x = 0.75$)	−0.9% ($x = 0.2$)	−1.5% ($x = 0.1$)

[a]Sinusoidal function

hydrogen bond interactions with the cation, and the delicate structural changes occurring upon mixing affect the degree of deviation from ideal mixing behavior.

4 Conclusions

Ionic liquids are complex media in which a balance of various types and strengths of interactions affects the structure and dynamics of the system, hence often leading to unusual properties. We combine experimental and theoretical approaches with the goal of providing a holistic description of the nature of the interactions present in ionic liquids and their binary mixtures with solutes such as water or a second ionic liquid, to be able to predict the properties of not yet synthesized materials in the future.

In this chapter we have focused on the nature of hydrogen bonding, and have shown that, depending on the anion, strong hydrogen bonds may occur, and in the case of [C_2mim][OAc], the formation of a three-dimensional hydrogen bonding network exists.

A particularly interesting case to study hydrogen bonding and other interactions is the investigation of binary mixtures of ionic liquids of the type [cation1][anion1]/[cation1][anion2]. In these mixtures, competing interactions are to be expected. We present both a through property meta-analysis of the literature and new data covering a wide range of anions, i.e., mixtures of 1-ethyl-3-methylimidazolium acetate with either trifluoroacetate, tetrafluoroborate, methanesulfonate, or bis-(trifluoromethanesulfonyl)imide.

One might expect that the multitude of interactions existing in ionic liquids, including Coulomb, van der Waals, and hydrogen bonding, should lead to distinctive non-ideal behavior of binary ionic liquid mixtures. Surprisingly, it is found that many of the bulk physical properties such as density, refractive index, surface tension, and in many cases viscosity are predictable for any molar composition with high accuracy by presuming ideal mixing behavior. It is therefore sufficient for many applications to obtain data from the pure components, and extrapolate to the composition under investigation. Group contribution methods, albeit developed for organic non-ionic chemicals, also yield values in good agreement with experiments.

Using binary ionic liquid mixtures proves to be a tool to tune the bulk physical properties of an ionic liquid. The future will show whether this strategy can be used

to reduce the overall solvent cost of a process, or whether further improvements of the performance in a process can be achieved, e.g., by reducing viscosity while improving conductivity in electrochemical reactions, or by increasing the selectivity in separation processes. Some examples have been published highlighting pioneering work on the beneficial application of binary ionic liquid mixtures. Preferential interactions may tune the nucleophilicity of one of the anions, which can be used to affect the reaction performance in organic and organometallic reactions, hinting at new research fields to exploit in the future.

Nevertheless, subtle structural rearrangements between the ions occur upon changing the molecular composition of the mixtures, as witnessed from the analysis of the excess properties, and from spectroscopic and computer based studies. Deviations from ideal behavior occur for binary mixtures containing very unlike cations and or anions, leading in extreme cases to phase separation.

Interpretation of the meta-analysis has shown that, just as for pure ionic liquids, hydrogen bonding (beside Coulomb interactions) is one of the most important features that affect both chemical and physical properties. It is well known that, for the much investigated 1,3-dialkylimidazolium salts, H2 is the most acidic and hence the main interaction site for hydrogen bonding interactions, depending strongly on the make-up of the cation and the basicity of the anion. When adding a second ionic liquid, its anion may compete for interaction leading to delicate changes in the interaction pattern. Further studies, in particular spectroscopic and molecular dynamic studies, should prove valuable for the elucidation of the fundamental structural arrangements and various subtle effects occurring in ionic liquids systems affecting the macroscopic properties. Understanding what each of these effects contributes to the microscopic properties of an ionic liquid would give a rule of thumb for the creation of ionic liquids for specific applications.

As far as we know today from several studies and our own work, there are three aspects that should be taken into account while analyzing or tuning the properties of ionic liquids. Each aspect might lead to a slight or pronounced change of the global characteristics of an ionic liquid, depending also on how much the changed feature affects the other aspects. These three aspects are:

1. Molecular interactions such as electrostatics, London forces, hydrogen bonding features
2. Geometric influences such as bulkiness, side chain effects, charge concentration
3. Group contributions constituting features such as hydrophobicity, lipophobicity, and molar mass

For molecular non-ionic liquids it is already known that several of these aspects can be responsible for the resulting physicochemical properties. It is obvious that for ionic liquids the same is true; it is “just” the ionicity that is added to the medium’s environment, surely influencing each of the above-mentioned aspects in a way we do not completely understand yet. Our present picture is based on a conventional salt where the organization is driven by electrostatic interactions providing a “grid” of favored ion positions. The above-mentioned aspects disturb, stabilize, or rearrange the grid, leading to changes in the macroscopic properties of the system.

Dispersion (which is additionally connected to the geometric and group properties) often destabilizes the grid by forces that stabilize non-ionic (for example aliphatic) positions of the ions.

Hydrogen bonding can have a similar effect on the grid. For example in [C_2mim][Cl], the transition between the favored positions of the anion on top of the imidazolium ring to the C2–H2 in plane position is stabilized, which again disturbs the ionic grid. Hydrogen bonding may become the main driving force, e.g., in [C_2mim][OAc], where the grid is then built of the favored hydrogen bonding positions, introducing entropy in the system by means of the anion geometry and its poorly ordered three-dimensional network. Hydrogen bonding depends on the strength of the interaction, which again depends on the anion, the cation, and the overall electrostatics of the system. Again, [C_2mim][OAc] can serve as an example which is able to solvate cellulose due to its ability to build strong hydrogen bonds (which are enhanced by the electrostatics in that system) and its ionic character.

Geometrical influences such as the lengths of the cation's side chains introduce entropy by the side chain rotation disturbing the ionic grid. Upon further elongation, the increasing mass of the side chain and other factors slow the rotation leading to solidification of the system. In the same way, the bulkiness of the ions on the one hand shields the ionic charge, but on the other hand increases the mass, hence counterbalancing the effects with a minimum somewhere in between.

Thus, all these molecular aspects build up a complex potential energy landscape which affects the physical as well as the chemical properties of the ionic liquid. For the physical properties, we can state as a rule of thumb that the more balanced the features, the more flat this potential energy landscape, and the more fluid the system.

Taken together, and given the intrinsic complexity of ionic liquids, understanding the interactions occurring on a molecular level by means of theoretical tools, and exploiting these in chemical or engineering applications is still in its infancy, but there are some exciting examples presented in this chapter which allow a glimpse at what is still to come.

Acknowledgments This work was supported by the DFG, in particular by the projects KI-768/4-1 and KI-768/4-2 from the ERA-chemistry, KI-768/5-2, KI-768/5-3, STA-1027/2-1, STA-1027/2-2, and STA-1027/2-3 from the priority program on ionic liquids (SPP 1191). The participation of ASP was made possible by a postdoctoral fellowship granted by the DFG through SPP 1191. Computer time from the RZ Leipzig is gratefully acknowledged. Likewise, we would like to thank M. Ramzan, M. Reichelt, H. Rudzik, A. Foerster, C. Birkemeyer, and L. Hennig for experimental support. Figures 3, 4, 5 and 6 were visualised using TRAVIS [131].

References

1. Plechkova NV, Seddon KR (2008) Chem Soc Rev 37:123
2. Howlett PC, MacFarlane DR, Hollenkamp AF (2004) Electrochem Solid State Lett 7
3. Markevich E, Baranchugov V, Aurbach D (2006) Electrochem Commun 8:1331

4. Shin JH, Henderson WA, Scaccia S, Prosini PP, Passerini S (2006) J Power Sources 156:560
5. Dai Q, Menzies DB, MacFarlane DR, Batten SR, Forsyth S, Spiccia L, Cheng YB, Forsyth M (2006) C R Chim 9:617
6. Kuang D, Wang P, Ito S, Zakeeruddin SM, Grätzel M (2006) J Am Chem Soc 128:7732
7. Oda T, Tanaka S, Hayase S (2006) Solar Energy Mater Solar Cells 90:2696
8. Wei D (2010) Int J Mol Sci 11:1103
9. Armand M, Endres F, MacFarlane DR, Ohno H, Scrosati B (2009) Nat Mat 8:621
10. Zhang Y, Feng H, Wu X, Wang L, Zhang A, Xia T, Dong H, Li X, Zhang L (2009) Int J Hydrogen Energy 34:4889
11. Jiménez AE, Bermúdez MD (2010) Tribol Lett 37:431
12. Palacio M, Bhushan B (2010) Tribol Lett 40:247
13. Zhou F, Liang Y, Liu W (2009) Chem Soc Rev 38:2590
14. Campbell PS, Podgorsek A, Gutel T, Santini CC, Padua AAH, Costa Gomes MF, Bayard F, Fenet B, Chauvin Y (2010) J Phys Chem B 114:8156
15. Campbell PS, Santini CC, Chauvin Y (2010) Chim Oggi Chem Today 28:36
16. Olivier-Bourbigou H, Magna L, Morvan D (2010) Appl Catal A Gen 373:1
17. Podgorsek A, Salas G, Campbell PS, Santini CC, Padua AAH, Costa Gomes MF, Fenet B, Chauvin Y (2011) J Phys Chem B 115:12150
18. Dupont J, Scholten JD (2010) Chem Soc Rev 39:1780
19. Greaves TL, Drummond CJ (2008) Chem Soc Rev 37:1709
20. Ohno H, Fukaya Y (2009) Chem Lett 38:2
21. Bernard UL, Izgorodina EI, MacFarlane DR (2010) J Phys Chem C 114:20472
22. Grimme S, Hujo W, Kirchner B (2011) Phys Chem Chem Phys 14:4875
23. Hunt PA, Gould IR, Kirchner B (2007) Aust J Chem 60:9
24. Izgorodina EI (2011) Phys Chem Chem Phys 13:4189
25. Izgorodina EI, MacFarlane DR (2011) J Phys Chem B 115:14659
26. Li H, Ibrahim M, Agberemi I, Kobrak MN (2008) J Chem Phys 129:124507
27. Tsuzuki S, Tokuda H, Hayamizu K, Watanabe M (2005) J Phys Chem B 109:16474
28. Tsuzuki S, Tokuda H, Mikami M (2007) Phys Chem Chem Phys 9:4780
29. Zahn S, Bruns G, Thar J, Kirchner B (2008) Phys Chem Chem Phys 10:6921
30. Zahn S, Uhlig F, Thar J, Spickermann C, Kirchner B (2008) Angew Chem Int Ed 47:3639
31. Lehmann SBC, Roatsch M, Schöppke M, Kirchner B (2010) Phys Chem Chem Phys 12:7473
32. Thar J, Brehm M, Seitsonen AP, Kirchner B (2009) J Phys Chem B 113:15129
33. Wendler K, Thar J, Zahn S, Kirchner B (2010) J Phys Chem A 114:9529
34. Goswami M, Arunan E (2009) Phys Chem Chem Phys 11:8974
35. Arunan E, Desiraju GR, Klein RA, Sadlej J, Scheiner S, Alkorta I, Clary DC, Crabtree RH, Dannenberg JJ, Hobza P, Kjaergaard HG, Legon AC, Mennucci B, Nesbitt DJ (2011) Pure Appl Chem 83:1637
36. Arunan E, Desiraju GR, Klein RA, Sadlej J, Scheiner S, Alkorta I, Clary DC, Crabtree RH, Dannenberg JJ, Hobza P, Kjaergaard HG, Legon AC, Mennucci B, Nesbitt DJ (2011) Pure Appl Chem 83:1619
37. Pimentel GC, McCleallan AL (1960) The hydrogen bond. W. H. Freeman and Co., San Francisco
38. Qiao B, Krekeler C, Berger R, Delle Site L, Holm C (2008) J Phys Chem B 112:1743
39. Skarmoutsos I, Dellis D, Matthews RP, Welton T, Hunt PA (2012) J Phys Chem B 116:4921
40. Brehm M, Weber H, Pensado AS, Stark A, Kirchner B (2012) Phys Chem Chem Phys 14:5030
41. Spickermann C, Thar J, Lehmann SBC, Zahn S, Hunger J, Buchner R, Hunt PA, Welton T, Kirchner B (2008) J Chem Phys 129
42. Bader RFW (1990) Atoms in molecules: a quantum theory. Oxford University Press, Oxford
43. Abdul Sada AK, Greenway AM, Hitchcock PB, Mohammed TJ, Seddon KR, Zora JA (1986) J Chem Soc Chem Commun 1986:1753

44. Bowron DT, D'Agostino C, Gladden LF, Hardacre C, Holbrey JD, Lagunas MC, McGregor J, Mantle MD, Mullan CL, Youngs TGA (2010) J Phys Chem B 114:7760
45. Dhumal NR, Kim HJ, Kiefer J (2009) J Phys Chem A 113:10397
46. Fumino K, Peppel T, Geppert-Rybczynska M, Zaitsau DH, Lehmann JK, Verevkin SP, Koeckerling M, Ludwig R (2011) Phys Chem Chem Phys 13:14064
47. Fumino K, Wulf A, Ludwig R (2008) Angew Chem Int Ed 47:8731
48. Fumino K, Wulf A, Ludwig R (2009) Phys Chem Chem Phys 11:8790
49. Gao Y, Zhang L, Wang Y, Li H (2010) J Phys Chem B 114:2828
50. Kempter V, Kirchner B (2010) J Mol Struct 972:22
51. Kiefer J, Obert K, Boesmann A, Seeger T, Wasserscheid P, Leipertz A (2008) ChemPhysChem 9:1317
52. Kiefer J, Obert K, Himmler S, Schulz PS, Wasserscheid P, Leipertz A (2008) ChemPhysChem 9:2207
53. Noack K, Schulz PS, Paape N, Kiefer J, Wasserscheid P, Leipertz A (2010) Phys Chem Chem Phys 12:14153
54. Papanyan Z, Roth C, Paschek D, Ludwig R (2011) ChemPhysChem 12:2400
55. Peppel T, Roth C, Fumino K, Paschek D, Koeckerling M, Ludwig R (2011) Angew Chem Int Ed 50:6661
56. Roth C, Peppel T, Fumino K, Koeckerling M, Ludwig R (2010) Angew Chem Int Ed 49:10221
57. Stoimenovski J, Izgorodina EI, Macfarlane DR (2010) Phys Chem Chem Phys 12:10341
58. Wulf A, Fumino K, Ludwig R (2010) Angew Chem Int Ed 49:449
59. Wulf A, Fumino K, Michalik D, Ludwig R (2007) ChemPhysChem 8:2265
60. Xing DY, Peng N, Chung T (2011) J Memb Sci 380:87
61. Youngs TGA, Holbrey JD, Mullan CL, Norman SE, Lagunas MC, D'Agostino C, Mantle MD, Gladden LF, Bowron DT, Hardacre C (2011) Chem Sci 2:1594
62. Liu X, Zhao Y, Zhang X, Zhou G, Zhang S (2012) J Phys Chem B 116:4934
63. Mendez-Morales T, Carrete J, Cabeza O, Gallego LJ, Varela LM (2011) J Phys Chem B 115:11170
64. Podgorsek A, Macchiagodena M, Ramondo F, Gomes MFC, Padua AAH (2012) ChemPhysChem 13:1753
65. Rabideau BD, Ismail AE (2012) J Phys Chem B 116:9732
66. Mele A, Tran CD, De Paoli Lacerda SH (2003) Angew Chem Int Ed 42:4364
67. Dupont J (2004) J Braz Chem Soc 15:341
68. Suarez PAZ, Einloft S, Dullius JEL, de Souza RF, Dupont J (1998) J Chem Phys Phys Chim Biol 95:1626
69. Antonietti M, Kuang D, Smarsly B, Zhou Y (2004) Angew Chem Int Ed 43:4988
70. Bonhôte P, Dias A-P, Papageorgiou N, Kalyanasundaram K, Grätzel M (1996) Inorg Chem 35:1168
71. Hunt PA (2007) J Phys Chem B 111:4844
72. Endo T, Kato T, Nishikawa K (2010) J Phys Chem B 114:9201
73. Bhargava BL, Balasubramanian S (2005) J Chem Phys 123:144505
74. Bhargava BL, Balasubramanian S, Klein ML (2008) Chem Comm 3339
75. Krekeler C, Schmidt J, Zhao YY, Qiao B, Berger R, Holm C, Delle Site L (2008) J Chem Phys 129:174503
76. Schmidt J, Krekeler C, Dommert F, Zhao YY, Berger R, Delle Site L, Holm C (2010) J Phys Chem C 114:6150
77. Hunt PA, Kirchner B, Welton T (2006) Chem Eur J 12:6762
78. Tsuzuki S, Tokuda H, Hayamizu K, Watanabe M (2005) J Phys Chem B 109:16474
79. Hunt PA, Gould IR (2006) J Phys Chem A 110:2269
80. Brehm M, Weber H, Pensado AS, Stark A, Kirchner B (2013) Z Phys Chem 227:177
81. Becke A (1988) Phys Rev A 38:3098
82. Lee C, Yang W, Parr R (1988) Phys Rev B 37:785

83. Grimme S (2006) J Comput Chem 27:1787
84. Brüssel M, Brehm M, Pensado AS, Malberg F, Ramzan M, Stark A, Kirchner B (2012) Phys Chem Chem Phys 14:13204
85. Brüssel M, Brehm M, Voigt T, Kirchner B (2011) Phys Chem Chem Phys 13:13617
86. Swatloski RP, Spear SK, Holbrey JD, Rogers RD (2002) J Am Chem Soc 124:4974
87. Sellin M, Ondruschka B, Stark A (2010) In: Liebert TF and Edgar KJ (eds) Cellulose solvents: for analysis, shaping and chemical modification, vol 1033. American Chemical Society, Washington, DC
88. Stark A, Sellin M, Ondruschka B, Massonne K (2012) Sci China Chem 55:1663
89. Pensado AS, Brehm M, Thar J, Seitsonen AP, Kirchner B (2012) ChemPhysChem 13:1845
90. Gilli P, Bertolasi V, Ferretti V, Gilli G (1994) J Am Chem Soc 116:909
91. Gilli P, Bertolasi V, Pretto L, Ferretti V, Gilli G (2004) J Am Chem Soc 126:3845
92. Gilli P, Pretto L, Gilli G (2007) J Mol Struct 844:328
93. Seddon KR (1999) In: Boghosian S, Dracopoulos V, Kontoyannis CG, Voyiatzis GA (eds) The international George Papatheodorou symposium, Patras, p 131
94. Niedermeyer H, Hallett JP, Villar-Garcia IJ, Hunt PA, Welton T (2012) Chem Soc Rev 41:7780
95. Castiglione F, Raos G, Battista Appetecchi G, Montanino S, Passerini S, Moreno M, Famulari A, Mele A (2010) Phys Chem Chem Phys 12:1784
96. Swatloski RP, Spear SK, Holbrey JD, Rogers RD (2002) J Am Chem Soc 124:4974
97. Vagt U (2010) In: Wasserscheid P, Stark A, Anastas PT (eds) Handbook of green chemistry, vol 6. Wiley-VCH, Weinheim, p 123
98. Ebner G, Schihser S, Potthast A, Rosenau T (2008) Tetrahedron Lett 49:7322
99. Heinze T, Dorn S, Schoebitz M, Liebert T, Koehler S, Meister F (2008) Macromol Symp 262:8
100. Liebert T (2008) Macromol Symp 262:28
101. Bini R, Chiappe C, Marmugi E, Pieraccini D (2006) Chem Commun 897
102. Garcia S, Larriba M, Garcia J, Torrecilla JS, Rodriguez F (2012) Chem Eng J 180:210
103. Finotello A, Bara JE, Narayan S, Camper D, Noble RD (2008) J Phys Chem B 112:2335
104. Lungwitz R, Friedrich M, Linert W, Spange S (2008) New J Chem 32:1493
105. Lungwitz R, Spange S (2008) New J Chem 32:392
106. Canongia Lopes JN, Cordeiro TC, Esperanca JMSS, Guedes HJR, Huq S, Rebelo LPN, Seddon KR (2005) J Phys Chem B 109:3519
107. Navia P, Troncoso J, Romani L (2007) J Chem Eng Data 52:1369
108. Shiflett MB, Yokozeki A (2009) J Chem Eng Data 54:108
109. Stoppa A, Buchner R, Hefter G (2010) J Mol Liq 153:46
110. Ning H, Hou MQ, Mei QQ, Liu YH, Yang DZ, Han BX (2012) Sci China Chem 55:1509
111. Aparicio S, Atilhan M (2012) J Phys Chem B 116:2526
112. Larriba M, Garcia S, Navarro P, Garcia J, Rodriguez F (2012) J Chem Eng Data 57:1318
113. Fox ET, Weaver JEF, Henderson WA (2012) Phys Chem Chem Phys 116:5270
114. Tariq M, Freire MG, Saramago B, Coutinho JAP, Canongia Lopes JN, Rebelo LPN (2012) Chem Soc Rev 41:829
115. Stark A, Wild M, Ramzan M, Azim MM, Schmidt A (2013) In: Bröckel U, Wagner G, Meier W (eds) Product design and engineering, volume III: liquid, paste and gel formulations. Wiley-VCH, Weinheim
116. Navia P, Troncoso J, Romani L (2008) J Solut Chem 37:677
117. Annat G, Forsyth M, MacFarlane DR (2012) J Phys Chem C 116:8251
118. Shimizu K, Tariq M, Rebelo LPN, Canongia Lopes JN (2010) J Mol Liq 153:52
119. Deetlefs M, Seddon KR, Shara M (2006) Phys Chem Chem Phys 8:642
120. Macleod DB (1923) Trans Faraday Soc 38
121. Sudgen S (1924) J Chem Soc Trans 125:32
122. Knotts TA, Wilding WW, Oscarson JL, Rowley RL (2001) J Chem Eng Data 46:1007
123. Wildman SA, Crippen GM (1999) J Chem Inf Comput Sci 39:868

124. Gardas RL, Coutinho JAP (2012) Fluid Phase Equilib 263:26
125. Almeida HFD, Teles ARR, Lopes-da-Silva JA, Freire MG, Coutinho JAP (2012) J Chem Thermodyn 46:1007
126. Kilaru P, Baker GA, Scovazzo P (2007) J Chem Eng Data 52:2306
127. Every H, Bishop AG, Forsyth M, MacFarlane DR (2000) Electrochim Acta 45:127
128. Seddon KR, Stark A, Torres MJ (2000) Pure Appl Chem 72:2275
129. Arce A, Earle MJ, Katdare SP, Rodriguez H, Seddon KR (2007) Fluid Phase Equilib 261:427
130. Arce A, Earle MJ, Katdare SP, Rodriguez H, Seddon KR (2006) Chem Commun 2548
131. Brehm M, Kirchner B (2011) J Chem Inf Model 51:2007

Index